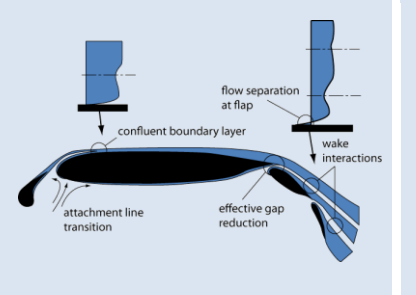
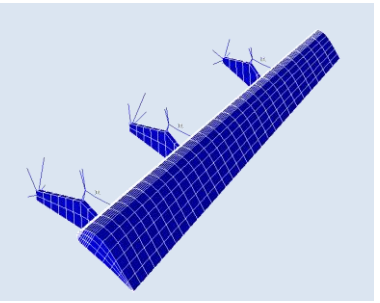


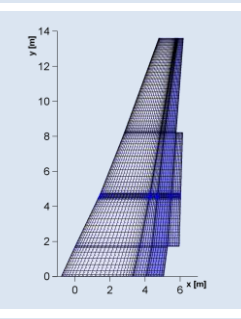


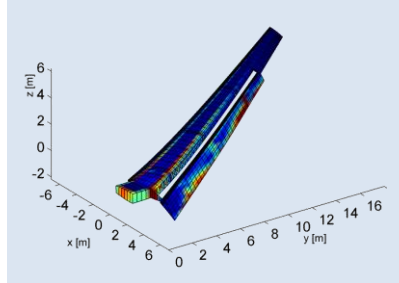
Development of an aeroelastic analysis tool for structural sizing of high-lift devices during preliminary design

Master Thesis Report









Author | Erwin Moerland, B.Sc.

Chair Systems Engineering & Aircraft Design

Date | April, 2011

Supervisor Dr. Ir. R. Vos





Development of an Aeroelastic Analysis Tool for Structural Sizing of High-lift Devices During Preliminary Design

Master of Science Thesis

For obtaining the degree of Master of Science in Aerospace Engineering at Delft University of Technology

Erwin Moerland, B.Sc.

April 8th, 2011

Faculty of Aerospace Engineering · Delft University of Technology





Delft University of Technology

Copyright © E.Moerland, B.Sc. All rights reserved.



Delft University of Technology

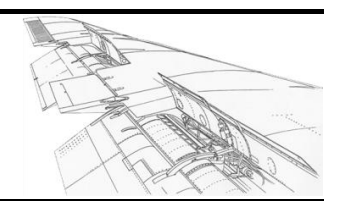
Department Of

Design, Integration and Operations of Aircraft and Rotorcraft

The undersigned hereby certify that they have read and recommend to the Faculty of Aerospace Engineering for acceptance a thesis entitled "Development of an Aeroelastic Analysis Tool for Structural Sizing of High-lift Devices During Preliminary Design" by E. Moerland B.Sc. in partial fulfilment of the requirements for the degree of Master of Science.

	Dated:		
Head of Department:			
		Prof. dr. ir. M.J.L. van Tooren	
Chairman exam committee:			
		Dr.ir. L.L.M. Veldhuis	
Thesis supervisor:		De in D. Vee	
External exam committee member:		Dr.ir. R. Vos	
		DiplIng. B. Nagel	

Preface



When once you have tasted flight, you will forever walk the earth with your eyes turned skyward, for there you have been and there you will always long to return

Leonardo da Vinci (1452-1519)

December 17th, 1903: two bicycle repairers manage to achieve the first heavier-than-air powered aircraft flight, sustained over a distance of 120 ft.

Wilbur and Orville Wright (1867-1912, 1871-1948)

The quote and achievement by these pioneers of flight have been the driving force behind my aerospace engineering study at Delft University of Technology, of which this master thesis report is the final result. The field of aerospace engineering has been progressing rapidly since the first attempts to fly, and I am really looking forward to be involved in future developments in this inspiring environment.

Effective high-lift design has a significant impact on the performance of aircraft. Within the current design of airplane wings, ever increasing computational power is used to investigate future opportunities on these high-lift systems by providing more knowledge of the design in early design stages. This thesis focuses on the development of an application in which both structural and aerodynamic design considerations are closely coupled. Increased knowledge of the high-lift system parameter dependencies will eventually lead to more efficient airplanes, providing a contribution to solutions of the sustainability challenges faced by future air transportation systems.

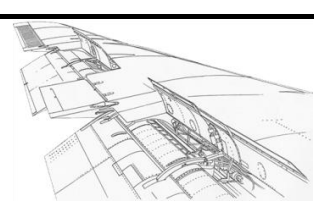
In developing this thesis, several people have been of great aid. I would like to use this opportunity to show my gratitude to dr.ir. Roelof Vos for his helpful guidance, inspiring ideas and tremendous patience during the course of the thesis. Many thanks go out to Björn Nagel of the institute for air transportation systems and technology assessment of the German Aerospace Centre in Hamburg for hosting the preceding internship and providing the subject of this thesis. The technical guidance of Felix Dorbath of aforementioned institute has also been of great help in developing the aeroelastic model underlying the thesis.

I owe much gratitude to my parents for providing a great foundation of moral values, social skills and above all perseverance, and the opportunity to study at Delft University of Technology. Finally, I would like to thank my wife for providing calmness when I was in one of my programming crises, for her patience which approaches infinity and for her useful feedback on the structure and contents of this thesis report.

Delft, the 28th of March 2011

Erwin Moerland

Contents

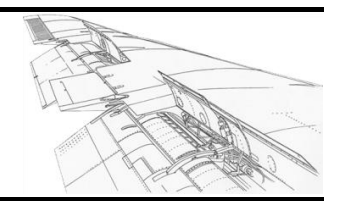


<u>Pre</u>	face		vii
Cor	ntents		ix
Sur	nmary		X
No	menclat	ture	xiii
<u>1</u>	Introc	luction and Problem Statement	1
<u>2</u>	Resea	rch background	5
	<u>2.1</u>	High-lift devices	5
	2.1.1	The need for high-lift systems	5
	2.1.2	Current trends in high-lift systems for large commercial transport aircraft	8
	2.1.3	Flow physics and topology of high-lift systems	14
	2.1.4	High-lift system design process	20
	2.2	Parametric modelling techniques	24
	2.2.1	The need for parametric modelling techniques in early design phases	24
	2.2.2	Current trends in the usage of parametric modelling techniques	25
	2.2.3	Parametric wing modelling using ParaMAM	32
	<u>2.3</u>	Aerodynamic calculation methods in wing conceptual design	35
	2.3.1	Requirements on aerodynamic tools in conceptual design	35
	2.3.2	Overview of available aerodynamic methods	38
	2.3.3	Wing modelling using a vortex-lattice method	48
<u>3</u>	Aeroe	lastic modelling	51
	<u>3.1</u>	Main goals and general structure of the aeroelastic sizing tool chain	52
	3.1.1	Main goals of the aeroelastic sizing tool chain	52
	3.1.2	Structure of the aeroelastic tool chain	53
	3.1.3	Initial approach and future opportunities	55
	<u>3.2</u>	Basic wing model generation	56
	3.2.1	The iGreen / LamAir wing model	56
	3.2.2	Model generator connection to CPACS	58
	3.2.3	Possibilities and limitations in wing modelling	58
	<u>3.3</u>	High-lift device deployment using ANSYS multibody dynamics	60
	3.3.1	Extending the high-lift devices using ANSYS	60
	<u>3.4</u>	Aerodynamic loading calculation using a vortex-lattice method	63



	3.4.1	Vortex-lattice model generation for AVL	64
	3.4.2	Load extraction from AVL result datadecks	76
	<u>3.5</u>	Structural calculations	83
	3.5.1	ANSYS structural model	83
	3.5.2	Stress and displacement data extraction	84
	<u>3.6</u>	Aeroelastic iterations	87
	<u>3.7</u>	Preliminary wing thickness sizing	89
	3.7.1	Working principles of sizing routine S_BOT	89
	3.7.2	Incorporating the sizing routine in the aeroelastic tool chain	90
<u>4</u>	<u>Aerod</u>	ynamic model validation	91
	<u>4.1</u>	The Fokker-100 wing model	91
	4.1.1	Geometry and base model of the Fokker-100 wing	91
	4.1.2	Structural and aerodynamic wing model generation of the Fokker-100 wing	93
	<u>4.2</u>	Aerodynamic result validation using the Fokker-100 wing	95
	4.2.1	General calculation setup including effective flap angle correction method	95
	4.2.2	Validation of spanwise lift distribution results for the Fokker-100 wing	97
	4.2.3	Validation of lift curve calculation results for the Fokker-100 wing	100
	<u>4.3</u>	Grid convergence analysis of the Fokker-100 wing	102
<u>5</u>	Applic	ation in preliminary wing sizing	107
<u>6</u>	<u>Conclu</u>	sions and Recommendations	113
	6.1 of high	Conclusions concerning the developed aeroelastic analysis tool for structural sol-lift devices	sizing 113
	6.2 prelim	Recommendations for future work on high-lift system investigations defining design	uring 115
Refe	erences		117
<u>APP</u>	ENDIX	Overview of applied high-lift devices	A-1
<u>APP</u>	ENDIX	Overview of applied support systems	B-1
<u>APP</u>	ENDIX	Numbering conventions for ANSYS structural wing models	C-1
<u>APP</u>	ENDIX	D Fokker 100 wing geometry	D-1

Summary



The design of complex aircraft elements such as high-lift devices has large influence on the performance of modern transport airplanes. At the cost of increased wing weight, these devices are included in the wing to ensure safe takeoff and landing. In order to meet sustainability challenges on future air transportation systems, high-lift devices need to be designed as efficiently as possible. Therefore, multidisciplinary design considerations should already start in preliminary design phase.

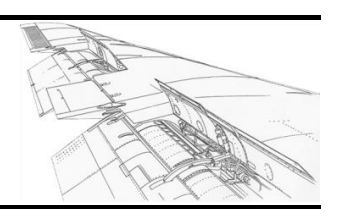
Up to now the focus of high-lift flow-physics research has been mainly on the creation of high-fidelity aerodynamic analysis methods which are not applicable to early aircraft design stages. The increase in computational power in the last decade allows both a shift of design methodologies from empirical to computational methods and a more extensive incorporation of disciplines other than aerodynamics.

The goal of this thesis is to present an initial solution to the requirement for improved high-lift system representations on preliminary design level. Structural and aerodynamic disciplines are jointly considered in the developed high-lift system analysis tool.

First, a literature research is conducted considering high-lift device characteristics, parametric modelling techniques and possible aerodynamic calculation methods. Herewith a theoretical basis for development of the analysis tool is obtained. Based on the outcomes of an existing structural model generator, a link is established to a low-fidelity aerodynamic vortex-lattice calculation method. Obtained wing loads are thereafter applied at the structural wing representation to acquire stress and displacement distributions. Knowing these, an aeroelastic coupling method is established and extended with a structural sizing routine. Aerodynamic results are validated using existing data of the Fokker-100 wing. Finally, an application of the routine is shown by performing initial structural sizing of a forward-swept wing including a trailing edge flap.

The aeroelastic analysis tool developed during this thesis provides a solid basis for enhancement of the understanding of interconnections and sensitivities between the aerodynamic and structural disciplines involved in preliminary high-lift device design. Although the initial results of the analysis tool are quite promising, extension of the aerodynamic analysis method, as well as incorporation of additional modelling capabilities are required for the methodology to become generally applicable.

Nomenclature



Latin Symbols

а	speed of sound	[m/s]
b	wing span	[m]
С	wing chord	[m]
C_p	pressure coefficient	[-]
C _I	lift coefficient in two-dimensional flow conditions	[-]
C _m	moment coefficient in two-dimensional flow conditions	[-]
C_{L}	lift coefficient in three-dimensional flow conditions	[-]
C_{T}	engine/thrust specific fuel consumption	[g/(s·kN)]
d_{f}	fuselage diameter	[m]
D	drag	[N]
g	gravitational acceleration	[m/s²]
G	gap in high-lift device definitions	[%c]
h _{cruise}	airplane cruise altitude	[m]
h _s	screen height	[m]
М	Mach number	[-]
0	overlap in high-lift device definitions	[%c]
p	pitch rate	[deg/sec]
q	roll rate	[deg/sec]
r	yaw rate	[deg/sec]
R	airplane range	[m]
Re	Reynolds number	[-]
V	airplane velocity	[m/s]
V_1	takeoff decision speed	[m/s]
V_2	lowest speed to ensure adequate and safe climb out with critical engine inoperative	[m/s]
V _{approach}	landing approach speed	[m/s]
V_{C}	climb out speed	[m/s]
V_{LOF}	liftoff speed	[m/s]
V_{MC}	minimum control speed	[m/s]
V_{MU}	minimum liftoff or unstick speed	[m/s]
V_{MS}	minimum stalling speed	[m/s]



Latin Symbols (continued)

V_{Sx}	reference stall speed in configuration 'x'	[m/s]
V_{R}	rotation speed	[m/s]
W_{i}	airplane initial weight (at start of flying mission)	[N]
W_{e}	airplane final weight (at end of flying mission)	[N]

Greek Symbols

α	angle of attack	[deg]
β	sideslip angle	[deg]
γ	flight path angle	[deg]
Γ	dihedral angle	[deg]
δ	deflection angle	[deg]
$\delta^{^*}$	boundary layer displacement thickness	[m]
λ	taper ratio	[-]
Λ	sweep angle	[deg]
ρ	air density	[kg/m³]

Acronyms

APDL ANSYS parametric design language

B-spline Bezier-spline

CAD computer aided design

CFD computational fluid dynamicsCSM computational solid mechanicsCS Certification Specifications

DLR Deutsches Zentrum für Luft- und Raumfahrt (German Aerospace Centre)

EASA European Aviation Safety Agency

FBSM feature-based solid modelling

FEA finite element analysis **FFD** free-form deformation

FM Fowler motion

IBL integral boundary layer methodKBE knowledge-based engineering

LE leading edge

MLW maximum landing weightMTOW maximum takeoff weight

NURBS non uniform rational Bezier-spline

PDE power drive unit (part of high-lift system)

PDE partial differential equation (parameterization method)



Acronyms (continued)

PDR pressure difference rule (for predicting lift values at high-lift conditions)

RANS refers to methods based on the Reynolds-averaged Navier Stokes equations

RSM Reynolds stress turbulence model
 SA Spallart-Almaras turbulence model
 SH shroud length (used in flap definition)

SOA soft object animation

SST shear stress transport turbulence model

TE trailing edgeTO takeoff

VC variable camberWF wing-fuselage

WFN wing-fuselage-nacelles

Definitions

L/D	lift over drag ratio	[-]
R/C	rate of climb	[m/s]
T/W	thrust over weight ratio	[-]
U _e / U _∞	effective velocity to freestream velocity ratio	[-]
W/S	wing loading	[N/m²]

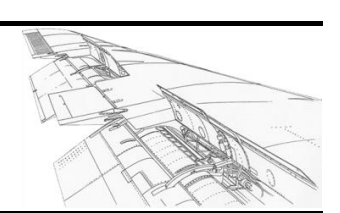


Program acronyms

	expanded	Analysis systems
ANSYS	purpose	multipurpose CAE software tool including FEA methods and multibody dynamics simulations
AVL	expanded	Athena vortex lattice
7172	purpose	inviscid three-dimensional flow solver using vortex-lattice technique
CPACS	expanded	common parametric aircraft configuration scheme
	purpose	aircraft configuration information model
007	expanded	class shape transformation
CST	purpose	parameterization method based on B-splines (Kulfan)
MASSOUD	expanded	multidisciplinary aerodynamic structural shape optimization using deformation
WASSOOD	purpose	parameterization tool based on FFD (Samareh)
MATLAD	expanded	matrix laboratory
MATLAB	purpose	programming environment used for generating and controlling the aeroelastic high-lift device analysis tool
1414C	expanded	multi model generator
MMG	purpose	parametric modelling tool incorporating multiple parameterization techniques (TU Delft)
	expanded	
MSES	purpose	coupled viscous/inviscid Euler method for airfoil design and analysis
NPLS	expanded	non-planar lifting surface programme
	purpose	vortex-lattice analysis programme used by Fokker
D		
ParaMAM	expanded	parametric simple and fast mesh-based aircraft modelling tool
	purpose	modelling tool for aircraft structures at advanced preliminary design level
D 400	·	modelling tool for aircraft structures at advanced preliminary design
PrADO	purpose	modelling tool for aircraft structures at advanced preliminary design level
	purpose expanded	modelling tool for aircraft structures at advanced preliminary design level preliminary aircraft design and optimization tool parametric modelling and analysis tool incorporating multiple
PrADO S_BOT	purpose expanded purpose	modelling tool for aircraft structures at advanced preliminary design level preliminary aircraft design and optimization tool parametric modelling and analysis tool incorporating multiple parameterization techniques (DLR)

Chapter 1

Introduction and Problem Statement



In this chapter, an introduction in the problems encountered during preliminary design of highlift devices is presented. The general problem statement of the thesis is provided, as well as the way the problem is approached. Finally, the structure of this report is described.

Airplane wings that are optimized for efficient flight in cruise conditions need to be fitted with powerful high-lift devices to meet lift requirements for safe takeoff and landing. These high-lift devices have a significant impact on the total airplane performance and therefore need to be considered already in early design stages. Incorporating efficient high-lift system design methods can lead to more efficient airplanes, ready to face the envisaged sustainability challenges of future air transportation systems.

Unfortunately, when it comes to high-lift flow-physics investigations, up to now the focus has been on the creation of high-fidelity methods such as full RANS simulations. These methods require too large computational effort and too detailed geometry modelling to be applicable to early design stages. Since one wants to assess a large number of system concepts and variations in a quick and concise manner during early design, lower fidelity aerodynamic design tools are required. A second observation in the high-lift design process during early design stages is the underrepresentation of design disciplines other than aerodynamics. The underrepresentation of structures and systems thereby leads to difficulties in proper estimation of one of the most fundamental system parameters, high-lift system weight.

The ever increasing computer power enables a shift in today's design process: empirical design methods are gradually being superseded by the application of computational methods. This enables a more multidisciplinary design approach to be started already in conceptual and preliminary design phases. At the institute of air transportation systems and technology assessment of the German aerospace centre (DLR) in Hamburg, an overall wing design and optimisation chain on an advanced pre-design level is being developed. The goal of the tool chain is to close the expensive gap between preliminary and detailed design phases. Additionally, the tool chain is intended to be extremely flexible, so that methods of different fidelity levels can easily be interchanged. Improved knowledge on the complete high-lift system gained in preliminary design level enables the design team to consider relevant sensitivities in other disciplines earlier in the design cycle. This increases the knowledge level of the complete design in early design phases and this in turn can lead to more efficient high-lift system topologies.

The goal of this thesis is presenting an initial solution to the requirement for improved high-lift system representations on preliminary design level. The applied parametric design method is used for gaining enhanced understanding of both the disciplinary components involved in high-lift system design and the effectiveness of the lower fidelity design methods. Two main objectives in the investigation subdivide the project in two major phases, as indicated in figure 1.1. After fulfilling these main objectives, sizing of high-lift devices during early aircraft wing design phases can be done with more confidence, reducing the risk of encountering expensive redesign in the detailed design phase.

Chapter 1



Construction of an improved aeroelastic representation of high-lift systems with a focus on rapid load estimations, which can be incorporated in the DLR wing design chain

Enhancement of the understanding of the interconnections as well as sensitivities between different disciplinary components of the high-lift system, with a focus on structural sizing and weight estimation

Figure 1.1 Main thesis objectives

In order to be able to assess a large number of system concepts and their derivatives, a flexible parametric wing modelling technique has to be applied. During a preceding study [1], a structural modelling tool was created for wings incorporating trailing edge high-lift devices. This tool serves as the basis for creating the improved aeroelastic representation. Starting the master thesis, first a literature research is performed. The results of this literature research cover the three main pillars on which the research is based; high-lift device characteristics, parametric modelling techniques and possible aerodynamic calculation methods. In the first part of this literature research, the current trends in high-lift systems, as well as the accompanying flow physics are investigated. The second part puts the created model generator in perspective to parametric design methods applied in the aerospace industry. The last part provides a survey of aerodynamic calculation methods applicable to the preliminary design phase aimed for, after which the most appropriate aerodynamic approach is chosen.

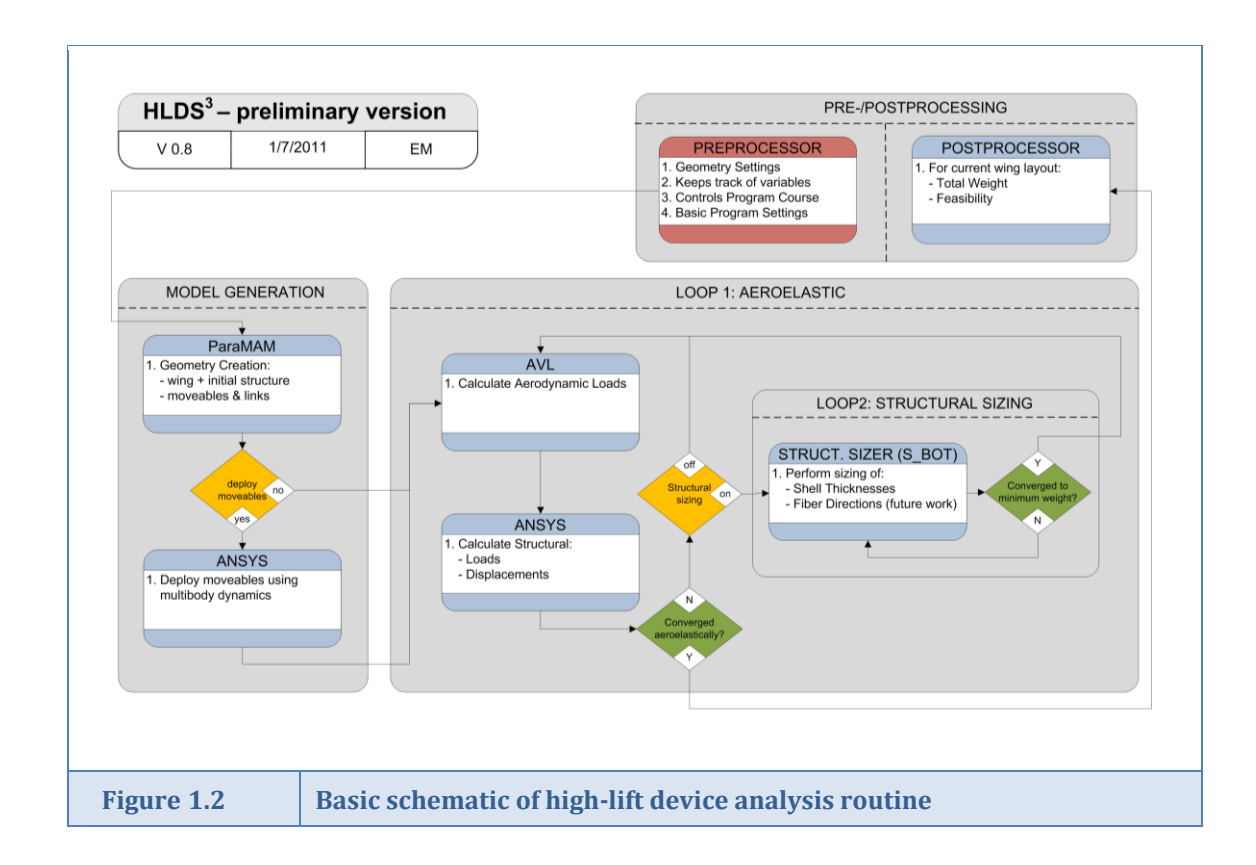
After the literature research, the capabilities of the wing and high-lift system model generator are expanded by incorporating a link to the chosen low-fidelity aerodynamic calculation method. The aerodynamic calculation method is verified by comparing results to existing wing aerodynamic data and calculations. After completion of the aerodynamic part, an aeroelastically coupled calculation procedure is created, indicated by 'LOOP 1' in figure 1.2. The part indicated by 'model generation' in figure 1.2 represents the work already performed during the aforementioned study, although some adjustments need to be made in order to automate each subfunction when a complete analysis is to be run. Once the aerodynamic coupling runs in an efficient way, a structural sizing routine can be incorporated and applied to general wing models containing basic high-lift systems. The sizing routine S_BOT will be available from the DLR and applies a direct sizing technique to the skin, rib and spar thicknesses of the wing model. After main convergence of the coupled software infrastructure, a total mass estimation of the structurally sized model can be performed. With the high-lift device analysis routine working, studies can be performed to better understand the sensitivities between wing topology and mass estimation.

Since research is performed at a preliminary design level, it is important to keep the boundaries of applicability of the software tool in mind. To be able to perform quick aerodynamic calculations losses in accuracy have to be accepted. Furthermore, the structural sizing routine performs a sizing based on basic principles valid for preliminary design and thereby does not take all material failure possibilities into account. The underlying assumptions made in the choice for calculation methods implicate only qualitative system assessments are allowed. The tools will however be programmed in such a way that individual software parts can be exchanged without much effort, allowing incorporation of tools possessing different levels of fidelity and computational cost.

The reader interested in the results of the literature research is referred to chapter 2. The two chapters thereafter describe the creation and aerodynamic validation of the high-lift device analysis routine. First, chapter 3 shows the applied aerodynamic calculation method, along

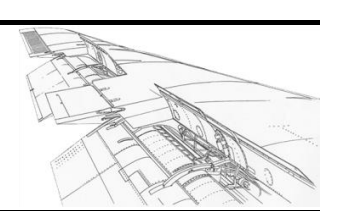


with the principles used for extracting the aerodynamic wing representation from the parametric design tool. The aeroelastic coupling routine is presented and a structural sizing addition is incorporated. Subsequently, chapter 4 validates the aerodynamic calculation method by comparing results to a Fokker-100 wing model. Chapter 5 provides an application of the developed tool, by performing an initial structural sizing of a forward-swept wing model. The report concludes with an evaluation of the applied analysis method and recommendations for future work in chapter 6.



Chapter 2

Research background



In the current chapter, the three main pillars on which the research is based are introduced, along with their similarities and differences with current aircraft design methods. The chapter starts with a general discussion on high-lift devices in section 2.1. Trends in high-lift device design, as well as aerodynamics of high-lift systems will be highlighted. Thereafter the parametric wing modelling method is treated in section 2.2, along with its relation to other parametric modelling techniques. Finally the possible aerodynamic calculation methods in conceptual design are reviewed in section 2.3.

2.1 High-lift devices

The present section first shortly indicates why airplanes need high-lift devices, after which the current trends in high-lift systems are given. Thereafter, the general flow physics of high-lift devices are explained and finally the general structure of a current high-lift design process is given.

2.1.1 The need for high-lift systems

Section Sources:

[2], [3], [4], [5]

High-lift systems: a necessity

To increase maximum speeds of military aircraft and cruise speeds of commercial airliners, the aircraft design of the early days was altered by the introduction of the swept wing concept and by increasing the wing loading. This increased wing loading leads to requirements for larger lift coefficients at low speeds, as can be seen from equation 2-1.

$$C_{L,req} = \frac{1}{\frac{1}{2}\rho(V^{\downarrow})^{2}} \cdot \left(\frac{W}{S}\right)^{T}$$
 (2-1)

The wing that is optimized for efficient flight in cruise conditions needs to be fitted with powerful high-lift devices to meet the lift requirements. A numerical example provided by van Dam [3], summarized in table 2.1 confirms this statement. In this example, two airplane configurations with an equal flight mission are compared: airplane A which is optimized for cruise conditions and airplane B which is able to take off and land without use of high-lift devices. As can be seen, both airplanes face problems in their design:

- **Airplane A** needs to be able to attain a lift coefficient of 2.35 in landing conditions. This is far beyond the capabilities of a clean airplane wing without any high-lift devices, which can reach maximum lift coefficients of 1.2.
- **Airplane B**, having the maximum attainable clean wing lift coefficient of 1.2 at landing conditions, the loss in range is unacceptable. It can only fly 0.817 times the distance of airplane A, as is calculated using Breguets' equation of range, equation 2-2.



$$R = \frac{aM}{C_T} \cdot \frac{L}{D} \cdot \ln\left(\frac{W_i}{W_e}\right)$$
 (2-2)

To be able to meet commercial requirements on airplane velocity and range and governmental requirements, it must therefore be concluded that a commercial transport aircraft should be equipped with high-lift devices.

Table 2.1	The need		Based on source: [3]							
variable		symbol	basic values for both airplanes							
cruise mach nu	mber	M			0.80	0 [-]				
initial cruise alt	itude	h _{cruise}		30	0000 [ft] ?	≈ 9144 [m]				
landing approach	speed	V _{approach}		14	15 [kn] ≈	74.6 [m/s]				
drag character	istics	D	á	assumed	l similar i	for both airpla	nes			
engine specific fuel co	C _T	á	assumed	l similar i	for both airpla	both airplanes				
			airplane A ^(*)		calc. dir.	airplane	airplane B ^(**)			
range ratio		RR	1	[-]		0.817	[-]			
cruise lift coeffi	cient	$C_{L,cruise}$	0.52	[-]		0.27	[-]	. ↑		
lift over drag r	atio	L/D	18	[-]		14.8	[-]			
wing loading	v (+)	(W/S) _{takeoff}	7.0 ·10 ³	[Pa]	\downarrow	$3.6 \cdot 10^{3}$	[Pa]			
wing loading	J	(W/S) _{landing}	5.3 · 10 ³	[Pa]		$2.7 \cdot 10^{3}$	[Pa]			
approach lift coeff	icient ⁽⁺⁺⁾	C _{Lapproach}	1.55	[-]		0.79	[-]			
required maximum lift of	required maximum lift coefficient(+++) C _{Lmax}					1.2	[-]			
required maximum lift coefficient $(+++)$ C_{Lmax} 2.35 [-] 1.2 [-] (*) airplane A: optimized for cruise conditions, includes high-lift devices airplane B: able to perform takeoff and landing without high-lift devices assumption: $(W/S)_{landing} = 0.75 * (W/S)_{takeoff}$ $C_{Lapproach} = (W/S)_{landing} / (0.5 * p * V_{approach}^2)$ C_{Lmax} , required = 1.23 2 * $C_{Lapproach}$ in which the multiplication factor is governed by CS25.125 on landing [4] comment: italic values are assumed values, bold values are calculation results										

High-lift device design: a large compromise

Takeoff and landing procedures are governed by regulations of the European Aviation Safety Agency (EASA). For commercial transport aircraft these are listed in Certification Specifications Number 25 (CS-25) [4].

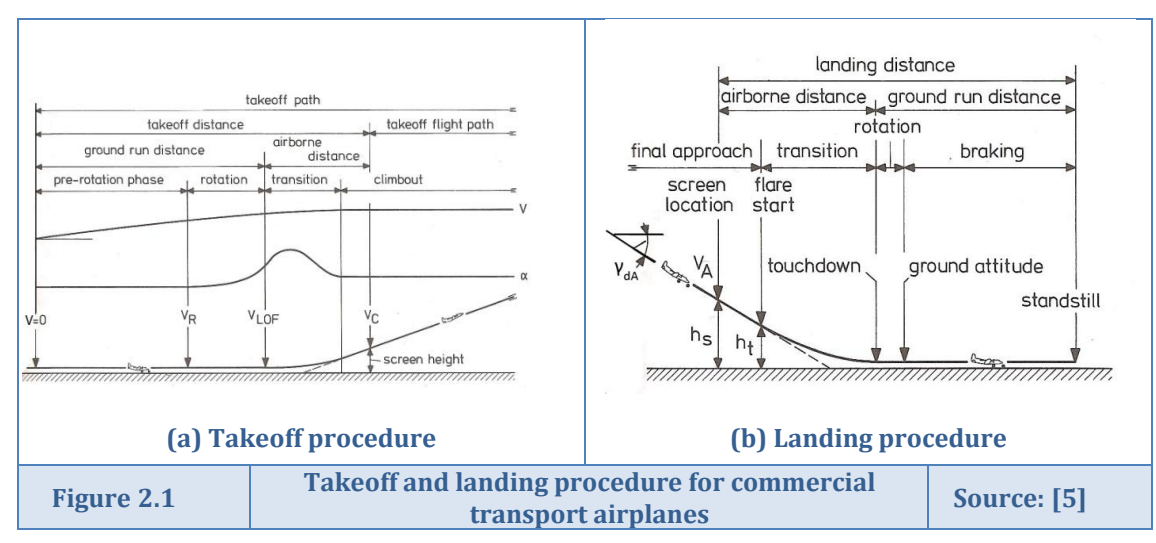
The takeoff procedure of a commercial transport airplane is illustrated in figure 2.1(a). The velocities and climb gradients encountered in this procedure are bound to minimum values enforced by the regulations stipulated in CS-25. Without getting into further detail, the most important regulations are listed in table 2.2. The takeoff performance strongly depends on the rotation speed V_R , since this velocity can significantly influence the total takeoff distance. The value of this speed can be influenced by the attainable lift coefficient at takeoff $C_{L,TO}$, which increases for increasing flap setting. After becoming airborne, the airplane has to attain a certain climb gradient when passing the screen height. This climb gradient is governed by equation 2-3. It is seen that for good climb performance, the lift-over-drag ratio L/D should be maximized. Unfortunately, L/D decreases with increased flap setting (see figure 2.2). It is therefore concluded that the design of the takeoff configuration consists of finding the optimal compromise between maximum lift capabilities and lift-to-drag ratio.

$$R/C = \tan \gamma = \frac{T}{W} - \left(\frac{L}{D}\right)^{-1} \tag{2-3}$$



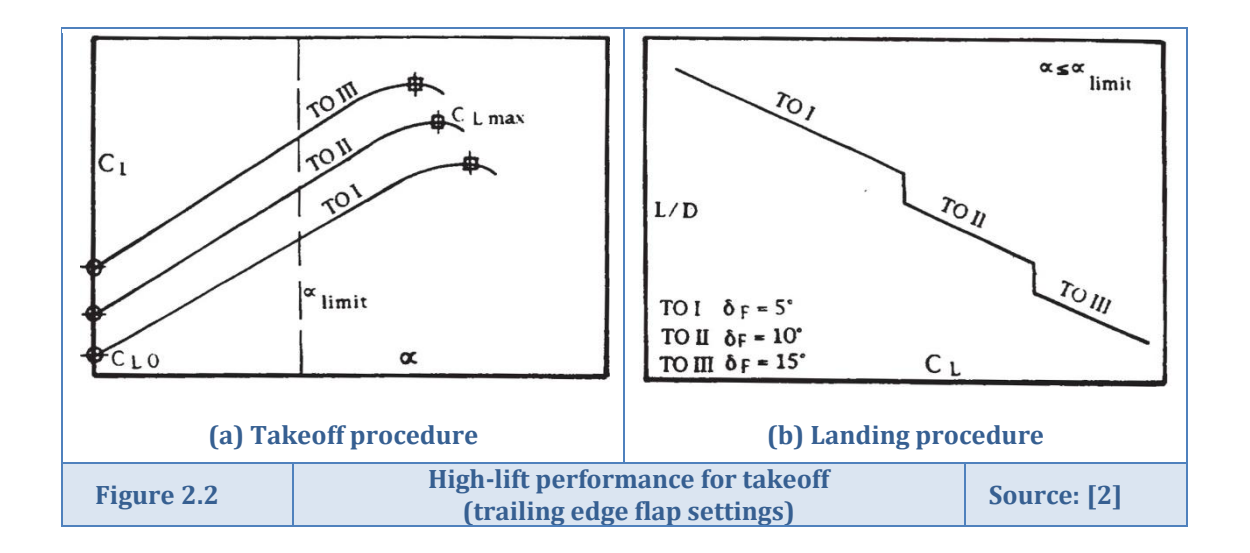
The landing procedure of a commercial transport airplane is illustrated in figure 2.1(b). Just as for the takeoff procedure, the minimum velocities and attainable climb gradients for go-around situations are enforced by airworthiness requirements. These are also listed in 2.2. The approach angle of attack of the aircraft might be governed by either maximum lift capabilities or by pilot visibility. Since there are requirements on climb gradient when a go-around has to be performed, the lift-to-drag ratio of the airplane also plays a role during landing manoeuvres.

From the above, it can be concluded that the (aerodynamic) design of high-lift devices is a trade-off between maximum lift capabilities, lift-to-drag ratio, lift capabilities at the tail-scrape angle on takeoff and landing approach angle.



Та	Tania / /			ness requireme ocedures as is s	Source: [4]						
		ve	locity requiren	nents	climb gradient requirements						
	re	equire	ement	condition	req	uire	ment	# engines	condition		
	V ₁	≥	V _{MC}		tan γ	≥	2.4%	2	OEI		
ē	V_R	≥	V_1		tan γ	≥	2.7%	3	OEI		
npəc	V_R	≥	1.05 · V _{MC}		tan γ	≥	3.0%	4	OEI		
proc	V_{LOF}	≥	1.10 · V _{MU}	AEO							
takeoff procedure	V_{LOF}	≥	1.05 · V _{MU}	OEI							
tal	V_2	≥	1.13 · V _{S1g}	OEI							
	V_2	≥	1.10 · V _{MC}	OEI							
	V _A	≥	1.23 · V _{S1g}		tan γ	≥	3.2%		OEI, GU, 8 s. after FT		
ling dure					tan γ	≥	2.1%	2	OEI, GD, 8 s. after FT		
landing procedure					tan γ	≥	2.4%	3	OEI, GD, 8 s. after FT		
ū					tan γ	≥	2.7%	4	OEI, GD, 8 s. after FT		
А	vEO: All En	gines	Operative, OEI:	One Engine Inoper	ative, Gl	D: G	ear Down	, GU: Gear Up	o, FT: Full Throttle		





2.1.2 Current trends in high-lift systems for large commercial transport aircraft

Section Sources: [2], [6], [7], [8]

Types of high-lift systems applied

After the introduction of the first simple high-lift systems on a swept wing aircraft, system complexity steadily increased to end up with very complex devices designed for airplanes built in the 1960's. The large increment in system complexity was required to accommodate the high-lift demands of commercial airliners requiring wings that provide efficient cruise flight. Nowadays it is realized that such complex devices require a tremendous amount of maintenance. Increased understanding and capabilities considering high-lift aerodynamic design have changed the general vision on high-lift design: a tendency to achieve high levels of lift with the usage of simpler devices is seen [2], [6].

The basic types of high-lift systems are summarized in table 2.3 for leading edge devices and in table 2.4 for devices at the trailing edge of the main wing. For leading edge devices, a consensus is seen between all aircraft manufacturers: the *three-position slat* is the most appropriate device to use on transport airplanes. Table 2.4 shows again a current tendency for application of simpler high-lift devices at the trailing edge of the wing.

For a more extensive overview of applied high-lift devices, the reader is referred to APPENDIX A . In the overviews presented in this appendix, a qualitative assessment of high-lift devices is based on the following criteria:

- Simplicity: maintenance and building costs are generally reduced when the device is simple
- Maximum attainable lift coefficient: high C_L allows a shorter takeoff distance and lower approach velocity during landing (see section 2.1.1)
- Attainable L/D ratio at takeoff: a high L/D ratio implies good climb performance (see section 2.1.1)



Table	Table 2.3 Leading edge devices and their year of application Based on Sources: [2], [2]								[6]			
Type	Cubi	avno.	Schematic	Simplicity	Approximate year of introduction							
Туре	Subt	ype	Schematic	Simplicity	NC ^(*)	1960	1970	1980	1990	2000	2010	
Fixed Slot	-			+++	х							
Nose	Hinge Nose			++	х							
Flap	Variable camber LE			+	х							
	Simple Krüger			-		х						
Krüger Flap	Folding, bull-nose Krüger					х	х	х				
	VC Krüger						х	х				
Clot	Two-pos	ition slat		+	х							
Slat	Three-pos	sition slat		+/-	х	х	х	х	х	х	х	
^(*) NC: n	ot used on c	ommercial t	ransport airplanes	3								

Table 2.4 Trailing edge devices and their year of application Sources: [2], [[6]		
Type	Subtype		Schematic	Simplicity	Approximate year of application							
Турс			Concinatio	Cimpliony	early	1960	1970	1980	1990	2000	2010	
Non- slotted	Split	flap		+++	х							
Flap	Plain flap			+++	х							
	Simple sl	otted flap	*	++	х							
	Single slot		~	+					х	х	х	
0, ,,	Fixed vane/main double-slotted flap		*	+		х	х	x	x			
Slotted Flap	Articulating vane/main double-slotted flap			-		х	х	x	x			
	Main/aft double-slotted flap						х	х				
	Triple-slotted flap					x	х	х				



Support systems for high-lift devices

The two main purposes of high-lift device mechanisms are to provide support in all required positions (stowed, takeoff and landing position) and to provide deployment kinematics that are as ideal as possible. For trailing edge devices, the second purpose implicates to provide as much initial Fowler motion (see section 2.1.3) as possible in initial deployment of the system, to maximize takeoff efficiency.

The purposes described above must be satisfied under a large amount of constraints, of which the most important ones are to ensure smooth flow in stowed configuration and to minimize drag and slot blockage ¹ in extended configurations. Smooth flow can be obtained by minimizing skin irregularities. For leading edge device mechanisms, the requirement not to protrude the skin of the main wing is often the most important mechanism design factor. To ensure proper deployment curves, trailing edge mechanisms are often placed partially in fairings that extend outside the main wing structure. To minimize drag and slot blockage, the supports and their fairings should be placed as far away from the slots' high speed region as possible and the fairing depths should be minimized.

In general, two support mechanisms are required per high-lift panel, however the application of more spanwise supports allows better control over the positioning of the device. Better control over positioning makes sure that a more optimal gap distribution (see section 2.1.3) is achieved. However, this comes at the cost of increased slot blockage. Niu [7] provides an extensive overview of high-lift support systems and the advantages and disadvantages of their arrangements.

Since of all high-lift system components the support and actuation mechanism is the most vulnerable one, fail-safe criteria are Boeing 777 outboard flap support

Figure 2.3 Source: [2]

used during their design. This leads to double presence of critical structural elements (see for example figure 2.3), so that often two connections are created per support. This however makes the system statically redundant, possibly introducing counteracting forces during deployment. If the panel has a large span, a third support may be added at midspan location to avoid excessive bending and gain better control over the deployed position. This however poses a large increase in system complexity, since additional force fights might be introduced. When a panel is held by two supports, in general these are placed at 25% and 75% of the panel span.

Actuation of the high-lift mechanism can be managed per individual panel, but in most designs it is centrally managed by a power drive unit (PDU) which is located in the centre of the wing. The second setup guarantees synchronized flap deployment, shows self-locking behaviour and can be designed such that it is insensitive to jamming. Therefore it is considered the safest system against deployment failures.

.

¹ Slot blockage is the blockage of flow through the slots of the high-lift system due to the supports and fairings, leading to early flow separation implying reduced lift and L/D



APPENDIX B provides an overview of the several known support mechanisms for both leading and trailing edge devices. A qualitative assessment is based on the following important criteria for linkage systems:

- Fowler motion development possibilities (see section 2.1.3)
- Simplicity: maintenance and building costs are generally reduced when the mechanism is simple
- Actuation loads (for LE devices): some devices deploy against airstream forces and thereby require large actuation loads implying heavy actuator requirements
- Fairing aerodynamic shaping possibilities (for TE devices): deep and wide fairings produce more drag, which is especially significant in cruise flight conditions
- Streamwise conical motion adaptability (for TE devices): if this is not possible, extra drag will be created due to exposure of the aft fairing to the airflow and due to the skewed inboard ends of the corresponding high-lift device. Furthermore, this leads to difficulties in the sealing of multiple high-lift panels for creating spanwise continuity

Weight of high-lift systems

System complexity is a very strong driver for weight and cost. The most complex high-lift devices in general provide the best high-lift performance (e.g. the triple slotted flaps on Boeings 727, 737 and 747), but lead to high weight and system complexity. This in turn results in high costs, both for manufacturing and maintenance during its service life. In many cases a better overall airplane design solution with the lowest life cycle cost imposed by the high-lift system is found by applying a simpler systems and accepting the lower aerodynamic performance [6].

Two methods of weight estimation can be distinguished during conceptual design of a high-lift system. The first is using empirical data based on previous airplane designs and the second, becoming possible due to the increase in available computer power, is calculating initial weight estimations based on coarse initial wing designs.

Empirical weight data on high-lift systems is unfortunately not generally available. Rudolph [2] has however generated a simplified overview of general specific weights per system type, given in tables 2.5 for leading edge devices and 2.6 for trailing edge devices. The values in both tables are based on modified versions of weight estimation formulae published in a report on weight and cost estimates for lifting surfaces [8]. The estimation formulae were originally based on Boeing airplanes designed until 1976. Rudolph has modified these formulae in such a way to take the introduction of composite materials in airplane design into account. It must however be stated that the data used by Rudolph is based on airplane designs until 1996, the year in which [2] was published. Therefore, the data given in tables 2.5 and 2.6 must be handled with care when conducting research on high-lift system weight for future commercial transport aircraft.



Table	e 2.5	5 Leading edge devices and their specific weights Source: [2					rce: [2]			
				Specific weights ^(*) [kg/m ²]						
Туре	vpe Subtyp	oe .	Support	fixed LE	moving panels	actuation	total			
Krüger	Simple Krüger		simple hinge without slave link	11.0	7.32	7.32	25.6			
Flap	VC Krüger		four bar linkage with slave track	11.0	10.3	8.54	29.8			
Clat	Three-positi	ion slat	with slave tracks	10.8	12.2	6.35	29.3			
Slat	Three-position slat		without slave tracks	10.3	11.7	6.35	28.3			
^(*) weigh	ts related to v	ving lead	ding edge area forward o	of the front spar						

Table 2.6 Trai			iling edge devices	ights	Source: [2]						
				Specific weights ^(*) [kg/m²]							
Туре	Subtype		Support	flap panels ⁽ⁱ⁾	supports ⁽ⁱⁱ⁾	actuation ⁽ⁱⁱⁱ⁾	fairing ^(iv)	total			
	Single slotted Fowler flap		Link/Track end support	13.2	7.32	9.76	0.488	30.8			
	Single slotted Fowler flap		Hooked track	13.2	14.6	10.7	4.88	43.5			
Slotted	Fixed vane/main double-slotted flap			14.6	15.6	10.7	4.88	45.9			
Flap	Articulating vane/main double- slotted flap Main/aft double- slotted flap Triple-slotted flap			17.1	18.6	11.2	5.61	52.5			
				23.4	22.9	11.7	6.35	64.4			
				26.9	27.3	12.2	6.84	73.2			

weights per projected area of the nested flaps

weight savings for composites taken into account in modified formulae from [8]

hooked track used as baseline mechanism, simple hinges and some link/track mechanisms are lighter. Complex four-bar linkages are however heavier
a synchronized shaft drive with jack screw actuation is assumed
fairing area is calculated using a constant unit weight and fairing area/flap area ratio dependent on support type



One can however distil some trends from the specific weight tables. When combining tables 2.5 and 2.6, the logical relation between system complexity and specific weight is seen. The triple-slotted flap is about 1.7 times heavier than the simple single slotted Fowler flap. One can also see, from table 2.6, that support and actuation concept can have a large influence in highlift system weight, when considering the single slotted Fowler flap with a link/track end support at the one hand and a hooked track support at the other hand. Comparing both specific weight tables (2.5 and 2.6), it can be concluded that the weight saving potential is much higher for trailing edge devices than it is for leading edge devices.

Aside the overview of typical weights provided by Rudolph, empirical weight estimation methods are described by Roskam [9], Raymer [10] and Torenbeek [11]. These methods are based on the same underlying principles as empirical methods used in aerodynamic design, therefore the reader is referred to section 2.3, in which these empirical methods will be described.

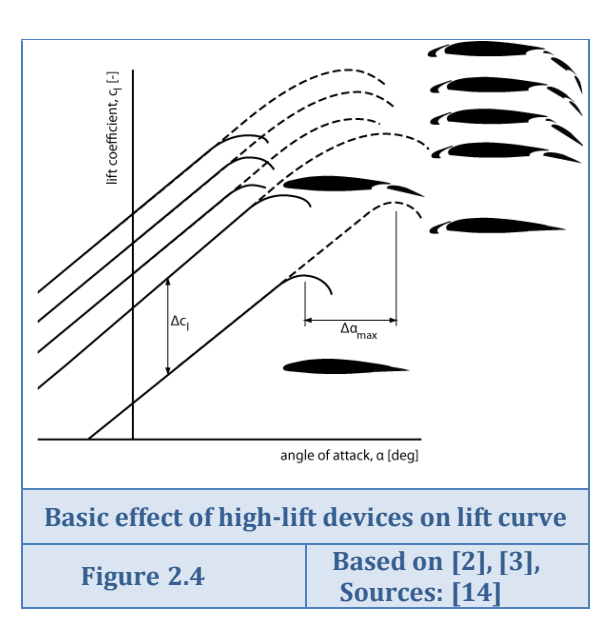


2.1.3 Flow physics and topology of high-lift systems

Section Sources: [2], [3], [12], [13], [14], [15], [16], [17], [18], [19], [20]

Aerodynamics of extending high-lift devices

In figure 2.4, the effect of extending leading and trailing edge devices on the lift curve is seen. A leading edge device extends the stall angle of attack ($\Delta \alpha_{max}$ in figure 2.4) by changing the local curvature of the airfoil, whereas a trailing edge device increases the lift coefficient (ΔC_L in figure 2.4) by increasing the local camber of the airfoil. It can be seen that the highest lift levels can be attained by the most complex high-lift systems. When compared to current highlift designs satisfying all basic requirements on takeoff and landing, an extra increase in complexity is however not outweighed by the obtained increase in lift level, as was already stated in section 2.1.2.



Besides changing the curvature or camber of the airfoils, extension of high-lift devices can increase the effective chord by generating Fowler motion (see formulae 2-4 and 2-5 for a definition), implying an increase in generated lift. Especially in takeoff situations this increase in lift is very beneficial, since it is the most effective way to increase the L/D-ratio of the airplane.

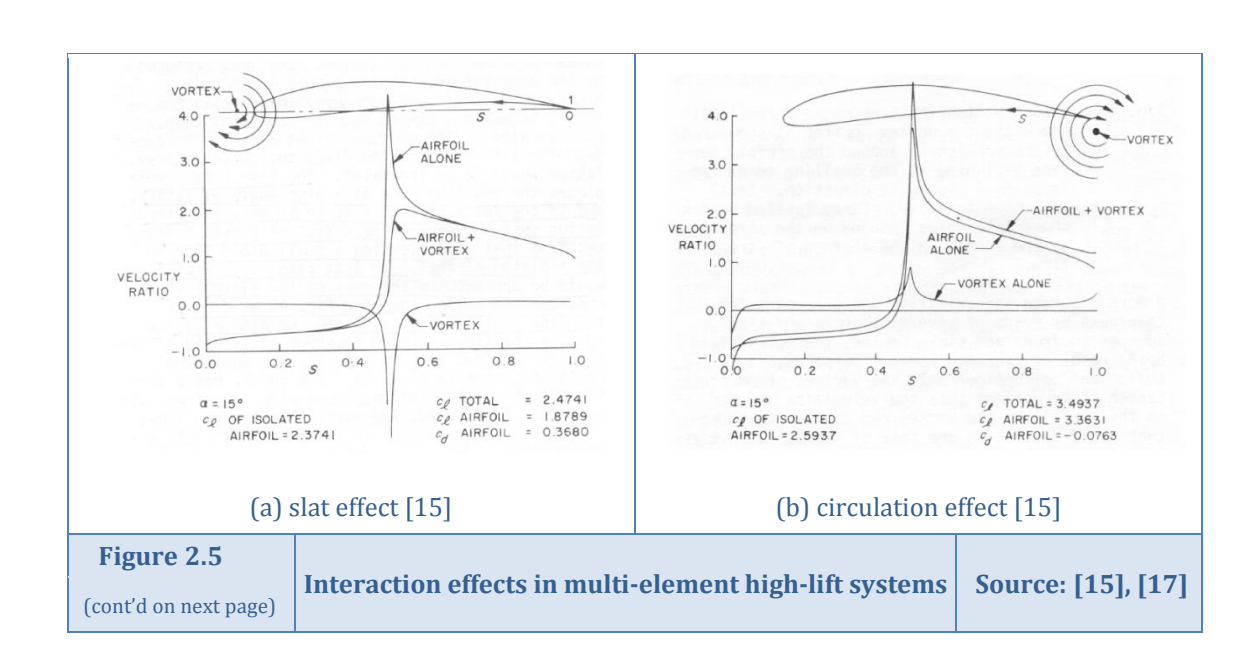
It took aerodynamicists a long time before the last effect of multi-element high-lift devices was properly understood. A.M.O. Smith was the first to properly describe the five effects that occur due to interaction of properly placed wing elements [15]. The five interaction effects are described hereafter:

- Slat effect: pressure peaks on downstream elements are reduced due to the circulation of an upstream element. In practice this effect is used to reduce the chance of flow separation on the main element of a multi-element airfoil. Figure 2.5 (a) shows that a deflected slat can be represented by a point vortex, reducing velocities and thereby pressure peaks on the leading edge of the main element.
- Circulation effect: velocities on an upstream element are increased and inclined to the mean line due to the circulation of a downstream element. Figure 2.5 (b) shows that a deflected flap can be represented by a point vortex, increasing velocities and thereby pressure differences on the upstream element. The larger pressure differences lead to higher lift generation. In terms of circulation of the upstream element, one can say that the increased flow inclined to the mean line implies circulation has to be increased to keep satisfying the Kutta condition².

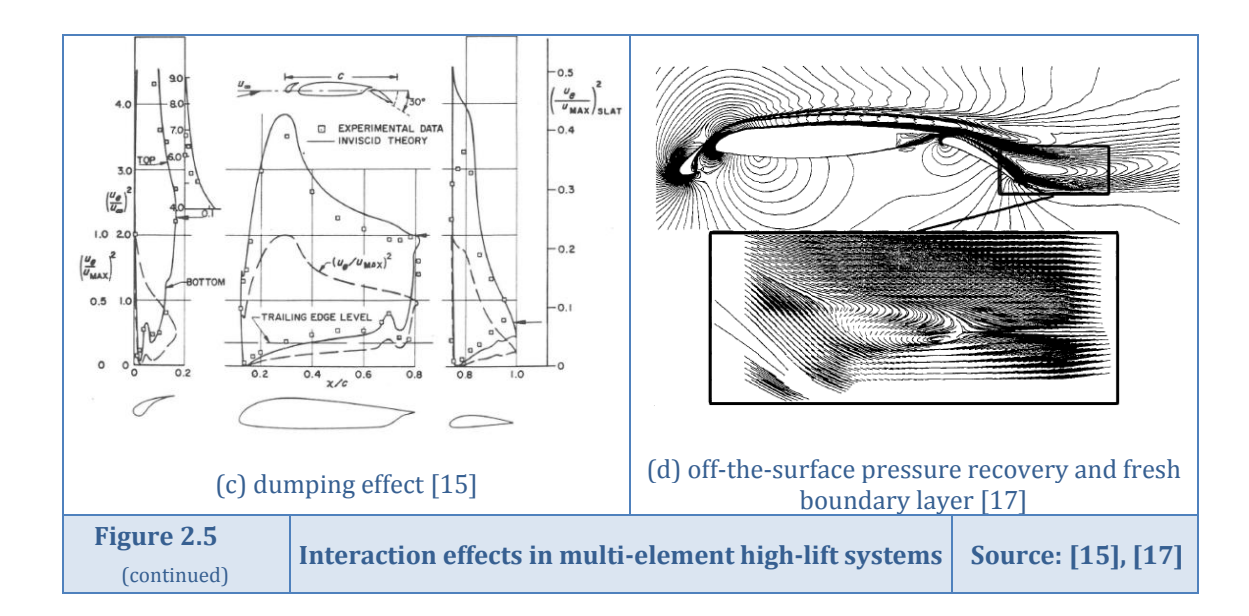
² Kutta condition: the circulation value around an airfoil attains a value which makes sure the flow is smoothly leaving the top and bottom surfaces of the airfoil at the trailing edge



- Dumping effect: the flow around the leading edge of a following element makes sure the trailing edge of a forward element is positioned in a velocity region that is considerably higher than freestream. Therefore, the boundary layer of the forward element is dumped at a higher velocity. This lowers the required pressure increase in the boundary layer, which allows larger pressure differences to be built up due to postponement of separation effects on the forward element. Figure 2.5 (c) shows the increased $(U_e/U_{\infty})^2$ values allowed at the trailing edges of the first and second element making up the high-lift system. The encountered pressure gradients along the upper surface of these elements are significantly lowered due to the dumping effect.
- Off-the-surface pressure recovery effect: the boundary layer from upstream elements leaves the trailing edge at higher velocities than freestream velocity, therefore a wake is created. Due to this, deceleration to freestream velocity occurs out of contact with a wall, which is far more efficient than it would be when in contact. In the enlarged box of figure 2.5 (d), particle traces of the flow show off-surface recovery in the wake of the flap. In the upper part of the mentioned figure, velocity contours can be seen, indicating the same behaviour.
- Fresh boundary layer effect: each new element starts with a fresh boundary layer that is able to withstand larger adverse pressure gradients. The upper part of figure 2.5 (d), indicating velocity contours around the airfoil elements, clearly shows the start of new boundary layers at the leading edge of the individual elements.

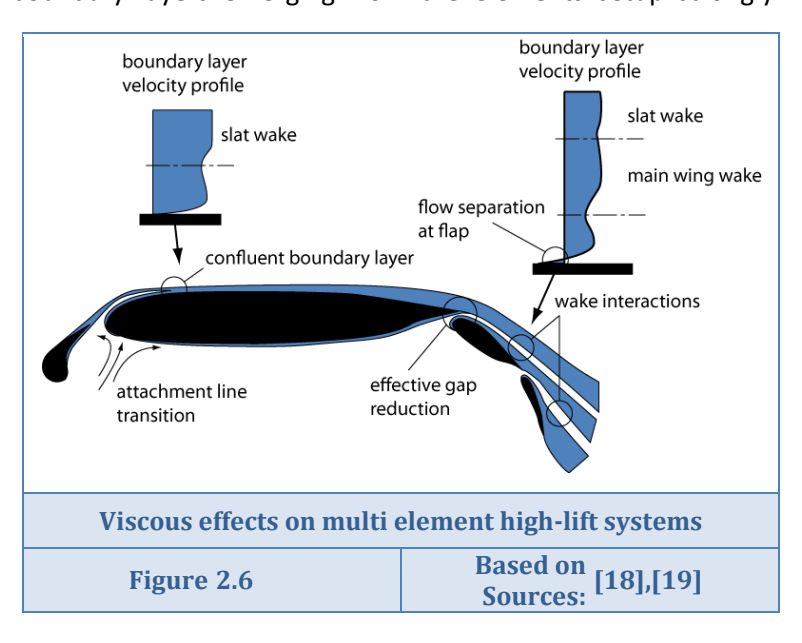






It is thought that the downwash emerging from the systems individual elements (see for an example figure 2.5(d)) provide a damping effect on the pressure peaks of downstream elements, reducing separation tendency of the flow. However, when the wakes merge with the fresh boundary layer of a following element, a confluent boundary layer is created (see figure 2.6). This boundary layer is much thicker than a normal boundary layer, which imposes an increase in the likelihood of separation and thereby deteriorates stall characteristics [3]. The occurrence of confluent boundary layers emerging from the elements setup strongly

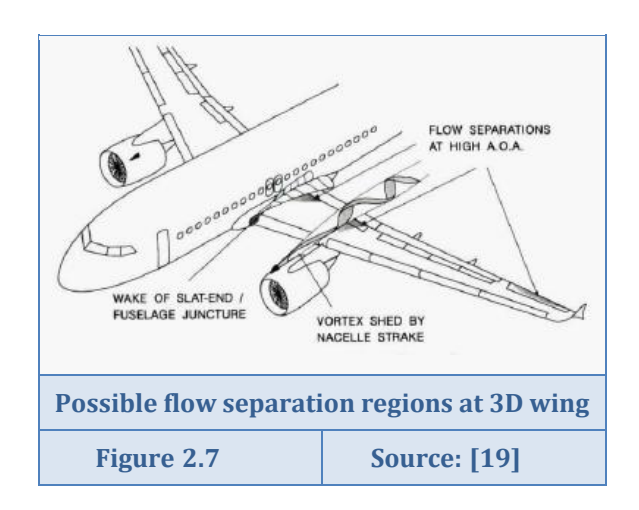
depends on viscous flow effects. Another important viscous flow effect is found in the thickness of the shear (boundary) layers. These thicknesses determine the effective gap between the elements (see figure 2.6), which in turn has a large effect on the positions of the wakes emerging from the elements. It can be concluded that viscous effects play an important role in the determination of high-lift flow characteristics.



The above described interactions between the several elements of a low-speed wing require a lot of tuning in the design. This tuning should lead to an optimum configuration of all elements to maximize high-lift performance.



When calculating 3D flow around wings with high-lift systems, more complications are introduced. Local 3D separation regions can adversely affect the performance of the high-lift system. These separation regions can be triggered by wing-fuselage junctions, nacelles, near wing tips and by other irregularities in the wing buildup. It is very difficult to model the complex interactions between flow in boundary layers and wake/vortex interactions (see figure 2.7) occurring on wing in high-lift a configuration.



For simulating 3D boundary layer flows around swept wings in high-lift configuration, determining the type and location of transition is one of the most important goals. When assessing and scaling 3D high-lift system aerodynamics, finding the properties of the flow along the attachment line of the 3D wing, to find out if attachment-line instabilities occur, can be a significant factor [3]. Other types of flow mechanisms that can trigger transition of course also need to be taken into account, for example due to cross flow at swept wings.

Three-dimensional design optimization is mainly focused on minimizing the above described detrimental effects on the aerodynamic characteristics of the high-lift system [19]. For the 3D flow around wings with extended high-lift devices, one of the most important design factors is maintaining spanwise continuity between the devices panels [2]. A spanwise discontinuity reduces lift and increases drag and noise considerably. This is since open ends of the high-lift panels cause unwanted vortices leading to early flow separation³. Engine struts can cause spanwise interruptions in leading edge devices, whereas inboard ailerons and/or thrust gates can cause this for trailing edge devices.

17

³ This is true for wings of transport airplanes having moderate to high aspect ratio's. Vortices on wings with a low aspect ratio however tend to delay flow separation.



Main topological design factors: gap and Fowler motion

Alongside the design of the aerodynamic shape of the main high-lift devices, two topological design factors play an important role in high-lift device design, being 'Fowler motion' and 'gap/overlap'. These will be treated here.

Fowler motion is defined separately for leading and trailing edge devices:

 Using figure 2.8(a), Fowler motion is defined for leading edge devices, more specifically for slats, as:

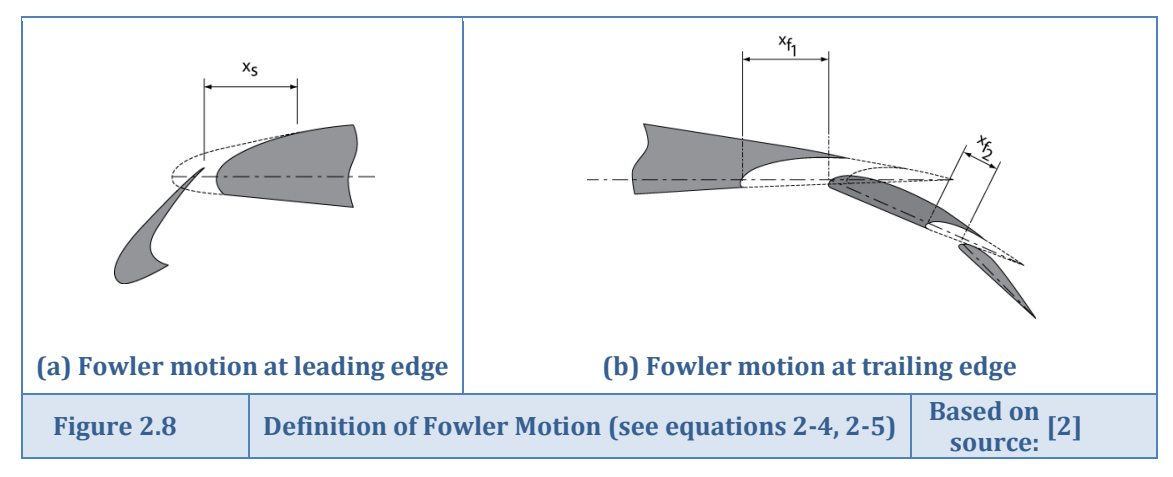
$$FM_{LE} = \frac{x_s}{c_w} \cdot 100\% \tag{2-4}$$

- Using figure 2.8(b), Fowler motion is defined for trailing edge devices as:

$$FM_{TE} = \frac{x_{f_1} + x_{f_2}}{c_w} \cdot 100\% \tag{2-5}$$

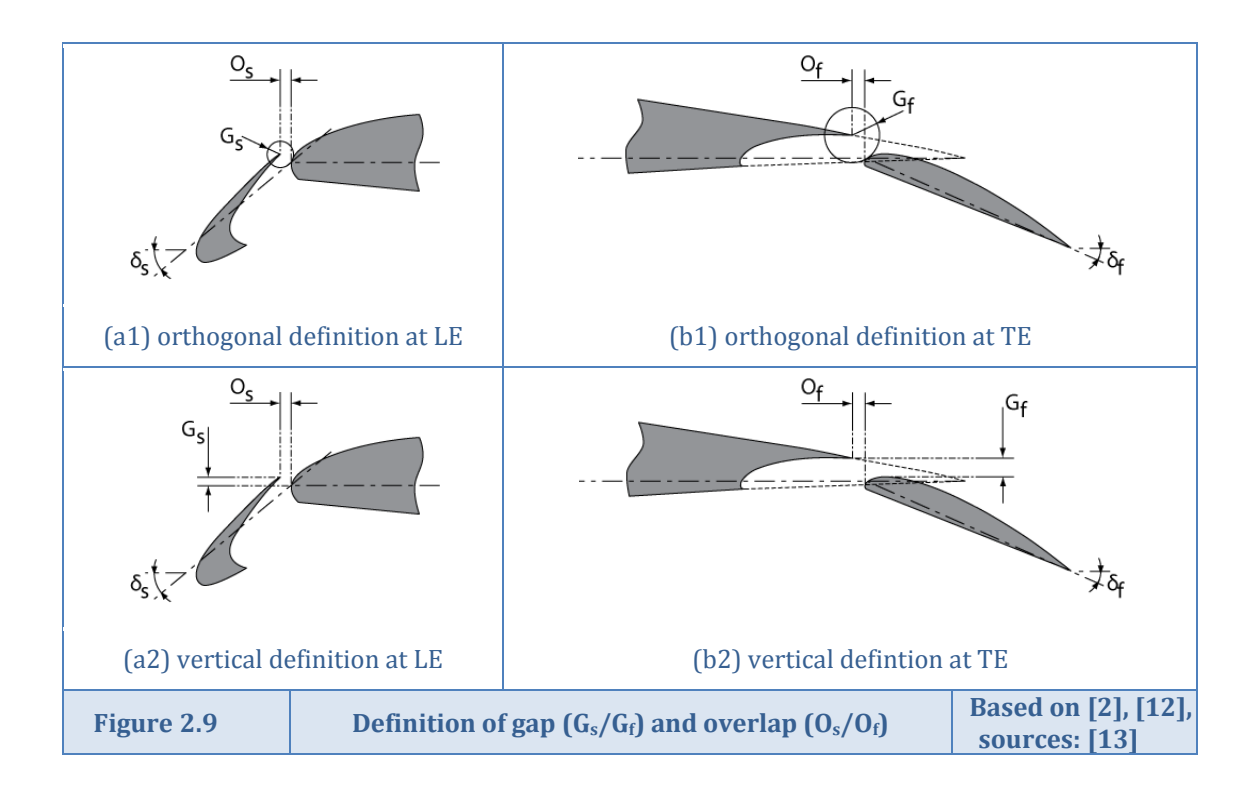
In other words, Fowler motion is defined as the incremental chord percentage due to extension of the device under consideration. When such a device consists of multiple elements, Fowler motion is measured as linear increments in the chord plane of the respective upstream element (see figure 2.8(b)).

For attaining the best L/D ratio at takeoff conditions, large Fowler motion during initial flap deployment is very beneficial. In this way, the lifting capability of the wing is initially increased by mainly increasing the effective wing chord. This comes at a lower drag cost than applying an increase in effective wing camber due to flap rotation. Flap mechanisms should therefore ideally provide large translational motion and low rotation at initial deployment and the opposite at the end of the deployment trajectory. An intermediate flap position can then be used during takeoff, whereas flaps are fully deployed in landing conditions.



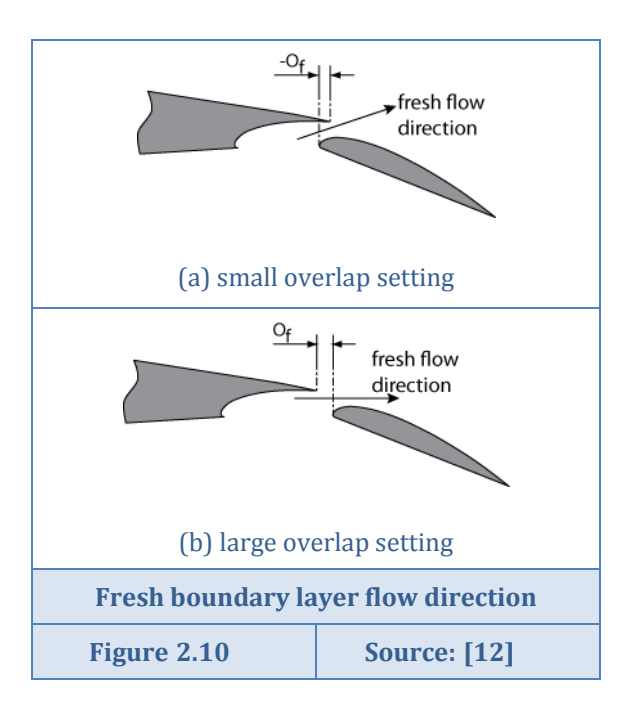
The gap between the high-lift device and its up- or downstream element largely influences the aerodynamic flow around the complete wing setup. The two-dimensional positioning of the high-lift device is defined by the parameters gap and overlap (sometimes called overhang in literature). Two ways of defining these parameters are common: the orthogonal definition depicted in figure 2.9(a1,b1) and the vertical definition depicted in figure 2.9(a2,b2).





To provide some insight of the importance of the gap and overlap in the airfoil topology, a wing-flap combination is considered. The maximum attainable lift coefficient on this geometry is limited by flow separation phenomena at the upper side of the flap. A careful choice of gap and overlap can postpone this limiting flow separation, by introducing a proper fresh boundary layer on the flap. When the gap (G_f in figure 2.9(b1,b2)) is too small, the air between the wing

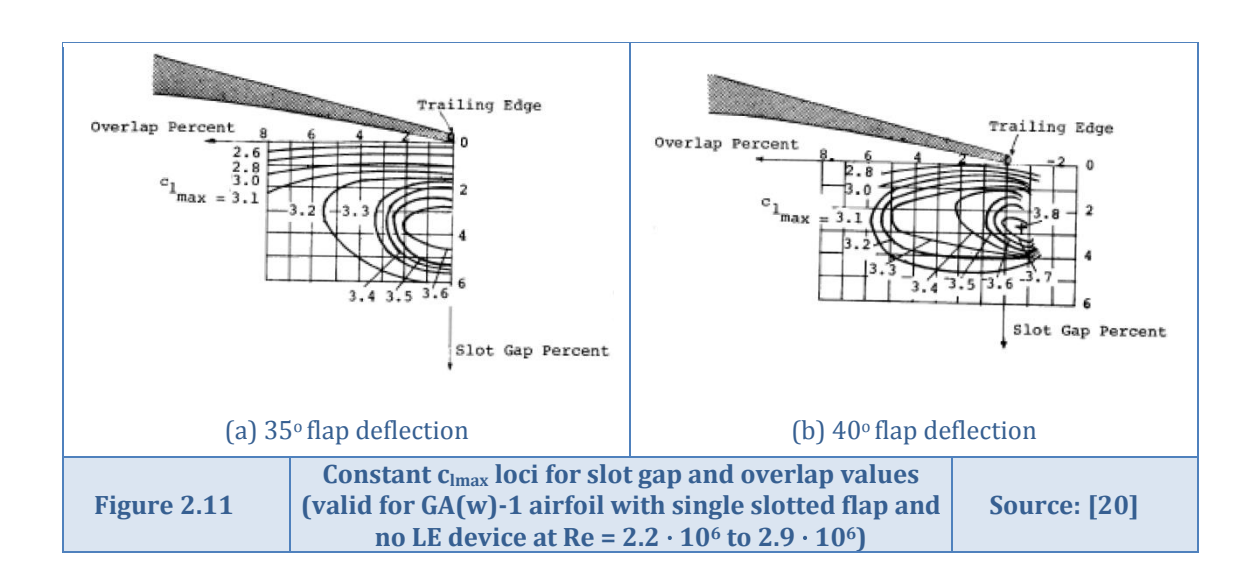
and flap will clog and the volume flow of fresh air will reduce considerably. If, on the contrary, the gap G_f is too large, the acceleration of flow on the upper side of the flap is only marginal, which also leads to early flow separation on the flap. The relative positioning of the flap with respect to the wing is also important, defined by the overlap parameter (O_f in figure 2.9(b1,b2)). Increasing the overlap implicates that the acceleration direction of the fresh flow on the upper side of the flap is tilted more backwards, increasing the accelerative effect on the boundary layer of the flap (see figure 2.10). A too large overlap is however not beneficial, since the kinetic energy of the fresh boundary layer dissipates due to friction along the skin of the flap and the influence is only felt at a small region of the flow field.



The aerodynamic performance of multi-element high-lift devices is very sensitive to small changes in the gap and overlap setting. This is seen in figure 2.11, where the loci of gap and overlap values with constant c_{lmax} value are given. These loci are the result of an optimization of the flap position for the development of a high performance Fowler flap system. Notice the



high maximum lift coefficient of 3.8 that can be achieved for a flap at 40° deflection angle (figure 2.11(b)) with 2.7 % gap and negative overlap of 0.7%. An even more important point to be noted from the figure is the large sensitivity of achievable c_{lmax} value on the flap positioning. The difference in loci between figures 2.11 (a) and (b) further indicates the large sensitivity of optimal flap setting to flap deflection angle. This is the reason why the design of support and actuation systems is a very complicated task: it can considerably influence the achievable lift levels of the complete wing setup. Properly taking the aeroelastic deformation of the wing, high-lift device and support system into account even further complicates this design task.



2.1.4 High-lift system design process

Section Sources: [2], [19], [21], [22], [23]

Historically, the design and analysis of high-lift systems was a very experiment- and time-intensive process. A large amount of physical experiments was required to assess the large complexity of high-lift system design, since flow physics, geometrical considerations and the incorporation of support and actuation systems had to be taken into account simultaneously. In the recent past and current design of high-lift systems, a new trend has occurred: the empirical methods are gradually being superseded by the application of computational methods. The application of computational methods is made possible due to the rapid development in computational hard- and software. It reduces the development time of high-lift systems considerably and opens up possibilities to explore a larger amount of high-lift system setups [2].

The application of computational methods to design high-lift devices also opens up the doors for a more multidisciplinary design approach to be started already in preliminary and conceptual design phases. This may improve the resulting high-lift system design in a considerable way. To show this, first a high-lift design process of the 1990's is considered. Figure 2.13 shows an overview of the Airbus high-lift design process, as described by Flaig and Hilbig in 1992 [19]. In this scheme, it can be seen that during the predevelopment phase, the main focus of the design process is on aerodynamics. Furthermore, the main wing geometry is governed by cruise requirements, largely constraining the design space for high-lift devices. The majority of structural and kinematic design considerations were taken into account not earlier than in the development phase, where a lot of design choices have already been frozen.

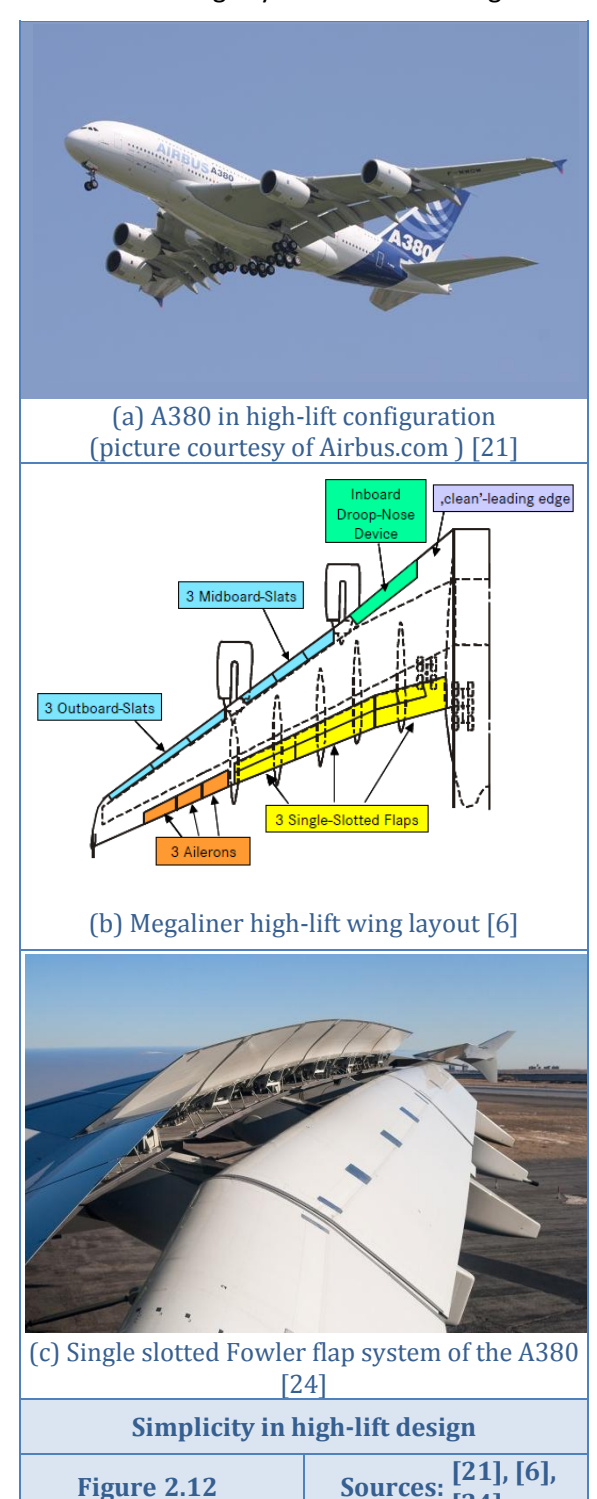


Van Dam [3] indicates the limitations of such a sequential design approach, where after the creation of a high-lift system design with its optimum positions, the aerodynamicists tend to hand everything over to mechanical designers. These designers are in charge of the development of the mechanism that supports and deploys the devices, but are largely limited in design space due to the boundaries set by the aerodynamic design. In the end, this might lead to kinematic systems with inferior performance at a too large system cost and weight.

Among others, van Dam [22] and Reckzeh [23] provide examples of large weight and complexity savings that can be achieved when strong cooperative design efforts between the various disciplines are made, already in the early design stages. Reckzeh describes that the interactions between the high speed cruise wing design team and highlift design team led to the possible application of simple high-lift devices at the newest and largest airplane of Airbus, the A380. The cruise wing design profile shapes were thickened to accommodate a single slotted Fowler flap system with increased thickness influencing the flow quality in slow flight considerably and thereby saving weight and complexity (see figure 2.12). The strong cooperative efforts between various design disciplines are also seen in the schematic sequence of CFD-based high-lift design process, indicated in figure 2.14. This schematic was used to design the high-lift wing for a megaliner aircraft, on which the above described A380's design is based.

It can be concluded that the current high-lift design process has to show strong multidisciplinary design work, which should already be started in the early design phases of a new airplane concept.

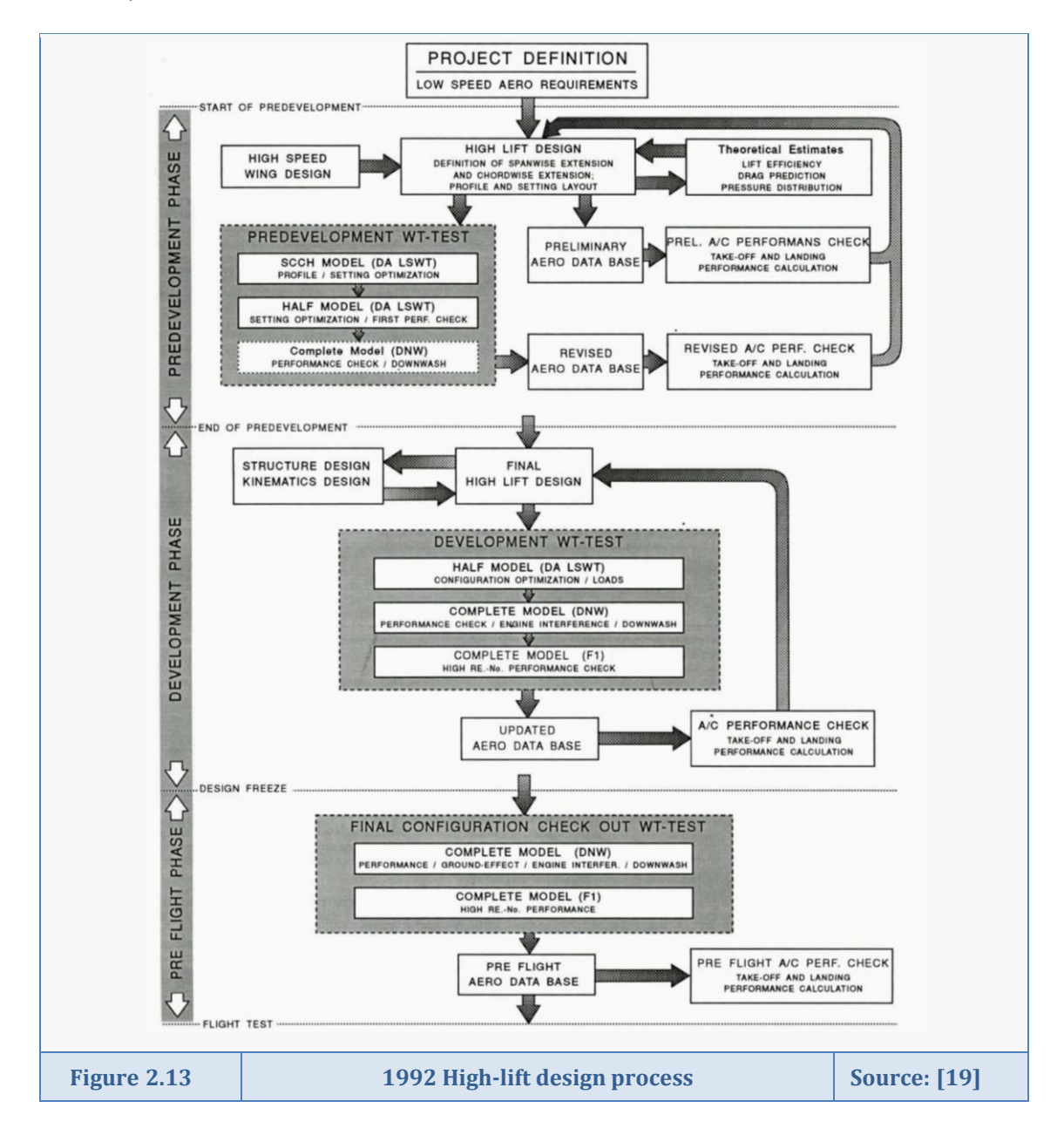
During previous designs of novel complex systems such as airplane high-lift systems, the design team is asked to make important design decisions in the early phases of the design process. These decisions have to be made with little knowledge, reducing the design freedom and considerably affecting committed the costs [25]. Strong multidisciplinary design work in the early design phases of a new concept can introduce the desired change in available knowledge to the earlier design phases, see figure 2.15.



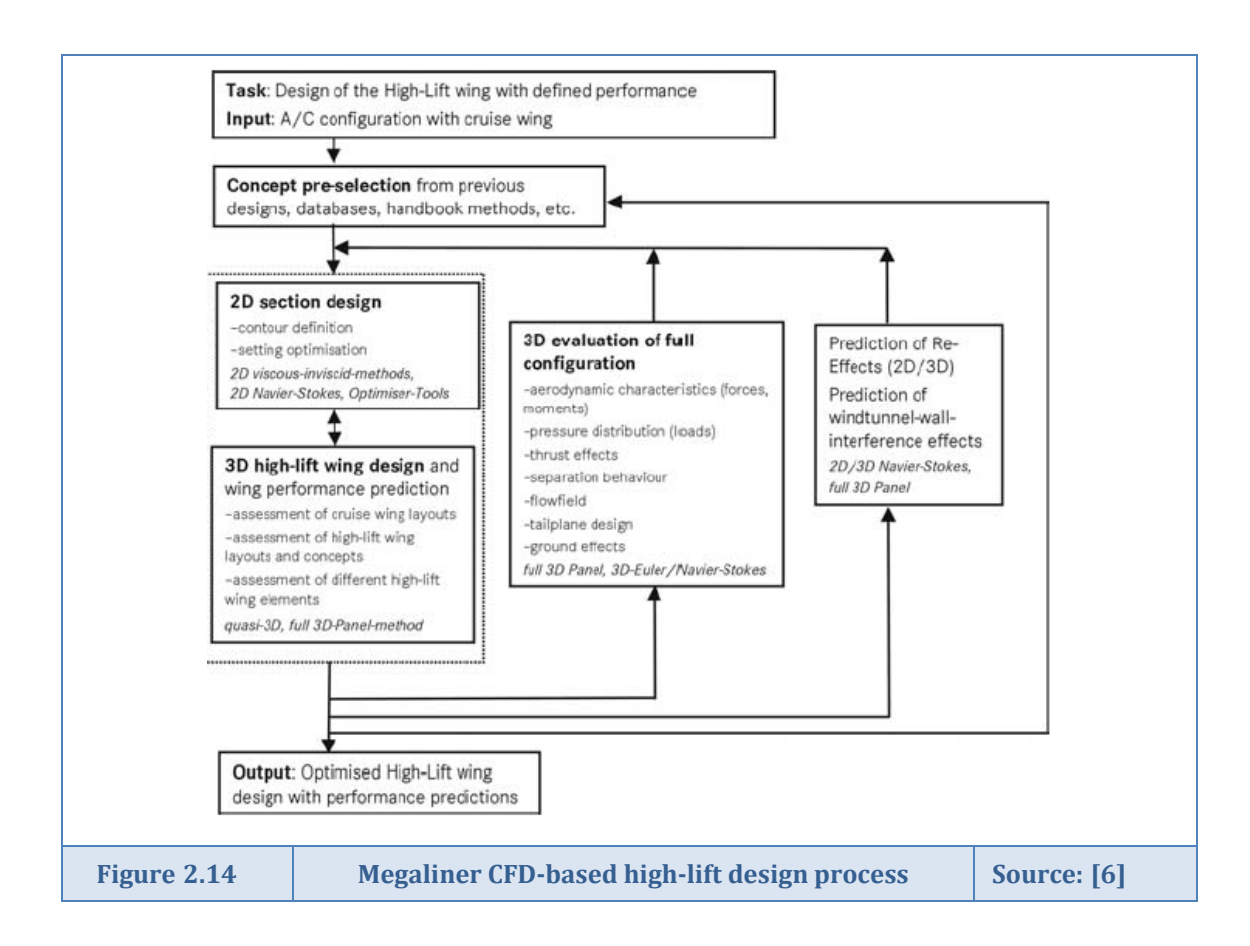


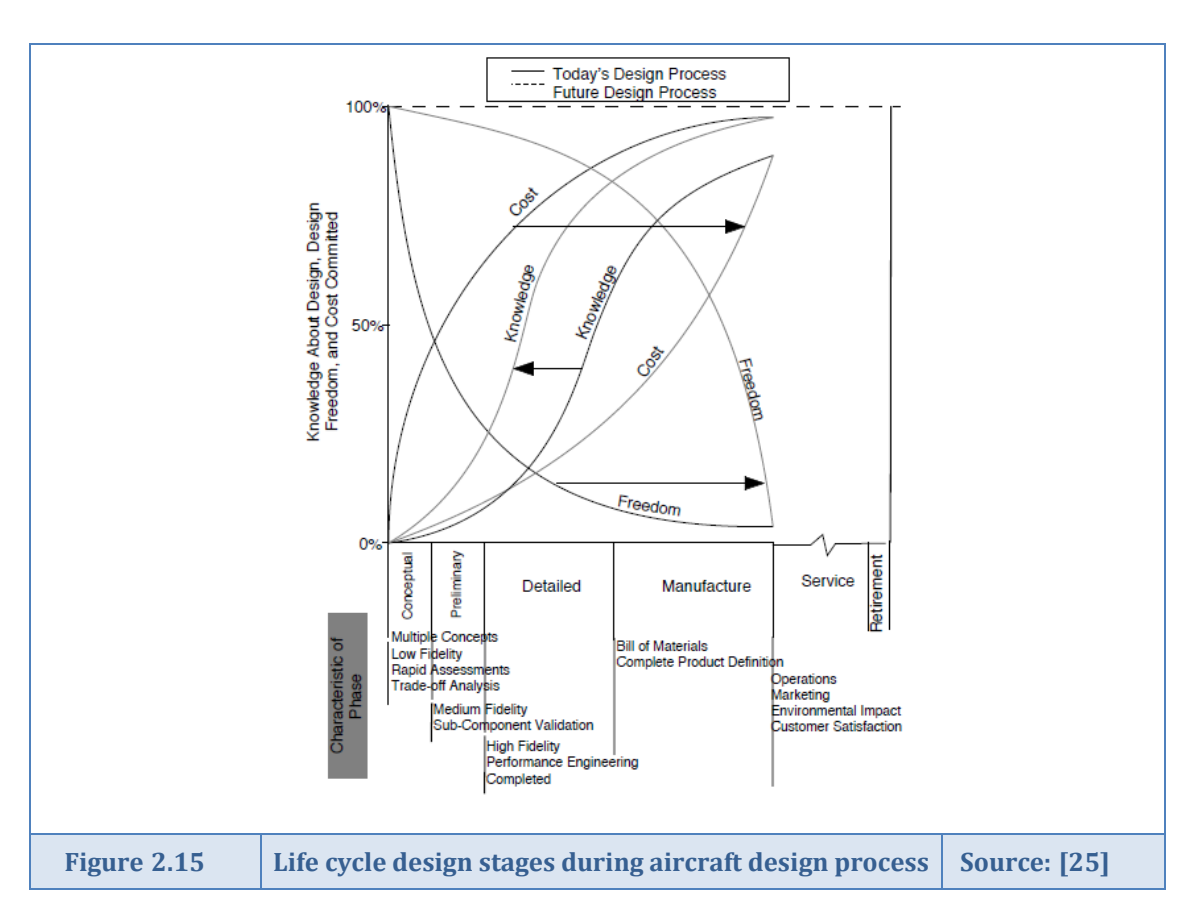
Design of support systems

A good overview of the design considerations of support systems is given by Niu [7]. As explained in section 2.1.3, support systems can substantially influence the topology and thereby the performance of high-lift systems. Figure 2.13 shows that in the former design method of high-lift devices, the kinematics were taken into account after finishing the predevelopment phase. Van Dam [3] indicates that there is still a notable discrepancy in choices for support systems, especially in those that actuate trailing edge devices. These mechanisms however play an important role in the high-lift device optimization process, since they provide critical kinematic constraints. Therefore, as soon as incorporation of these mechanisms in the early design phases of a new airplane concept is possible, this should definitely be done.











2.2 Parametric modelling techniques

The current section starts with a description of the need for parametric modelling techniques in conceptual design. Thereafter the current trends in parametric modelling techniques are indicated by describing a number of techniques available in literature. The section ends with a description of 'ParaMAM', the technique that will be used throughout the project for modelling wings with high-lift devices and their support systems on an advanced conceptual design level.

2.2.1 The need for parametric modelling techniques in early design phases

Section Sources:

[26]

Within conceptual design phase, designers want to be able to assess the advantages and disadvantages of a large number of aircraft concepts. At the end of this design phase it can be decided which aircraft concept best fits the flying mission aimed for. Using flexible parametric design methods, concepts and their derivatives can be compared in a quick and comparable way. After the best concept for the mission is chosen, the preliminary design phase starts, in which a large number of topological setups need to be assessed for all conditions that can be encountered during the intended mission. During this second phase in aircraft design, parametric design tools can be of large help in evaluating the high number of configuration settings. After convergence to a final airplane setup is found, the final setup is to be designed in detail in following phases.

In short: one needs parametric modelling techniques for flexibility and fast modelling purposes during conceptual and preliminary design.

The parameterisation of a high-lift wing can be divided into three parts [26]:

- Outlining parameters are all parameters that can be observed in the planar view of the wing, for example shown in figure 2.12(b). Most important are the spanwise extent of leading and trailing edge devices, local chord length of the devices and the geometry of the fixed main wing.
- Positioning parameters define the deflection of the deployed high-lift devices. These are for example seen in figures 2.8 and 2.9.
- Shape parameters cover the shape of the devices. In general this shape is largely constrained by the clean airfoil/wing designed for efficient cruise conditions.

Beside aerodynamics, discussed in sections 2.1 and 2.3, the most important constraints in high-lift design are imposed by structural design. Constraints are in the form of deformation aspects and boundaries set due to front and rear spar locations. A second part of constraints comes from the kinematics used for deploying the high-lift devices. Currently these are mostly designed for landing configuration, defining the maximum deflections to be generated. Other kinematic settings have to be derived using kinematical laws based upon this design [26]. Using parametric design methods, data exchange possibilities are created between the different disciplines involved in the design.



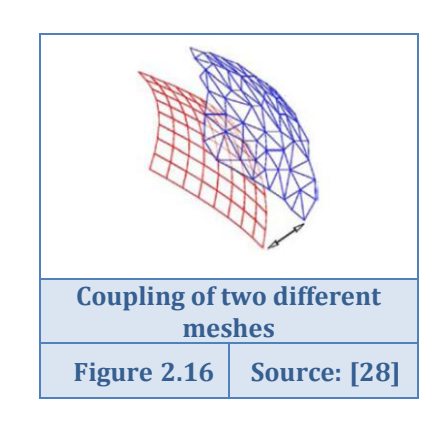
2.2.2 Current trends in the usage of parametric modelling techniques

Section Sources: [27], [28], [29], [30], [31], [32], [33], [34], [35], [36], [37], [38]

The current section will provide a short insight in some current parametric modelling techniques used by aircraft designers/design groups. This is done to put the model generator based on ParaMAM, explained in the subsequent section, in perspective to other methods applied in aerospace industry.

Vehicle parameterization is not a trivial task. The largest difficulties are found in determining the configuration rules as well as in defining suitable shape controlling parameters [27]. Once these parameters are determined, they can be used to express a parameterized vehicle. Creating the parameterization method is often found to be an easier task than defining the shape controlling parameters, properly capturing the design intent.

One of the problems emerging in multidisciplinary geometrical parameterization is the variety in grid requirements. The most prone example is the difference between grids for computational fluid dynamics (CFD) and for computational solid mechanics (CSM) studies. CSM methods generally require a relatively coarse and equally spread grid which must be able to handle very complex internal and external geometric components to retrieve accurate results. CFD grids on the other hand are very fine but only need to model external geometric components. This implies that often difficult interpolation algorithms need to be applied in order to create a coupling between



the different meshes (see figure 2.16). A necessary prerequisite to do this is that both CFD and CSM studies use information based on the same geometrical model.

Kulfan [29], Vandenbrande [27] and Samareh [30] present lists of fundamental and desirable features a parametric geometrical representation technique should have. According to them, the methods should:

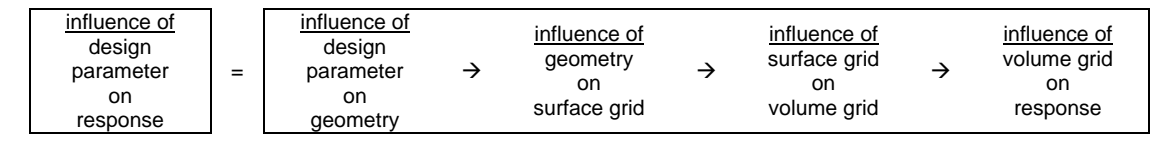
- be well behaved and produce smooth and realistic shapes. Within their specified regions, any combination of parameter values should produce a sensible and realizable configuration. To make sure realistic shapes are created by the modelling technique, explicit shape control is aspired. This ensures no unintended inflection points can be introduced into the design. Controlling the geometric shape using explicit shape control is however a nonlinear and expensive operation.
- be a mathematically efficient, geometrically robust and numerically stable process that is fast, accurate and consistent. When geometric curves do not change due to transformations, they are geometrically robust.
- require a compact and effective set of design variables that represents a large enough design space. Thereby, the choice of variables and parameterization technique has to be such, that it fits into the product development cycle times. Specification of key design parameters is in this sense preferred. Examples of such parameters for airfoil design are: LE radius, boat-tail angle and airfoil closure; for a wing these might be: planform, twist, camber and thickness.
- be easy to control when it comes to editing the shape of a curve. Changing the geometry should be very intuitive to the user. This is achieved by creating a systematic and consistent parameterization method, applicable to all types of geometries.



- support a link to all analysis codes involved in a design approach. Either all different geometrical manifestations should be producible from a single geometry source, or consistent geometry changes should be provided across all disciplines.
- possess the ability to embed engineering knowledge in the script performing the geometry generation. When constraints are directly incorporated in the geometry generation principle, the searching space is reduced and the chance of a successful design is improved by increasing the percentage of design space which contains feasible designs
- *produce designs automatically.* No interactive steps should be involved that are to be executed by the user.
- provide sensitivity derivatives. Especially when gradient-based optimization is aimed for, analytical availability of sensitivity derivatives is required. This is elaborated later in this section
- form a continuous function of the input parameters. Small changes in the design parameter values have to lead to small changes in the values of computed performance characteristics. Values of the aforementioned sensitivity derivatives can provide information on the continuity of the geometrical response to changing input parameters.

In his work performed in 2001, Samareh [30] provides a survey of shape parameterization techniques for multidisciplinary shape optimization. Although focus of the study is assessing the suitability of the available methods for application to complex configurations using high-fidelity analysis tools, it provides a useful insight in available parameterization methods.

One of the assessment criteria used by Samareh is the availability of sensitivity derivatives. Sensitivity is in this sense defined as the 'partial derivative of a response with respect to a design variable'. The availability of sensitivity derivatives forms an essential building block for gradient-based optimization techniques. Although not of interest for the current research, since only a structural sizing routine will be involved, the definition of sensitivity derivatives indicates the possible geometrical difficulties in consistent parametric modelling. The following chain of influence needs to be taken into account in calculating the sensitivity derivatives:



To be able to compare several concepts during a conceptual or preliminary design study, it is necessary to make sure no errors are made due to differences in geometrical modelling. The occurrence of the four separate entries in the aforementioned influence chain indicates the difficulty that might be involved in making sure the assessment is not influenced by the geometrical problem formulation.

Positioned at the end of the current section, table 2.7 lists the considered parameterization techniques, along with a qualitative assessment of their properties. Hereafter, each parameterization technique is first shortly described.

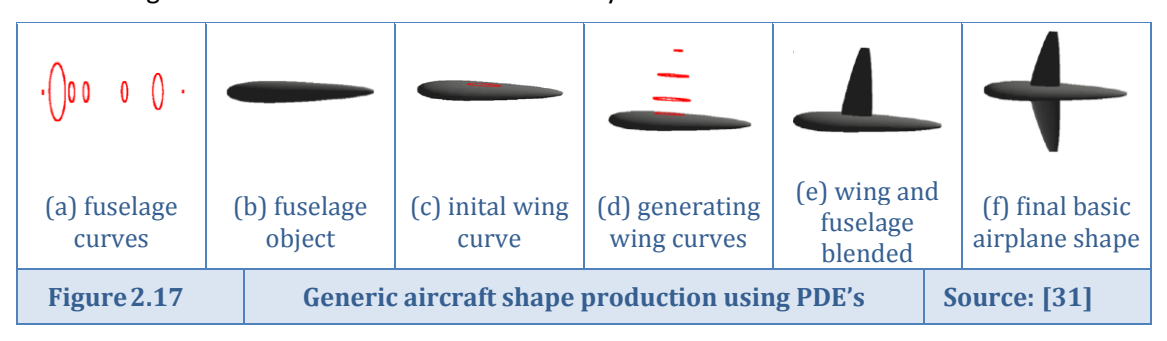
Parameterization methods using basis vectors

Within this parameterization technique, a baseline shape is adjusted by the addition of a combination of predefined basis vectors which are based on several proposed shapes. The proposed shapes must share same grid topology for the method to work. Since only the changes in shape are parameterized, a compact set of design variables can be provided. A big disadvantage of the basis vector approach is however the required generation of consistent design vectors which are valid across all disciplines.



Parameterization methods using partial differential equations

Within this method, surface generation is considered as a boundary value problem. Surfaces are produced as the solution of elliptic partial differential equations (PDE's). This leads to a small set of design variables, implying a significant reduction in computational cost associated with designing and optimising either given airplanes or specific components such as wings. A disadvantage of PDE's is found in that it is not very intuitive to use.



Athanasopoulos et al. [31] created a parametric design method based on PDE's. In their method, each surface is generated by a number of curves that represent the character lines of a given part of the aircraft shape. Other surfaces then blend to create the full shape of the airplane as shown in figure 2.17. The shapes are defined through boundary conditions and a small set of design parameters. These design parameters are associated with the curves defining the surfaces. In the software of Athanasopoulos, a user interface had to be created for users to be able to modify the aircraft without having any knowledge of the mathematical theory behind the PDE methods applied.

Discrete parameterization methods

Within discrete parameterization methods, the coordinates of grid points are used as design variables. These methods are relatively easy to implement and allow all kinds of geometry changes. Having such a large amount of local design variables can however introduce problems in maintaining a smooth geometry. Furthermore, sizing or optimization requiring additional constraints to avoid unrealistic geometries may be impractical to set-up. The large amount of design variables may lead to high demands on computational power and difficult solver setup. Another large difficulty is found in the usage of grid points as design variables. Since for each incorporated design discipline individual grids are parameterized, consistent shape parameterization across multiple disciplines cannot be guaranteed. The ability to use existing disciplinary grids is the most attractive feature of the discrete parameterization method. When optimization or sizing is aimed for, no separate grid generation processes have to be incorporated. The process is only slightly dependent on model complexity and local control on shape changes is easily possible.

The parametric simple and fast mesh based aircraft modelling tool ParaMAM, serving as a basis for the wing model generator in this master thesis is an example of a discrete parameterization method. It will be discussed in more detail in section 2.2.3.

Parameterization methods using domain elements

This parameterization technique, grid points are linked to a macro element that controls the shape of the model. Model movement is based on inverse mapping between gird points and the defined domain element: if the nodes of the domain element move, the grid points belonging to the domain move as well. The method is considered very efficient and is relatively easy to implement. Grid automatically moves along with the domain elements, due to which it



forms a consistent shape parameterization method across all disciplines within a multidisciplinary application.

Polynomial and spline parameterization methods

Within this parameterization category, three sub methods are discussed: geometrical representation using polynomials, using Bezier representation and finally, using B-spline methods.

Since polynomials can describe a curve in a very compact form, the total number of design variables can be significantly reduced. Disadvantages are however that the coefficient vectors of the polynomial weighing factors convey very little insight about the geometrical shape. When applying a polynomial parameterization method having a power basis form, round off errors might pose problems. For simple curves however, it is a powerful and compact representation method.

Bezier representation methods provide a far better representation method than the above described power-based polynomials. Round off errors are minimized due to the usage of Bernstein polynomials as a basis. Furthermore, control points are more closely related to the curve position, increasing the geometric insight conveyed by the control point vectors. Sensitivity derivatives stay constant during optimization process, lowering demands computational power. Problems arise when trying to represent complex curves using higher-degree Bezier forms, since the round off error increases and calculation of coefficient vectors becomes inefficient.

An improvement over the aforementioned Bezier representations is created by combining several low-degree Bezier segments to cover complex geometrical curves. This so-called B-spline method can give efficient and accurate representations of complex curves. Again, sensitivity derivatives stay constant during shape changes, making the method very attractive for sizing and optimization processes. For regular B-spline methods, the only drawback is the inability to accurately create representations of conic sections. A special form of the B-spline representation overcomes this problem: non uniform rational B-spline (NURBS). NURBS can be used to represent cylinders and cones, as well as free-form geometry in a very efficient way, and is therefore widely used in CAD software packages.

Polynomial and spline techniques are very well suited for both two- and three-dimensional model representations. When three-dimensional models are complex, a large number of curves might be required for proper model representation. This makes the techniques difficult to apply without usage of a sophisticated CAD system. Another factor to keep in mind is that irregular or wavy geometry might be the result of a sizing or optimization process applied to complex models.

Examples of Bezier-polynomial parameterization methods are the class shape transformation (CST) method of Kulfan [29] and its expansion by using B-spline based refinement functions created by Straathof [32].

Commercial CAD-based parameterization methods

Development time can be saved by using commercial CAD packages for geometry modelling. Most of these CAD systems however use faceted boundary representations or constructive solid geometry methods to represent physical objects, methods that are very difficult to parameterize. Grid generation for CFD and CSM usage can thereby require long computational times. A solution for this problem might be the usage of Feature-based solid modelling (FBSM) CAD systems, since these are capable of creating dimension-driven objects. The driving dimensions are then automatically capturing the design intent of the model creator and allows



for incorporation as variable in design environments. However, sensitivity derivatives cannot be obtained without large efforts, posing a large drawback of optimization using CAD methods.

Ledermann [28] presents an associative parametric computer aided engineering method applicable to aircraft preliminary design. For the main model CATIA V5 is used; allowing parameterized geometries, associating different components and building hierarchical assemblies making up the complete aircraft model. Several parametric CAD representations of involved geometrical parts of increasing fidelity are created. Since the labour of creating the generic geometry increases with the number of parameters involved in the model, the user has to select the most appropriate geometrical representation based on a trade off between modelling efficiency and flexibility. The created knowledge-based geometry can serve as a basis for all disciplines involved in a design cycle. A large advantage for usage of CAD based methods in airplane design is that mass derivations are very straightforward.

Parameterization methods based on an analytical approach

The analytical approach provides a compact formulation for airfoil section parameterizations. In order to create a new shape, analytical shape functions based on a set of previous airfoil designs are linearly added to a known baseline shape. In most literature, Hicks-Henne shape functions are used, created by Hicks and Henne in 1978. The weight of the added shape functions are then the design parameters. The method is very effective for airfoil parameterization.

In a comparison study of geometric airfoil representations, Wu et al. [33] conclude that Hicks-Henne shape function method reaches optimum designs much faster than discrete methods, although at a lower accuracy. This directly indicates the largest advantage of analytical methods: sizing and optimization require relatively low computational power.

Parameterization methods using free-form deformation algorithms

The free-form deformation (FFD) algorithm is a subset of soft object animation (SOA) algorithms used in computer graphics methods. In these graphics methods, SOA algorithms are used for morphing and deforming three-dimensional models. Since the FFD formulation is independent of grid topology and consists of a reduced number of design variables, it can serve as a basis for efficient shape parameterization techniques. From the FFD-based geometrical models, a wide variety of both low and high-fidelity analysis tools can be controlled. Analytical sensitivity derivatives are available if gradient based optimization is wanted. A large disadvantage is that design variables in the FFD description have no physical significance, making it difficult to interpret these.

In the MASSOUD (multidisciplinary aerodynamic structural shape optimization using deformation) method of Samareh [34], the deformation of the shapes is parameterized rather than the shape itself. This idea is based on the notion that optimization of an airplane surface such as a wing starts with an existing wing design, and geometry changes are often very small. SOA algorithms are used for shape parameterization and deformation is related to aerodynamic shape design variables such as thickness, camber, twist, and wing planform. The method of Samareh is not applicable to the present design work, in that it does not focus on the detailed optimization of a wing, but on exploring several topologically different concepts and obtaining the corresponding sensitivities on airplane weight.

L: low, M: medium, H: high



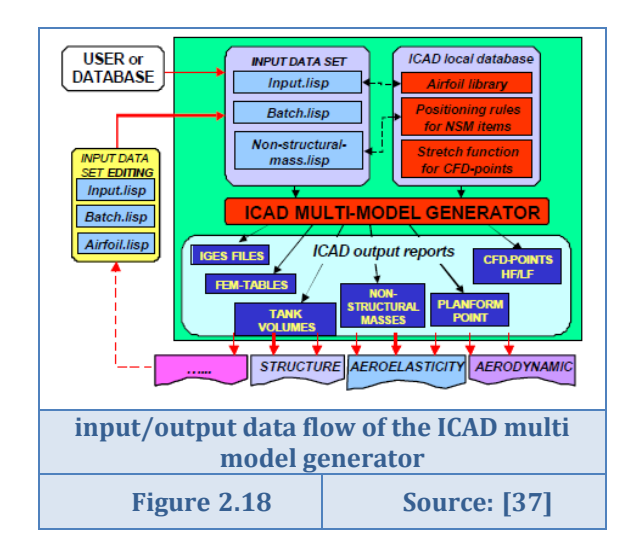
Table 2.7 Multid		Multidis	sciplinary shape parameterization approaches						Main Source: [30]	
Method	indicative figure		parameterizing capabilities ^{(*), 4}	consistent across disciplines	reverse engineering req'd	automatic grid generation req'd	possibility of large geometrical changes	sensitivity derivatives available	level of complexity for geometry changes ^(**)	source / example
basis vectors	1 state of the sta		G	N	N	N	N	Y	L	[29]
domain elements			G	Y	N	N	N	Y	L	[30]
partial differential equations			S	Y	Y	Y	Y	Y	М	[31]
discrete	<u></u>	and the second s	G	N	N	N	N	Y	L	[30], [35]
polynomial and spline	0		S	Y	Y	Y	Y	Y	М	[30], [29], [32]
CAD-based	<u> </u>		S	Y	Y	Y	Y	N	Н	[28]
analytical	10 0 0 0 0 0 0 0 0 0 0 0 0 0 0 0 0 0 0	1 1 1 1 1 1 1 1 1 1 1 1 1 1 1 1 1 1 1	G/S	Y	N	N	N	Y	L	[33]
free-form deformation (FFD)			G/S	Y	N	N	N	Y	М	[36], [34]
G: disciplinary grid parameterization, S: surface parameterization (from which the disciplinary grids can be calculated)										

As already mentioned, the parameterization method used in this thesis is based on a discrete geometrical representation method. As can be seen from table 2.7, the largest threat in using this method is consistency problems across multiple disciplines. Since a coupling between aerodynamic and structural analysis modules will be created, this parameterization problem requires extra attention.

Two more aircraft geometrical representation methods will be discussed: the multi model generator of the TU Delft [37] and the preliminary aircraft design tool PrADO of the German

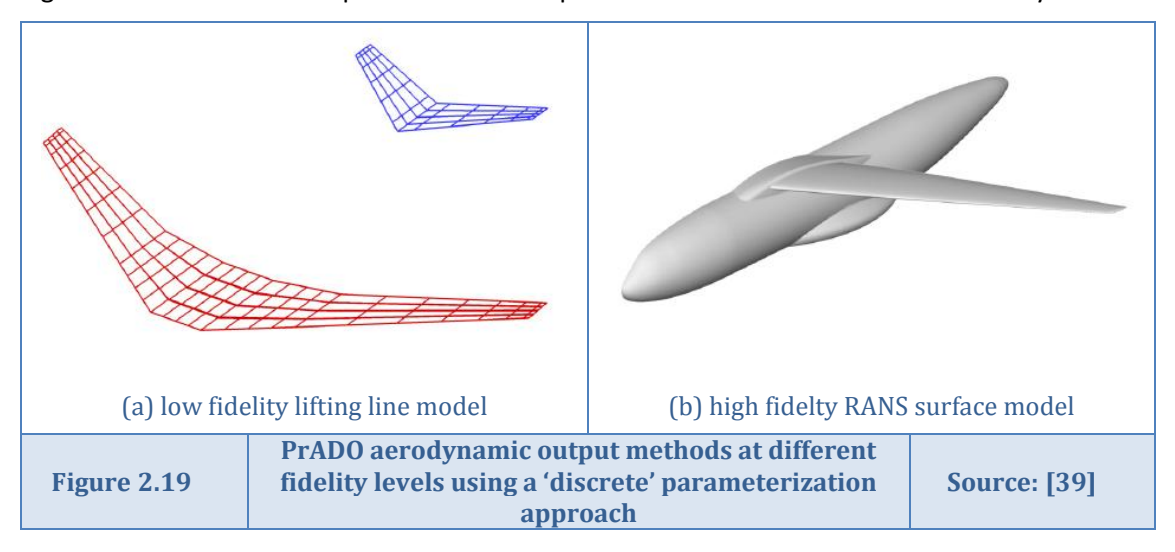
⁴ Parameterizing the grid has as advantage that the grid topology stays fixed throughout a sizing or optimization session. Existing grids can thereby be used for optimization. Disadvantage is that large shape changes could produce unacceptable grids. The advantage of geometry parameterization is that only one representation needs to be parameterized. However, automatic grid generation tools are required in optimization sessions, which are not always available and require extra calculation time





Aerospace Centre [38]. Both methods cannot be assigned to a single parametric method, since they allow geometrical model output multiple using parameterization techniques. Both methods parameterize the surface of the aircraft geometries and serve as a knowledge base for generation of consistent models of different levels of fidelity which are suitable for various disciplines involved in a design effort. As can be seen from figure 2.18, the multi model generator can generate several output reports. Among others, IGES and cloud of points output is supported. IGES is NURBS-based and thereby falls in the

parameterization category 'polynomial and spline', whereas point cloud output falls in the 'discrete' parameterization category. Another parameterization technique incorporated in the multi model generator is related to the 'domain elements' method. Grouped surface patches of for example wing models can be assigned the same design variable, such that the complete group will be sized with the same thickness when subjected to a sizing routine. PrADO is the German Aerospace Centre's preliminary aircraft design and optimization tool. It applies a multidisciplinary integrated iterative design process and can, just as the multi-model generator, provide airplane model descriptions using multiple parametric description methods. Figure 2.19 shows an example of discrete output methods at different levels of fidelity.





2.2.3 Parametric wing modelling using ParaMAM

Section Sources: [35], [40]

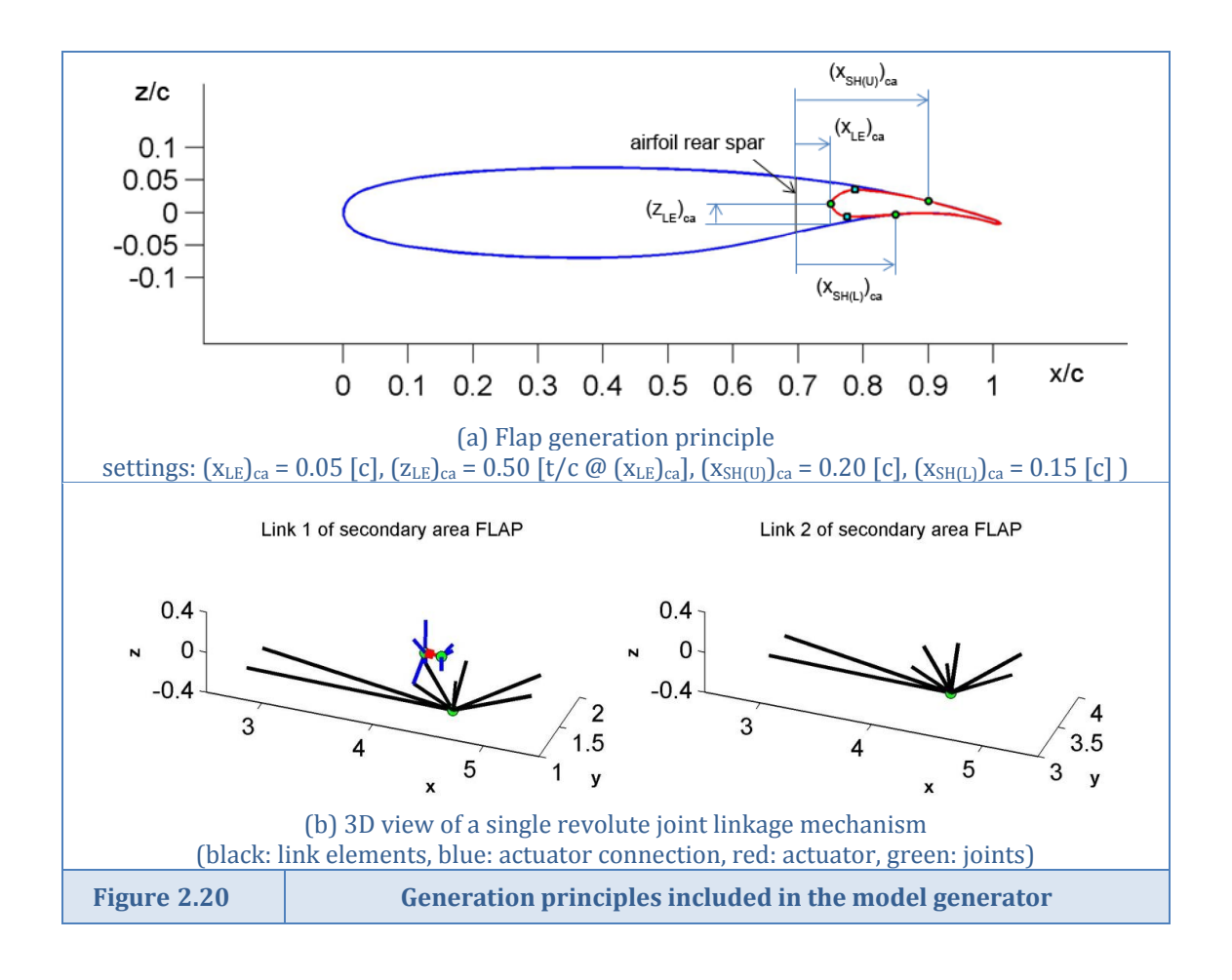
In the current section, the wing model generator using the MatLab based software package 'ParaMAM' will be shortly described. The model generator can be used to generate models containing high-lift devices positioned at the trailing edge of the wing. Furthermore, support systems and simple actuators for deployment are included. For an elaborate overview of the working principles of the model generator, the reader is referred to [1].

ParaMAM stands for 'Parametric simple and fast Mesh based Aircraft Modelling tool', and serves as a structural modelling tool which generates input decks for finite element analysis (FEA) software. Within the package, a sophisticated interpolation algorithm for interpolating data between different mesh representations of the wing model is used. This so-called 'gridapprox'-routine is based on advanced branch and bound searching strategies well-known from ray tracing principles used in photorealistic rendering software. Besides its usage in the model generator, it can serve as a tool for interpolating loads from aerodynamic to structural grids later on in this thesis. An extensive description of the working principles of ParaMAM is given by Nagel in [35], the principles behind gridapprox are explained by Rose in [40].

During the preceding internship at the institute of air transportation systems of the German Aerospace Centre, a wing model generator extension to ParaMAM was created for two reasons. First, the routine could be used to generate arbitrary wing shapes instead of being dependent on known aerodynamic grids. Second, the ability to include high-lift devices in the wing representation was added. The obtained geometrical wing representation can replace the expensive generation of CAD drawings, this is especially beneficial in early and intermediate design stages of the aircraft design process. The obtained wing model can include multiple section distributions, sweep, taper, twist and dihedral, as well as centre wing box extensions and rib/spar distributions in arbitrary directions. Emphasis was put on structuring and logically building-up the input files for the model generator, so that the user can focus on the design problem instead of spending hours in setting-up the wing geometry. Furthermore, the generator contains routines checking both completeness and, at important parts, correctness of the user input.

Trailing edge high-lift devices are 'cut-out' from the wing using a procedure based on the design of movables during actual wing design processes. The outer shape of the wing, designed for optimal cruise conditions, implicates the shape of flaps is predefined from the shroud points onwards to the trailing edge of the wing. As a first approximation, an interpolating polynomial is used to define the nose shape of the trailing edge device. The user has to only input the shroud points and leading edge position of the device, as depicted in figure 2.20(a). In later stages of the design, the nose shape of the flap can be readjusted to cope with aerodynamics of the high-lift device in its deployed position. Another user option, more applicable to later stages in the design, is to provide an actual flap geometry file defining the cut-out. Using the described method, single-, double- or even triple-slotted flaps, as well as ailerons can be generated.

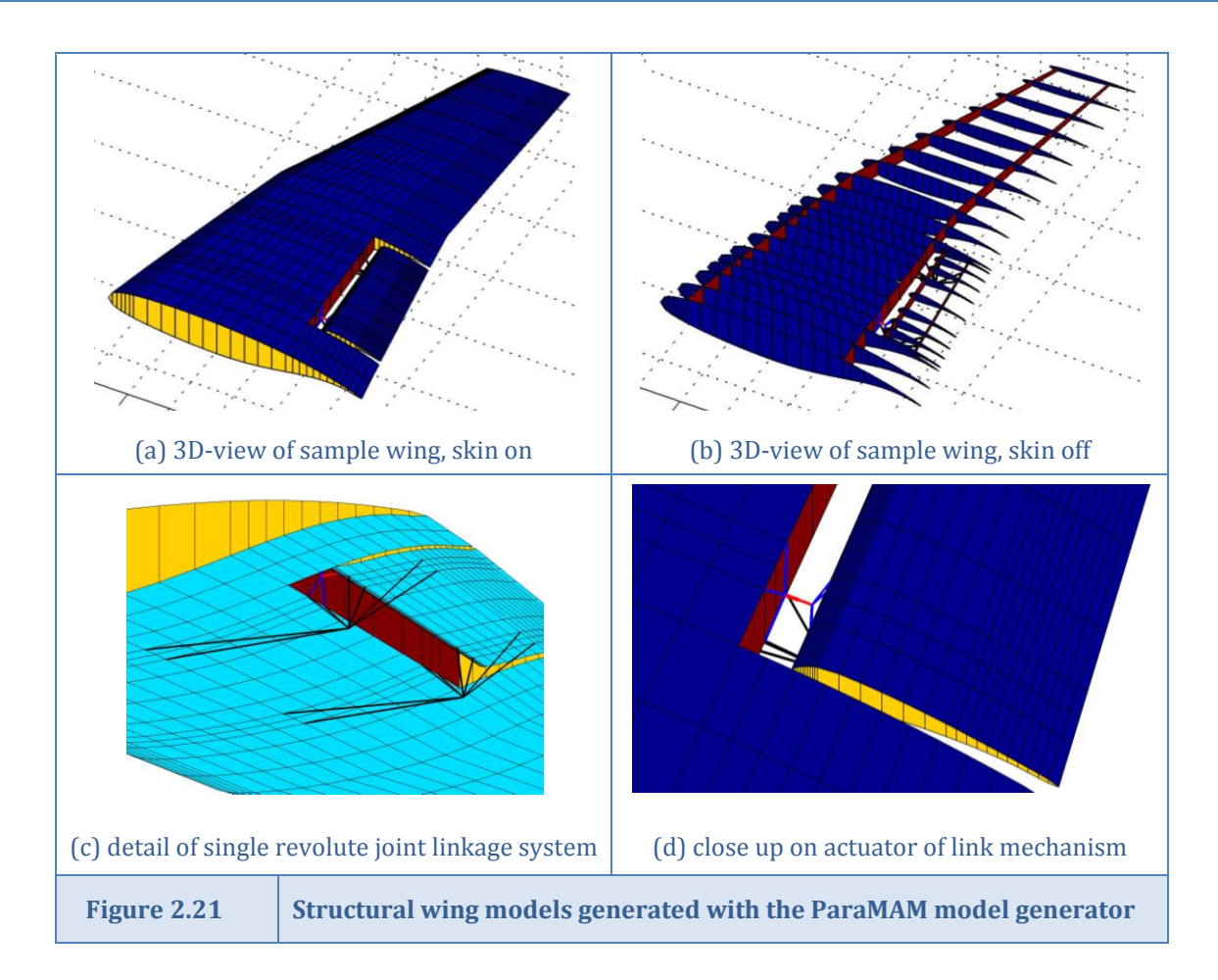




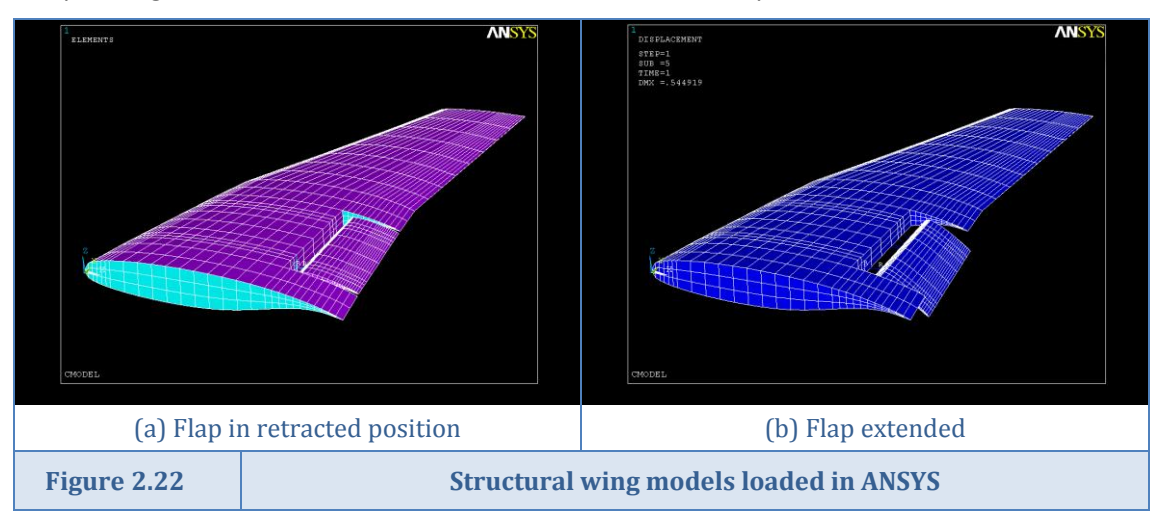
Within the current version of the model generator, a simple link model representing the earliest of link types used in commercial aircraft is pre-programmed: a single revolute joint link mechanism. This link mechanism serves as a basis for the generation of more linkage types in the future and serves at this moment as an initial flexible connection possibility between the main wing and flap system. Since the linkages are currently only designed to create a physical connection between the separate areas within the structural model, it is suggested to exclude these from aerodynamic calculations in the initial design of the modules in this thesis. Figure 2.20(b) shows a three-dimensional view of the discussed linkage system. Extension to create fairings around the linkages and/or create linkages including sliding mechanisms for guiding rails have shown to be possible, but proper inclusion of these remains a challenge for the future.

In figure 2.21(a-d) visual outputs generated by the described structural model generator are presented. As can be seen, all relevant geometrical wing properties can be incorporated in the model: a kink is present at half-span, airfoil definitions change along the span and washout and dihedral are applied. Finally, the wing model includes a single slotted flap system, linked to the main wing via a simplified linkage system. The model generator provides direct input datadecks for usage in the finite element analysis software ANSYS and currently a connection with aerodynamic vortex-lattice method AVL is being created.





Combined usage of multibody dynamics and structural analysis is possible using the multiphysics software package of ANSYS. The multiphysics package allows removal of software specifically needed for representing the kinematics of wings incorporating high-lift devices, reducing both modelling complexity and requirements on calculation time. The model generator incorporates a routine that writes batch input command listings for ANSYS in its specific parametric design language called 'APDL'. After loading the model in ANSYS, movables can be extended or retracted and loads can be added for structural calculations. Extension of the movables is done by prescribing a stroke to the linear actuator. Figure 2.22(a-b) show the sample wing loaded in ANSYS, with retracted and extended flap.





2.3 Aerodynamic calculation methods in wing conceptual design

The current section provides an overview of possible aerodynamic calculation methods that can be applied in conceptual design of airplane wings. Comments are provided on the applicability of the methods, including applicability to wings including a high-lift system. After stating the requirements on aerodynamic tools in conceptual design, an overview of the methods is given. A subdivision is made in: empirical methods, 2D methods, 3D methods and quasi-3D methods. The last section elaborates in further detail on wing modelling by using a vortex-lattice method.

2.3.1 Requirements on aerodynamic tools in conceptual design

Section Sources:

[3], [6], [41], [42]

Since designers want to explore a large number of high-lift wing concepts and variations during the conceptual design phase of an aircraft, one of the most fundamental requirements on aerodynamic tools is computing speed. When a lot of concepts can be evaluated using theoretical tools, the following detailed aircraft design phase can be started using an already pre-optimized design. This reduces the expenses in testing and allows a more targeted optimisation procedure [6].

As already stated in section 2.1, the flow around high-lift systems is governed by inviscid⁵ as well as viscous effects. When assuming inviscid flow, the equations governing the fluid flow can be simplified by removing viscosity and heat conduction terms. This simplifying step reduces the computational cost of a flow simulation considerably, since the system of equations to be solved is much simpler. Assumptions like these however come at the expense of losing fidelity in the obtained flow solution. The large difference in viscous and inviscid flow solutions can be seen in figure 2.23(a), where calculated inviscid and viscous pressure distribution of a single element airfoil is compared to experiments. As can be seen, the inviscid calculation highly overestimates the lift generated by this section. For multiple segment sections, where viscous effects play an even larger role than for single element sections, this can have large consequences for wing design. A very illustrative example is provided by [3], in which inviscid flow solutions are compared to real-life wind tunnel data for a slotted twoelement airfoil optimum gap determination. Inviscid flow calculations indicate an ever increasing lift coefficient for decreasing gap size (see figure 2.23(b)). However, confluence of main element wake and flap boundary layer largely reduces the lift coefficient for gap sizes smaller than 0.2 [%chord] in real flow, as is indicated by the wind tunnel measurements. The lift loss at gap sizes larger than 0.2 [%chord] can be attributed to boundary layer development along the main and flap elements. The example shows that both viscous and inviscid effects should be taken into account when calculating the flow around high-lift systems.

35

⁵ Inviscid flow: theoretical flow which is assumed to have no friction, thermal conduction or diffusion. Theoretically this flow is approached in the limit as the Reynolds number (ratio of inertial forces to viscous forces within a flow) goes to infinity.



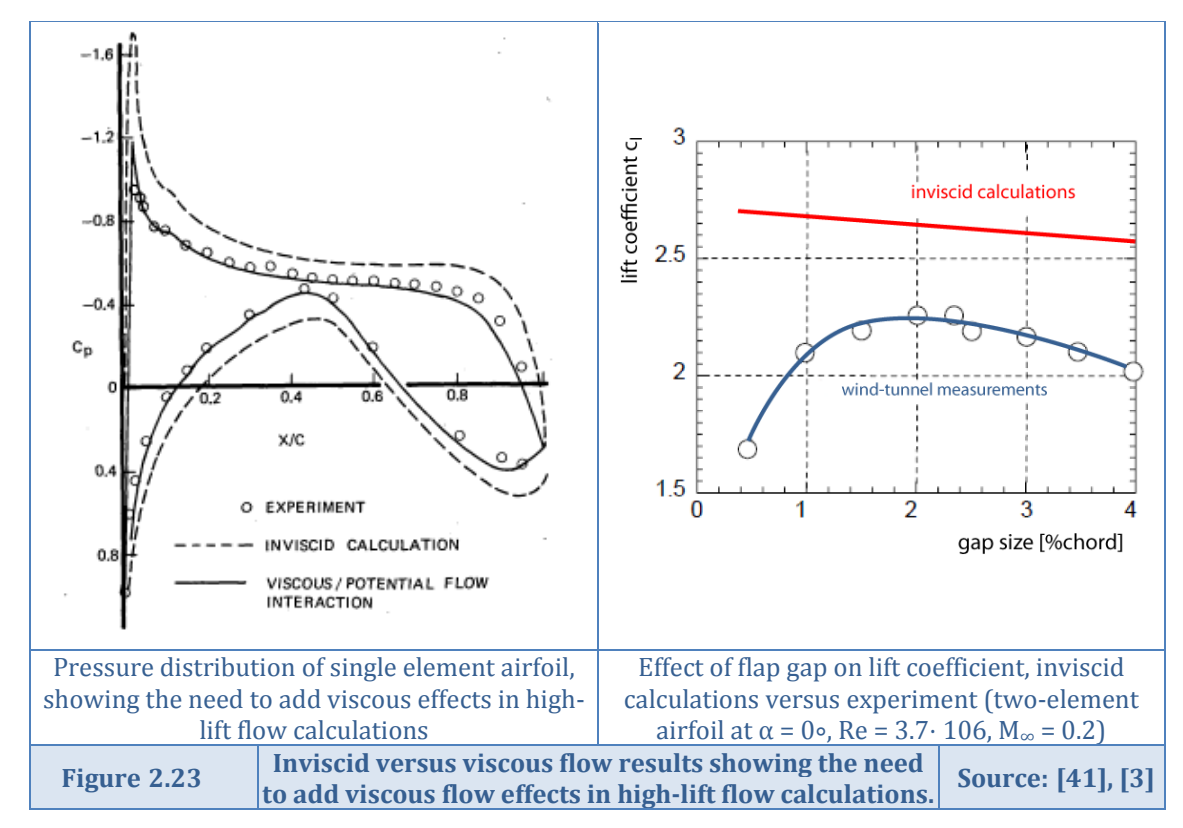


Table 2.8 gives a short overview of the demands on aerodynamic design tools within the three main design levels distinguished in aircraft design. It can be seen that the requirements on accuracy within the preliminary design phase are quite loose when compared to those of the detailed design phase. It is this preliminary design phase for which the mass sensitivity analysis is investigated during the thesis research.

Table 2.8	Low speed ae	Source: [42]					
Design level	Accuracy	Accuracy required		Cost	Method ^(**)		
conceptual	approximate	10% - 20%	negligible	negligible	handbook and calculator		
preliminary	good	5% - 10%	rapid	low	semi empirical		
detailed (project group)	high	2% - 5%	reasonable	moderate	full analysis and design (viscous 2D, inviscid 3D)		
note that this overview stems from a paper made in 1984 within current design principles, the increase in available computer power creates the possibility of performing aerodynamic analyses already in early design, phases							

Since a large amount of high-lift configurations need to be assessed during preliminary and conceptual design phases, it is concluded that the main requirement on aerodynamic tools for design of high-lift systems in the conceptual design phase is: *finding a flow solution taking both inviscid and (simplified) viscous flow phenomena into account with as little computational power requirements as possible*.

The above describes the general crux of computational fluid dynamics, for each design phase one has to find the right balance between solution accuracy and computational requirements. The following section will provide an overview of the available aerodynamic methods that can be applied in aerodynamic design, along with their computational requirements, accuracy and some other advantages and disadvantages. These methods are summarized in table 2.9, along



with a qualitative assessment of their main properties. Taking the requirements described above into account, it can be concluded that quasi-3D methods seem the most appropriate choice for the design level aimed for in this thesis work. Since two-dimensional viscous section data is not available to the writer, a quasi-3D method where inviscid three-dimensional calculations are combined with either empirical two-dimensional data or a two-dimensional panel+IBL method seems the most appropriate aerodynamic approach. For a description of the methods, the reader is referred to the next section.

T-1-1- 2 0	01:4-4:		
Table 2.9	Qualitative overviev	v of aerodynamic design	methods for high-lift systems

Table 2.5 Qualitative overview of aerodynamic design methods for high-intesystems								i iiic systems
Туре	Method	coding easiness	Program size	computa- tional speed	accu- racy	gap handling	design phase applica -bility ⁽¹⁾	comments
2D	empirical	very easy	very compact	very fast	very poor	possible	С	no geometry coding required
	inviscid panel	easy	compact	fast	very poor	unknown	С	no viscosity or compressibility
	panel + IBL ^(*) interaction	poor	extensive	average	very good	good	C/P	problems with robustness of calculations involving wakes, confluence and separation
	Euler ^(**)	poor	extensive	slow	poor	not possible	N/A	barely used for high-lift design due to absence of viscosity [43]
	RANS ^(***)	very poor	very extensive	very slow	excel- lent	excel- lent	D	more robust than panel + IBL methods, but often less accurate
	empirical	very easy	very compact	very fast	very poor	possible	С	no geometry coding required
3D	inviscid panel	average	compact	fast	very poor	unknown	С	no viscosity or compressibility
	panel + IBL ^(*)	poor	extensive	slow	very good	good	C/P	difficult step from 2D to 3D coding
	Euler ^(**)	poor	extensive	slow	poor	poor	N/A	barely used for high-lift design due to absence of viscosity
	RANS ^(***)	very poor	very extensive	very slow	excel- lent	excel- lent	D	fluid mesh creation required (time consuming)
quasi - -3D	3D inviscid panel + 2D empirical	average	average	fast	poor	unknown	C/P	least degree of geometrical flexibility
	3D inviscid panel + 2D experiments	poor	average	average	very good	good	C/P	experimental (wind tunnel) test data must be available
	3D inviscid panel + (2D panel + IBL)	poor	extensive	slow	very good	good	Р	very promising results due to incorporation of viscous effects
	3D inviscid panel + 2D RANS	very poor	very extensive	very slow	excel- lent	good	Р	RANS pre- calculations are time-consuming
(1)	0 () ()	D 0 1	The second second	D 1 4 11 1 1				

C: conceptual design, P: preliminary design, D: detailed design

^(*) IBL: Integral Boundary Layer method, used to incorporate viscous boundary layer effects

EULER: methods based on the Euler equations

RANS: methods based on the Reynolds Averaged Navier Stokes equations



2.3.2 Overview of available aerodynamic methods

Section Sources:
[3], [6], [9], [10], [11], [23],
[39], [41], [43], [44], [45],
[46], [47], [48], [49], [50],
[51], [52], [53], [54], [55],
[56], [57], [58], [59], [60]

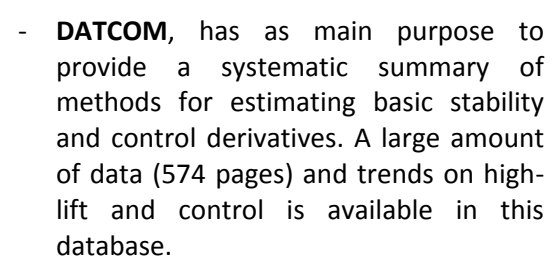
Before starting the current section, a concise introduction into the types of aerodynamic equations is at its place. The most fundamental equations governing airflow, the Navier-Stokes equations, are reduced to the Euler equations by assuming inviscid flow (no friction, diffusion or thermal conduction). When the flow is then further assumed irrotational, the full potential equations are obtained. A final step is linearizing these equations to obtain the linearized potential equations, the lowest order of equations that can be explicitly solved for obtaining the aerodynamic properties of high-lift devices.

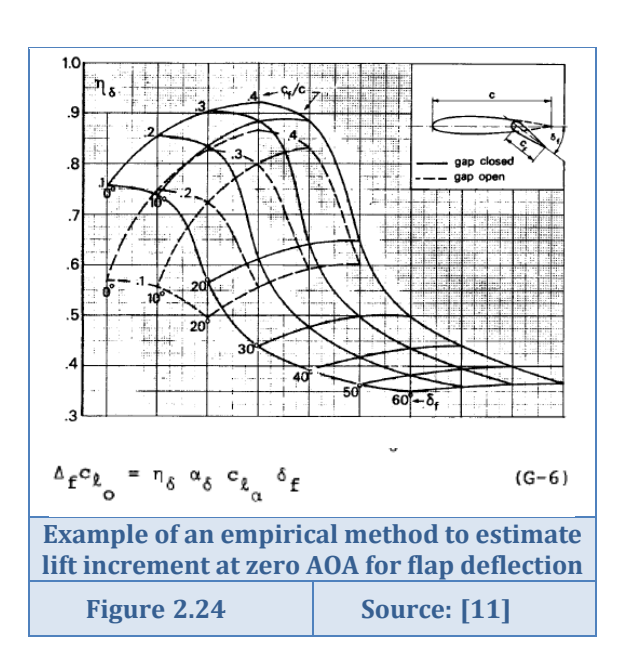
The first class of aerodynamic methods available for high-lift system design are 'empirical methods', based on experience with previous designs. Using trends obtained from historical data, aerodynamic behaviour can be predicted when only a few system parameters are known. An increase in accuracy of the calculations can be obtained by explicitly modelling the high-lift system geometry and applying computational fluid dynamic (CFD) methods. After indicating some well known empirical methods, first CFD methods for two-dimensional flow will be highlighted, after which three-dimensional methods are indicated. Finally, this section ends with a description of hybrid 'quasi-3D'-methods in which both two- and three-dimensional methods are combined in a single procedure; a method applicable to preliminary design of high-lift systems.

Empirical methods

The basis of empirical methods is formed by the collection of a large amount of data from previous similar designs. From this data obtained from previous experience, general trends are deducted and often captured in the form of trend-formulae describing the general dependency between investigated parameters.

Two large databases containing a lot of airplane historic data are USAF DATCOM [44] and IHS ESDU [45]:





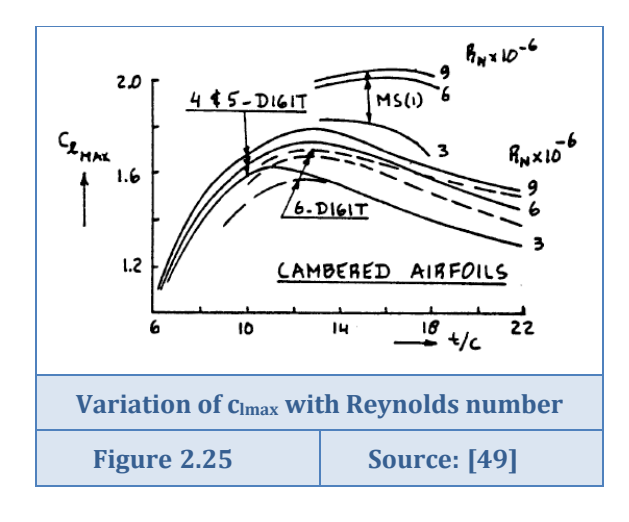
 ESDU provides a large amount of validated engineering databases for design and validation purposes. Data item 97002 [46] provides an overview of the data items and their usage when high-lift design is pursued. Data items are available for finding changes in lift, pitching moment and drag of both two-dimensional airfoils and three-dimensional wing setups due



to high-lift device deployment. Among others, data items of interest are 91014 on 'maximum lift of wings with trailing-edge flaps at low speeds' [47] and 96032 on 'Wing lift coefficient increment at zero angle of attack due to deployment of leading-edge devices at low speeds' [48].

Another example of empirical methods are the so-called 'textbook methods', in which methods to estimate properties of high-lift systems in preliminary design are derived. These methods are based on data from past designs and therefore two factors should be considered before application: the outdatedness of the basic data and conformity of flow similarity parameters between the database and intended airplane design. Well known examples of textbook methods are by Raymer [10], Roskam [9], [49], Howe [50] and Torenbeek [11]:

- Raymer has a very concise section on high-lift devices (within section 12.5) providing
 merely two basic equations on estimating maximum lift coefficient and change in zero-lift
 angle of attack, coefficients can be based on approximations of lift contributions due to
 high-lift devices learned from past designs.
- Roskam subdivides the high-lift system in two components: leading-edge and trailing-edge devices. For given maximum deflection angles, statistical values on the effects of different device types have on the lift, zero-lift drag and pitching moment coefficients are provided in table 2.10. Aside provided trend formulae not mentioned here, this tabular data can be used to make estimations of lift coefficient changes due to device deflection when the clean wing lift coefficient is known. This highly empirical method is for example applied by Werner-Westphal [39], to correct three-dimensional viscous flow lift coefficients during preliminary design phases. They assume a linear relation between flap deflection and change in lift-coefficient. One however has to take into account the large variation of the change in lift-coefficient with Reynolds number as is mentioned by Roskam (see figure 2.25), a dependency not mentioned by Werner-Westphal.
- **Torenbeek** provides prediction methods for high-lift and drag in the low-speed configuration in Appendix G of his book [11]. The methods are restricted to passive high-lift devices and are mainly based on Glauert's linear theory for thin airfoils; correction factors for taking nonlinearities and flow separation into account are also presented. See for an example figure 2.24.

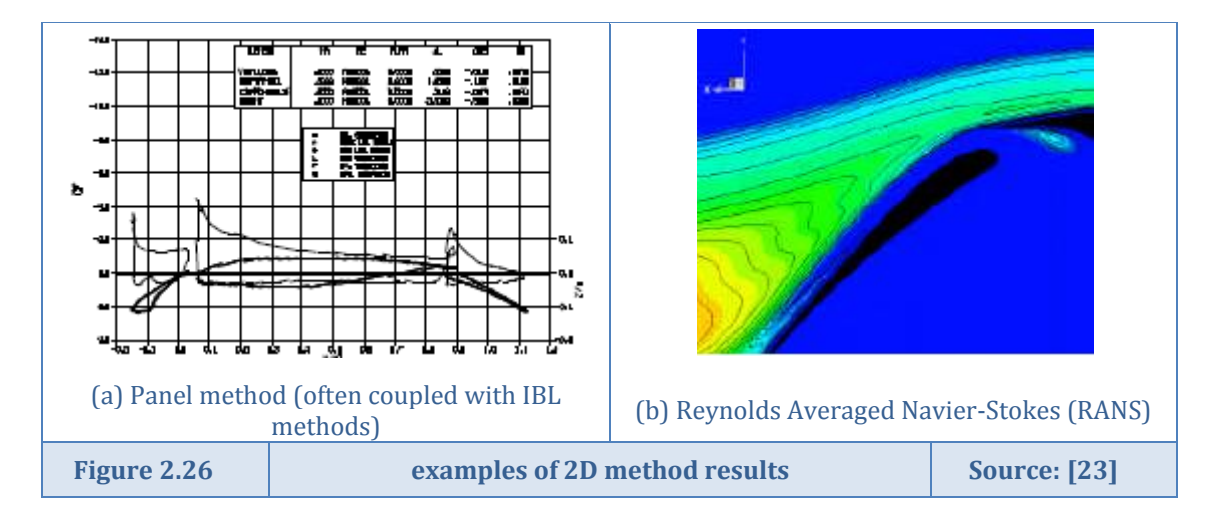


Empirical methods are based on statistical data derived from past designs. This approach can be restrictive in that it cannot be safely applied to novel concepts since they only apply to aircraft designs and highlift types for which they are properly calibrated. Furthermore, estimations based on empirical methods should be handled with care, since these are very dependent on the topicality of the database the methods are based on.



Table 2.10		Empirical high-lift system performance prediction Source: [49]						
Type	Subtype	Schematic	maximum deflection	Reynolds number of	Coeffic	ient change a	ent change at δ _{max}	
Туре	angle δ_{max}			ΔC_L	$\Delta C_{\text{D(CL=0)}}$	ΔC_m		
Nose Flap	Hinged LE		30∘	6·10 ⁶	0.55 - 0.75	0.00	-0.09	
Krüger Flap	Simple Krüger		40°-45° (straight wings) 60° (swept wings)	8.2·10 ⁵	0.50	0.00	-0.10	
Slat	Three- position slat		26°-30° (straight wings) 45°-60° (swept wings)	6·10 ⁶	0.93	0.00	+0.11	
Non- slotted Flap	Split flap		60∘	6·10 ⁶	0.8	0.23	-0.275	
	Plain flap		60∘	6·10 ⁶	0.90	0.12	-0.275	
Slotted Flap	Simple slotted flap	× /	40°	3.5·10 ⁶	1.18	0.13	-0.33	
	Single slotted Fowler flap	1	30∘	3.5·10 ⁶	1.67	0.10	-0.42	
	double- slotted flap		30°/55°	6·10 ⁶	1.4	0.23	-0.41	
	Triple- slotted flap		30°/44°/55°	6·10 ⁶	1.6	0.23	-0.44	

2D methods

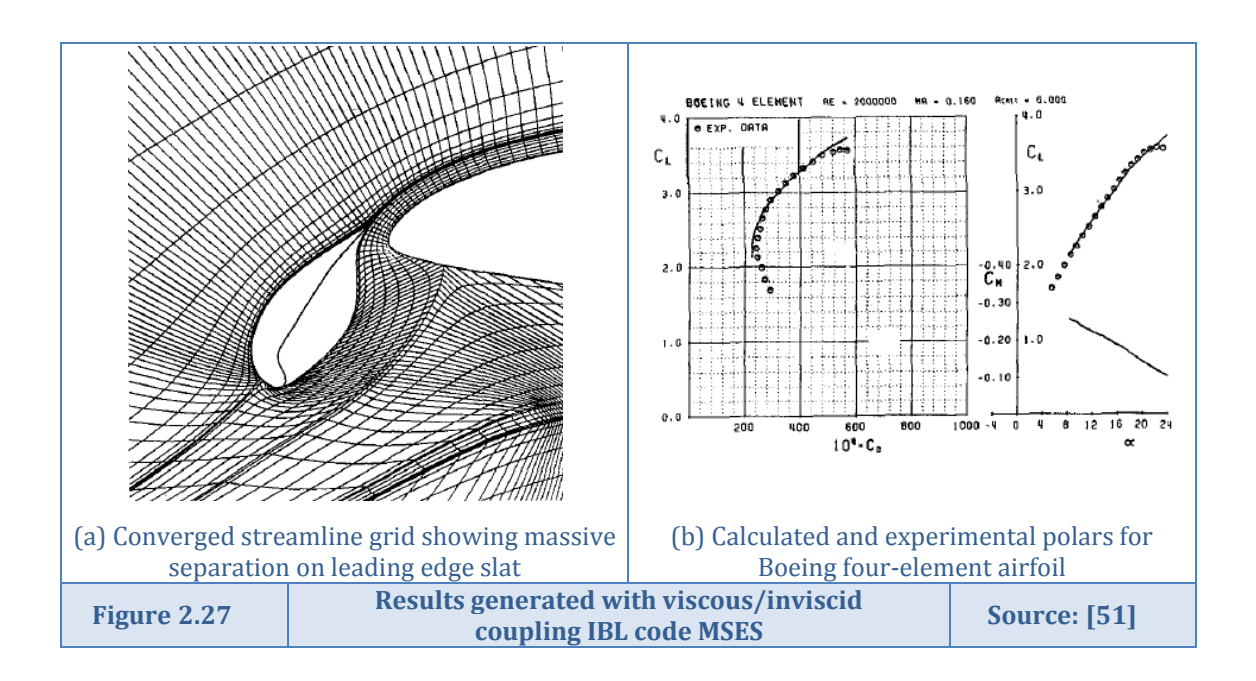


Until quite recently, interaction methods in which panel codes are combined with integral boundary layer (IBL) calculations (see figure 2.26(a)) were used to calculate the flow characteristics of multi-element airfoils. The usage of separate viscous and inviscid flow solvers allows calculations requiring moderate calculation times and can yield quite realistic results. The advances in computer power and understanding of two-dimensional flow phenomena, especially in the form of improved turbulence models, has led to a wider usage of computer



methods solving the Reynolds Averaged Navier-Stokes (RANS) equations [43]. The two most often used turbulence models are the Spalart-Allmaras (SA) one-equation model and the shear stress transport model (SST) developed by Menter. It is beyond the scope of this thesis to go into detail on the turbulence modelling methods. Full Reynolds stress models (RSM) solvers, representing the highest fidelity level of RANS methods, are not widely available for complex configurations. Hereafter, first the interaction method MSES will be discussed, after which some more in-depth information will be provided on RANS methods.

Drela and Gilles [51] have created a viscous/inviscid method for the calculation of multielement flows around airfoils. In their program MSES, the steady Euler equations are solved to find the inviscid flow solution and simultaneously a two-equation integral boundary layer method is used to perform a viscous calculation. This solution is coupled through the displacement thickness of the airfoil: the inviscid streamline adjacent to the airfoil is displaced from the surface by the local calculated displacement thickness. On the wake, the gap between its bounding inviscid streamlines is set equal to the wakes total displacement thickness and the pressure jump along this gap is set to zero. Multi-element airfoil flows show two important characteristics: strong wake asymmetry and confluence of adjacent shear layers (see figure 2.6 in section 2.1). Wake asymmetry has a positive influence on the dissipation rate of the shear layers and resistance to adverse pressure gradients, whereas confluent wakes negatively influence these properties. These effects are taken into account by the creation of an integral multi-layer representation of the boundary layers, elaborated in detail in [51]. The program shows quite good agreement with experimental data around a four-element high-lift configuration (see figure 2.27(b)). The advantage of the applied displacement body model is that the inviscid streamline closest to the surface accurately models the free shear layer in the real situation, which can be seen in figure 2.27(a). The coupling method was first suggested by Prandtl, it however has two drawbacks [41]. The first is that the influence coefficient matrix representing the geometry of the configuration needs to be re-inverted during each inviscid flow calculation. This can be avoided as is described in the method of Dvorak and Woodward, see the part on 'quasi-3D methods'. The second drawback is that it is usually necessary to smooth the new geometry before the inviscid flow calculation can be performed.



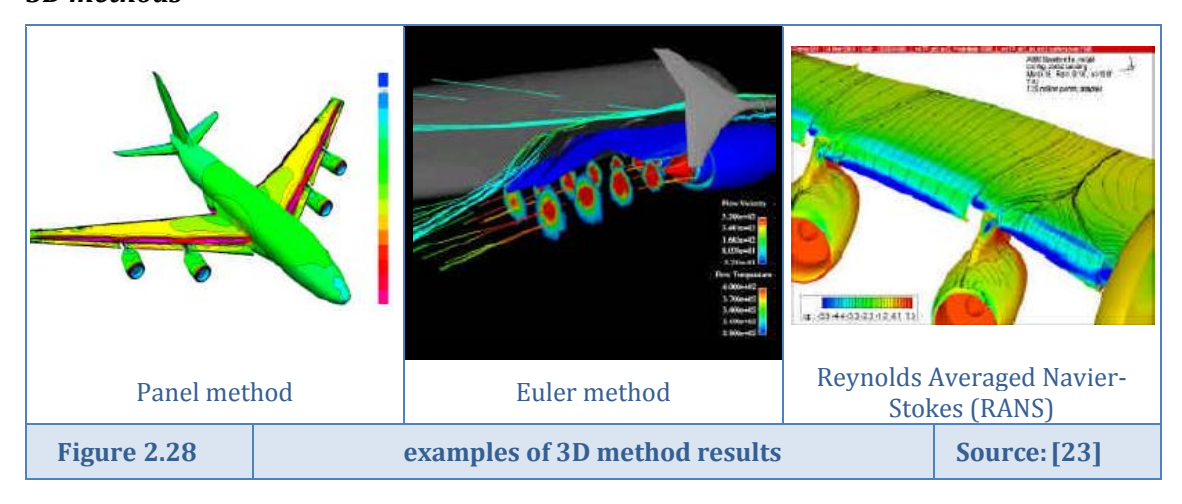


Although some viscous/inviscid interaction codes provide excellent results, methods based on the Navier-Stokes equations are nowadays being applied more often. First, this is due to robustness problems within wake calculations, at confluence of boundary layers and at massive separation situations when performing interactive calculation methods. Secondly, the extension to three-dimensional flow problems is more straightforward for RANS than for interaction methods. Figure 2.26(b) shows the results of a RANS calculation. When solving this type of problem, generation of a proper grid capturing all flow phenomena is of main importance. In figure 2.31(b)), such a grid is represented showing the high density required along the boundary layer, in the wakes and along profile discontinuities such as a flap slot. Especially for multi-element airfoils it is difficult to generate consistent grids for all high-lift device settings, and time-consuming grid convergence studies are required. Besides the large computing time requirements on grid generation, obtaining the solution of the RANS equations at every node of the grid require difficult algorithms, posing large demands on computational power. It has to be concluded that two-dimensional RANS calculations provide results closest to the real flow, however at the cost of large requirements on computational power.

Interaction methods often show discrepancies when predicting the maximum lift coefficient, therefore RANS calculations are required to be able to do this. However, predicting the sectional maximum lift coefficient and the angle at which it occurs still remains a problem, since a large amount of flow separation mechanisms need to be taken into account which are often difficult to model.

For an overview and assessment of software titles able to perform two-dimensional calculations on high-lift systems (for both panel+IBL and RANS methods), the reader is referred to [43].

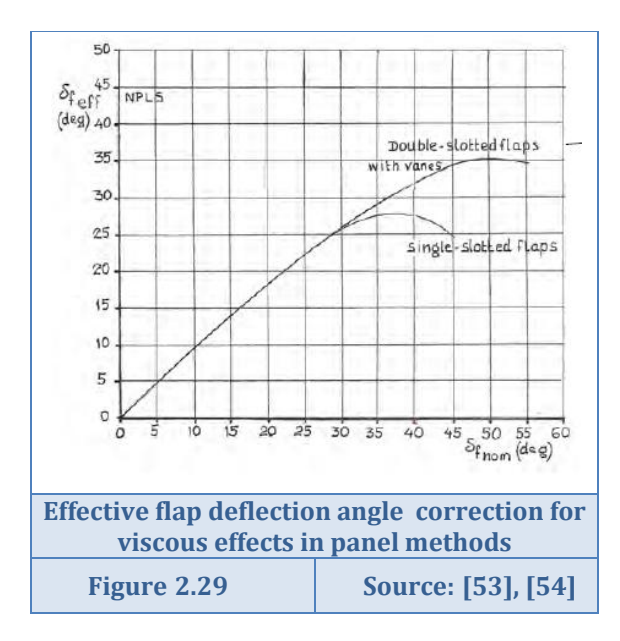
3D methods



For obtaining the aerodynamics around three-dimensional bodies, a distinction can again be made between panel methods in which a flow solution is found at the body, and more sophisticated methods for which the complete fluid around the body is discretized.

Performing inviscid calculations using panel methods is the method requiring the least computational power. The surface of the three-dimensional body is discretized using panels and the linearized potential equation is solved along this body. Including IBL methods in these three-dimensional calculations is shown to be a difficult task [3]. When properly included, the viscous/inviscid coupling using IBL methods is then often found too weak to predict stall





characteristics. Among others, the pressure difference rule (PDR) of Valarezo and Chin [52] can be used as a first approximation for predicting high-lift for complex threedimensional configurations. This semiempirical method predicts stall on each spanwise element of the representation, based on the pressure difference between the suction peak and trailing edge. The results obtained with this method show quite accurate maximum lift predictions. Another common practise in three-dimensional panel methods correcting flap deflection angles to account for viscous effects on flap effectiveness. Flap angle reduction information should however be available to be able to do this,

often posing a problem for preliminary design stages of high-lift systems. Vos indicated in his lecture on aircraft design and operation [53], that it is worth investigating if the method of Obert can be used as a first estimate in this respect. As part of a method to estimate trimmed drag polars for Fokker transport aircraft with deflected flaps, Obert [54] provides a relation between the actual and effective flap angle, based on comparison of inviscid calculations with wind tunnel tests. This relation is depicted in figure 2.29 for single-slotted flaps and double-slotted flaps with vanes. When full use is made of the method described in the report of Obert, possibly initial L/D estimations can be included in the calculation procedure presented in this master thesis, providing a qualitative estimate of the climb performance (see also section 2.1).

In spite of the low fidelity of the inviscid calculations, panel methods can be used to rapidly gain insights in the flow around three-dimensional bodies, as for example seen in figure 2.28(a). By correlating the results of panel methods to experimental data, it is revealed that pressure distributions of multi-element wings can be reasonably predicted for the linear range of the lift curve. Reckzeh [6] describes that for the design of the megaliner aircraft at Airbus the three-dimensional panel method (VSAERO) was supplemented by 'in house'-developed extensions to incorporate the strong viscous effects found at high-lift devices. Both empirical data as well as extensions for the prediction of flow separation were used to capture the viscous discrepancies of the applied panel method. This proved to be a very valuable tool in assessing a large number of high-lift system setups during the preliminary design phase.

Although providing much more realistic results, Euler and especially RANS calculations require very large computational sources. Rumsey and Ying [43] indicate that methods solving the Euler equations are rarely used in the design of high-lift systems, due to the absence of viscous phenomena in the flow solutions. Reckzeh [6] however indicates that, among other methods, also Euler equations were used in the design of the megaliner aircraft of which the Airbus A380 is the result. These Euler equations are probably used in areas where inertial forces are much more profound than viscous effects, as is the case for the engine outflow depicted in figure 2.28(b).

The reason why RANS solvers are not as widely applicable to the design of high-lift systems is that in the past the development of these tools was mainly focussed on transonic airfoil and wing design [55]. Only recently attempts of creating RANS solvers for full three-dimensional flows around high-lift configurations have been made. In Europe, both the EUROLIFT and

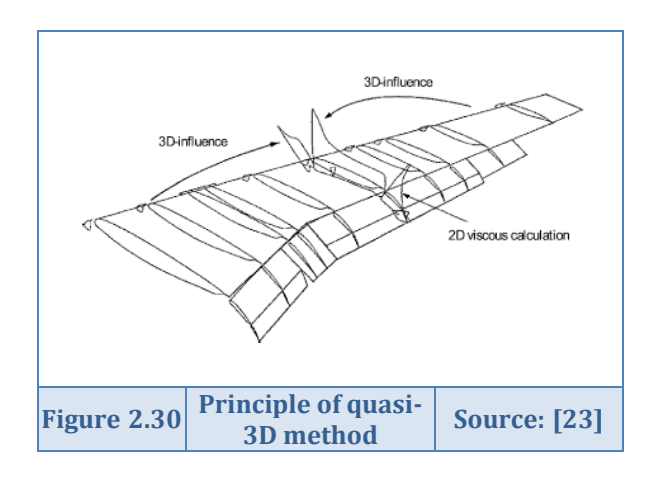


EUROLIFT II project (see for example [56]) aim to validate RANS solvers for these highly complex types of flow. The level of accuracy has demonstrated that this type of simulation is a promising method for aerodynamic design of high-lift devices in the near future. However, these design methods probably remain part of the detailed design phase for the upcoming years due to the large associated computational demands.

Other disadvantages of considering the usage of RANS equations in conceptual and preliminary design phases are related to mesh requirements and lack of detailed geometrical data. Due to the large complexity of meshes for three-dimensional configurations including high-lift devices, generation without manual intervention is very difficult. This is a large disadvantage in preliminary and conceptual design, since one wants to automatically assess the feasibility of a large number of configurations. Furthermore, maintaining a constant mesh quality is a second challenge as the change of geometry can be rather large [57]. Another problem with complex three-dimensional methods is that an exact representation of the outer geometry of the complete aircraft is required for the calculations to be valid. In early stages of aircraft design, this kind of data is often not available in the required level of detail [39]. See figure 2.28(b) for an example of the level of detail required for a proper RANS calculation. As a last comment on RANS calculation methods, it can be stated that compressible methods are preferred over their incompressible counterparts, since flows over high-lift systems usually possess noticeable compressibility effects [43].

For an overview and assessment of software titles able to perform three-dimensional calculations on high-lift systems (for both panel+IBL and RANS methods), just as for the two-dimensional case the reader is referred to [43].

Quasi-3D methods



In so-called quasi-3D methods, twoviscous simulations dimensional coupled to three-dimensional inviscid calculations. In this way, a calculation method demanding moderate computer power is created, in which the most important viscous effects of multielement flows are taken into account while no time-consuming complete threedimensional viscous calculations have to be performed. It serves as an attractive 'best of both worlds' method, applicable for predicting trends in high-lift system design variations during preliminary and

conceptual design stages. Hereunder three different quasi-3D analysis methods will be discussed, those of Antunes et al. [58], Dvorak and Woodward [41] and the combined method of Liersch and Werner-Westphal [59], [39], along with a similar approach by van Dam et al [60]. Although more methods exist, only the aforementioned are described, since these provide indicative and dissimilar approaches on the coupling of two- and three-dimensional aerodynamic data.

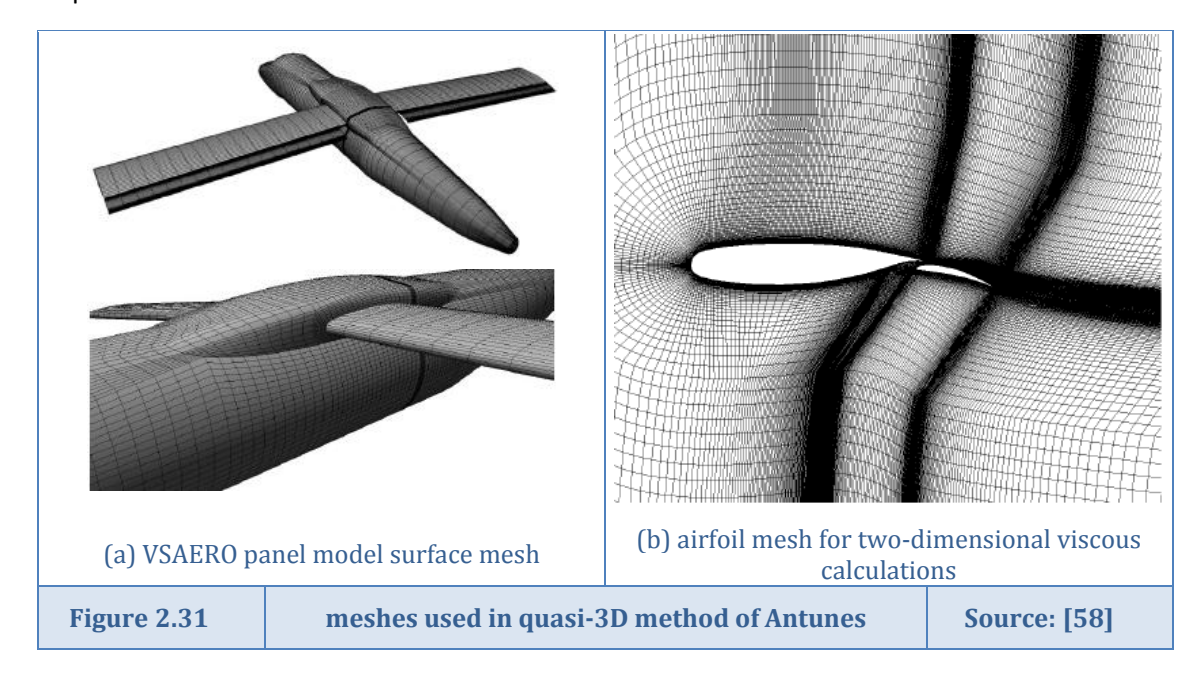


Antunes et al. [58] couples two-dimensional viscous simulations to a three-dimensional panel method (VSAERO) in the following way:

- The three-dimensional simulation is used to determine the spanwise loading distribution for a predefined C_L level (i.e. the wing is trimmed at a condition that provides this three-dimensional lift-coefficient). Figure 2.31(a) shows the mesh generated for the VSAERO code used to obtain the spanwise lift distribution.
- For a number of spanwise stations, two-dimensional viscous flow simulations based on solving RANS equations are used to determine maximum sectional lift coefficient c_{I} . From these local values a spanwise c_{Imax} distribution is interpolated. Figure 2.31(b) shows the mesh generated for the viscous calculations.
- If the inviscid spanwise loading exceeds the c_{lmax} distribution, wing stall is assumed and the spanwise loading is corrected at these positions.

The above described method is quite straightforward, but has the problem that a slight error in the prediction of sectional c_{lmax} can impose large consequences on the correctness of spanwise lift distribution. All assumptions and errors made in the two-dimensional calculation are completely transferred to the three-dimensional C_L prediction method. Of course, the usage of a panel method for the calculation of the spanwise lift distribution also introduces errors in the simulation, these were discussed earlier in this section. The two-dimensional calculations incorporated either a Spallart-Allmaras (SA) model or the shear-stress transport (SST) model for turbulence modelling, and was calibrated using known two-dimensional wind tunnel data.

The method of Antunes showed some discrepancies for the quasi-3D method applied. For the method including the SST turbulence model, C_{Lmax} was overpredicted by about 6% when compared to a full three-dimensional RANS calculation of the same setup. Application of the SA turbulence model showed even larger prediction errors, but had lower computational requirements.





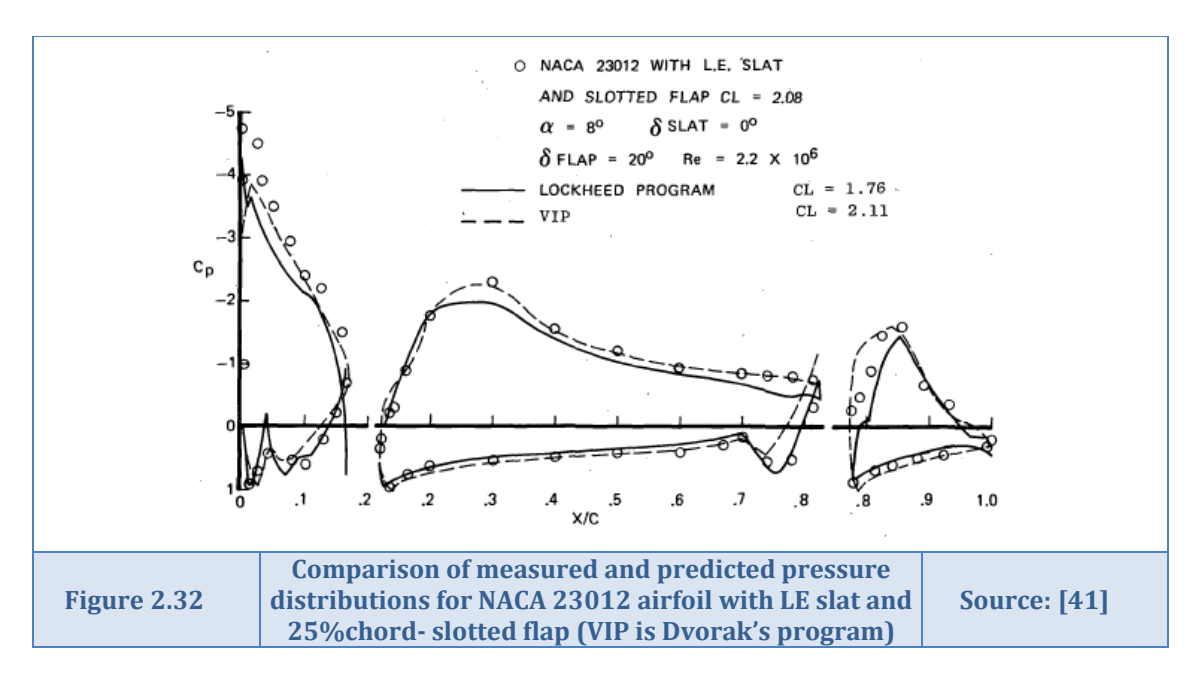
Dvorak and Woodward [41] describe a viscous/inviscid coupling method based on a different approach, applicable to multi-element infinite swept wings. This makes it essentially a two-dimensional calculation problem. It is however suggested that an extension to three-dimensional modelling is a possibility. The approach is as follows:

- The inviscid pressure distribution is determined using a two dimensional potential flow solver making use of a vortex lattice technique
- For each individual element of the high-lift configuration, the boundary layer development is determined using either integral boundary layer theory or using finite differences
- A source distribution is then determined and added at the profile boundary, to account for viscous effects. This source distribution is a function of the boundary displacement thickness (δ^*) and pressure distributions
- A new inviscid calculation is performed incorporating the extra source distribution. This is done until solution convergence

Although being a little less straightforward than simply adding the displacement thickness to the geometry (as in the method of Drela, see the part on 2D methods and figure 2.27), the approach is claimed to be much more efficient. This is due to the influence coefficient matrix representing the geometry of the configuration needs to be inverted only once at the start of the calculation procedure. The boundary calculations must at least include for each element:

- stagnation line initial conditions
- laminar, transitional and turbulent boundary layer developments
- laminar or turbulent separation predictions

A last advantage of using distributed sources is the possibility to model separated flow regions in the potential flow analysis. The authors however did not yet include that possibility in their program. A resulting two-dimensional pressure distribution for a three-element airfoil is given in figure 2.32, showing good agreements with experimental data.



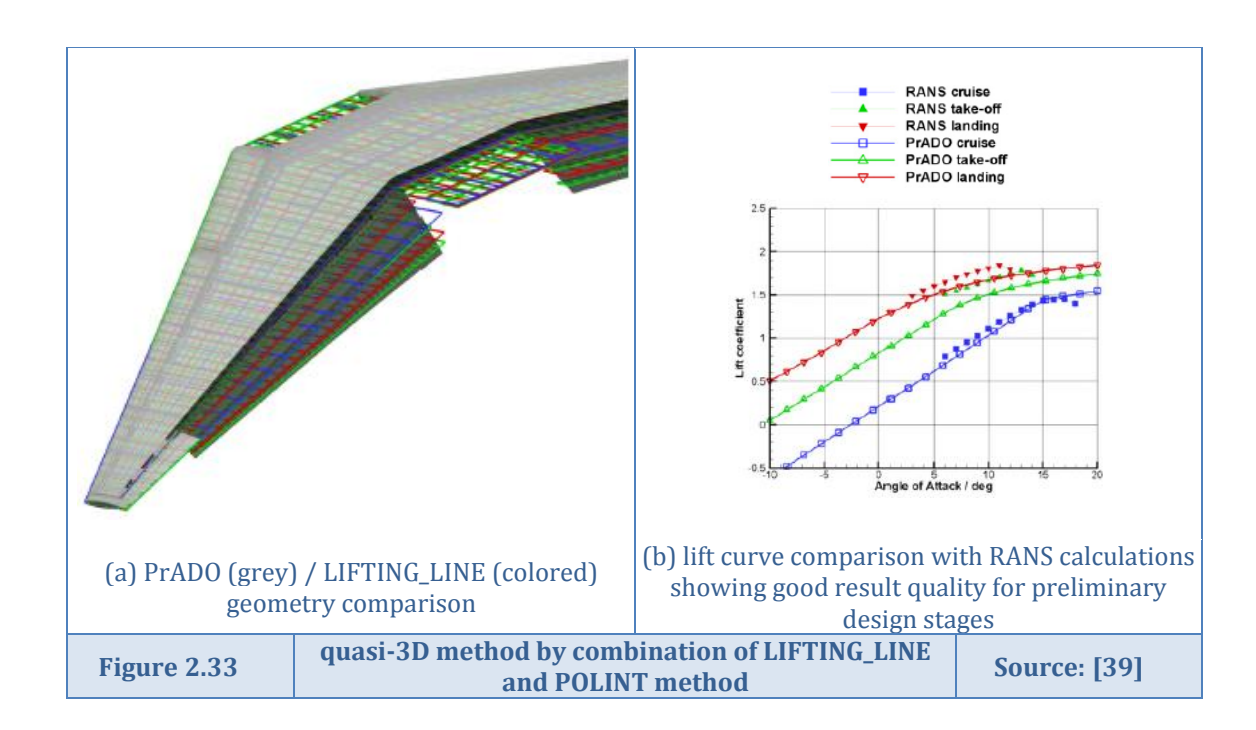
The last quasi-3D method to be discussed is that applied by **Liersch and Werner-Westphal** [59], [39]. They combine a three-dimensional multi lifting line method called LIFTING_LINE with two-dimensional airfoil polar interpolation tool POLINT to design high-lift systems in preliminary design phases. The combined tool covers the effects of flap deflections, transonic



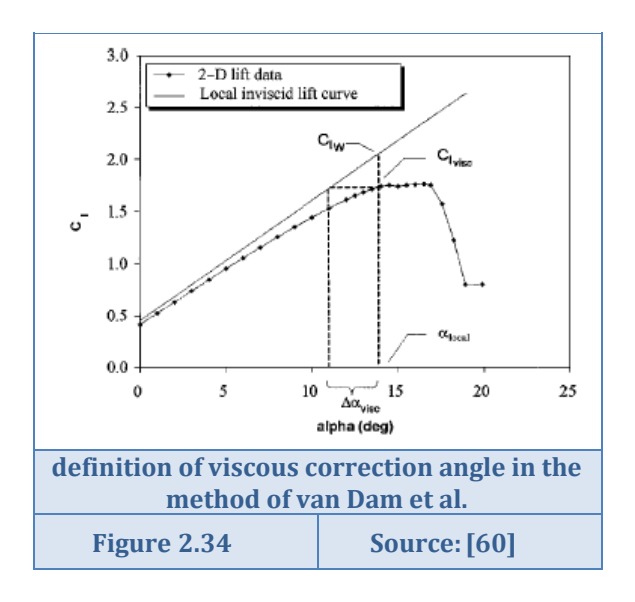
drag and nonlinear behaviour around maximum lift coefficient. LIFTING_LINE is a panel method using a multi lifting line method to solve the linearized potential equation, and uses in large sense the same ideas as applied in a general vortex-lattice method. First order transonic accuracy is provided by taking a compressibility correction rule into account. POLINT uses known data from airfoil polars to modify the spanwise aerodynamic coefficients obtained by LIFTING_LINE, thereby assuming two-dimensional flow in each wing section. This implies however, that airfoil polars with correct Mach and Reynolds numbers are required at the spanwise wing sections. These can be either obtained from experiments or calculated using higher-fidelity computations, such as RANS simulations. The method build-up is as follows:

- A three dimensional lift-coefficient distribution is calculated using LIFTING LINE.
- POLINT interpolates known airfoil polars to obtain a two-dimensional lift curve at each spanwise wing section.
- Local normal force coefficients are used to obtain the local angle of attack of the section.
 This angle of attack is used inside interpolated airfoil polar to recalculate the normal force coefficient, drag and pitching moment coefficient. If the angle of attack is beyond maximum/minimum angle in the interpolated polar, the last existing value will be used.
- The new local coefficients are integrated over the wing to obtain new total coefficients.

The method is integrated in the multidisciplinary preliminary aircraft design process PrADO, shortly discussed in section 2.2.2. From the PrADO database, a wing surface model is extracted and put in a high-lift configuration. The high-lift devices are explicitly modelled as can be seen in figure 2.33(a). Angles of incidence due to flap deflection are set by adjusting the tangential flow condition for each panel. Using the described coupling method, building up a full aerodynamic database for all flight conditions takes approximately 10 to 12 hours. This is significantly more than when applying a coupling method based on Roskams' semi-empirical methods (described in the part on Empirical methods), taking only 15 minutes of computing time. Applying the more sophisticated coupling method however largely increases the validity of the results and allows one to study unconventional aircraft and high-lift system layouts.







It is noted that a method very similar to the last described quasi-3D method is applied by van Dam et al. [60], where a modified lifting-line method originally developed by Weissinger is coupled to results of sectional viscous calculations. Just LIFTING LINE/POLINT method, analysis of complete aircraft lifting surface configurations is allowed. Models can be created, consisting of wings with high-lift systems, horizontal and vertical tails, including sweep, taper, twist and dihedral. In a non-linear C_{Lmax} prediction routine, a viscous correction angle is predicted per spanwise section, based two dimensional viscous section data.

correction angle is then used to adjust the inviscid three-dimensional wing model, after which a new calculation is started. This is repeated until convergence. Figure 2.34 shows the definition of the applied correction angle, which has large similarities with the effective flap angle calculation method described by Obert [54], depicted in figure 2.29. Just as in the LIFTING_LINE/POLINT method, van Dams' method shows very good correlations with experimental data.

2.3.3 Wing modelling using a vortex-lattice method

Section Sources: [61], [62], [63], [64]

At the institute of air transport systems of the DLR in Hamburg, it was suggested to use the publicly available vortex-lattice code AVL [61], written by Mark Drela, for performing the inviscid three-dimensional wing calculations. This code has a good reputation, and a batch version is available for quick calculation purposes. During the internship preceding this master thesis, an input generator and output reader was written, creating the possibility to control AVL from MatLab. This connectivity can serve as a basis for creating aerodynamic wing models in AVL based on wings generated by ParaMAM (see section 2.2). When modelling using the vortex lattice method AVL, the following main assumptions need to be taken into account [61]:

- A vortex lattice method is best suited for configurations consisting mainly of thin lifting surfaces at small angles of attack and sideslip.
- Surfaces and trailing wakes are represented as single-layer vortex sheets, the trailing legs of horseshoe vortex filaments are assumed parallel to the x-axis.
- Quasi-steady flow is assumed, implying unsteady vorticity shedding is neglected.
- Compressibility is treated using the Prandtl-Glauert compressibility correction, which is expected to be valid for a wing-perpendicular Mach number up to 0.6.



Some important rules have to be followed for proper modelling of wing geometries in vortexlattice codes:

- Trailing vortex legs are not allowed to closely pass downstream control points. This implies surfaces lined up in the x-direction must have the same spanwise vortex spacing.
- Spanwise vortex spacing must be smooth, no sudden changes in strip width are allowed. Bunched spacing is required at positions where the circulation changes rapid; i.e. at taper, dihedral and chord brakes, as well as at control surface ends and especially at wing tips.
- If a control surface is present, the discontinuity in camber line angle needs to be modelled with an adequate amount of chord wise vortices at the hinge line.

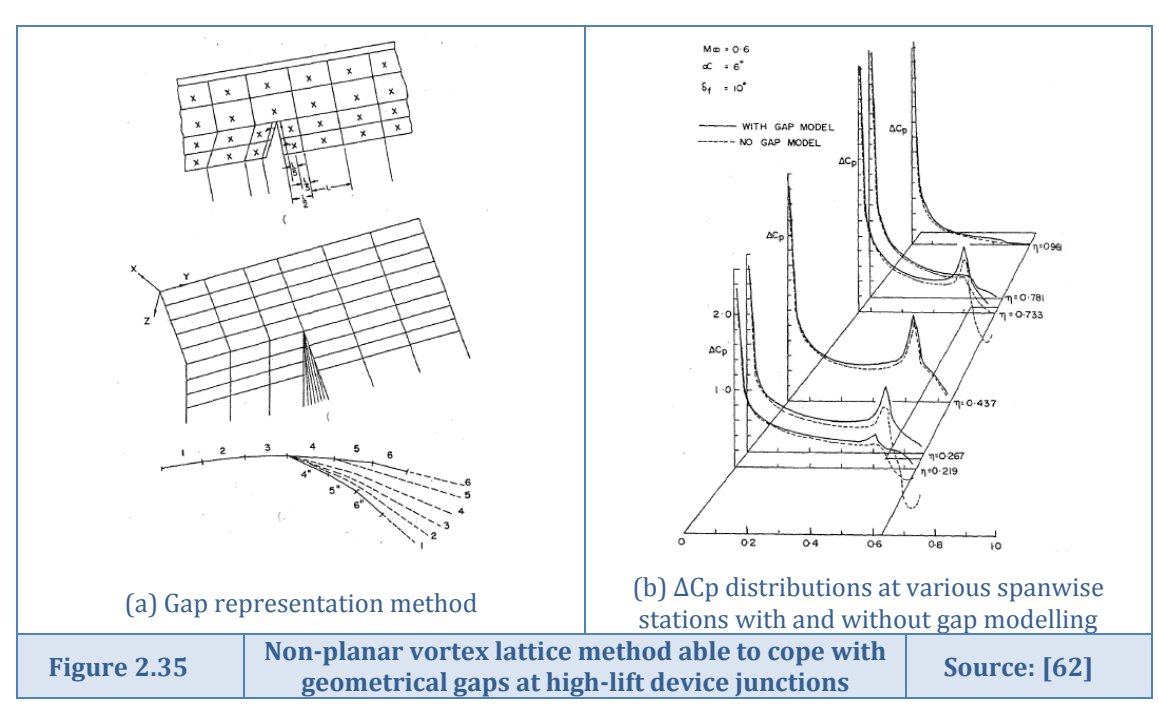
Difficulties arise when trying to model high-lift devices using a vortex-lattice method. In the limits of linear theory, a common way of approaching the problem of high-lift device modelling within a vortex-lattice method is to treat the flap deflection as an additional local incidence distribution, as is done in the AVL method described above. Chord extension effects can also be modelled without large problems, although outlining of the horseshoe vortices might pose some difficulties. It is to be investigated if creating an actual gap in the three-dimensional vortex lattice representation of a wing concept increases or decreases the accuracy of the results. Unfortunately, not much information on this matter is available in literature. Rajeswari Ramamurthy [62] proposes a method for proper gap treatment. Although it is not possible to incorporate his method in the AVL method, it is shortly described hereafter.

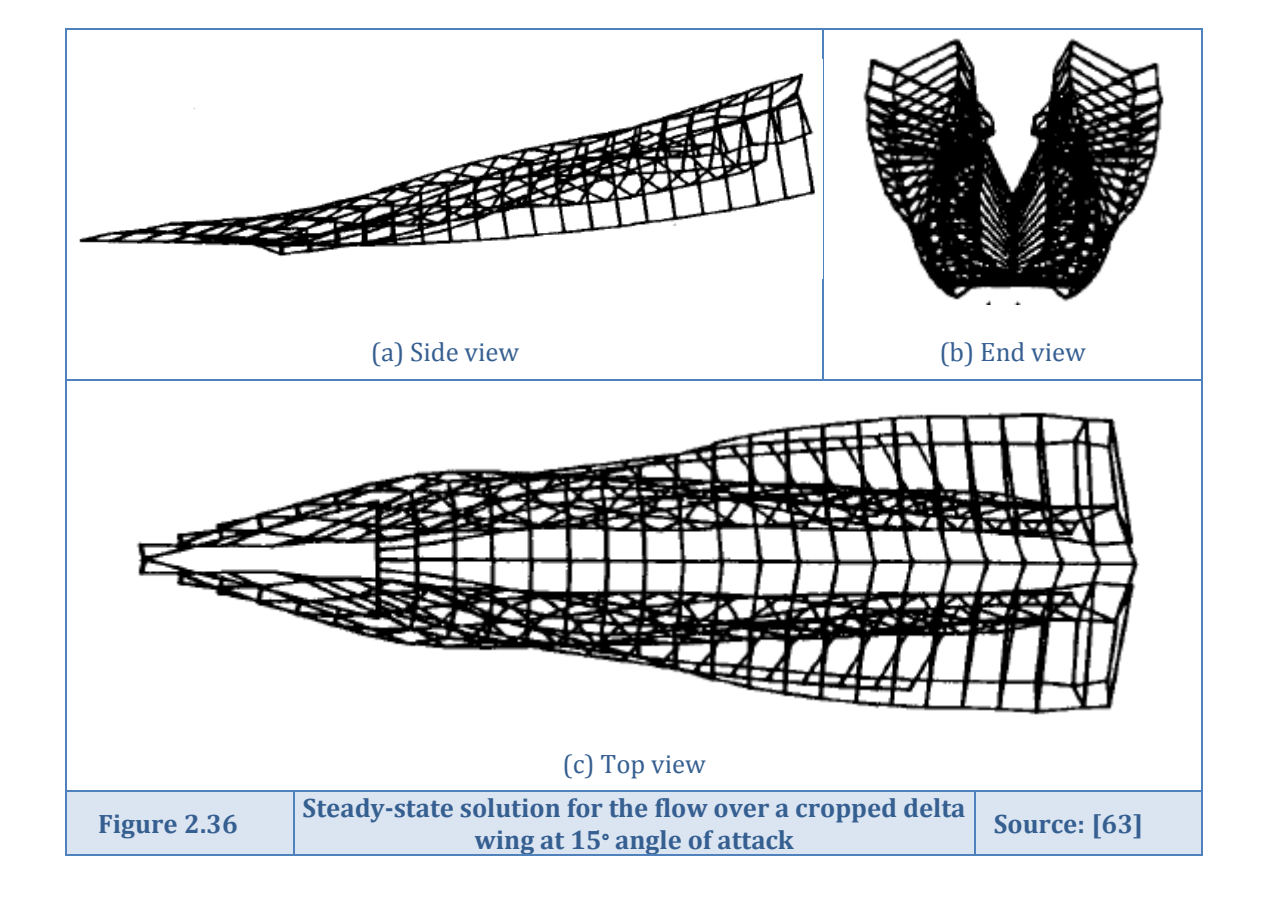
According to Ramamurthy, a more exact way of representing deflected flaps is to distribute the singularities on the actual wing flap surfaces. Through the gap formed in the x-z plane flow can then communicate from the lower to the upper side of the wing, the gap itself carries no load. This gap has to be modelled in such a way that the load on both panels at the side of the gap and upstream of the gap are realistic. The error in computed vortex strengths can otherwise propagate to other panels and influence the total simulation results. This problem can be resolved by creating concentrated vortices at the junctures between wing and high-lift device. These vortices can then be diffused and spread into a sheet of vortices covering the gap to properly take the geometrical discontinuity into account. This method is schematically represented in figure 2.35(a). It is assumed that the vortex sheet filling the gap carries has no pressure difference across it and only properly transfers the loads from wing to high-lift device and the other way around. Figure 2.35(b) shows the calculation results with and without explicit gap modelling, showing that the problems with negative trailing-edge loads due to gap discontinuities are resolved using the described gap filling model.

Another problem occurring in the usage of AVL is modelling the influence of wakes generated by upstream elements on downstream elements. The wake representation applied in the method does not allow any rollup or influence of downwash, since it is represented as a singlelayer sheet in the x-y plane. The method of Mook and Nayfeh [63], does allow rollup of the wake using downstream vortex panel representations and is applicable to multiple lifting surfaces operating in close proximity. Unfortunately, it is based on leading edge vortex separation theory and is thereby restricted to setups for which separation occurs either along the sharp edges of the wing, or at other known locations. This data is generally not available in conceptual and preliminary design phases. When a further assumption that vortex bursting does not occur near any of the downstream surfaces is made, the method shows good agreement when compared to experimental data. It is suggested that for flows where the position of the strong shed vorticity in the wake is important, accurate treatment can most likely only be obtained when freely forming wakes are included. Figure 2.36 shows the steadystate solution for the wake of the flow over a cropped delta wing, as calculated by Mook and Nayfeh. In a validation of vortex-lattice methods for wing/wake interactions, Rossow [64] suggests reconfiguring the flow field and wing, such that the stream encountering the



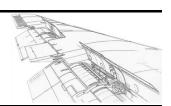
downstream element is uniform rather than rotational. To take the effects of the wake of upstream elements into account, the wing is re-twisted to match the angles of attack imposed by the vortex. In this way, the problem of simulating a wing in a wake flow is restored to being solvable with potential flow assumptions. This method would unfortunately also require alteration of the methods applied within the AVL programme.





Chapter 3

Aeroelastic wing modelling



In the current chapter, the software routine serving as a basis for quick aerodynamic and structural calculations during preliminary wing design is explained. The general structure of this software is provided in the first section. In section 3.2, generation of the basic wing model will be described, along with its coupling to the aircraft information model CPACS⁶. Section 3.3 considers generation of an updated wing model having high-lift devices extended according to prescribed deflection settings. Thereafter, the two main pillars of the aeroelastic routine, an aerodynamic vortex-lattice software connection and a coupling to structural software are explained in sections 3.4 and 3.5 respectively. Section 3.6 shows the results of performing a complete aeroelastic calculation. The final section of this chapter, section 3.7, discusses the effects of incorporating sizing routine S_BOT⁷ in the aeroelastic chain, which is used to size the material thickness distribution in the wing.

.

⁶ CPACS stands for 'Common Parametric Aircraft Configuration Scheme', which is an aircraft configuration information model currently under development at the German Aerospace Centre (DLR). It is to be used to exchange data between multidisciplinary and multifidelity software tools in aircraft design.

⁷ S_BOT is the acronym for 'sizing robot for ANSYS wing models', which is a structural sizing tool written in ANSYS' parametric design language (APDL) by Björn Nagel. It is capable of redistributing material thickness according to stresses in spars, ribs and skin panels. When composite materials are considered, fibre angles can also be adjusted according to stress states calculated by ANSYS.



3.1 Main goals and general structure of the aeroelastic sizing tool chain

The main goals and general structure of the aeroelastic tool chain including sizing routine is described in this section. The scheme provided in subsection 3.1.2 serves as a basis for the development of all individual software connections created in sections 3.2 to 3.5. The approach in building up the software, as well as opportunities left for future research are indicated in subsection 3.1.3.

3.1.1 Main goals of the aeroelastic sizing tool chain

Section Sources: no external sources used

In order to define the main goals of the aeroelastic routine, the main thesis goals defined in chapter 1 are repeated below:

- Construction of an improved aeroelastic representation of high-lift systems with a focus on rapid load estimations, which can be incorporated in the DLR wing design chain
- Enhancement of the understanding of the interconnections as well as sensitivities between different disciplinary components of the high-lift system, with a focus on structural sizing and weight estimation

The wing design chain of the DLR is focused on a preliminary design level. This implicates that the aeroelastic wing representation should be applicable to this particular design phase. The structural model generator created during a preceding internship is used as the generator of the structural model used within the design chain. The first and main goal of the software generation in this thesis is to use this structural model in order to create a connection to aerodynamic 'off the shelf' software being able to generate rapid load estimations. An important secondary target is to make sure the aerodynamic model generation, calculation and result processing uses as little computational effort as possible. The latter is required to be able to perform a large amount of design iterations during a sizing run, possibly covering a large amounts of wing setups. A third, somewhat more obvious target is to make sure incorporation in the wing design chain of the DLR is possible.

Knowing the aerodynamic loads, structural calculations need to be performed in an automated way. For this, input decks are to be automatically generated for usage in an interactive batch run of structural software. From the structural calculation result data, stresses and displacements need to be extracted for usage in the aeroelastic tool chain.

After completing the aeroelastic part of the software, incorporation of sizing routine S_BOT will finish-off the initial routine. With the complete tool chain finished, structural sizing and weight estimation are to be performed on wing models in order to provide an answer the second main thesis goal: enhancement of understanding the interconnections between structural and aerodynamic components of the high-lift system.



3.1.2 Structure of the aeroelastic tool chain

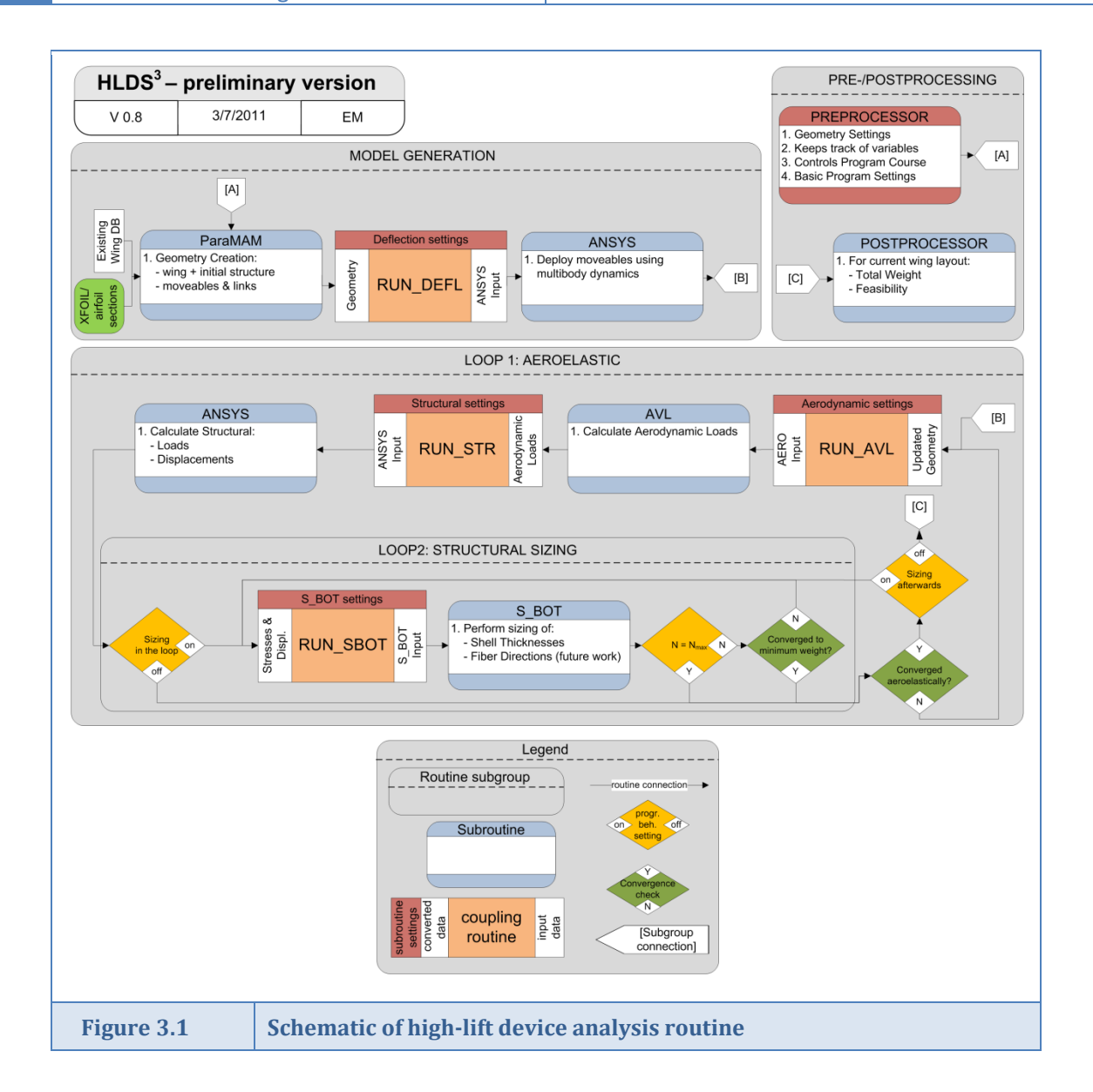
Section Sources: no external sources used

A basic schematic of the developed aeroelastic tool chain was shortly described in chapter 1. A more extensive version of this schematic is given in figure 3.1, which will serve as a basis for the development of all individual subroutines within the tool chain. As can be seen from the schematic, the tool chain is built up of four subgroups:

- *Pre-/postprocessing*: the preprocessor controls the course of the program, and loads basic program settings. The postprocessor generates a result summary, as well as plots of the results after finishing a complete aeroelastic program run.
- Model generation: in this subgroup, the structural wing model is built according to the wing definition provided in the CPACS aircraft information model. If required, the loaded movables are thereafter deflected using a multibody dynamics calculation. Structural model generation is described in section 3.2, deflection of the movables in section 3.3.
- Loop 1 'Aeroelastic': By coupling an aerodynamic load calculation method with structural deflection calculations an aeroelastic iteration process is created. Section 3.4 describes which methods are applied to extract an aerodynamic vortex-lattice wing model using the generated structural model from the model generation subgroup as a basis. The 'RUN_AVL' block in the program schematic indicates the relative position of this procedure within the complete tool chain. The obtained aerodynamic loads are converted from the vortex-lattice result data to proper input for the structural wing model and passed on to the 'RUN_STR' coupling routine. After generating input datadecks in the ANSYS parametric design language, ANSYS performs a batch run, of which the results are explained in section 3.5. This results in wing displacement data that can be used to update the aerodynamic model, as well as stress data that can be used to perform initial wing sizing in the structural sizing subgroup.
- Loop 2 'Structural sizing': the coupling routine 'RUN_SBOT' restarts ANSYS, this time for performing a third type of calculation cycle in order to size the skin thickness of the wing. After reaching either convergence or the maximum number of sizing iterations, the updated wing is fed back to the aeroelastic subgroup. This structural sizing can be done either 'in the loop' during aeroelastic calculations, or after the aeroelastic calculation routine has reached convergence.

MatLab is chosen as basic controlling software, calling all other externally incorporated software packages where necessary. The reason for choosing MatLab is twofold: the basic wing model generator is coded in this software package and runs of external software can be intuitively controlled. All coupling routine functions and executables are located in individual folders on the hard disk, and use a standardized subfolder structure to exchange data. The data exchange method allows structured program runs, which are controlled by a single main running function. Calculations from intermediate stages can be resumed if desired. Furthermore, interchange of individual software parts can be done without much administrative effort, which allows either increasing or decreasing the fidelity level and computational cost of program subgroups. Exchanging software within subparts of the routine can also be used to validate and compare result data.







3.1.3 Initial approach and future opportunities

Section Sources: none external sources used

Initial development approach

In order to fulfil the thesis goals described in subsection 3.1.1 within the time limited by the graduation project, it is chosen to focus on building up the entire high-lift device analysis routine using basic external software. Keeping the software flexibility requirements in mind, individual parts of the routine can then be improved in future work by exchanging calculation methods. Four main steps are distinguished in the programming approach:

- 1. Automating basic wing model generation and high-lift device extension
 Both program parts should be easy controllable using a selected set of input parameters.
 Initially, only single-slotted trailing edge devices are considered in order to reduce the required programming effort. Wing model generation is described in section 3.2, high-lift device deployment in section 3.3.
- 2. Creation of an automated parametric connection with three-dimensional aerodynamic software to obtain load distributions.
 - Although in section 2.3.1 it was concluded that a quasi-3D analysis method is probably the most appropriate approach for obtaining wing loading in the design phase aimed for, it is chosen to first model the wing aerodynamics using a pure three-dimensional vortex-lattice method. This implies viscous flow effects are excluded from the routine, due to which flow results should be interpreted with care. Section 3.4 describes the aerodynamic connection created within the tool chain.
- 3. Applying the obtained aerodynamic loads to the wing model and performing structural calculations
 - Initially, a constant material distribution is applied and no sizing is performed. Relatively stiff beam connections combined with simple hinge mechanisms are used to connect the high-lift devices to the main wing. Specialized design of these connections is not considered in the current study. Structural results are used to update the parametric wing model for usage in a following calculations. In section 3.5, the structural connection and results are given.
- 4. Closing the aeroelastic loop, enabling initial aeroelastic iterations

 First, initial aeroelastic iterations are performed using the basic wing model with different high-lift device settings. Thereafter, sizing routine S_BOT is to be incorporated to upgrade the software routine with structural sizing capabilities. The aeroelastic loop is described in section 3.6, whereas incorporation of S_BOT is described in the final section of this chapter: section 3.7.

Future improvement and extension opportunities

Due to the choices made in the development approach as described above, major improvements in the high-lift device tool chain are possible in the part concerning aerodynamics. One could imagine the creation of a coupling to two-dimensional viscous flow calculation software to correct the three-dimensional pressure distribution viscous flow effects. This would lead to more realistically modelled aerodynamics within the high-lift device analysis procedure, thereby allowing analysis of interconnections between structures and aerodynamics on a more solid basis.

Besides improving parts of the software, extensions to the tool chain are also possible in the future. An example of this is the incorporation of a routine checking whether unwanted aeroelastic behaviour such as flutter or divergence occurs.

Chapter 3



3.2 Basic wing model generation

This section discusses the generation of the basic wing model used in the remainder of this chapter. To generate the wing model, the earlier developed parametric model generator 'ParaMAM' described in section 2.2.3 is used.

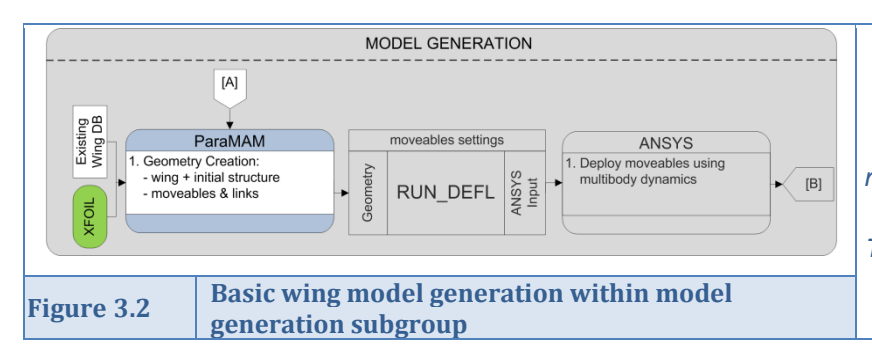


Figure 3.2 shows the model generation part of the high-lift analysis routine, which is treated in the current section. The used wing database is of the CPACS format.

3.2.1 The iGreen / LamAir wing model

Section Sources: [65], [66]

Since the generated software must be incorporated in the DLR wing design chain, it is chosen to use a wing model of a project in which the institute of air transportation systems and technology assessment is involved. The project is named 'iGreen' and is shortly described below, alongside with the general dimensions of the wing under consideration.

The iGreen/LamAir project

The acronym 'iGreen' stands for 'integrated green aircraft', which is a DLR project in which the aeroelastic effects of different technological innovations for future green aircraft are investigated [65]. Examples of such innovations are: the application of larger engines, using thinner wings with laminar-flow profiles or applying new control surface methods. Specific aeroelastic phenomena are explored by using computer simulations and wind tunnel experiments.

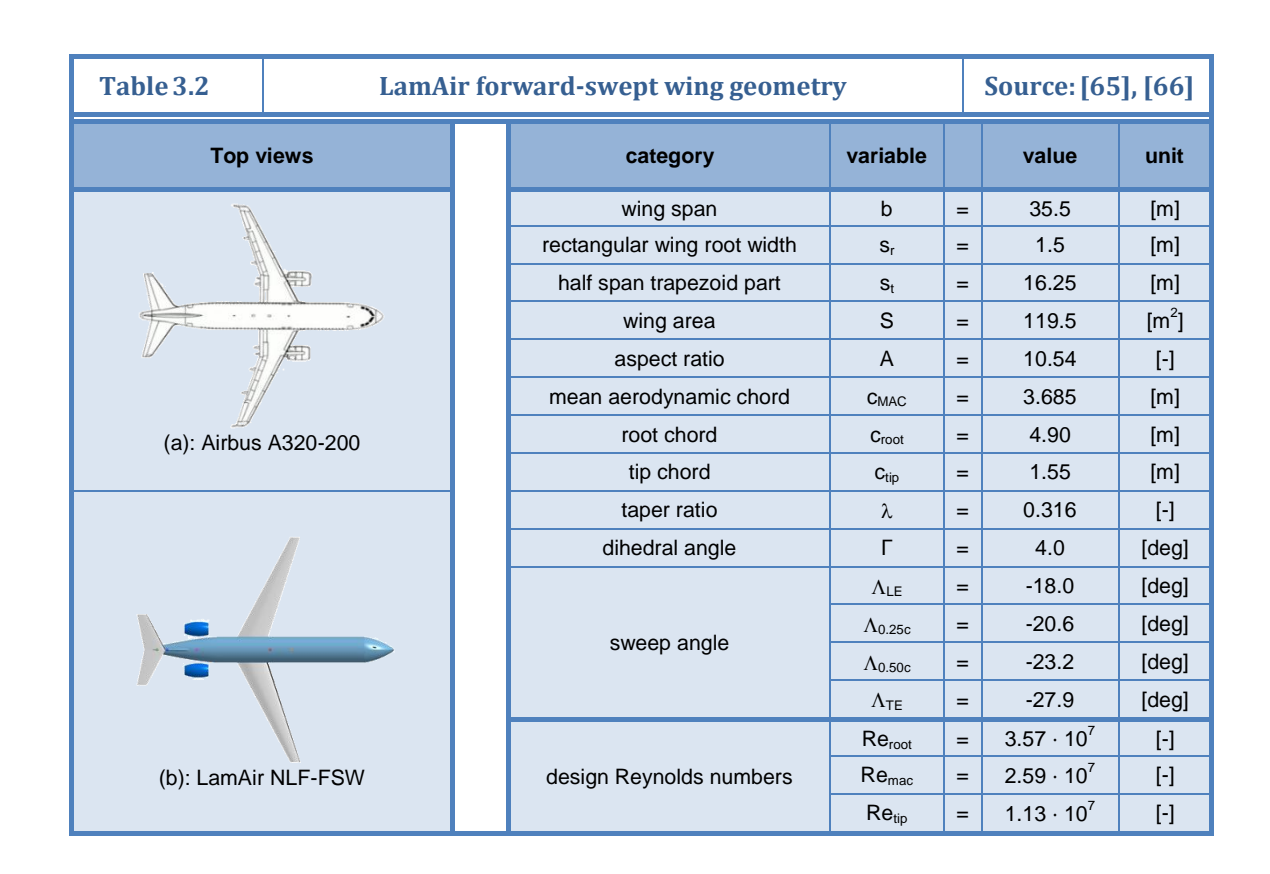
Since one of the technologies to be researched considers the usage of laminar flow technology, it was chosen to use the same aircraft configuration as used in a second project called 'LamAir'. Within this project, a forward-swept transonic laminar wing for short and medium range transport aircraft is designed. The application of forward sweep is chosen within this project to reduce flow instabilities that might cause transition from laminar to turbulent flow conditions. For a constant quarter-chord sweep and taper-ratio, the leading edge sweep angle is lower for a forward swept wing than for a backward swept wing. Thereby cross-flow instabilities and attachment-line transition mechanisms are reduced, making the application of laminar flow technology possible [66]. Large disadvantages of a forward swept wing are found in the reduction of flap and aileron effectiveness due to an increase in trailing edge sweep angle, and an increase in tip-stall problems. The forward swept wing of the iGreen/LamAir project is described hereafter.

The iGreen wing model

Table 3.1 lists the mission requirements the iGreen/LamAir aircraft has to fulfil. The basic wing dimensions are provided in table 3.2, together with a top view comparison of the concept aircraft with an Airbus A320.



Table 3.1	Top-level LamAir mission requiremen	Source: [6	Source: [65], [66]			
category	variable		value	unit		
cruise	M	≥	0.78	[-]		
conditions	altitude	~	30000	[feet]		
payload	150 pax + luggage		13.95	[t]		
	LD3 container		4.00	[t]		
	MTOW	≤	73.5	[t]		
weights	MOE	≤	44.0	[t]		
	MLW/MTOW		0.85	[-]		
ranges	R _{max. payload}	>	1810	[NM]		
	R _{max. fuel}	>	2930	[NM]		
othor	take-off field length	≤	2500	[m]		
other	b	≤	36	[m]		



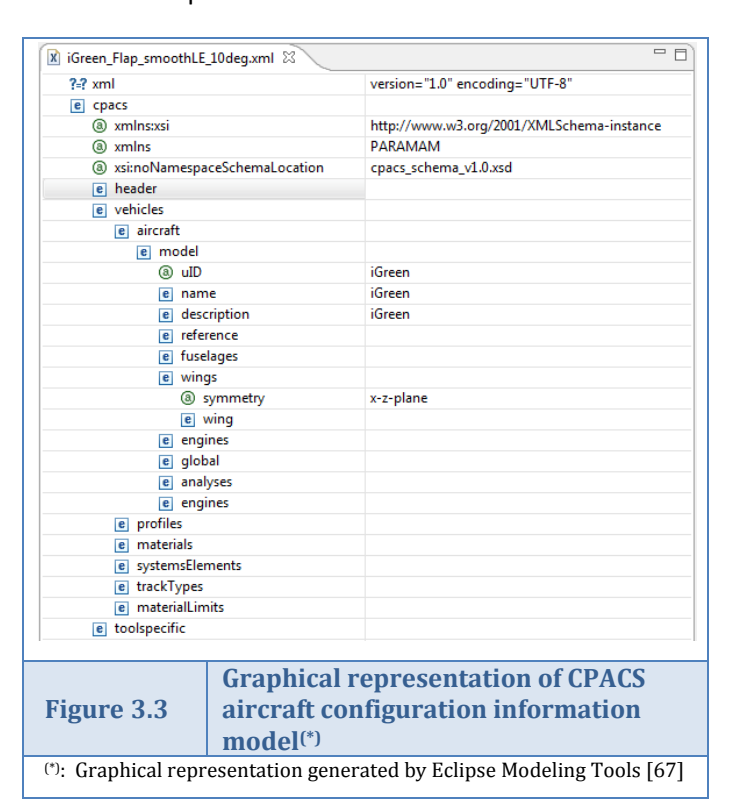
Chapter 3



3.2.2 Model generator connection to CPACS

Section Sources: [67]

The model generator described in section 2.2.3 has been connected to the common parametric aircraft configuration scheme (CPACS)⁸. This aircraft configuration information model is used as an input interface for defining the complete wing geometry. Aside wing geometric data, tool-specific settings controlling the general behaviour of the model generator are also incorporated in CPACS.



One of the major benefits of working with the xml-based CPACS scheme is the possibility to generate graphical representations of the model input settings. This eases the generation of flexible input decks representing complete aircraft models. Figure 3.5 shows a small part of а graphical representation of the iGreen model used in the remainder of this thesis.

3.2.3 Possibilities and limitations in wing modelling

Section Sources: [35], [40]

Currently, the ParaMAM wing model generator is capable of generating a structural base wing model, extended with secondary areas in the form of trailing-edge devices. With usage of the current connection to the CPACS wing information model, these trailing-edge devices can consist of a single-slotted section only. Previous applications of the model generator showed that multiple-segmented trailing-edge devices can be generated using the modelling logic. This is however left as an opportunity for future extensions of the tool chain. The same holds for generation and assessment of leading-edge devices.

The structural model consists of ribs, spars, skin panels and linkage connections. Stringers are represented by added skin panel layers. The thickness and material properties of these layers are set different from the basic skin panel layer, in order to properly represent the added

58

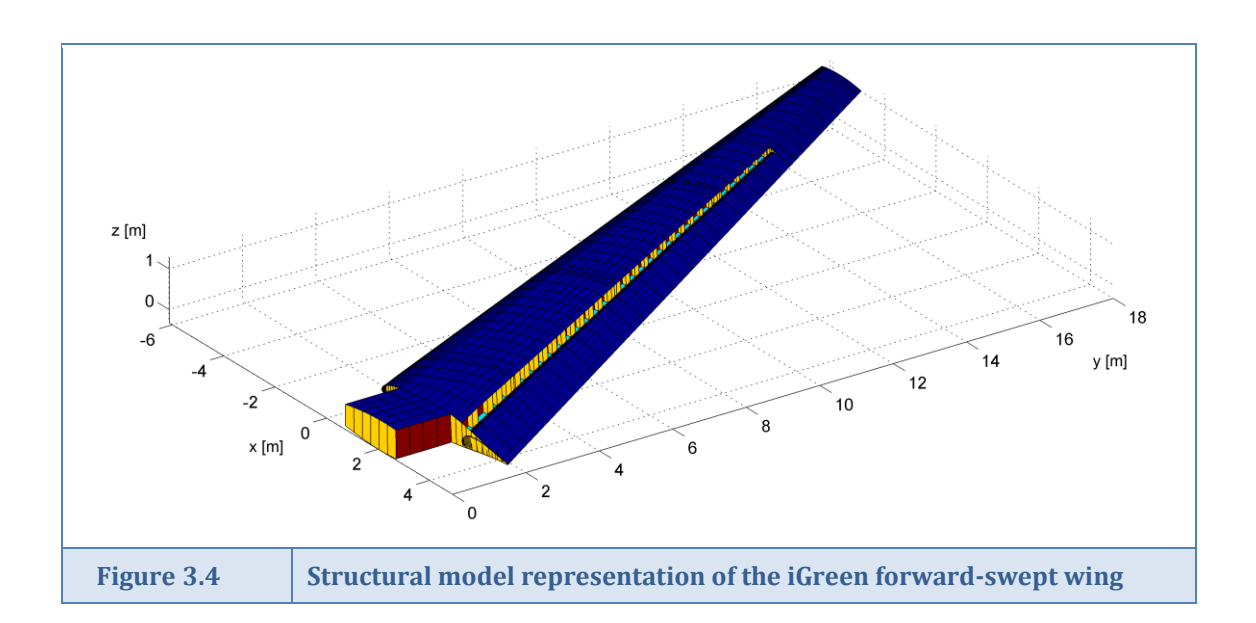
⁸ This connection has been created by co-workers of the German Aerospace Centre (DLR)



stringer stiffness and inertia. Linkages consist of simplified structural connection elements (either circular tubes or a combination of circular tubes and shell areas), which have a double function: structurally connecting the trailing edge devices to the base wing and providing proper degrees of freedom to make the devices deployable. Actuator elements within the linkage definitions provide the means to deploy the high-lift devices to their predefined deflection angle.

Other wing elements, such as spoilers, engine pylons, gear attachments, fuel tanks and winglets are not yet included in the current automated model generator. Most of these were however manually generated in early versions of the ParaMAM wing model generator and can thereby be included in future versions of the automated model generator if required.

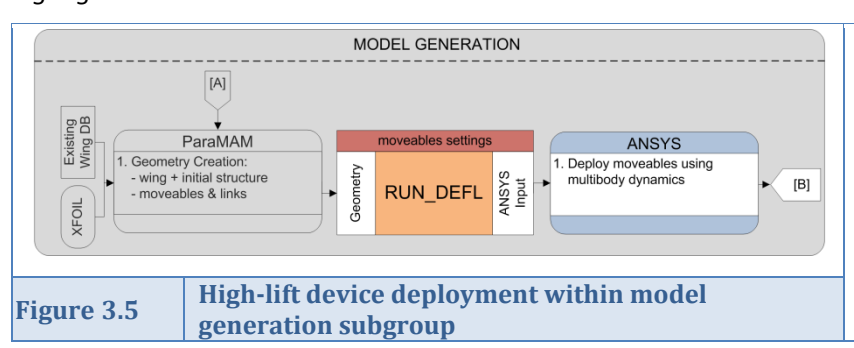
After loading geometrical information from the CPACS aircraft configuration definition, ribspar intersection points are calculated using an advanced branch-and-bound interpolation method based on ray-tracing principles (see [35], [40]). The 'gridapprox' routine that performs these interpolations is used at a later stage in the high-lift device analysis routine to interpolate aerodynamic loads on the upper and lower skin of the structural wing model. Aside the wing geometry, material properties and sizing regions are loaded from the CPACS input file and converted to input decks for usage in ANSYS. The loaded jig-shape of the structural wing model of the iGreen wing is provided in figure 3.5. The figure clearly shows the applied forward sweep angle of the wing, and an uninterrupted single-slotted flap definition covering a large part of the trailing-edge span. At the three spanwise positions where linkages connect this single flap to the base wing, ribs are accumulated to ensure proper structural load transmission. A centre wing box section is added to the model, providing the application of clamped boundary conditions during structural calculations.





3.3 High-lift device deployment using ANSYS multibody dynamics

The multibody dynamics package of ANSYS is used to deploy the high-lift devices according to the prescribed angle(s) defined by the user when setting up the routine. An updated model of the wing is generated, which will be used for aerodynamic model extraction and structural calculations in the following sections. The applied methods within ANSYS multibody dynamics, as well as advantages and disadvantages of using ANSYS for device extension will be highlighted in the current section.



The high-lift devices present on the basic wing model are deployed into their predefined positions, schematically indicated in figure 3.5.

3.3.1 Extending the high-lift devices using ANSYS

Section Sources: no external sources used

At the German Aerospace Centre, one of the finite element software environments used to perform structural calculations is ANSYS. Since ANSYS incorporates a multiphysics software package, complex coupled-physics behaviour of airplane wings can be simulated.

Multibody dynamics using ANSYS

With respect to the current design approach, the main advantage of using the multiphysics package of ANSYS is found in the combined multibody dynamics simulation and structural analysis within a single software title. This largely reduces modelling complexity, since no extra software and model interfacing step is required to represent the kinematics of high-lift devices. Large deformation/rotation effects are directly built into the formulation of the structural finite element mesh and can be turned on or off, dependent on the intended type of structural simulation. Proper modelling of inertial effects is performed by usage of either a consistent mass formulation or by point mass representations when rigid body motion is considered (as discussed in the following paragraph). Interconnection of body parts is done by defining finite motions at joint connections between two nodes, which are located exactly at the same position as in the definition of the wing geometry.

Three major disadvantages can be identified in the usage of ANSYS multibody dynamics to define the kinematic constraints between multiple bodies. To begin with, a multibody analysis requires a nonlinear solution method which is more computationally extensive than a linear structural analysis. However, deployment calculations on high-lift devices is required only once per high-lift system setting to be analyzed, since it is applied before starting the iterative structural sizing module (see figure 3.1). Another disadvantage is that load case combinations are usually not valid for nonlinear analyses. Therefore, extending the high-lift devices has to be performed in a separate ANSYS run and cannot be performed when actual flight loads are



applied to the wing structure. Since ANSYS cannot automatically detect overconstrained models, a last disadvantage is found in increased modelling difficulty. Overconstrained models most often result in non-convergence of the solution, and can even yield incorrect results in some cases. The last disadvantage of using ANSYS for high-lift device deployment calculations implies that joint connections between bodies have to be carefully defined. Performing a modal analysis on the system can provide insight in possible constraining problems. When the obtained number of zero eigenvalues is larger than the number of rigid body modes, the system is underconstrained. On the other hand, when the number of eigenvalues is smaller than the intended number of rigid body modes, the system is overconstrained. Missing or extra constraints can be created by redundant joints performing either the same function or contradictory motion, or by redundant rigid bodies or boundary conditions.

Model reduction using rigid bodies

As described in the foregoing paragraph, no external loads can be applied to the wing during the nonlinear high-lift device extension calculation. The only load applied to the structural model is generated by defining either a stroke to a linear actuator or a rotation to a rotating actuator (which is mostly the case for current transport aircraft). Since internal deformations are not generated during device extension, defining rigid bodies can significantly speed-up calculation time.

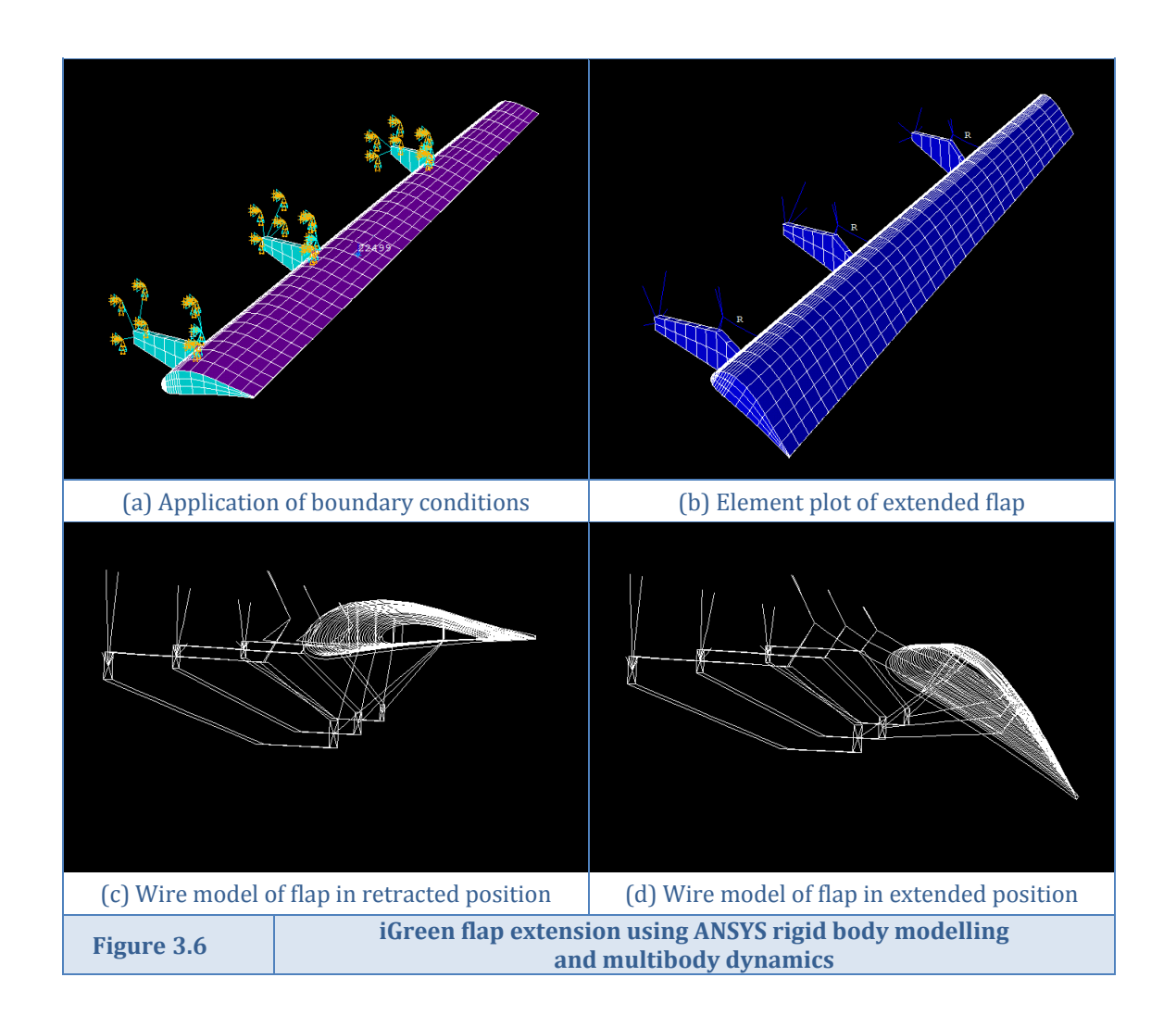
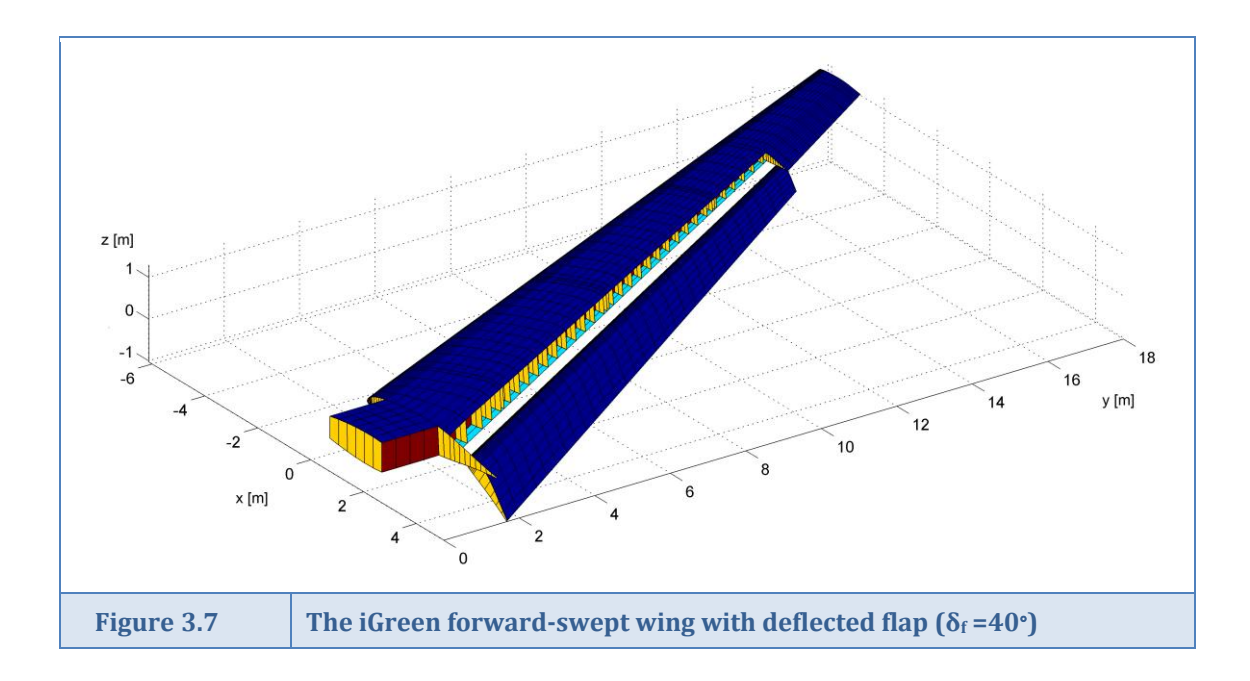




Figure 3.6 provides an overview of the rigid body definition process and subsequent flap extension of the iGreen wing in ANSYS. When comparing figure 3.6(a) to figure 3.7, it can be seen that almost the entire base wing definition has been deselected when performing the nonlinear multibody analysis. To create a basis for constraining the flap subsystem, attachment pods and their wing attachment beams are the only parts left in the calculation. As can be seen in figure 3.6(a), zero displacement constraints are applied to the open ends of the attachment beams, fixing the entire structural subsystem in space. After performing a partial-element solution on the flap elements, flap mass and inertia terms are obtained. Thereafter the structural elements of the flap are replaced by so-called contact elements and a point mass is added to the system to represent the mass and inertia of the deselected flap elements. Finally, a target element is placed at the same location as the point mass, to which all contact elements are rigidly linked. After applying the predefined stroke to the rotary actuator, the nonlinear analysis can be performed, of which the solution is represented in figure 3.6(b). After the solution is obtained, all rigid body elements are replaced by their original structural model parts. The 'R' symbols represent the joint connections of the three rotary actuators. Figures 3.6(c) and (d) contain wireframe plots of the flap system in both retracted and extended position, providing a better insight in the buildup of the structural support system.

After deploying the flap to its final position, the basic wing model generation is finished by updating the wing model in MatLab with the obtained flap displacement. Figure 3.7 shows the updated wing model. The large deflection angle of 40° is chosen to clearly indicate the differences between the wing model in its cruise and high-lift configuration.





3.4 Aerodynamic loading calculation using a vortex-lattice method

The first main pillar of the overall aeroelastic calculation method is the calculation of aerodynamic loads. As described in section 3.1.3, the aerodynamic vortex-lattice software AVL is used as a basis platform for generating the three-dimensional wing load distribution. Main assumptions and modelling rules concerning vortex-lattice models and AVL were discussed in section 2.3.3. The current section describes how basic wing models, either with or without extended trailing edge high-lift devices are converted to equivalent wing models to be used in AVL software. Furthermore, load extraction principles are shown, generating input load distributions which are to be used for loading the structural wing model as described in following section 3.5.

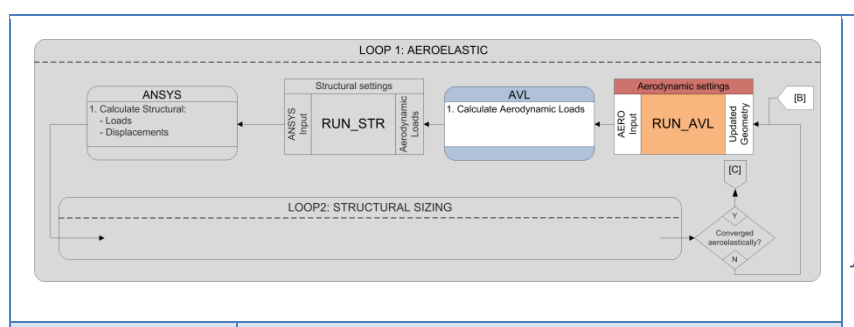


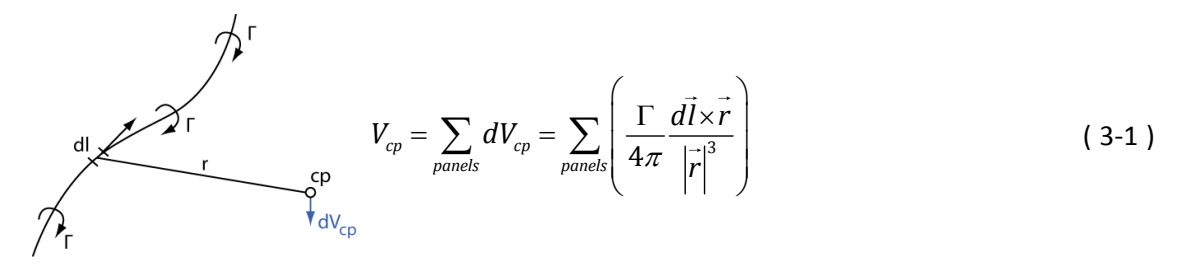
Figure 3.8 Aerodynamic loading calculation within aeroelastic subgroup

After completing the model generation, calculations are performed within the aeroelastic subgroup. Figure 3.8 shows the first subroutine included in this group: aerodynamic loading calculations.

Brief introduction to vortex-lattice methods

Vortex-lattice method is a numerical approach widely used to analyse aerodynamic properties of finite wings [16]. A finite number of horseshoe vortices of unknown strength Γ_i is superimposed on a panelled grid representing the wing, as sketched in figure 3.9(b). Per individual panel, a bound vortex line is placed at a distance I/4 from the front of the panel, and two trailing vortex lines extend to $+\infty$, as sketched in figure 3.9(a). Aside a horseshoe vortex, a control point is placed at around $\frac{3}{4}$ of the panel length, its exact position being dependent on the lift curve slope of the section it represents.

At each control point, the total normal velocity induced by the complete lattice of horseshoe vortices can be obtained by summing the individual contributions per horseshoe element calculated using the Biot-Savart law:



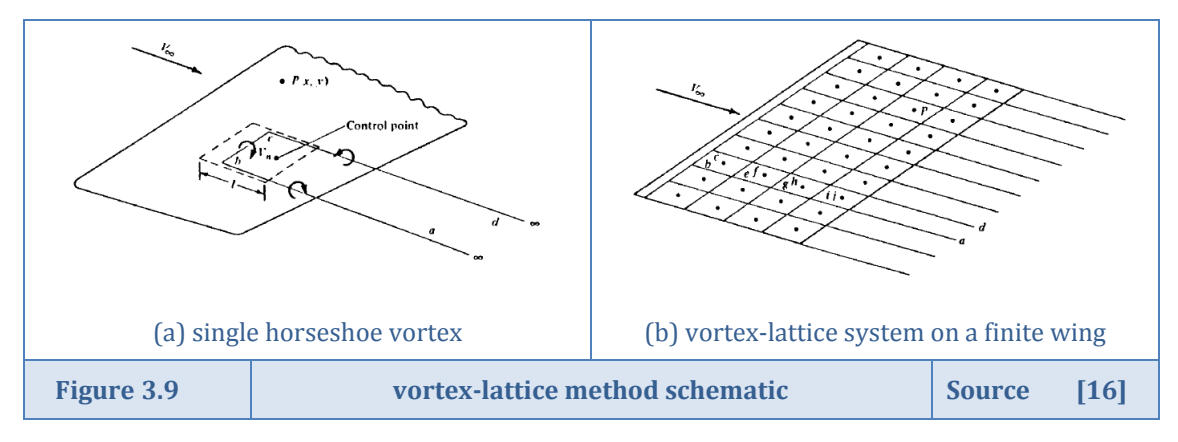
⁹ A vortex filament of strength Γ bound to a fixed location in a flow is not allowed to end in the fluid according to Helmholtz' vortex theorems. Therefore it is assumed to continue as two free vortices moving along with fluid elements through the flow and thereby extending to $+\infty$. Due to its shape, this set of vortices is commonly referred to as a *horseshoe vortex*



By applying flow-tangency boundary conditions at the control points, a system of equations is obtained, which can be solved for the unknown horseshoe vortex strengths Γ_i . Knowing the vortex strengths of the lattice representing the wing model under consideration, the Kutta-Joukowski theorem can be applied to obtain the lift distribution along the wing:

$$L_i = \rho_{\infty} V_{\infty} \Gamma_i$$
 (in which i = vortex filament number) (3-2)

For a more extensive description of vortex-lattice methods, the reader is referred to [16] and [68].



3.4.1 Vortex-lattice model generation for AVL

Section Sources: [61], [69], [70], [40]

The current subsection provides a step-by-step overview of the generation of the vortex-lattice model from the available basic wing model (see sections 3.2 and 3.3) used in aerodynamic calculation software AVL. First, geometrical modelling restrictions for usage within AVL are discussed, after which the model generation is described. The subsection ends with a description of the vortex lattice grid generation, including the way in which the model copes with vortex-lattice grid requirements.

AVL input method

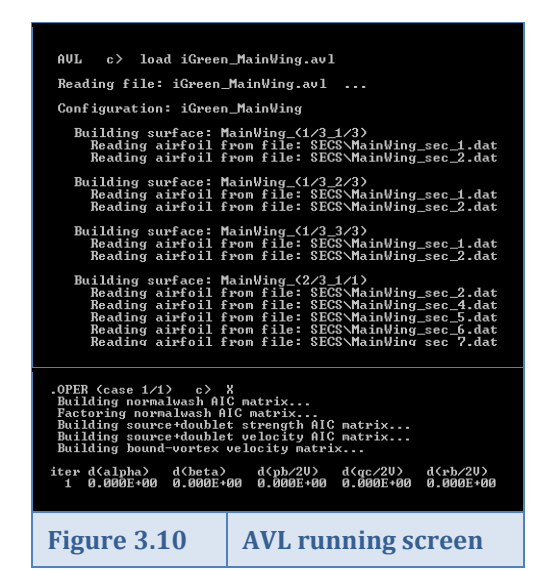
In order to run AVL in batch mode, the following input files need to be generated for the aerodynamic model named 'jobname':

- geometrical input file (jobname.avl)
 the geometrical input file describes the complete wing geometry and grid generation
 settings. The methods applied to obtain this input file are described in the paragraphs
 'aerodynamic model generation' and 'vortex-lattice grid generation' of the current
 subsection.
- runcase input file (jobname.run) and mass input file (jobname.mass)
 in the runcase and mass input files, the environmental and flight condition settings are
 provided. During the buildup of the aeroelastic subgroup, the single runcase as defined in
 table 3.3 is set during aerodynamic calculations. When performing a structural sizing run on
 a wing model, multiple flight conditions should be considered, thereby incorporating all
 boundaries of the airplanes' flight-envelope.



- batch file (jobname.bat)
 the batch file is called by the operating routine and runs AVL with the proper input command listing
- command listing (jobname.cli)
 contains AVL running commands, which loads all input files, performs the calculation and saves result datadecks
- section data files (area_section_##.dat)
 normalized and derotated airfoil coordinate files used for determination of wing camber distribution. These coordinate files are loaded by the geometry input file.

Table	3.3	AVL r	runcase definition for iGreen calculations								
input file	category		variable			value	unit				
runcase input	angles		angle of attack	α	=	0	[deg]				
			sideslip angle	β	=	0	[deg]				
	rotation rates		roll rate pb/2V		=	0	[-]				
			pitch rate	qc/2V	=	0	[-]				
			yaw rate rb/2V			0	[-]				
			flight Mach number	Mach	=	0	[-]				
mass	default		gravitational acceleration	g	=	9.80665	[m/s ²]				
input	consta	nts	air density	ρ	=	1.225	[kg/m ³]				



The latest release of AVL (v. 3.27, see [61]), can perform both interactive and batch runs. From the available AVL source code (written in Fortran 77), a renewed version was compiled¹⁰, which is able to perform quicker calculations in a batch run due to removal of all plotting functions. During the course of this master thesis, it was found that both aforementioned AVL versions are not able to handle wing models incorporating a large amount of vortex panels due to array size limitations. Using the G77 Fortran compiler (source [69]), a third AVL version, able to handle larger strip arrays was therefore created from the AVL source code by the author of this thesis. The original AVL version able to perform interactive runs should be consulted when proper loading of the model geometry is to

be checked. Figure 3.10 shows part of an automated AVL batch run.

In order to be able to perform batch calculations using MatLab as routine controlling software, automated AVL connection functions are programmed. Function AVL_INP generates the input decks listed above, based on user settings in predefined cell arrays. Functions AVL_OUT and subfunction AVL2MAT extract AVL result data and convert this to useable MatLab result arrays. The scarcely available result data is used to regenerate the wing grid and camber distribution and obtain the calculated dCp-distribution along the wing. Since the plotting capabilities of AVL

 $^{^{10}}$ AVL source code adjustments were made by Björn Nagel of the German Aerospace Centre (DLR)

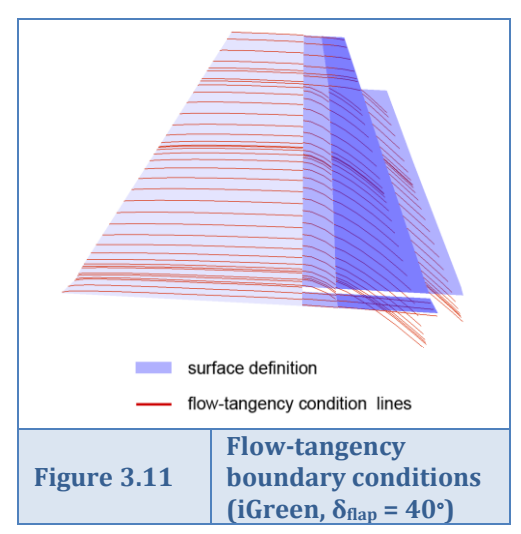


are very limited and in the inconvenient postscript format (and in a batch run even unavailable), the function AVL_PLOTRES provides plotting capabilities in MatLab.

Geometric modelling restrictions within AVL

A number of restrictions limit the geometrical modelling of the vortex-lattice calculation grid. As earlier discussed for general vortex-lattice methods in section 2.3.3; trailing vortex legs are not allowed to closely pass downstream control points, spanwise vortex spacing must be smooth and both spanwise and chordwise discontinuities in the wing model locally require denser grid spacing.

In AVL, surfaces and trailing wakes are represented by single-layer vortex sheets, due to which trailing legs area assumed parallel to x-axis. This implicates that the geometry of the wing itself is not rotated due to airfoil incidence angle, highlift device deflection angle or wing angle of attack. Instead, these conditions are considered in the model by modifying the flow-tangency boundary condition on the airfoil camber line. As an example of this modelling technique, figure 3.11 clearly shows the rotation of strip camber lines at surfaces representing the trailing-edge flap of the iGreen wing due to the applied deflection angle. The surfaces itself are neither cambered nor rotated.



Airfoil definition data has to be in a derotated and chord normalized format. Furthermore, the airfoil definition must have a sharp leading edge for the spline inversion method within AVL to work properly. Position and chord data within the geometric input file is used scale the sections and place these at their correct positions within three-dimensional space. Before writing the section data files, tolerance checks are performed on the input data to make sure airfoil point spacing is within AVL limits.

Multiple surfaces¹¹ having different chord ranges have to be used in order to resemble wing gaps within AVL. These surfaces have to align perfectly to avoid grid alignment problems. When a wing model consists of multiple chordwise surfaces, profile generation can be done by either interpolating a separate airfoil definition, or by indicating which chord range of the parent airfoil is represented. The latter method is used at the primary (base) wing area and when high-lift device deflection angles are set to zero.

Vortex-lattice model generation

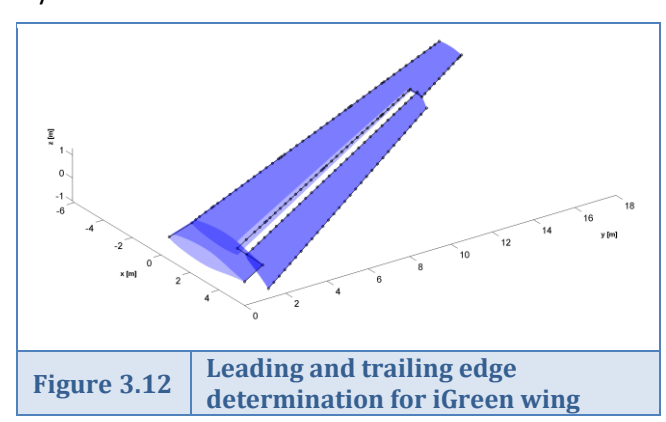
With the aforementioned modelling restrictions in mind, aerodynamic model generation is performed within two steps. First, airfoils for the vortex-lattice grid are obtained from the available structural model created by the model generator in sections 3.2 and 3.3. Thereafter, geometrical and section input files are created, in which grid settings for the vortex-lattice grid are provided. The parametric model description is coded as general as possible, such that a large range of wing models can be connected to the software routine by adjusting CPACS input data.

.

¹¹ in the aerodynamic wing model definition, a *wing* is built up of one or multiple *areas*, consisting of one or more *surfaces* having two or more *sections*.



To provide consistency across both the structural and aerodynamic discipline involved in the aeroelastic subgroup, the basic wing model description is adjusted to generate a proper basis for interpolating airfoil definitions. Since in a wing the largest part of the implied forces is transferred through the wing torsion box, this is the main region of interest for structural grid generations. Regions in front of the wing front spar and behind the rear spar therefore require a low amount of structural nodes. For aerodynamic model descriptions however, this nose section is of large interest since it influences the development of the flow around the wing. For this reason extra nodes are introduced in front of the leading edge, bunched at the leading edge of the wing. The improved roundness of the nose section however comes at the cost of increased structural computational requirements. The increase in computational effort is somewhat relaxed by assigning a relatively low stiffness to the additional elements generated by the extra nodes.



Since no actual aircraft fuselage section is modelled, the wing model is extended to the wing symmetry plane to incorporate root effects in the aerodynamic model. The centre wing box is replaced by this extended section. For this updated basic model, leading and trailing edge definitions are extracted using the known structural rib definitions, as shown in figure 3.12.

Knowing the outer regions of the wing hull, the positions requiring an airfoil definition are extracted from the wing model. It is thereby strived to obtain as little airfoil definitions as possible, in order to obtain the most elementary description of the wing geometry as required for performing rapid load calculations. Three categories of profiles are distinguished, as shown in figure 3.13 and described hereafter:

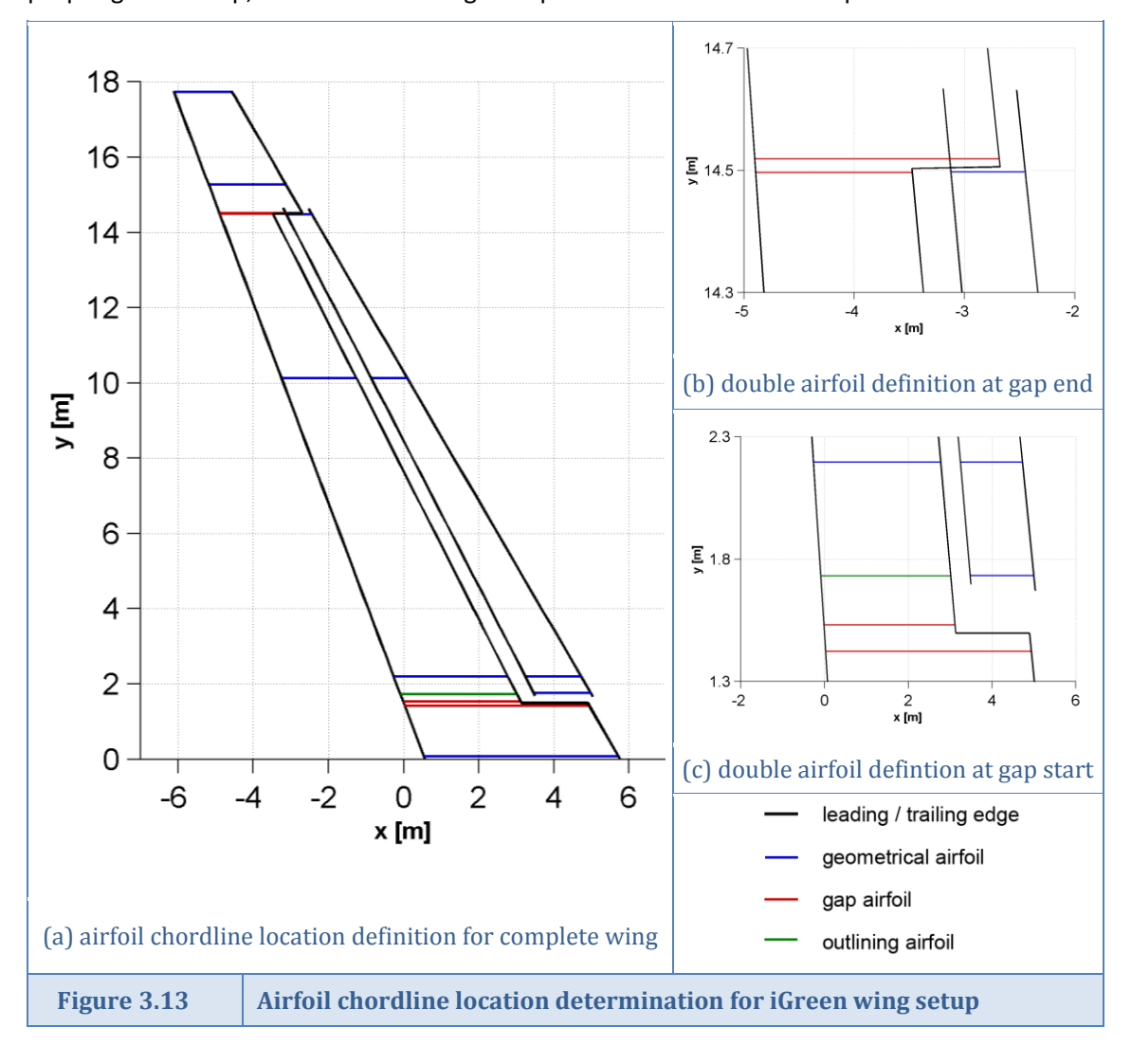
- geometric profiles are based on ribs that introduce changes in basic model geometry. Five types of geometric changes are under consideration: rib airfoil definition, wing sweep, wing dihedral, taper ratio and incidence angle changes. Root and tip profiles at the outer edges of wing area are included in this profile type, coloured blue in figure 3.13(a). At the main wing, the profiles at y-coordinates 2m, 10m and 14,5m introduce rib airfoil definition changes. The same holds for the profiles at these locations within the flap region of the iGreen wing. A small outboard and inboard offset is applied to respectively the root and tip profile, to guarantee profile points will be found by the interpolation routine. After completion, the resulting airfoils are placed at their original position.
- gap profiles mark the start or end of a gap in the leading or trailing edge of the areas making up the wing. For the iGreen wing model, a single trailing edge gap is present at the main wing area, providing space for flap storage in cruise conditions. Per gap profile, two airfoil interpolations are performed: one just outside and one just inside the gap definition. As depicted by the red coloured profile locations in figures 3.13(b) and (c), an offset from the exact geometrical location is applied to ensure obtainment of the correct airfoil definitions. After finishing the interpolation routine, the two resulting airfoils are placed exactly on top of each other and scaled accordingly.
- outlining airfoils are placed at spanwise positions where areas other than the area under consideration require profile definitions. These airfoils are marked green in figure 3.13. This last category of profiles is used to ensure proper spanwise vortex-lattice grid outlining.



Spanwise outlining is at its turn required not to let trailing legs of the horseshoe vortex filaments closely pass downstream control points. If this is the case, the flow solution becomes erroneous since the radius vector r from vortex filament segment dl to control point cp approaches zero in the numerator of equation 3-1.

Since the hinge line of the flap deployment system of the iGreen wing is skewed, the flap does not deflect purely in a streamwise direction but translates slightly in y-direction. After deflection, the root airfoil of the flap does not coincide with base wing airfoil distribution, due to which an outlining airfoil has to be placed at the main wing area of the iGreen wing.

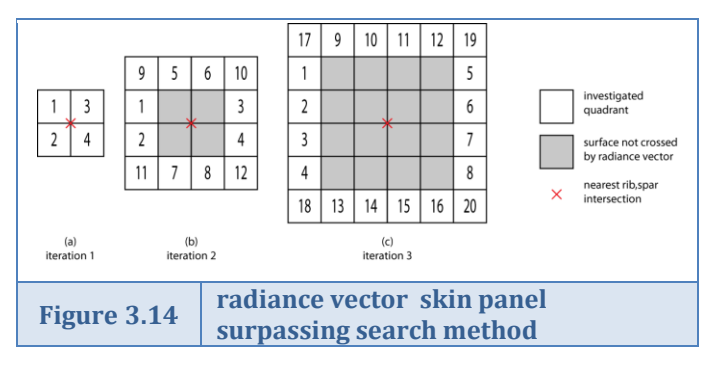
The complete distribution is checked for chordlines defined near to each other. Chordlines having a low in-between distance are merged in order to obtain a profile distribution allowing proper grid buildup, since at least a single strip has to fit in between the profiles.



With the airfoil locations known, base airfoil interpolation points are determined by applying cosine spacing along the known airfoil chordlines. Before applying the interpolation routine 'gridapprox' in order to obtain the vortex-lattice airfoil definitions, radiance vectors have to be determined, defining the search range per profile point. These radiance vectors are oriented perpendicular to the chordlines, as can be seen in figure 3.15(a) and (c). For each profile point,



barycentric coordinate logic¹² (see [70]) is used to determine the skin panel which is surpassed by the radiance vector. The four edge points of this specific skin panel are then used to determine the minimum and maximum distance between the base point and surpassed skin panel. A linear spacing is applied to generate radiance points along the radiance vector, with the determined minimum and maximum as extremes. An advanced branch and bound method is applied by gridapprox [40] to obtain the minimum distance to the wing skin for all radiance points. A final spline interpolation among the radiance vector points finally determines the x,z-coordinates for each profile point.



The order in which the skin panels are investigated for radiance vector surpassing is provided in figure 3.14. For each base airfoil interpolation point, the nearest structural rib-spar intersection marks the starting point for the search. Iterations are performed until the crossed skin panel is obtained. Using this method in

combination with the gridapprox routine allows finding arbitrary oriented wing slices, although in the current method pure x,z-interpolation is used. Figures 3.15(a) and (b) show the applied method for profile number 2, being the gap starting profile for the iGreen wing. Figures 3.153.9(c) and (d) show the method for the section placed at y = 14.5m. From the latter, it can be seen that multiple structural rib section definitions can be crossed when interpolating a single airfoil.

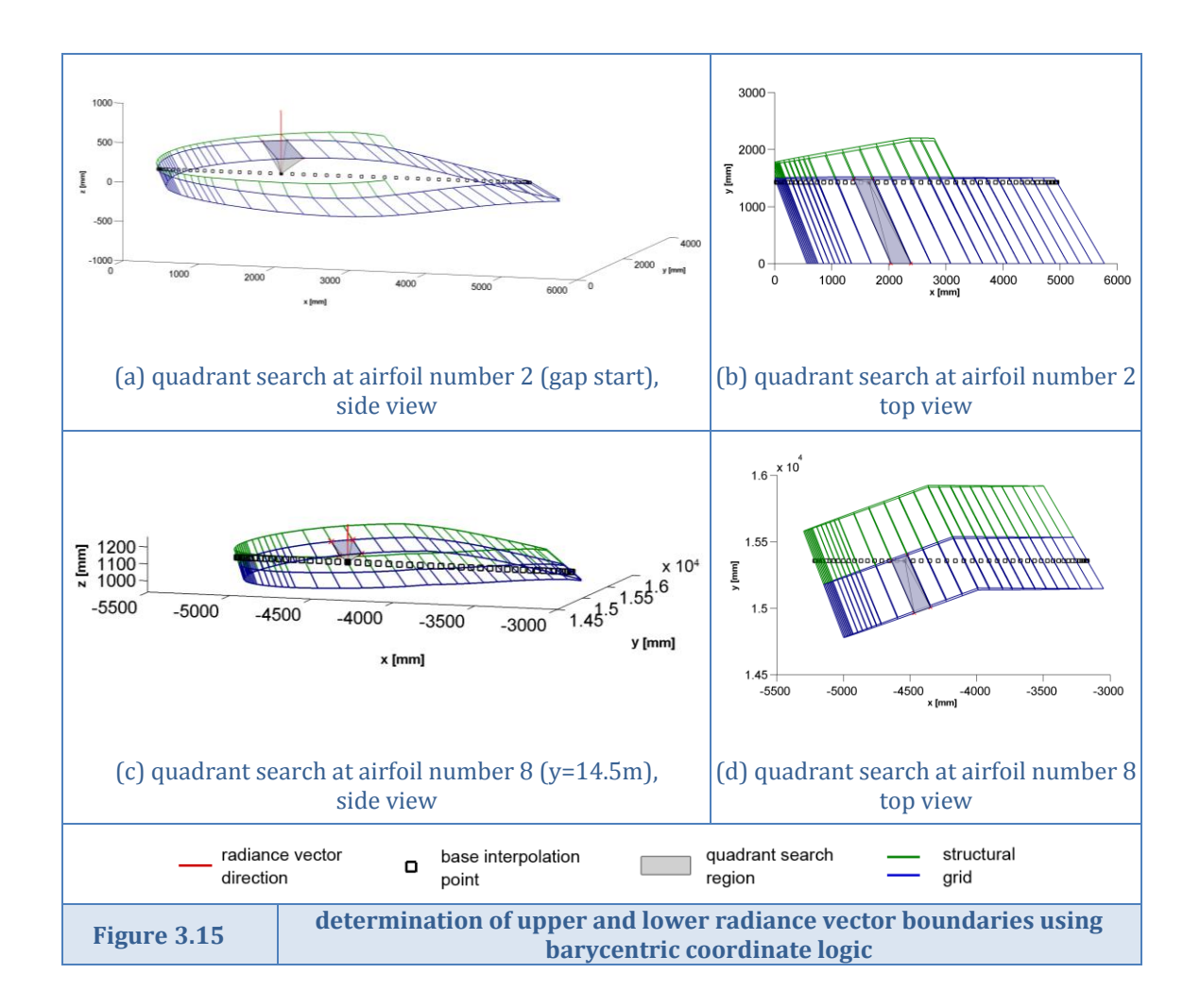
Figure 3.16 shows the obtained radiance vectors for the complete wing, as well as two-dimensional views of these vectors for gap starting sections and the section at y = 14.5m. For each base interpolation point, the radiance to the upper and lower skin is obtained and saved in the final airfoil coordinate array. The positioning of the root, tip and gap profiles is updated to comply with actual geometrical location and up-/downscaled accordingly. Among the profile definitions, basic positioning data is obtained for later usage in AVL input file arrays.

The final airfoil distribution for the iGreen wing setup is provided in figure 3.17. Due to the readily available structural grid and dense radiance vector point distribution, the uncertainty in interpolation for this wing is less than 1 cm.

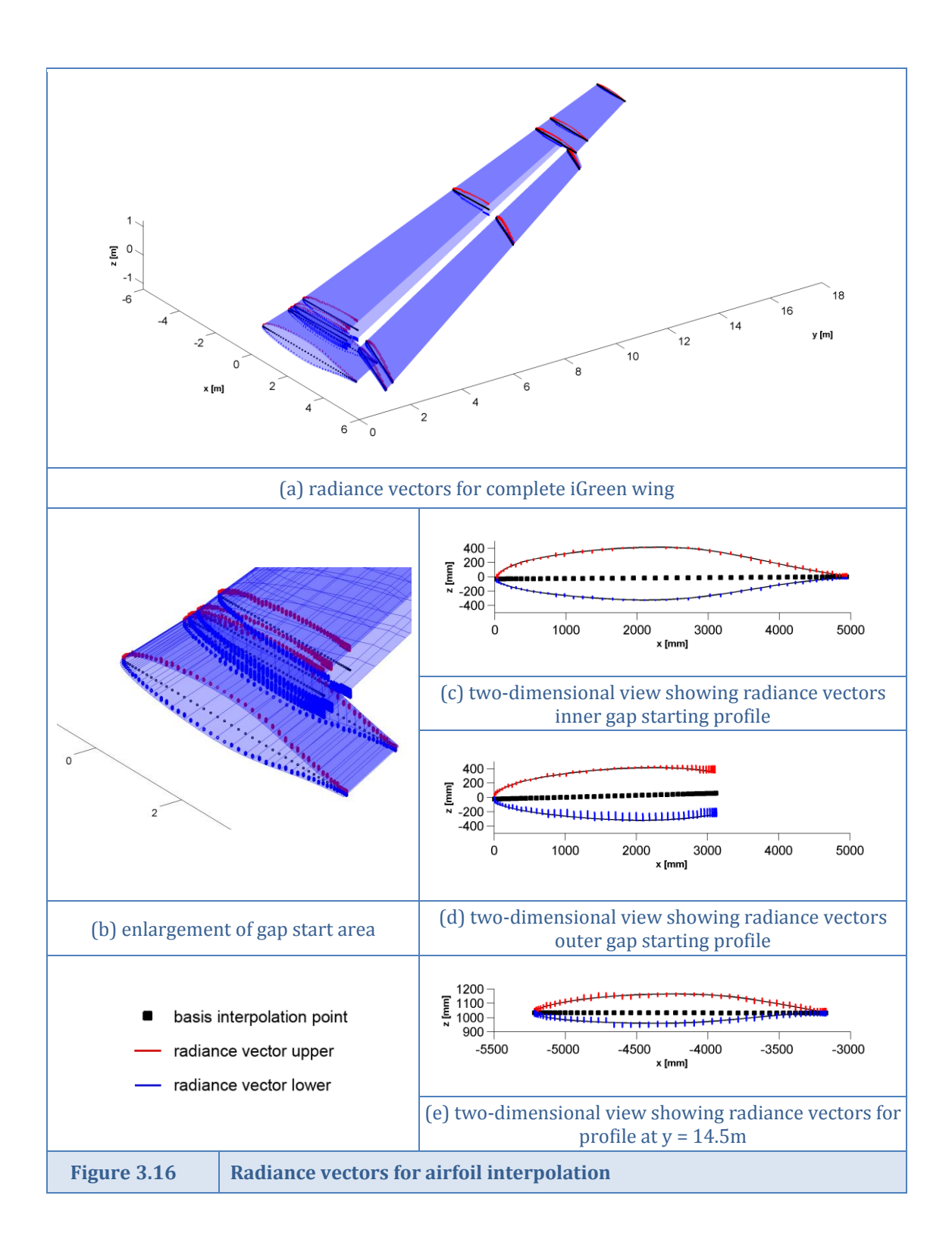
69

¹² barycentric coordinates describe the location of a point in two-dimensional space expressed in ratios of the vertices of a triangle, in three-dimensional space the location of a point is expressed in ratios of the vertices of a tetrahedron. If - for a specific point - all ratios are between 0 and 1, the point is contained within the triangle (2D) or tetrahedron (3D).

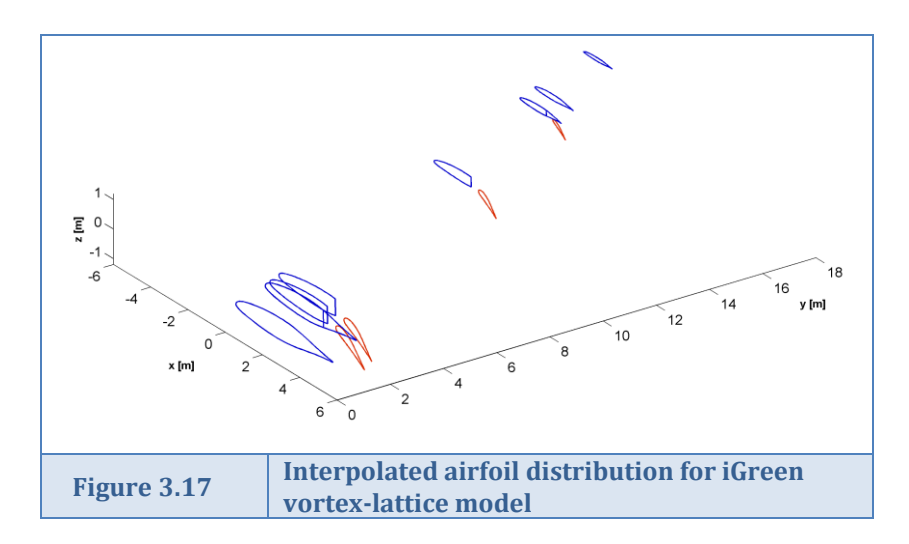












Vortex-lattice grid generation

Knowing the interpolated airfoil distribution as depicted in figure 3.17, two types of vortexlattice grids can be generated:

- a grid model representing the actual geometry (method 1 in figure 3.18(a))
 The gap in between the main area and the extended high-lift device(s) is modelled in the vortex-lattice grid. The actual gap and overlap values are converted to the positioning and axis system used within AVL, in order to properly place the high-lift devices. The flat vortex-lattice grid panels are coloured green in figure 3.18. The camber distribution, defining the normal velocity direction at the control points of the grid panels is coloured red.
- a grid model containing a filling panel distribution (method 2 in figure 3.18(a))
 The geometrical gap is replaced by a fill area connecting the high-lift device grid to the main wing area. As described in section 2.1.3, the five flow effects introduced by slots between wing and high-lift device surfaces mainly influence viscous flow effects, such as boundary layer development. Since vortex-lattice methods are based on potential flow theory, these viscous flow effects are absent in the vortex-lattice flow field. Therefore, filling the gap and thereby generating a more consistent panel distribution might be allowed. In section 4.2 it is investigated if the gradual increase of camber angle introduced by the filling area provides better or worse load distribution results than actual gap modelling. This second gap modelling method is often seen in literature.

Effects of extending high-lift devices other than the creation of slots between wing surfaces, being chord extension and local camber increase, are modelled similar in both methods.

To build up the vortex-lattice grid, the wing area is subdivided in multiple surfaces as shown in figure 3.18(b). The user defined spacing settings as shown in table 3.4 are used to calculate the number of spanwise and chordwise panels per individual surface. For surfaces regions requiring vortex outlining, the most dense vortex setting is used. A cosine spacing setting is applied to bunch vortex panels at positions where large vortex strength changes occur. The vortex-lattice grid and camber distribution in between the sections making up a surface is determined by linear interpolation.

A thick airfoil correction obtained from 2D potential flow theory is applied to the lift curve slope of the airfoil sections making up the wing:

$$\frac{dc_l}{d\alpha} = \left(1 + 0.77 \frac{t}{c}\right) \cdot 2\pi \tag{3-3}$$



Table 3.4 User input method of vortex-lattice spacing settings											
area	area spacing direction		# panels	p e r	chord/span range	# panels	p e r	chord range	# panels	p e r	chord range
main	chordwise	cosine	5	m	0.00 < c < 0.50	4	m	0.50 < c < 1.00	3	m	1.00 < c
wing	spanwise	cosine	4	m	0.00 < s < 0.50	3	m	0.50 < s < 1.00	2	m	1.00 < s
flap	chordwise	cosine	5	m	0.00 < c < 0.50	4	m	0.50 < c < 1.00	3	m	1.00 < c
пар	spanwise	cosine	4	m	0.00 < s < 0.50	3	m	0.50 < s < 1.00	2	m	1.00 < s

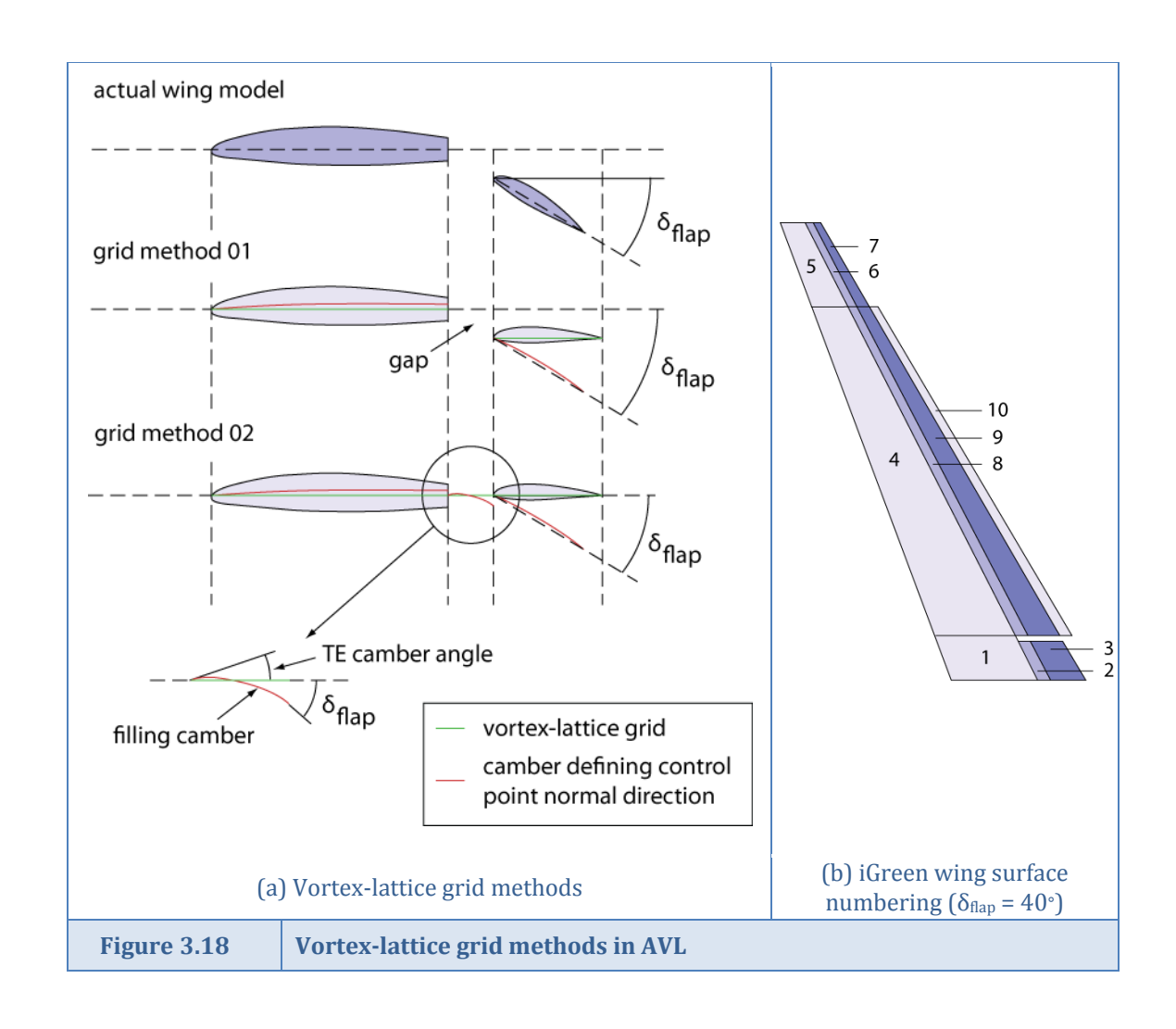
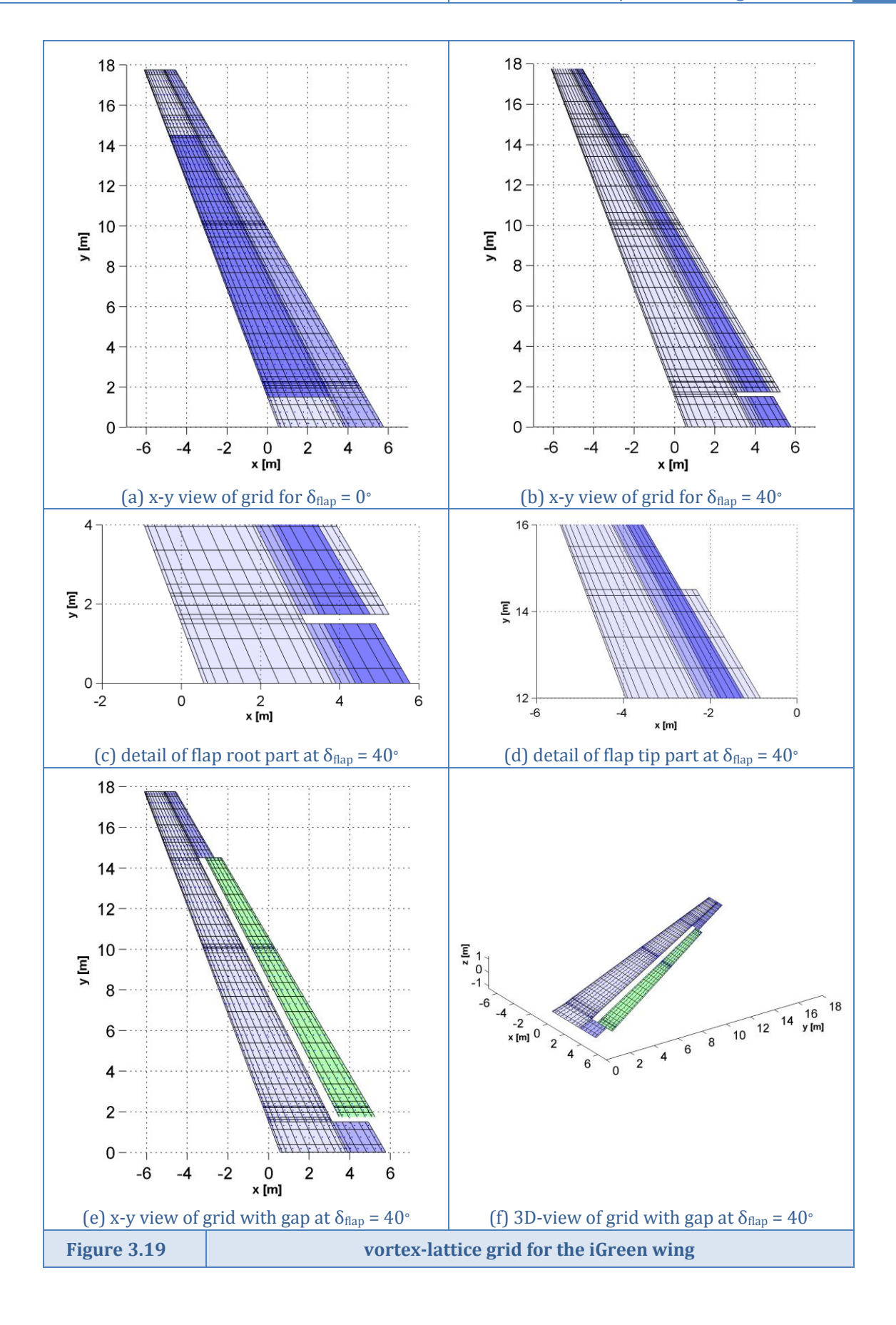




Figure 3.19 shows the vortex-lattice grid used for calculations on the iGreen wing. When the flap is not deflected, the wing is built up of six separate surfaces, as can be seen from figure 3.19 (a). The spanwise and chordwise bunching of vortex panels near locations introducing geometrical discontinuities is clearly visible. After application of a flap deflection, the number of surfaces making up the wing differs per grid generation method. The grid containing a filling surface at the location of the flap gap requires four additional surfaces to ensure proper chordwise vortex outlining as is seen in figure 3.19b(b). Parts (c) and (d) of this figure provide details of this grid, clearly showing the results of chordwise vortex outlining measures. When the gap between main wing and flap is maintained, no additional surfaces are required. As depicted in figure 3.19 (e), the wing is split up in two separate areas, the wing containing five surfaces and the flap containing a single surface. No chordwise outlining is required between the two individual areas. Spanwise vortex outlining methods are however maintained to make sure no vortex trailing legs closely pass control points of the flap at small deflection angles. Finally, figure 3.19 (f) provides a three-dimensional grid view showing the downward displacement of the flap area.

As stated earlier in this section, the required geometrical input file and section files describing the complete grid geometry are generated by the function AVL_INP. Having built up the grid, a AVL batch run can be performed. Extraction of the results and interpolation on the structural model representation are the subject of the next section.







3.4.2 Load extraction from AVL result datadecks

Section Sources:

[71]

The current subsection elaborates on processing the scarce available result data from AVL. The flat grid generated for the vortex-lattice calculation has to be adjusted in order to include camber and proper positioning of secondary wing areas, such as flaps. The method used for interpolating the aerodynamic pressure data on the structural grid is described as well.

Result data available from AVL

Four types of result datadecks are available after running an AVL calculation. In increasing order of detail these are: total force coefficient data applicable to the complete wing model, force and moment coefficient data per surface, force and moment coefficient data per strip and geometric as well as pressure difference data per vortex element. Since both bending and torsion of the structural wing model is to be considered within the structural calculation routine, force data per element is required in order to attain the required force distribution along the entire wing. Force and moment coefficient data per surface is used to check for correctness of the interpolation routine described in the paragraph hereafter.

Unfortunately, the element result datadecks only contain information concerning the location of bound vortex midpoints and resulting pressure coefficient difference (dCp) values across the panel represented by the bound vortex. Since a complete definition of the vortex-lattice geometry is required for performing force interpolations on the structural model, the entire grid definition has to be rebuilt in MatLab. Therefore, the grid generation method used by AVL was reprogrammed in MatLab with the aid of the source code of AVL in the Fortran77 coding language. Using the result point data, the original grid is re-obtained by applying the spacing rules extracted from AVL in combination with application of grid extrapolation methods.

With the original geometry of the vortex-lattice grid available, the dCp data can be extrapolated to the actual geometrical boundaries describing the wing model. Furthermore, the result data of the separate surfaces can be interconnected to avoid gaps at surface interconnections that causes incorrect force distribution results after interpolation. Two extrapolation methods are distinguished:

- Extrapolation and interconnection generating a continuous dCp-distribution

For three different flap deflection angle settings, resulting dCp-distributions using the continuous interpolation method are provided in figure 3.20. Large dCp-peaks occur along the leading edge of the main wing. This is as expected for vortex-lattice calculations (see for example [71], pp. 346), although the behaviour is somewhat exaggerated due to the applied extrapolation method. As can be concluded from part (c) of the figure, showing x-z views of the dCp-distribution along the wing model, the large peaks values are halved already at the start of the second vortex panel row. Adding the fact that vortex panels are bunched at the leading edge, the actual force contribution on the structural wing model is therefore not as large as the pressure peaks might initially suggest.

The influence of extending the large trailing edge flap of the iGreen wing results in an upward shift of the dCp-distribution area, indicating an increase in overall pressure on the entire wing. Furthermore, steep camber gradients introduce a second pressure peak near the leading edge of the flap section. The increased strengths of vortex filaments of the deflected flaps introduce higher upwash values at the main wing, thereby increasing the pressure on the main wing as well.



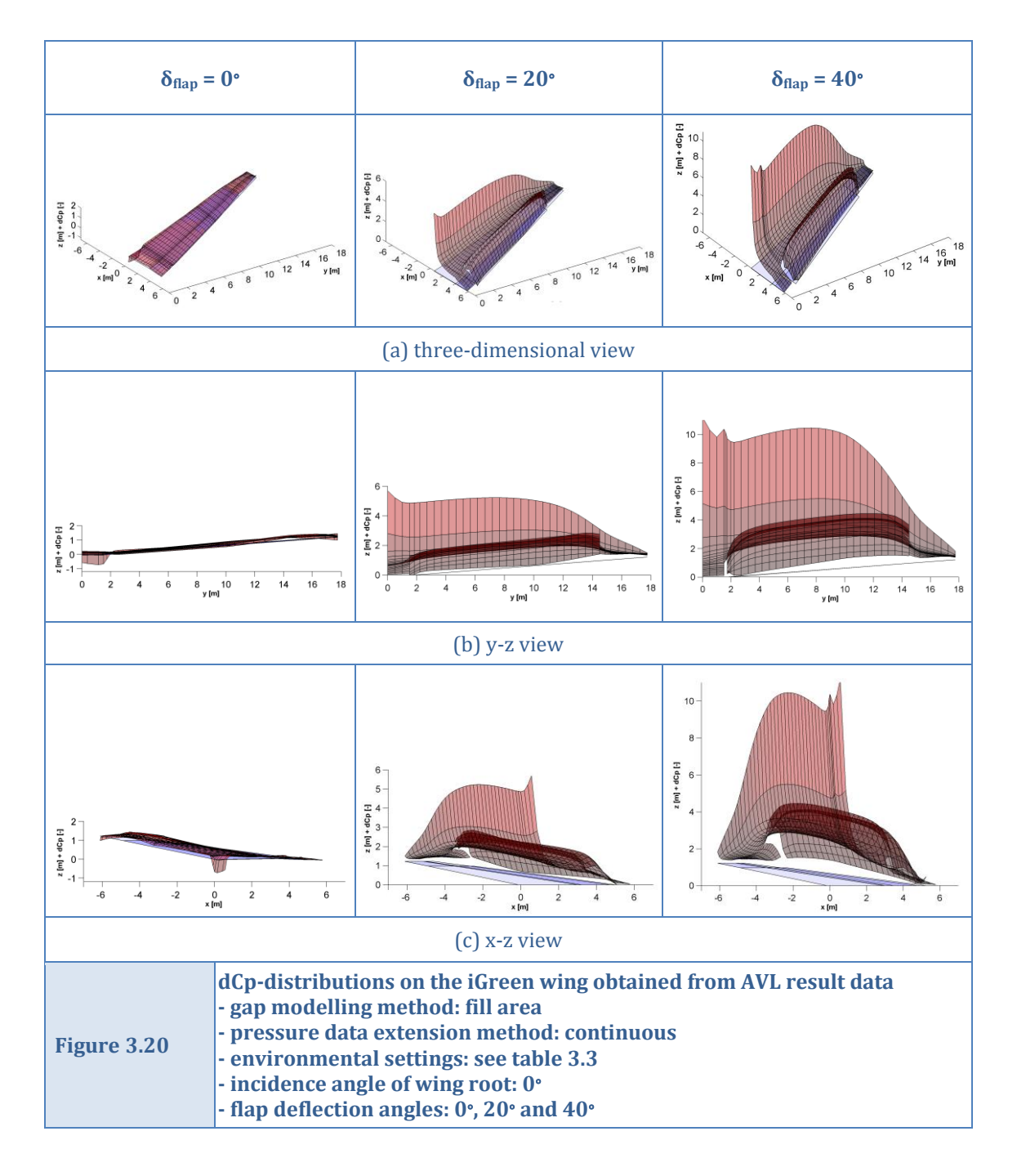
A last comment on figure 3.20 concerns the small negative pressure peak at the wing root in zero flap deflection conditions. A possible explanation for this small discrepancy is found in the interpolation of profile data. The two sections making up the wing root surface (0 m < y < 1.5 m) have the largest chord values. Since the number of interpolation points is constant for each profile, the nose roundness is the worst for the sections under consideration. Initial dCp-distribution results showed similar negative pressure peak behaviour, but extended along the complete leading edge of both main wing and high-lift devices. This has led to an updated definition of nose roundness in the generated wing model, as was described in section 3.4.1.

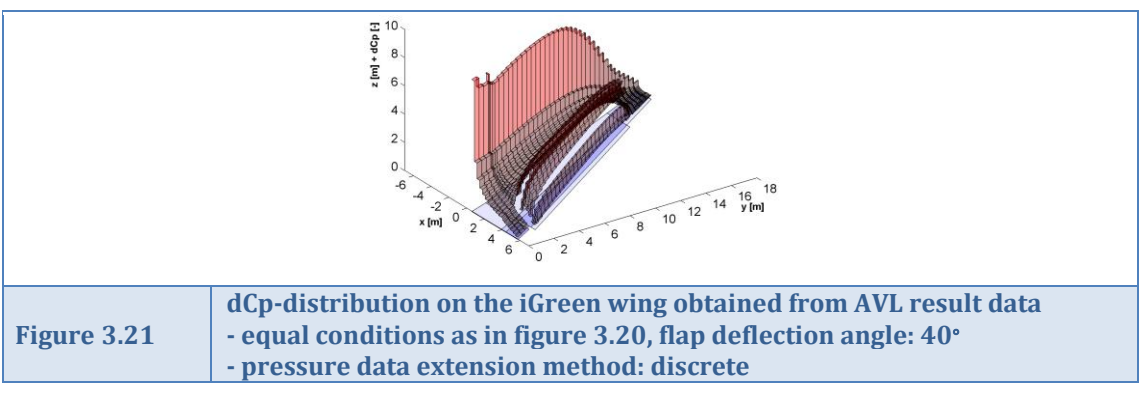
Extrapolation and interconnection generating a discrete dCp-distribution
 Figure 3.21 shows this second, discrete extrapolation method for the iGreen wing with flap deflection of 40°. When compared to continuous extrapolation, pressure peaks are less exaggerated at the boundaries of the wing definition, this however comes at the cost of the smoothness of the dCp-distribution.

Spanwise lift distributions are provided in figure 3.22 for the three flap deflection settings under consideration. It is clearly seen that the sectional lift coefficient increases in the flap region when extending the high-lift device. When comparing the root to the tip section of the flap, a decrease in flap chord is seen. Therefore, the increase in chord and camber is largest at the root section when extending the flap, explaining the larger increase in sectional lift coefficient at the root region of the flap.

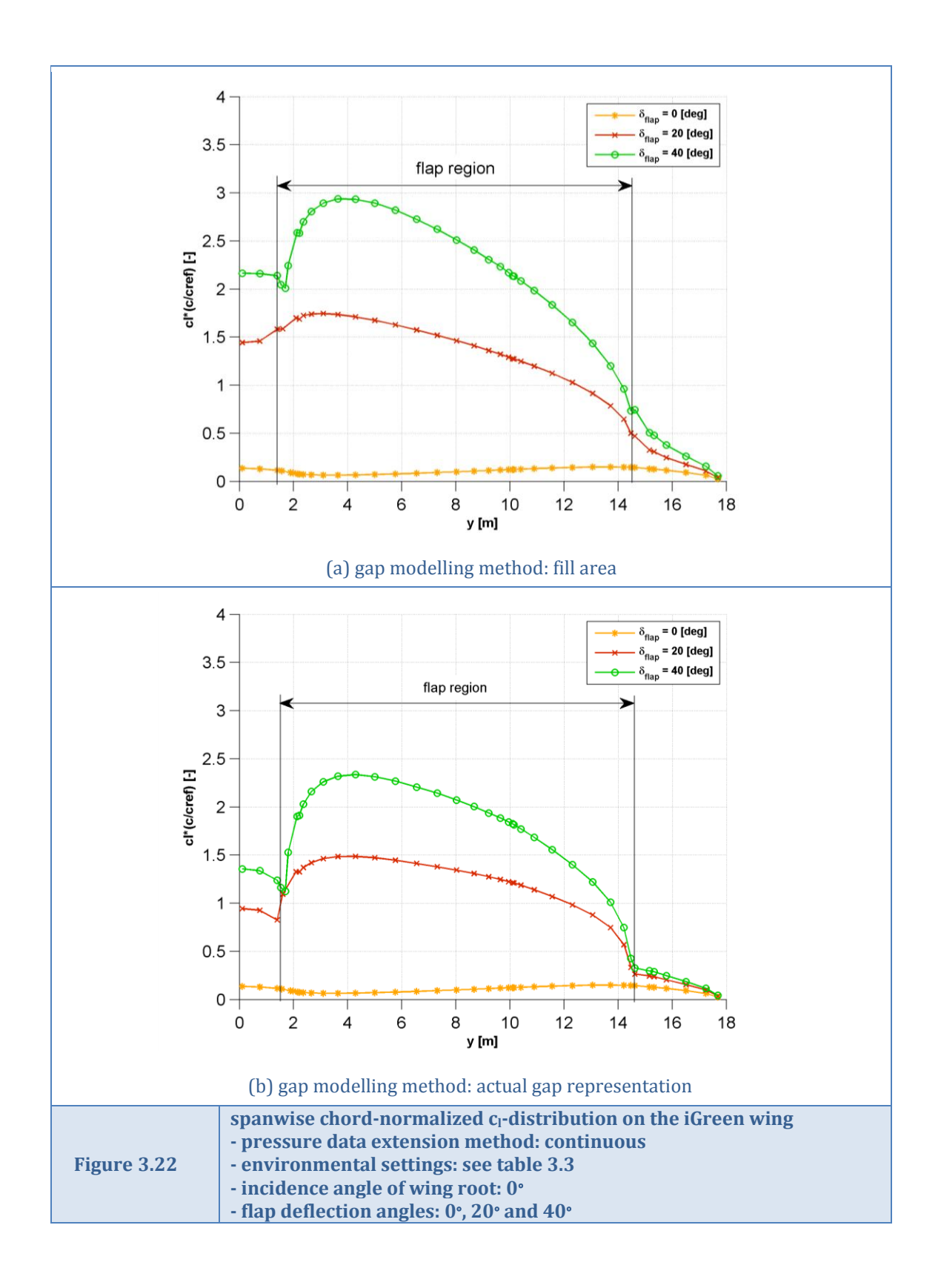
The sectional lift coefficient results of both grid representation methods are compared in figure 3.22(a) and (b). It can be concluded that the usage of a filling area results in larger lift coefficient values, although the qualitative behaviour of the curves is similar. In section 4.2, lift coefficient distributions will be compared to data available from literature, after which the most realistic gap representation method can be indicated. A significant difference in pressure distribution is observed when comparing the dCp-distribution for both gap modelling methods. Figure 3.23 clearly shows that the flap region is more highly loaded when a gap is included in the model. When modelling a filling surface for the gap, the pressure is not reduced to zero at the trailing edge of the main wing, but directly connected to the flap surface distribution. This lift dumping effect (see section 2.1.3) clearly introduces an overall increase in pressure, especially at the flap region of the main wing.





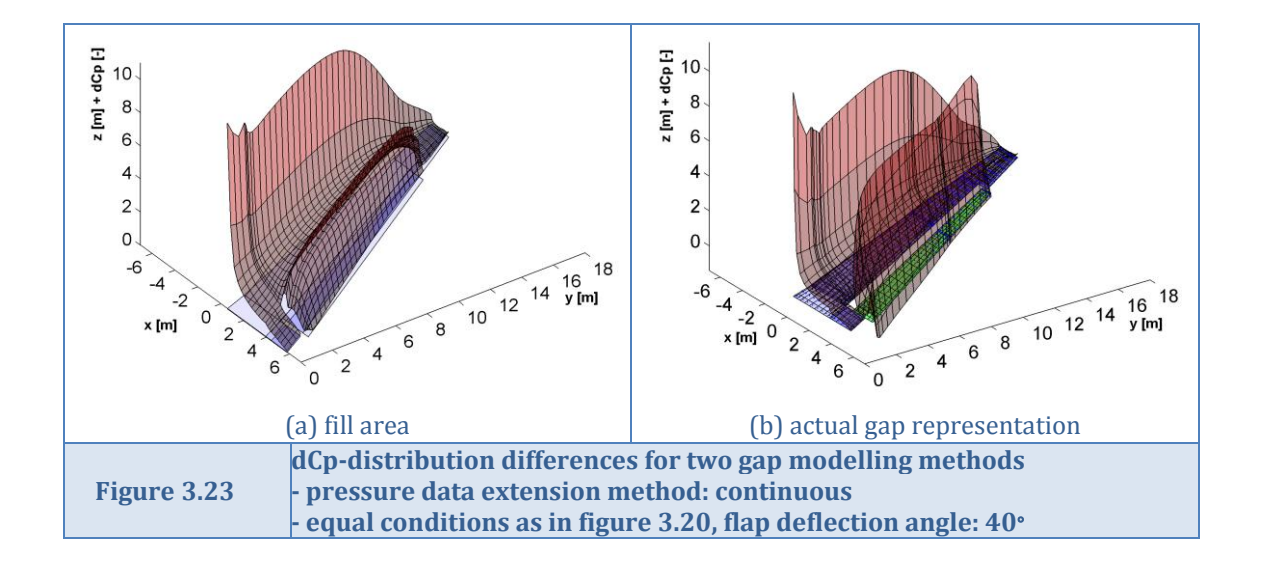






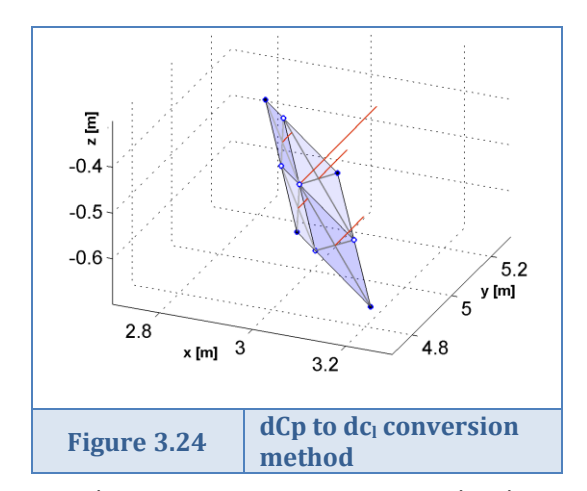
Chapter 3





Result interpolation on structural wing model

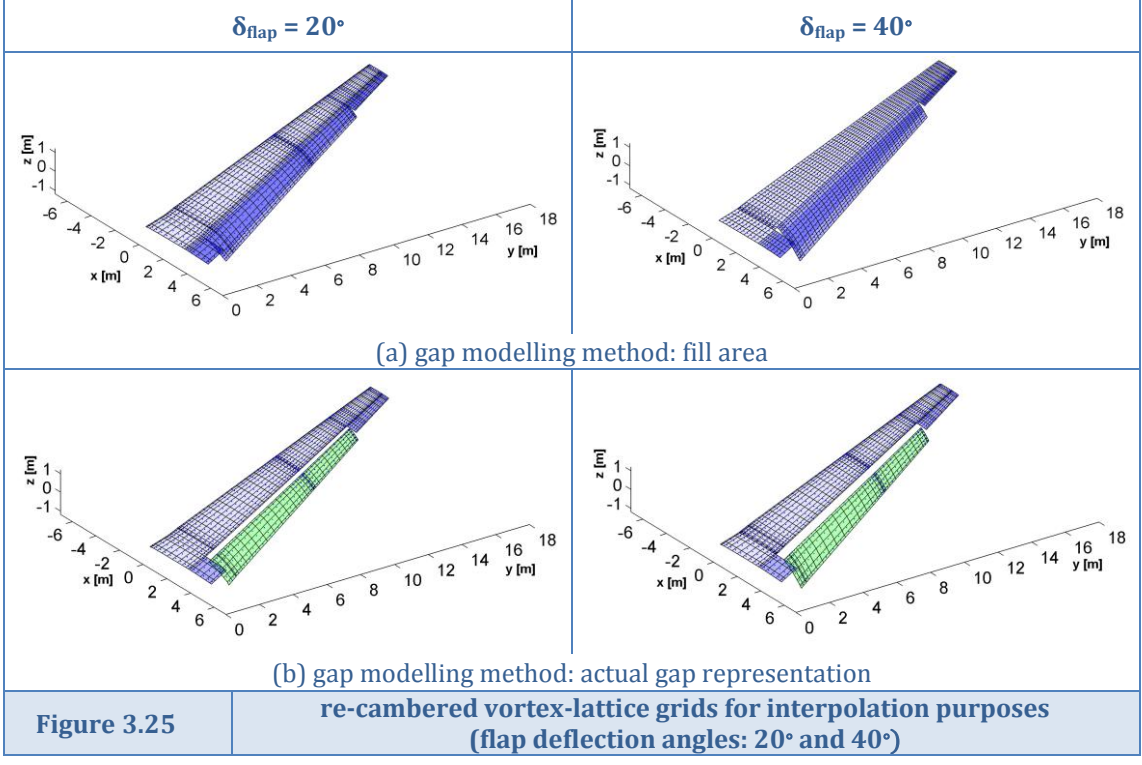
Before interpolating the wing loading to the structural wing model, the vortex-lattice grid requires the inclusion of actual camber. Camber data available at midstrip positions in the AVL result datadecks is inter- and extrapolated to strip boundaries and used to introduce proper curvature to the panelled wing representation. The positioning of extended high-lift devices is adjusted to the global coordinate system as applied in the original wing model generation to ensure proper overlap between both discrete grid representations. When applicable, the gap filling surface as well as the root extension surface are removed from the interpolated dCp-distribution (for the iGreen wing, these are surfaces 1,2,3 and 8 in figure 3.18(b)). Figure 3.25 shows the vortex-lattice grids for flap deflections of 20° and 40°, updated for interpolation.

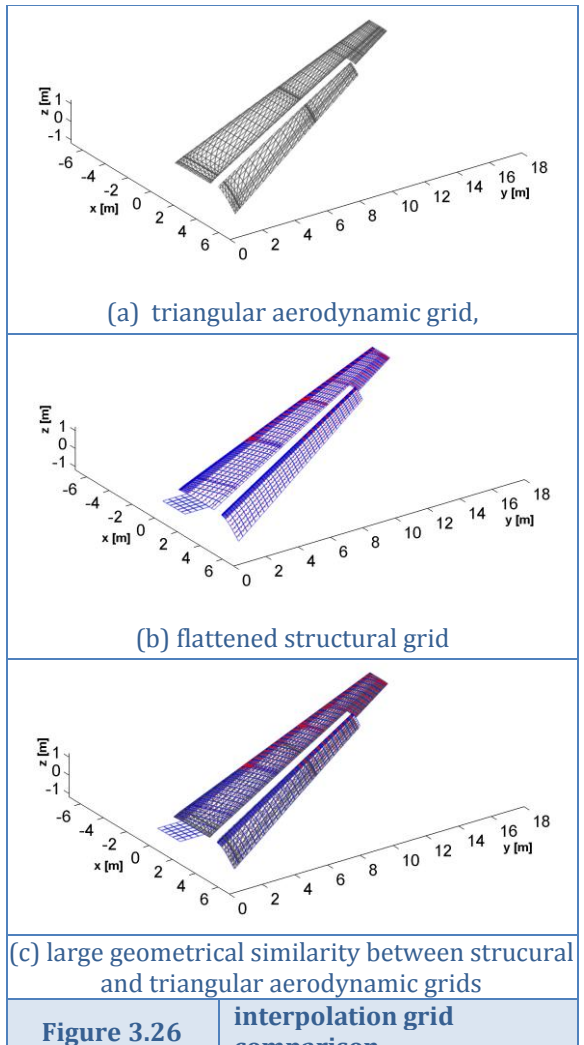


Before performing the actual interpolation using the 'gridapprox' routine, pressure coefficient values are converted to actual force vectors at the panel corner points. The applied method is schematically represented in figure 3.24. As illustrated in this figure, the pressure coefficient value at the bound-vortex midpoint is split up in four individual contributions per panel quadrant. Since camber and rotation was introduced to these panels, each quadrant has its individual normal vector. The pressure contributions are multiplied by the quadrant area to obtain the force contribution at the

panel corner point it represents. The direction of this force contribution is then set equal to the normal vector of the quadrant. This process is repeated for all panels of the cambered vortex-lattice grid and all contributions are added at the panel boundaries. Finally, a triangular element connectivity distribution is generated for gridapprox interpolation purposes, as depicted in figure 3.26(a).







comparison

Since the vortex-lattice grid for interpolation originated from a flat panel distribution, the structural model representation also needs flattening. The midpoints of structural keypoint pairs on upper and lower skin are structural for to define the interpolation grid. Figure 3.26(b) shows the resulting grid, along with force interpolation points at which an interpolated force value is obtained by the gridapprox routine. Figure 3.26(c) finally presents both the structural and aerodynamic interpolation grid on top of each other. Only very small geometric discrepancies are observed, mainly caused by misalignment due to spanwise outlining of the high-lift root and tip sections with gap starting and ending profiles of the main wing as depicted in figure 3.13.

The differences in grid and numerical roundoff errors in AVL result data introduces some differences in wing lift coefficient between the structural and aerodynamic model, as is shown in table 3.5. The difference in lift coefficient values is considered low enough to conclude that the correctness of the interpolation method is within acceptable boundaries.



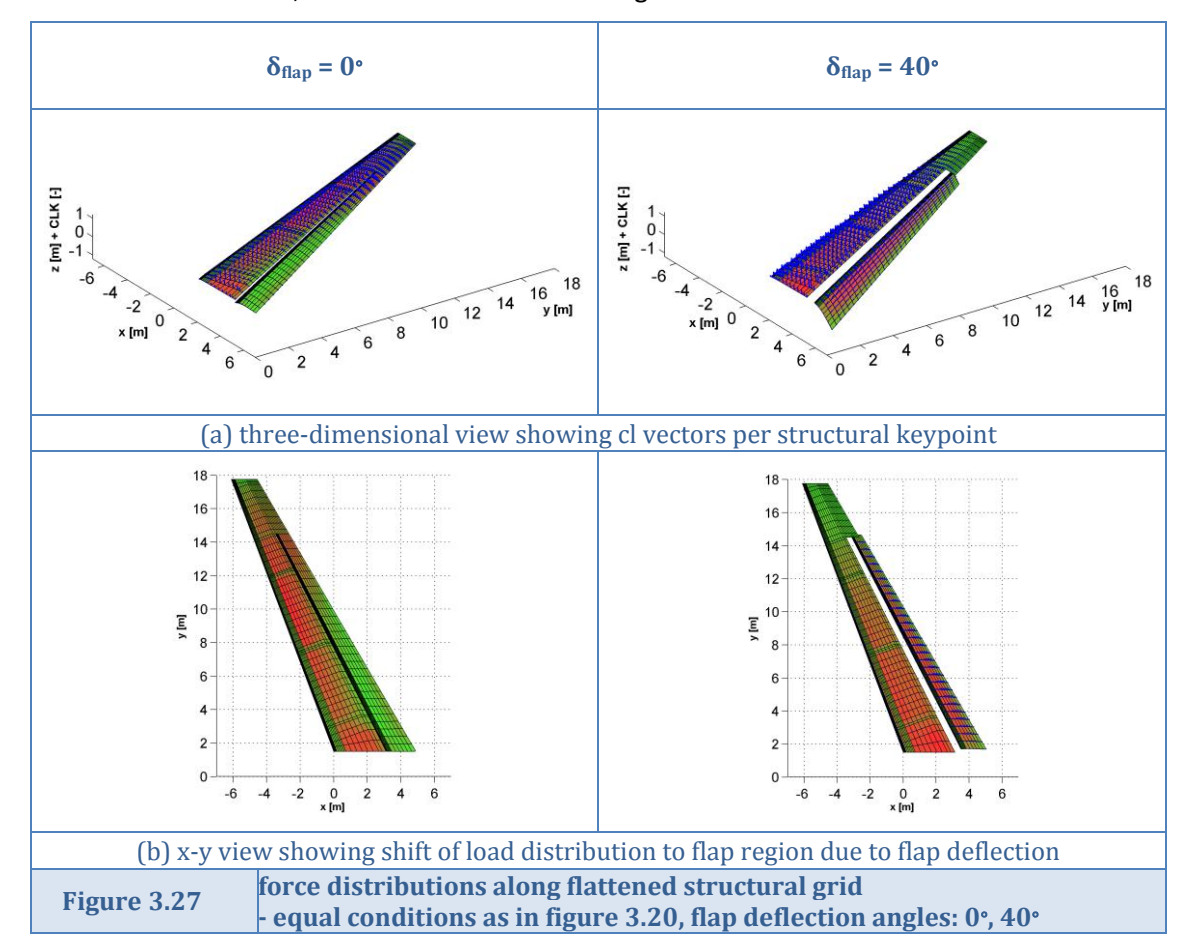
Table 3.5

total lift coefficient value comparison on structural grid and according to AVL output as a measure of interpolation certainty

- · pressure data extension method: continuous
- environmental settings: see table 3.3
- · incidence angle of wing root: 0°

δ _{flap} [deg]		C _∟ [-]		area [m²]					
[ueg]	interpolated AVL difference		difference [%]	interpolated	AVL	difference [%]			
0	0.116	0.118	-2.1	53.01	52.56	0.85			
20	1.347	1.337	0.73	53.01	52.93	0.15			
40	2.317	2.273	1.95	53.01	52.23	1.50			

Resulting force distributions are provided in figure 3.27 for the case with zero and maximum flap deflection settings. Part (a) of the figure shows three-dimensional views of the flattened structural wing geometry with the obtained force vectors placed on top. Part (b) of the figure is considered more indicative and shows the loading intensity along the entire wing setup. Clearly, an inboard shift of loading is introduced by extending the high-lift device. In its retracted position, the flap surface is only marginally loaded when compared to the main wing. After deflection however, the flap clearly contributes to the lift force generated by the wing setup. The resulting force vectors per grid point on the flattened structural grid are redistributed along the upper and lower skin of the original structural wing definition, according to a user defined ratio. The resulting force distribution is used for performing structural calculations, as described in the following section.





3.5 Structural calculations

Knowing the aerodynamic force distribution, the stress and displacement distribution of the wing model is obtained using finite element calculation software ANSYS. This forms the second main pillar of the aeroelastic routine. The current section describes the parametrically generated input data for ANSYS and result extraction methods. Resulting wing displacement data is used to update the geometric wing model and complete the aeroelastic chain described in section 3.6.

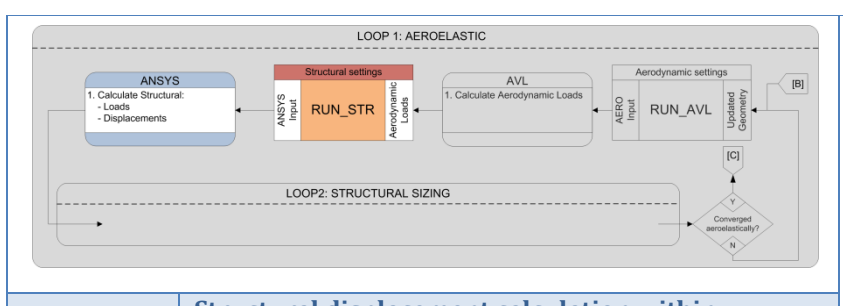


Figure 3.28 shows the part of the high-lift analysis routine concerning structural deflection calculations, which is the subject of the current section.

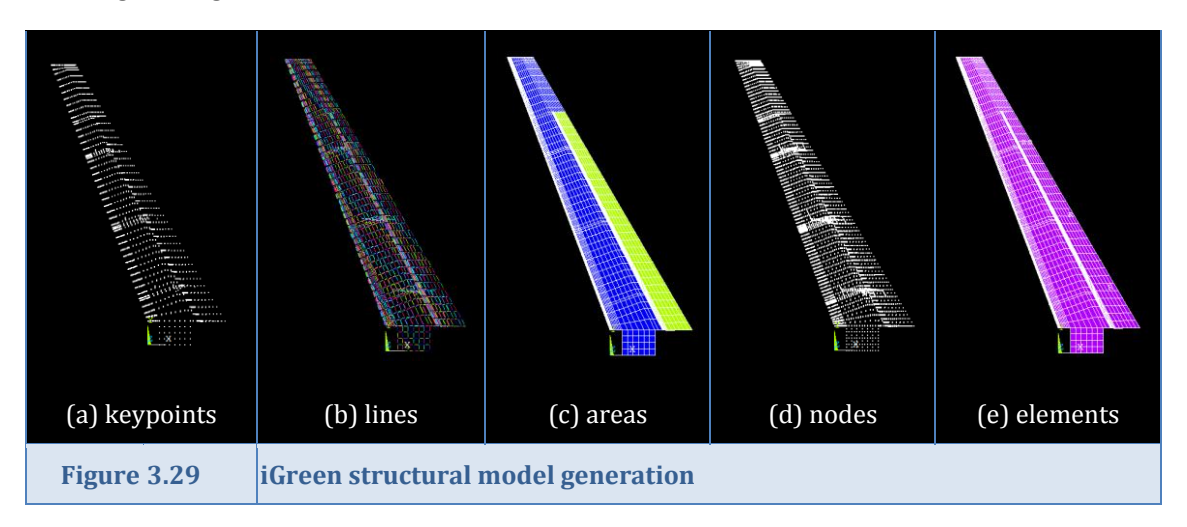
Figure 3.28 Structural displacement calculation within aeroelastic subgroup

3.5.1 ANSYS structural model

Section Sources: no external sources used

Structural model input using Ansys Parametric Design Language APDL

As described in section 3.2.3, the structural model generator ParaMAM includes functions for writing input data files for the generation of ANSYS structural models. When starting the first ANSYS batch run, all input files are sequentially loaded to define the structural model as depicted in figure 3.29. For generation of the basis wing model, keypoints define locations in space where rib-spar intersections occur. These keypoints are thereafter connected using line segments, which are at their turn used to generate areas. According to the user preferred element size setting, ANSYS converts these areas to shell elements and nodes representing skin, rib and spar panels. Additional keypoints locations are defined to provide a basis for the generation of support and linkage systems. Both the lines and areas connecting these keypoints are used for the generation of respectively beam and shell elements interconnecting the wing and high-lift devices.





Each keypoint, line and area is assigned an individual number, enabling selection of specific wing parts during model generation. The numbering system used by the original ParaMAM interpolation routine for basic wing models is extended for inclusion of linkage systems. APPENDIX C provides an overview of the numbering conventions used in the ANSYS structural wing model. Numbering conventions are also provided for possible future extensions, such as engines, gears and fuel tanks definitions.

Next to the geometrical wing definition, material properties and sizing regions are also loaded from the CPACS input file and converted to input decks for usage in ANSYS. Material properties are assigned to the elements involved in the calculation and sizing regions indicate which element types are allowed to be sized during an S_BOT structural sizing run. The meshed element model is saved after each run, allowing continuation of the generated wing model in following calculations. Especially during an aeroelastic iteration involving multiple structural runs, this saves a considerable amount of computational time.

Structural wing model calculations in ANSYS

The loads obtained from the aerodynamic calculations in section 3.4 are imported by ANSYS and applied at the geometrical keypoints. Instead of directly applying forces at the structural nodes, these are applied at the keypoints to take advantage of the aforementioned numbering system. Before the actual structural calculation starts, these loads are transferred from the keypoints to the nearest nodes using an internal ANSYS function. Gravity is simulated by accelerating the structure in the direction opposite to gravity, and the wing is clamped the structural wing box defined at the root of the structural wing model.

Having defined the complete wing geometry and loading, the linear structural calculation is performed by ANSYS.

3.5.2 Stress and displacement data extraction

Section Sources: no external sources used

After finishing the structural calculations, stress and displacement data is exported to result datadecks using APDL commands. These datadecks are thereafter loaded by the structural operating function 'RUN_STR' of the high-lift device analysis routine and used to update the geometrical wing model.

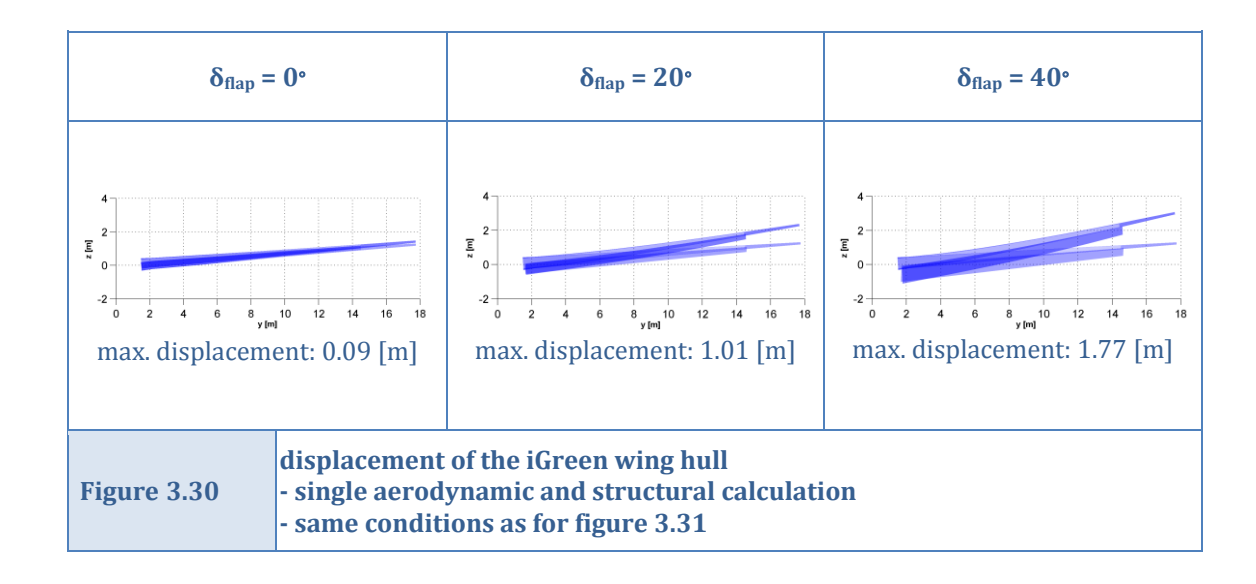
The postprocessing function of the high-lift device analysis routine provides the means for plotting stress and displacement results, as is done for the iGreen wing in figures 3.30 and 3.31. The first figure clearly shows the wing loads generated by the forces due to deflection of the large trailing edge flap of the iGreen wing. To provide insight in the stresses introduced to the wing box by the wing root structure, the wing box is switched off when creating the stress distribution figures.

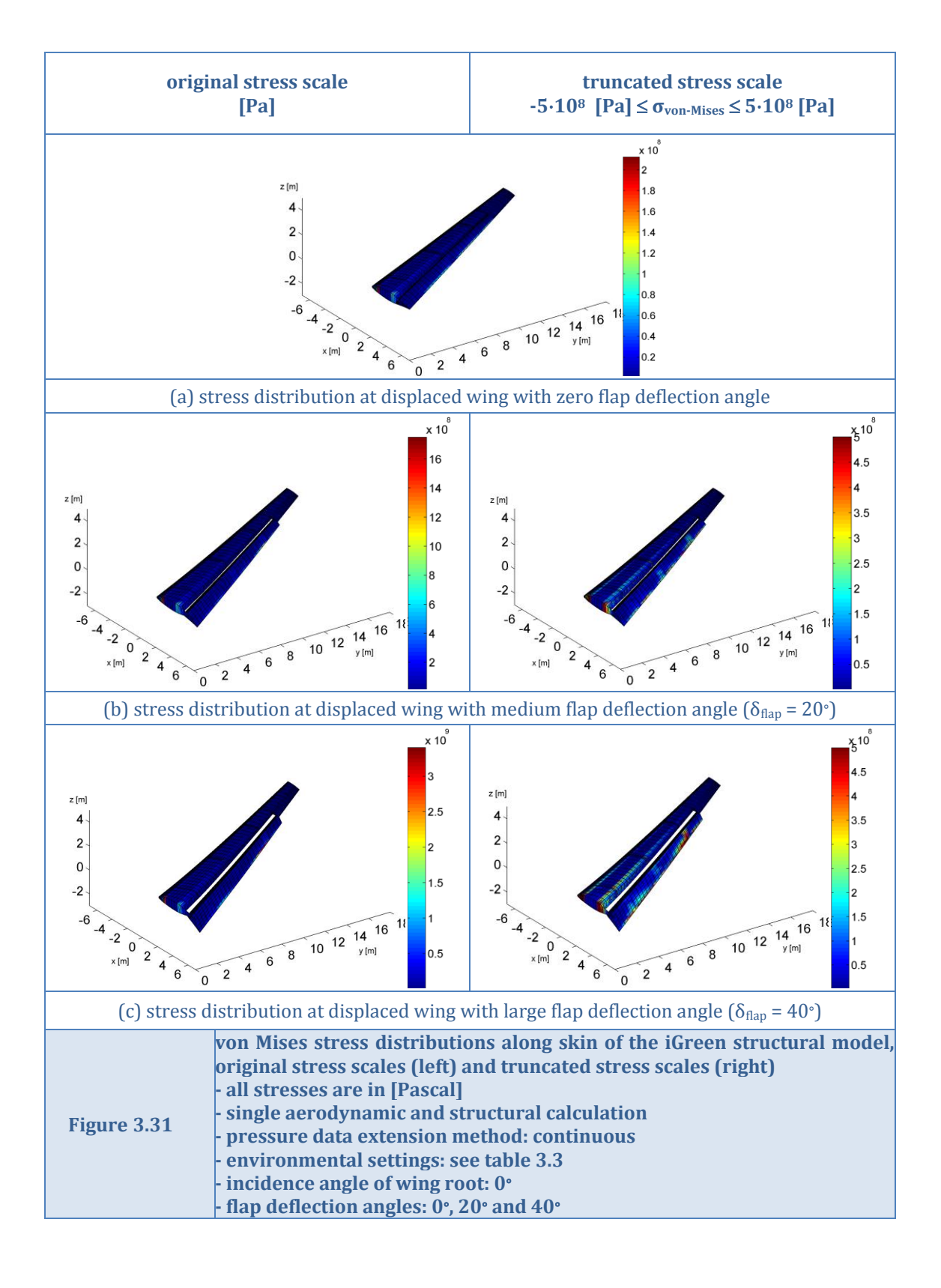
The wing deformations in figure 3.30 show behaviour as expected: increasing flap deflection angle lead to higher loads at the wing which at their turn result in larger wing tip displacements. The flap follows the general bending curvature of the main wing, indicating the support system is strong enough to cope with the aerodynamic flap loading.

The left-hand column of figure 3.31 provides stress distribution plots in the original stress scale. Due to the wing box definition in the structural model setup, large local stress peaks occur at the two spar-wingbox interconnections. A much better insight in the transfer of structural loads in the wing itself is obtained when truncating the scale of the stress plots. The



right-hand column of figure 3.31 provides stress distribution figures on a scale between -500 [MPa] and 500 [MPa]. Truncating the scale to this stress range has no effect on the distribution plot for the with undeflected flap case, since all stress values are contained within both scales applied. However, when considering the distribution plots for wing setups having deflected flap settings, it is shown that bending of the wing introduces large stresses at the trailing edge of the deflected flap. These stresses are the highest at the outboard linkage location, since at this position the bending moments are highest. The transfer of forces from the flap to the wing structure at the flap support system locations is also clearly shown by an increase in structural stress. For the main wing, it is seen that both the spars transfer large part of the wing loading to the root section, where the wing box connects the wing to the fuselage.

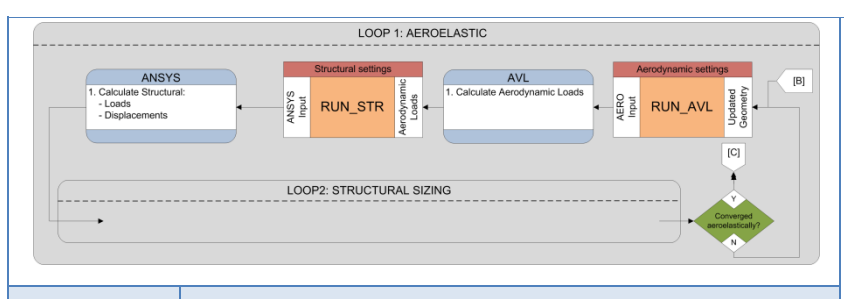






3.6 Aeroelastic iterations

The available aerodynamic and structural result data is coupled in order to create an aeroelastic calculation procedure. Using deformation data, the jig-shape of the wing as modelled in the CPACS information model is updated to the actual in-flight shape. Knowing this updated model, actual in-flight loading is obtained, which can be used in initial design methods such as the sizing routine described in section 3.7. The current section shows converged aeroelastic calculation results for the iGreen wing model for three different flap deflection settings.



calculation procedure within the aeroelastic subgroup is shown in figure 3.32. Each individual subpart was treated in the two previous sections.

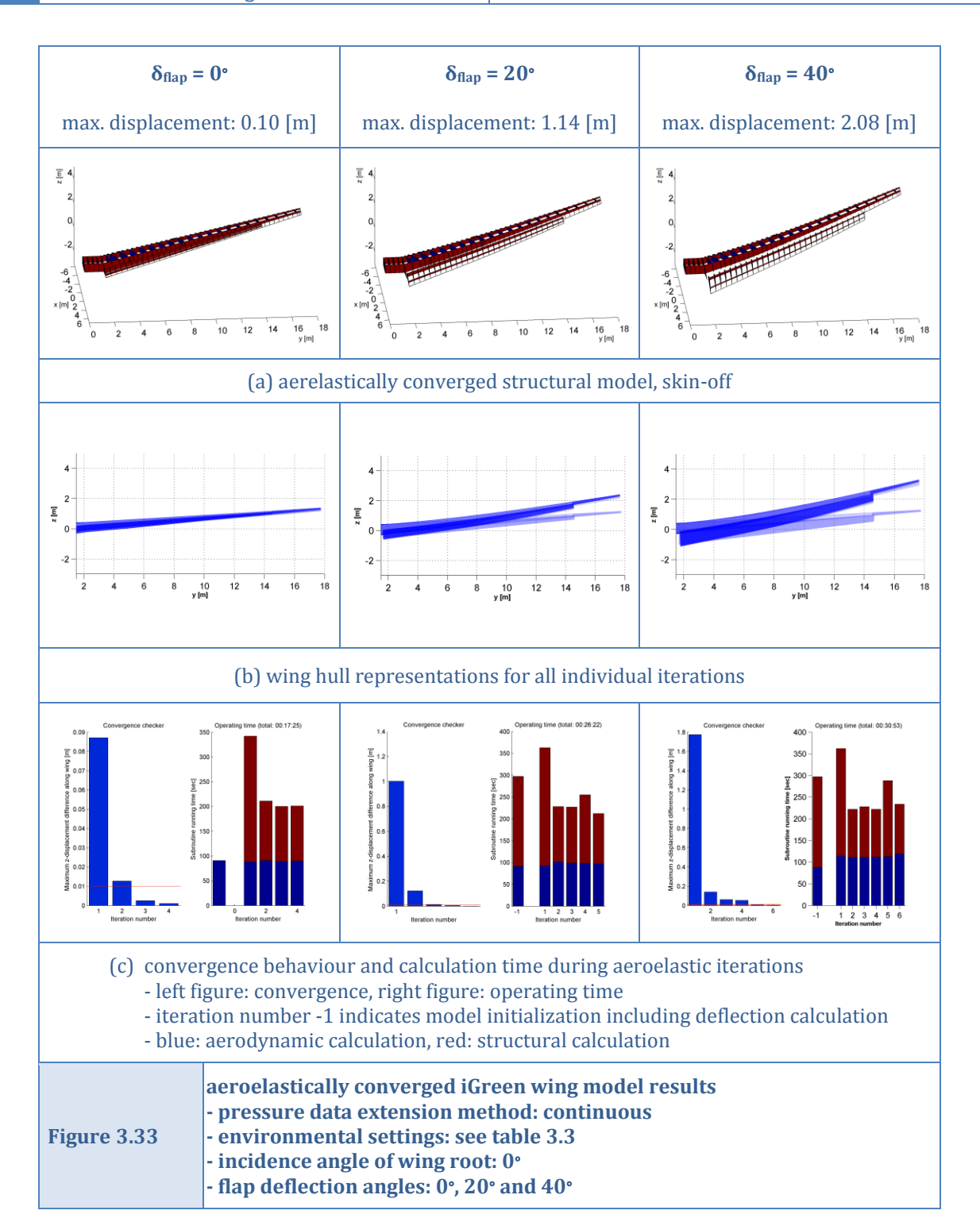
The complete

Figure 3.32 The complete aeroelastic subgroup

After each aeroelastic iteration, intermediate result data is internally saved to allow investigation of the development in stress and displacement distribution during the complete analysis. Figure 3.33 contains aeroelastically converged results for the iGreen wing model under consideration. Part (a) of this figure shows that the ribs and spars of the structural wing model in its flying condition. The influence of increased flap deflection clearly results in larger bending of the wing structure. Part (b) provides an y-z view of the wing hull for each individual iteration. It is concluded that the largest displacement occurs after the first structural calculation and the wing only marginally displaces further until convergence is obtained.

Convergence and operating time is finally shown in part (c) of figure 3.33. The applied convergence criterion is based on the displacement difference in z-direction along the entire wing. If for all structural keypoints the change in z-displacement is lower than 0.01 [m] for two consecutive aeroelastic iterations, the solution is considered converged. Convergence behaviour is depicted in the left hand graphs. The right hand graphs show the operating time of the high-lift device analysis routine. Iteration number -1 indicates model initialization, which consists of all calculations performed within the model generation subgroup of figure 3.1. The blue part of the bar represents loading the model, whereas the red part indicates the time used for deflection calculations on the flap system. From iteration number 1 onwards, blue bars indicate the time required for the aerodynamic calculations and red bars indicate the structural calculations time within the aeroelastic subgroup. For the first iteration, the structural calculation requires more time than the following iterations, since this initial calculation includes the time-demanding initial loading of the structural model generated by the model generator. After each iteration, the attained structural model is saved to a temporary database, which is resumed at the start of the following structural calculation in order to reduce demands on overall operating time.







3.7 Preliminary wing thickness sizing

Either during the aeroelastic iterations or after aeroelastic convergence, stress results can be used to size the thickness of groups of structural panels in the wing setup. For this purpose, sizing routine 'S_BOT' of the German Aerospace Centre is used. Using S_BOT, extra material is placed at highly-stressed locations and thickness is reduced where a material surplus is present. The principles behind the sizing routine are shortly indicated, followed by a discussion on the results of incorporating the sizing routine in the aeroelastic tool chain. A preliminary thickness sizing is performed on the iGreen wing in chapter 5.

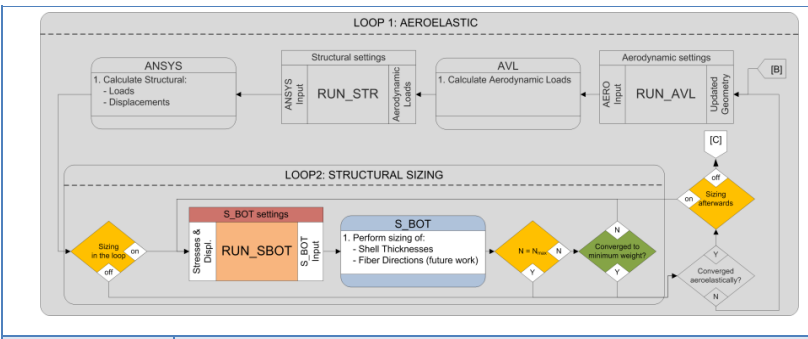


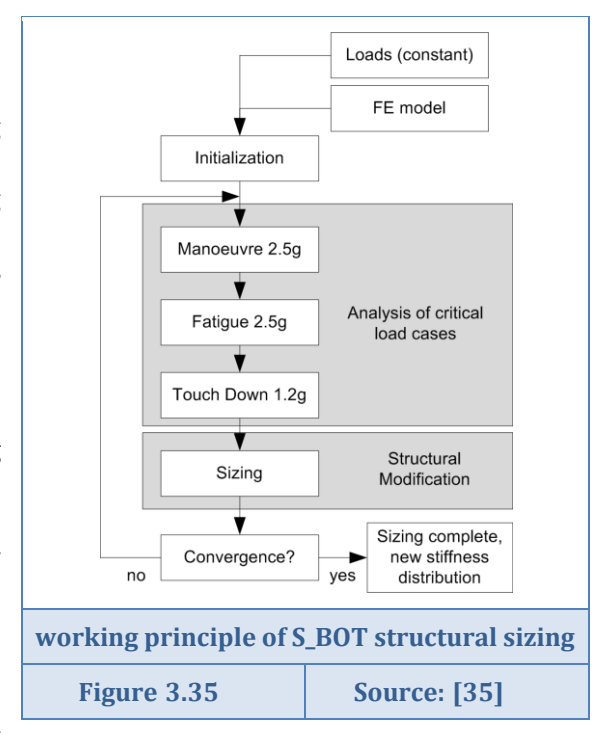
Figure 3.34 Structural sizing calculation within structural sizing subgroup

Figure 3.34 shows the final part of the preliminary high-lift device analysis routine, adding initial structural sizing capability within the aeroelastic subgroup.

3.7.1 Working principles of sizing routine S_BOT

Section Sources: [35], [72]

The structural finite element (FE) model created using the model generator described in section 3.2 is used as a basis for performing structural sizing of the panel thicknesses in predefined optimization regions. The sizing routine 'S BOT' developed by the German Aerospace Centre (DLR) is used for this matter. S_BOT consists of a set of modifiable macros written in Ansys Parametric Design Language (APDL) and thereby forms a modular framework for automated structural analysis within ANSYS [35], [72]. The working principle of the two-stage sizing process S BOT is schematically shown in figure 3.35. As can be seen, the FE model generated by ParaMAM, as well as sets of external loads have to be provided. These external loads remain constant during the ANSYS internal sizing loop. Multiple critical load cases are analyzed, after which the highest occurring



stresses are used to determine the best material and thickness properties per structural wing element. After structural modification of the wing model properties, internal loads within the wing change requiring an updated analysis of the critical load cases. This iterative process is



continued until convergence of both internal loading and structural properties. Sizing rules defined by the user define the way in which updated material properties are obtained. For homogeneous materials this for example includes putting the material at its ultimate stress state, or a fraction thereof. S_BOT also has functions incorporated concerning the sizing of composite materials. Calculations and sizing rules for the multiple-layered elements are generally more complicated due to the inclusion of variable fibre directions and layer stacking. Usage of composite materials is unfortunately beyond the scope of the current research, but might be included in future versions of the high-lift device analysis routine.

3.7.2 Incorporating the sizing routine in the aeroelastic tool chain

Section Sources: no external sources used

For the S_BOT connection incorporated in the high-lift device analysis routine, model sizing settings are read out from the CPACS aircraft information model described in section 3.2.2. Predefined sizing region settings are available, controlling which parts of the wing structural model are subjected to sizing rules and for which regions material settings and thicknesses are left unadjusted. In the most elementary region definition, the set of ribs, spars and skin panels included in the wing torsion box is subjected to sizing rules, all material in front of the front spar and behind the rear spar is left unadjusted.

As depicted in figure 3.34, the sizing using S_BOT forms an extension of the aeroelastic subroutine. Two sizing procedures are distinguished:

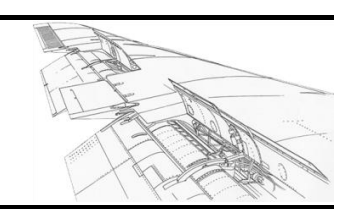
- Sizing after aeroelastic convergence First, the aeroelastic deformation and corresponding loading is obtained using the predefined material settings and skin thickness values set by the user in the CPACS input structure. After obtaining the wing in its actual flying shape, a single sizing run is performed using S_BOT, updating the structural model properties for the single aeroelastically converged wing loading distribution. After convergence of S_BOT, the entire analysis is considered finished and postprocessing is started to provide visual representations of the sized wing structure.
- Intermediate sizing during the aeroelastically coupled calculation

 This second, more complicated 'sizing-in-the-loop' procedure is designed for S_BOT to work with actual aerodynamic loading when applying the sizing rules to the structural properties of the wing. Based on each aerodynamic loading calculation, partial intermediate sizing is performed by either defining a finite number of S_BOT internal iterations, or stretching the internal convergence limits of S_BOT. In future work, it is to be determined if the result in this second procedure outweighs the added requirements on computational effort. Furthermore, optimal procedural settings such as the aforementioned number of S_BOT internal iterations need to be determined by comparing convergence analyses and results for several runs of the high-lift device analysis routine.

In chapter 5, an initial sizing example will be shown using the iGreen wing model. The reader is referred to this chapter for comments on computational requirements of sizing robot S_BOT.

Chapter 4

Validation of the aerodynamic model used in the high-lift device sizing routine



To judge the validity of the applied aerodynamic model, the vortex-lattice load result data is compared to experimental and computational data verified for an existing wing model. Unfortunately, very little aerodynamic pressure distribution data is available to the author for these load validation purposes. In order to make a first comparison between modelling results and validated aerodynamic data, this chapter describes the loading of a wing model different from the general model used throughout this thesis. Loading data of the Fokker-100 wing was made available for load comparison purposes and is used hereafter for validation purposes. It is concluded that the applied rapid aerodynamic load calculation method is capable of providing adequate result data using relatively low computational resources. These results are however obtained using a effective flap angle correction, based on a large amount of wind tunnel test data on two-dimensional airfoil sections. Results obtained without applying flap angle corrections show overprediction of wing loading values.

4.1 The Fokker-100 wing model

This first section provides an introduction to the Fokker-100 wing model used in the validation of the aerodynamic model used in the high-lift device sizing routine.

4.1.1 Geometry and base model of the Fokker-100 wing

Section Sources: [54], [73], [74]

The Fokker-100 is a medium-sized transport aircraft able to carry 107 passengers (standard single class seating), designed in the 1980's. As the successor of the F-28 Fellowship, it was Fokker's largest aircraft produced until the bankruptcy of Fokker in 1996. After the first flight

Fokker-100 flap system fully deployed

Figure 4.1

Source: [73]

on November the 30th in 1986, a total of 283 Fokker-100 aircraft have been built.

Fokker-100 wing geometry

Table 4.1 provides an overview of the external geometry of the Fokker-100 wing. The sweptback wing contains an aileron at the tip side of the wing and two flap segments at the root side. The first, inboard flap starts directly at the root of the wing and the second, outboard flap continues until a wing span fraction of $\eta = 0.60$. When fully deflected, the applied double-slotted flap has a deflection angle of 42° relative to the wing

91

¹³ Fokker report A-173 was made available by Dr. ir. R. Vos



chord. This maximum flap setting is only used during landing manoeuvres. Dependent on the environmental circumstances, either no flap deflection or a small single-slotted flap setting is applied for take-off manoeuvres. Figure (c) incorporated in table 4.1 provides an insightful schematic of the Fokker-100 wing geometry.

Table 4.1	Fokker 100 wing geometry Source: [74]									
Top views				category	variable		value	unit		
				wing span	b	=	28.076	[m]		
A	\			fuselage diameter	d_{f}	=	3.300	[m]		
1			ata	half span trapezoid part	b _t	=	12.388	[m]		
	1		main wing geometrical data	wing area (total)	S	=	93.5	[m ²]		
			netric	aspect ratio	Α	=	8.43	[-]		
	<u> </u>		yeor	mean aerodynamic chord	C _{MAC}	=	3.833	[m]		
1	-/		ing (root chord	C _{root}	=	5.280	[m]		
(a): Fokker	100 top view		w nix	tip chord	C _{tip}	=	1.257	[m]		
(a). I OKKEI	Too top view		Ë	taper ratio	λ	=	0.24	[-]		
				dihedral angle	Γ	=	2.5	[deg]		
				sweep angle	$\Lambda_{0.25c}$	=	17.45	[deg]		
				span inboard flap	$b_{f,i}$	=	3.320	[m]		
			ta	span outboard flap	b _{f,o}	=	2.640	[m]		
			al da	chord inboard flap (root)	C _{fr,inboard}	=	1.586	[m]		
			etrica	chord inboard flap (tip)	C _{ft,inboard}	=	1.347	[m]		
			flap geometrical data	chord inboard flap (root)	C _{fr,outboard}	=	1.323	[m]		
(b): Fokker 1	00 front view		ap g	chord inboard flap (tip)	C _{ft,outboard}	=	1.042	[m]		
			₩	max. deflection single slotted	$\delta_{\text{fmax,ss}}$	=	18	[deg]		
				max. deflection double slotted	$\delta_{\text{fmax,ds}}$	=	42	[deg]		
(c): wing geometry (c): wing geometry										
				(o). Willing geometry						



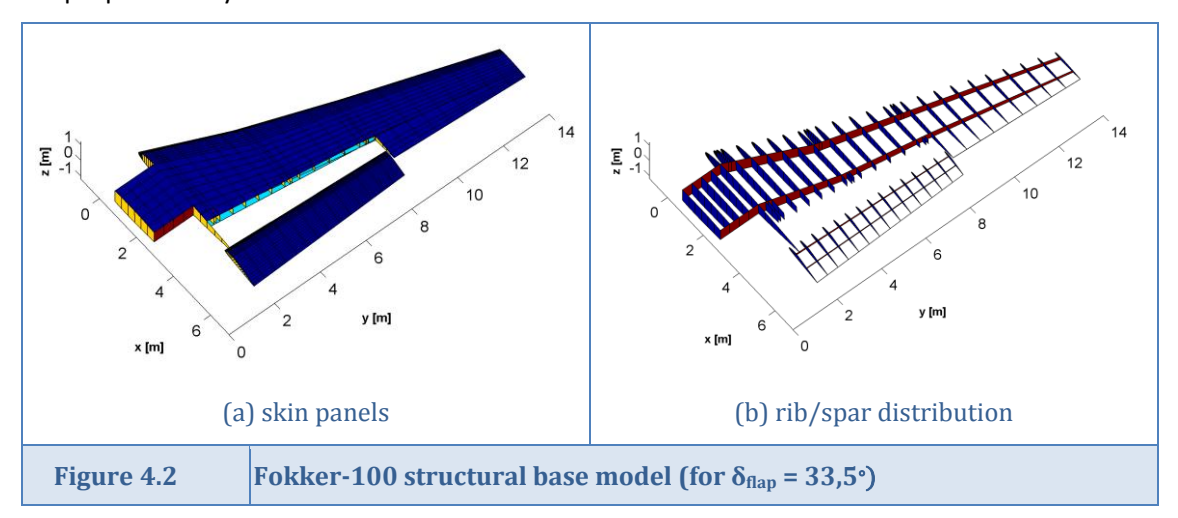
4.1.2 Structural and aerodynamic wing model generation of the Fokker-100 wing

Section Sources: [54], [74]

Structural base model of the Fokker-100 wing

Using the geometrical data provided in section 4.1.1 in combination with Fokker-100 Type Specification data [74] and geometrical data available from the available Fokker report on trim drag determination [54], a base model of the Fokker-100 is created in the CPACS¹⁴ aircraft information model environment. Since not all geometrical data is explicitly contained in the Fokker-100 reference reports, some dimensions such as flap Fowler motion and intermediate chord lengths are estimated using either three-view drawings or educated guessing. Main dimensions of the six sections making up the wing model are provided in table D.5 of APPENDIX D . Just as in the aforementioned Fokker report [54], it is assumed that the aircraft wing is built-up using symmetrical airfoil sections. Since on the actual Fokker-100 aircraft the applied profiles are adjusted versions of the NACA 0014 airfoil, it is chosen to use this airfoil as a basis for wing model generation.

Figure 4.2 shows the resulting structural wing model for the Fokker-100 wing. Within the aerodynamic model used for validation in the sections hereafter, the inboard and outboard flap of the actual wing model are merged into one single flap definition. To provide a proper base model for aerodynamic airfoil interpolations, this merging is also applied in the structural wing model. This introduces an extra complication when compared to the iGreen wing model used within the previous chapters: a kink occurs in the wing geometry within the range of the flap. This kink at wing station 4700 is clearly seen when viewing the rib/spar distribution in figure 4.2(b). From this figure, three more observations can be made. First, an extra spar is added at the trailing edge in order to close the gap that would else occur. Second, extra ribs are added at the three linkage positions of the F-100 wing, to provide suspension points for the flap support system. The third and last observation concerns the addition of virtual spars to ensure proper roundness of the leading edges of both the base wing and flap making up the complete wing model. As explained in section 3.4.1 and 3.5, these virtual spars are solely used for proper aerodynamic model extraction.



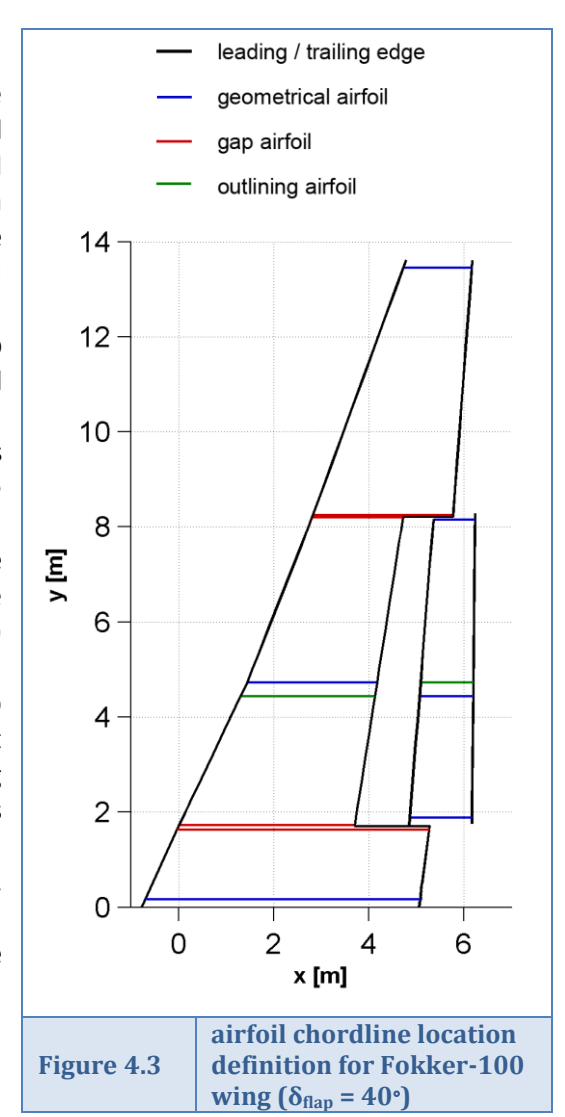
¹⁴ For a short description of the CPACS aircraft information model, the reader is referred to section 3.2.2

93

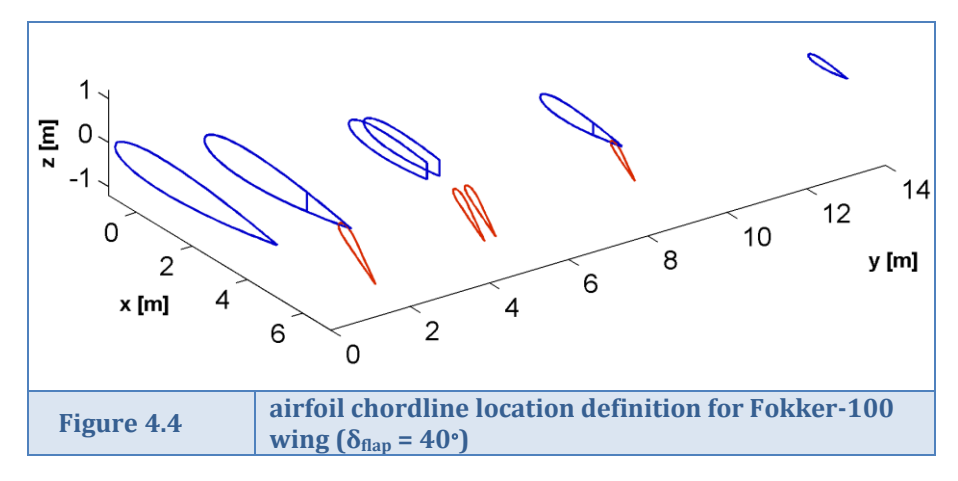


Aerodynamic model of the Fokker-100 wing

With the structural base model known, the methods described in section 3.4.1 are applied extract an aerodynamic wing model representation of the Fokker-100 wing. As a result of these methods, figure 4.3 shows the chordline locations introducing geometrical changes in the wing model. Aside the root and tip airfoil locations (coloured blue) and gap starting and ending airfoil locations (coloured red), one intermediate location requiring an additional airfoil definition is obtained. This geometrical airfoil at wing station 4700 of the main wing introduces the leading edge kink in the wing model. When the wing is in cruise configuration with retracted flap setting, the kink introducing airfoil locations (coloured blue) on both the main wing and flap area are aligned. As a consequence of the applied wing sweep angle, the hinge line of the flap deployment system is skewed with respect to the wing trailing edge. Therefore, the flap translates slightly in minus y-direction during deployment, causing the observed misalignment in figure 4.3. Outlining airfoils (coloured green) are required to ensure proper alignment of the vortex-lattice grid.



After applying interpolation methods to extract the actual profile definitions from the structural model, the profile definition serving as a basis for vortex-lattice grid generation depicted in figure 4.4 is obtained. Grids of varying density are extracted for performing grid convergence studies in section 4.3. First, the following section will compare results of aerodynamic calculations on the extracted Fokker-100 wing to experimental data and validated calculations.





4.2 Aerodynamic result validation using the Fokker-100 wing

In this section, aerodynamic results obtained using the Fokker-100 aerodynamic model as described in section 4.1 are used to perform an initial validation of the aerodynamic modelling technique applied within the structural high-lift analysis routine described in chapter 3.

4.2.1 General calculation setup including effective flap angle correction method

Section Sources: [54]

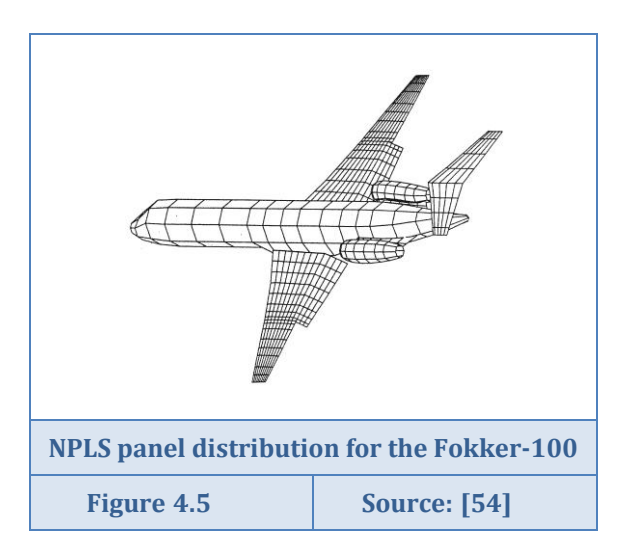
Reference data of the Fokker-100 wing is available for three flap settings [54]: a clean wing setting having undeployed flaps, an intermediate flap deflection setting of δ_{flap} = 20° and the maximum flap setting of δ_{flap} = 42°. The general environmental settings applied during the validation study are listed in table 4.2.

Three goals are identified in the verification process:

- comparing spanwise lift coefficient distributions (c_I-distributions) to reference data of the Fokker-100 wing (section 4.2.2)
 For angles of attack 0°, 3° and 6°, c_I-distribution reference data is available for all three flap settings described above. Comparison of spanwise c_I-distributions provides an indication of the correctness of the calculated load distribution along the wing.
- comparing lift curves (CL-curves) to reference data of the Fokker-100 wing (section 4.2.3)
 An angle of attack sweep from 0° to 15° is used to determine the linear range of the lift curve. Angles of attack higher than 15° are not concerned, since currently no stall prediction method is included in the software routine.
- performing a grid convergence study of the Fokker-100 wing model (section 4.3)
 The aerodynamic results of five different grid settings are compared in order to provide an indication for a proper grid settings for performing load calculations of geometries including trailing edge high-lift systems using the applied vortex-lattice method. Grid settings range from very coarse grids with very low computational demands to very dense grids requiring large computational effort.

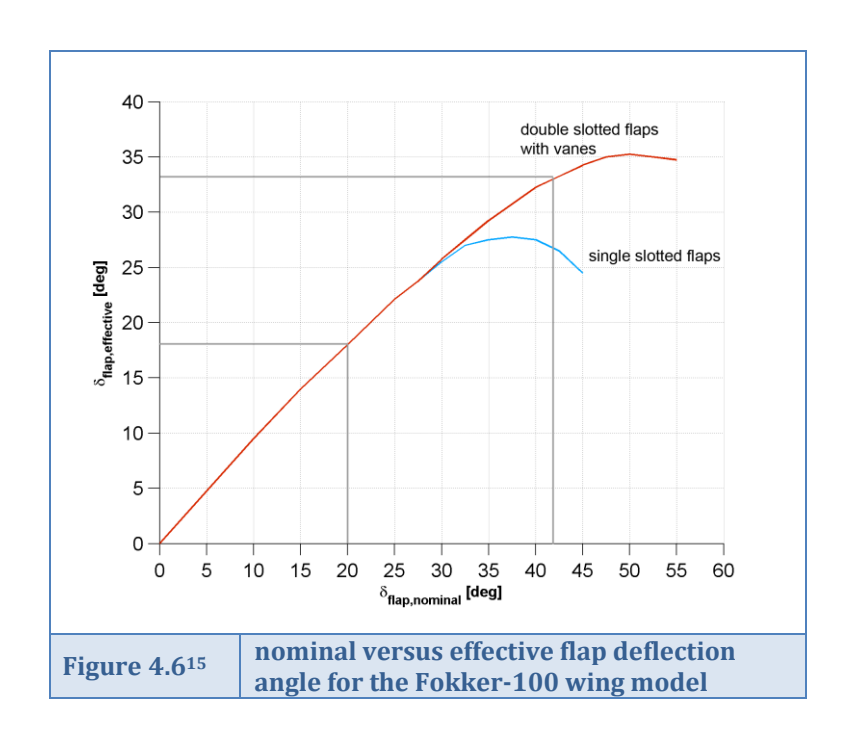
Table 4	4.2	Runc	ase definition for calc	ulations	on	the Fokker-1	00 wing
input file	catego	ory	variable			value	unit
	onalo	_	fuselage angle of attack	α	=	[0-3-6-9-12-15]	[deg]
	angle	S	sideslip angle	β	=	0	[deg]
runcase			roll rate	pb/2V	=	0	[-]
input	rotation r	ates	pitch rate	qc/2V	=	0	[-]
			yaw rate	rb/2V	=	0	[-]
	flight cond	dition	flight Mach number	Mach	=	0.19	[-]
mass	defau	lt	gravitational acceleration	g	=	9.80665	[m/s ²]
input	consta	nts	air density	ρ	=	1.225	[kg/m³]





The non-planar lifting surface (NPLS) programme developed at Fokker allows analysis of complete aircraft geometries. The Fokker-100 model as applied during the calculations of the reference report is figure depicted in 4.5. Fortunately, calculation results for wing and fuselage (WF) part of the model is separately available in the reference report. This allows for proper comparison of aerodynamic loading calculation results, as is performed in the section hereafter.

An experimentally based correction method is applied to the deflection setting of the flaps to account for flow-effects not captured by vortex-lattice methods. This essentially upgrades the inviscid three-dimensional aerodynamic method to a light form of a quasi-3D method in which a three-dimensional inviscid panel method is combined with two-dimensional experimental data (see table 2.9). From comparison between a predecessor of the NPLS vortex-lattice programme applied by Fokker and a large amount of windtunnel tests, the relation between nominal and effective flap deflection angle as shown in figure 4.6 is obtained. The deflection angle of the complete flap system is adjusted according to this relation, implying the usage of 0°, 17.6° and 33.5° flap setting for calculations on the Fokker-100 wing.



-

¹⁵ This figure is an updated version of figure 2.29, described in section 2.3.2



4.2.2 Validation of spanwise lift distribution results for the Fokker-100 wing

Section Sources:

[54]

To determine whether the spanwise lift-coefficient (c_I) distributions calculated by the applied aerodynamic routine show acceptable behaviour, these are compared to results obtained by the non-planar lifting surface (NPLS) programme for three flap deflection settings. The reference chord used in the determination of spanwise lift distributions in the report [54]is the extended chord after flap deflection. The spanwise lift distribution comparison is provided in figure 4.7. Blue lines represent the NPLS reference calculation performed by Fokker for the wing-fuselage model setup. Data is available from the root wing station to the tip of the wing model. Since the model used for calculations within the sizing routine incorporates an extension of the wing to the symmetry plane, for this model lift distribution data is available for the entire span range of the wing. Three different fuselage angles of attack are applied within the comparison: $\alpha_{fus} = 0^{\circ}$, $\alpha_{fus} = 3^{\circ}$, and $\alpha_{fus} = 6^{\circ}$. Comparisons are made for both flap extension method settings incorporated in the sizing routine. The upper row of the figure represents the method where the flap is rotated from its retracted to its extended method, thereby creating a gap between the main wing and flap system. Within the method represented in the lower row, this gap has been filled up by a surface containing a gradually increasing incidence angle to smoothly connect the main wing trailing edge to the flap leading edge. Both modelling methods were described in detail in section 3.4.1.

The following is observed when considering the spanwise lift distribution comparison contained in figure 4.7:

- For increasing fuselage angle of attack α_{fus} , the lift distribution shifts upward The upward shift of the lift distribution for increasing fuselage angle of attack implies an overall increase in lift forces on the wing model. The shape of the distribution remains constant along the considered angle of attack range. Since no stall correction mechanism is included in the current aerodynamic model, this is expected behaviour for even larger angles of attack.
- Both an upward shift and change of the shape of the list distribution is observed when varying the flap deployment setting
 As a consequence of increasing the flap deflection angle, the loading of the wing model increases over the complete wing span. This increase is the largest in the flap region itself, but is also seen in adjacent regions.
- Although the overall shape of the lift distribution shows large similarities between both calculation methods, overall wing loading of the high-lift device analysis routine calculation results is shifted outboard when compared to the NPLS calculations

 As will be shown in section 4.2.3, this shift in lift distribution does not result in a drastic change of the overall wing lift coefficient. It however does influence the overall spanwise wing loading, which at its turn has an effect on the local structural skin thicknesses obtained after sizing the wing as using the sizing routine incorporated in the analysis tool. The outboard shift of loads results in the introduction of larger wing bending moments in the structure, so care has to be taken when interpreting the results of a converged structural sizing run.



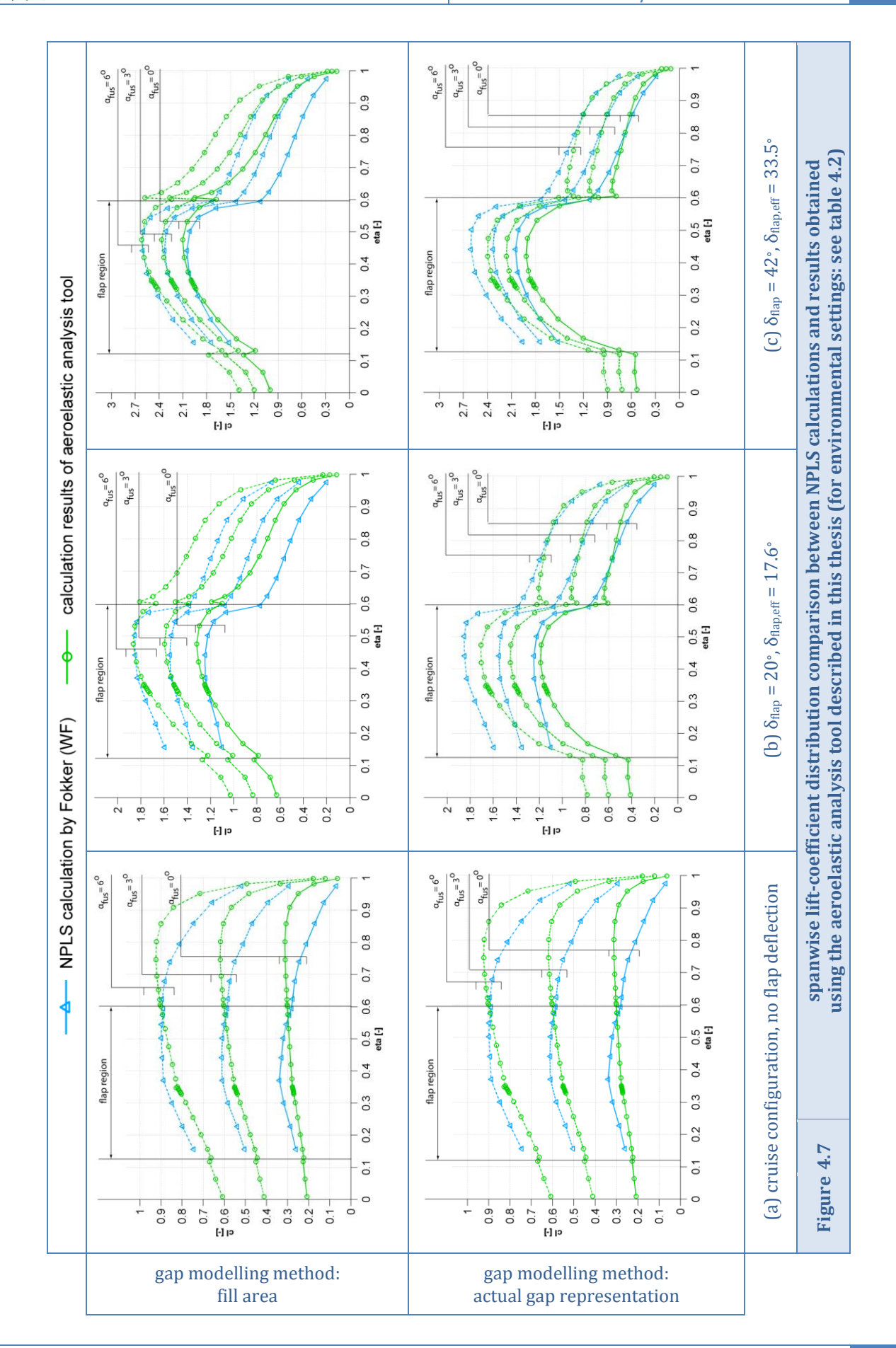
An explanation of this outboard shift of lift distribution peak can possibly be found in the difference in fuselage modelling. In the calculation performed by Fokker, an actual fuselage was modelled, as depicted in figure 4.5. In the vortex-lattice model used in the high-lift device analysis routine this fuselage is not explicitly modelled. Instead, the fuselage is represented by an extension of the wing from the wing root to the symmetry plane, using the overall wing sweep angle and taper ratio. This method might underestimate the influence of the fuselage induced flow accelerations on the lift distribution. Further research is required to find out if this difference is the cause of the discrepancy. Adding a fuselage representation to the wing is possible in AVL, unfortunately this is beyond the scope of the current investigation.

Since no experimental lift distribution data is available for comparison to the author, it is suggested to perform additional validation studies in order to gain a better insight in the correctness of the calculated lift distributions.

- Filling the gap between the main wing trailing edge and deployed flap surface in the vortex-lattice representation significantly improves the prediction of spanwise load distributions. When comparing the two applied gap modelling methods, a large difference in spanwise load distribution is observed. When using an actual gap representation, the lift is clearly underpredicted. This result should however be interpreted carefully, since results might be biased due to the absence of a flap covering area and spoilers in the wing model. This implies the gap representation is too large when compared to the actual wing model. On modern aircraft, spoiler panels are even used to actively control the size of the gap between both lifting surfaces. To allow actual conclusions on the differences in lift distributions for both gap modelling methods to be made, the wing model should first be improved by adding flap covering area and spoilers.

Although the gap is considered oversized in the wing model used for the lift distribution calculations, an indicative difference in load generation between both methods is already observed. Figure 3.23 showed that modelling a filling surface for the gap results in an overall increase in pressure due to the inclusion of lift dumping effect. This suggests using the gap filling method provides results more closely resembling actual load distributions along wings. Until further research is conducted, it is therefore suggested to use this particular method when performing calculations using the sizing routine designed during this thesis.







4.2.3 Validation of lift curve calculation results for the Fokker-100 wing

Section Sources: [54]

Aside computational data obtained using the non-planar lifting surface method (NPLS), the reference report of Fokker used in the current chapter provides actual wind tunnel data for total wing lift coefficient (C_L) curves. For the three flap deflection angles considered, lift curve data is available for the Fokker-100 aircraft in tail-off configuration (WFN). For the maximum flap deflection setting, an additional lift curve is provided concerning the model in wingfuselage (WF) configuration. These curves, along with the results of Fokkers' NPLS calculations are used in the current section to validate the aerodynamic results obtained using the vortex-lattice method applied in the sizing routine.

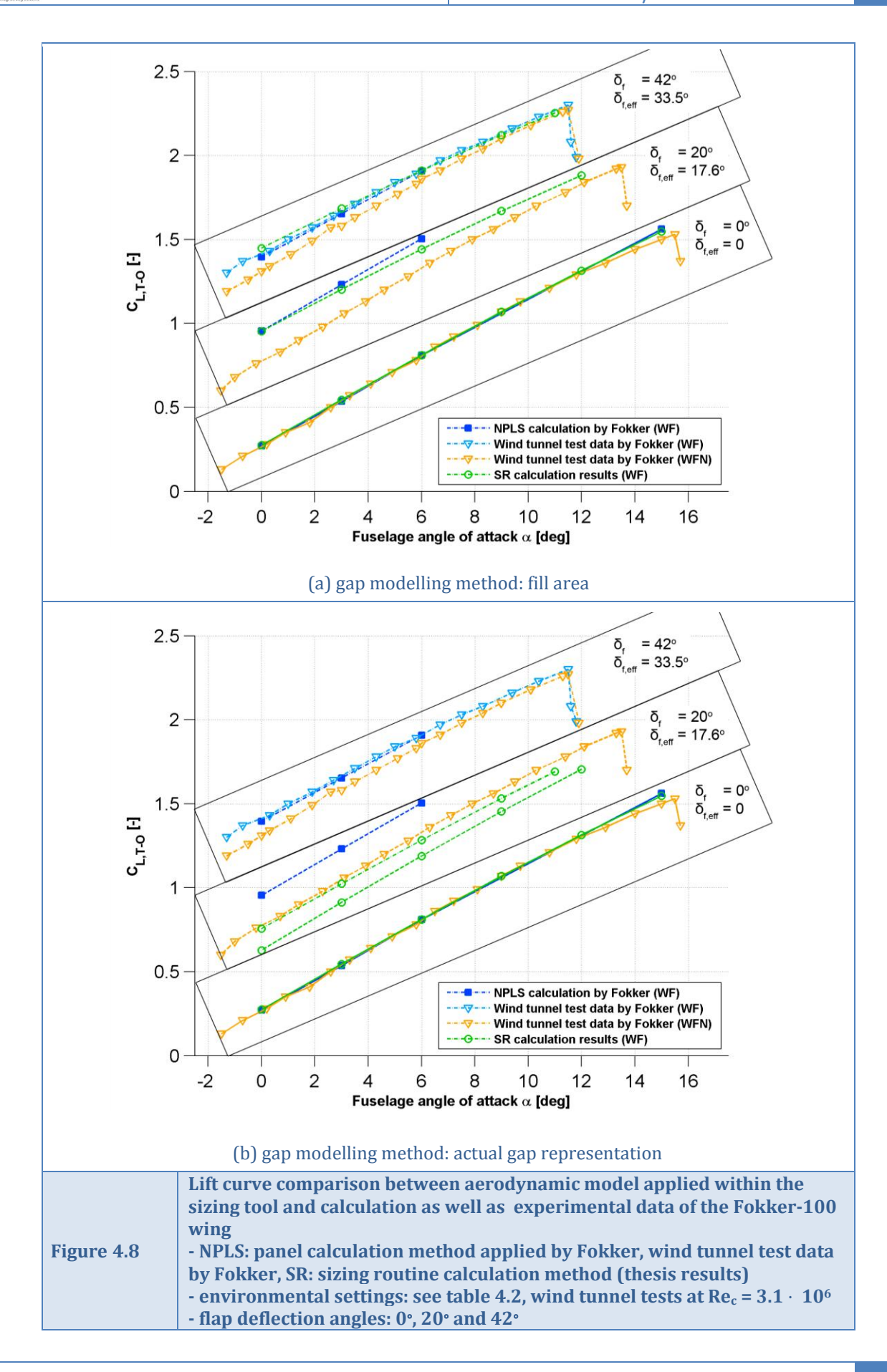
In determining total wing lift coefficient (C_L) values, a similar reference value determination method has been applied as was done when determining the spanwise lift distributions: the reference area is equal to the sum of all individual panel areas, using the geometry with flaps in the applicable deflected position. Environmental conditions as described in section 4.2.1 are again applied during the calculations.

The lift curve comparison is presented in figure 4.8, again for both gap modelling methods. Just as observed when comparing spanwise lift distributions, the model containing an actual gap representation underpredicts lift and is therefore considered an unreliable method in the high-lift device analysis routine. The results of the method using a fill area to represent the gap are however very promising. The following can be concluded from figure 4.8(a):

- For the cruise configuration having zero flap extension, both the results of the applied aerodynamic routine and those of the NPLS calculation performed by Fokker are in very good agreement with experimental data
 Since no stall prediction is included in the calculation methods, this conclusion refers to the linear range of the lift curve only.
- For the maximum flap deflection angle, results of both calculation methods are very similar. The wing total lift coefficient is only very slightly overpredicted when compared to experimental data. Especially when considering experimental data of the wing-fuselage model, sufficiently accurate lift coefficient predictions for preliminary design are obtained using the applied aerodynamic method in the current thesis

 Differences between the calculated and experimental data are probably mainly caused by the usage of experimentally corrected inviscid flow assumptions in the calculation methods, not capable of capturing all viscous effects of the actual flow field encountered during experiments. Another discrepancy might be introduced in the geometrical modelling assumptions made during the generation of the discrete wing model used within both calculation methods.
- Large differences are obtained between calculations and experimental data when considering the intermediate flap deployment position of δ_{flap} = 20° For the considered aeroelastic toolchain, the translational movement of the flap system for the intermediate flap position is restricted by the simple hinge linkage system used during flap deflection calculations. This uncertainty in model generation may have consequences on the obtained lift curve results. It is however noted that the NPLS results of Fokker show similar errors in predicting the lift curve for the intermediate flap position.







4.3 Grid convergence analysis of the Fokker-100 wing

In this section, the Fokker-100 aerodynamic model as described in section 4.1 is used to perform a grid convergence analysis. Sensitivity of the computed aerodynamic results to grid refinements is analyzed in order to obtain grid panelling settings providing adequate results using a low amount of computational resources.

In order to obtain an indicative basis grid setting for building wing models in the aerodynamic calculation subgroup of the sizing tool described in section 3.4, a grid convergence analysis is performed using the Fokker-100 wing model. For the five different grid settings listed in table 4.3, aerodynamic analyses are run using the same angle-of-attack range and flap settings as in the previous section. The vortex-lattice grids resulting from the panelling settings are provided for each individual flap deployment setting in figure 4.10. The very coarse grid in this figure contains the least amount of panels: 28 at the main wing and 4 at the flap area for the wing in cruise conditions. The largest amount of vortex panels is observed in the very dense grid model representing the Fokker-100 wing with a flap deflection angle of 42°: 2031 panels for the main wing and 756 for the flap.

The applied cosine spacing in both the chordwise and spanwise directions results in bunching of vortex panels at regions where geometrical discontinuities are present in the wing. Especially for the dense grid models, a large amount of panels is positioned at the wing kink and gap boundaries. As a final observation from figure 4.10, the automatic surface positioning ensuring proper chordwise vortex outlining for the complete wing setup is indicated. The spanwise surface boundaries of the base wing move along with the leading edge position of the flap.

Table 4	.3	Inve	estigated gr	id spacing setti	ngs durin	g grid conver	gence ana	llysis
grid type	spacir directi	_	# panels per [m]	chord/span range	# panels per [m]	chord/span range	# panels per [m]	chord/span range
V0W/ 000W00	chordw	ise	2		1		0.5	
very coarse	spanwi	ise	2		1		0.5	
	chordw	ise	3		2		1	
coarse	spanwi	ise	3	0.00 < c < 0.50	2	0.50 < c < 1.00	1	1.00 < c
01/04000	chordw	ise	5		4		3	0.5
average	spanwi	ise	4	or	3	or	2	or
dense	chordw	ise	8	0.00 < s < 0.50	6	0.50 < s < 1.00	4	1.00 < s
aense	spanwi	ise	7		5		3	
very dense	chordw	ise	12		9		6	
very dense	spanwi	ise	8		6		4	

Figure 4.11 provides spanwise lift coefficient distributions for the three flap deflection settings at both low and high angle of attack. The very coarse grid setting overpredicts the aerodynamic wing loading and is therefore considered inappropriate for usage within the sizing routine. The coarse grid already shows a large improvement in result behaviour, but still

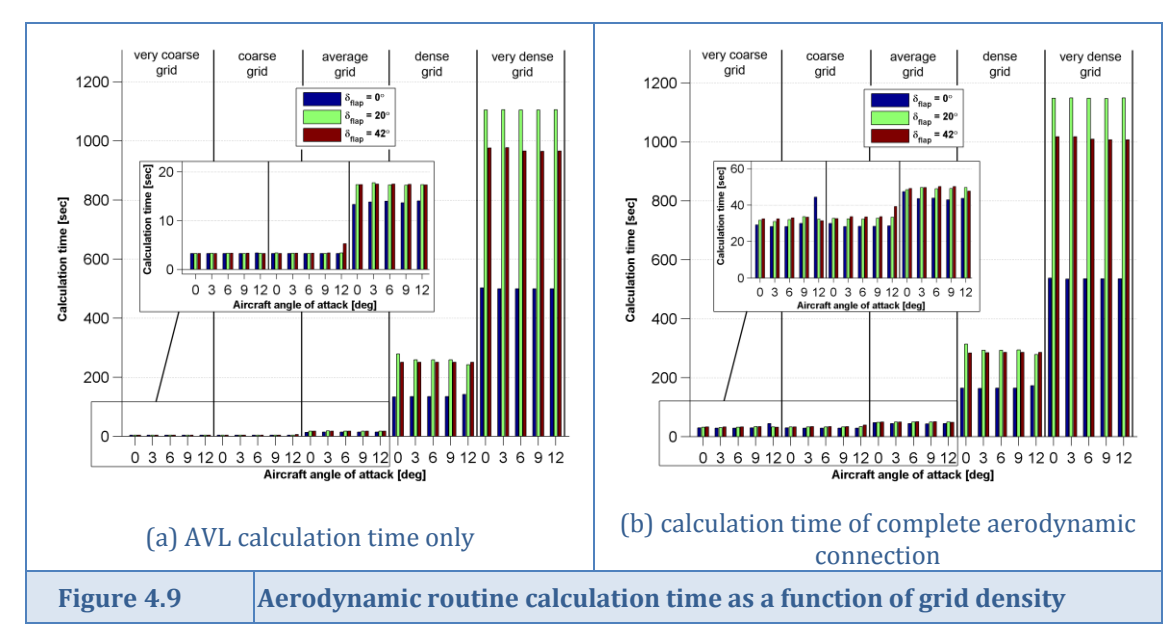


incorporates distinct jumps in the c_l -distribution curves. Discontinuities at the edges of the flap system are only marginally captured by this grid. Spanwise loading results of the models having average to very dense grids show no significant differences in behaviour, except for a small discontinuity at the kink position for the dense and very dense grids, almost not worthy of mentioning.

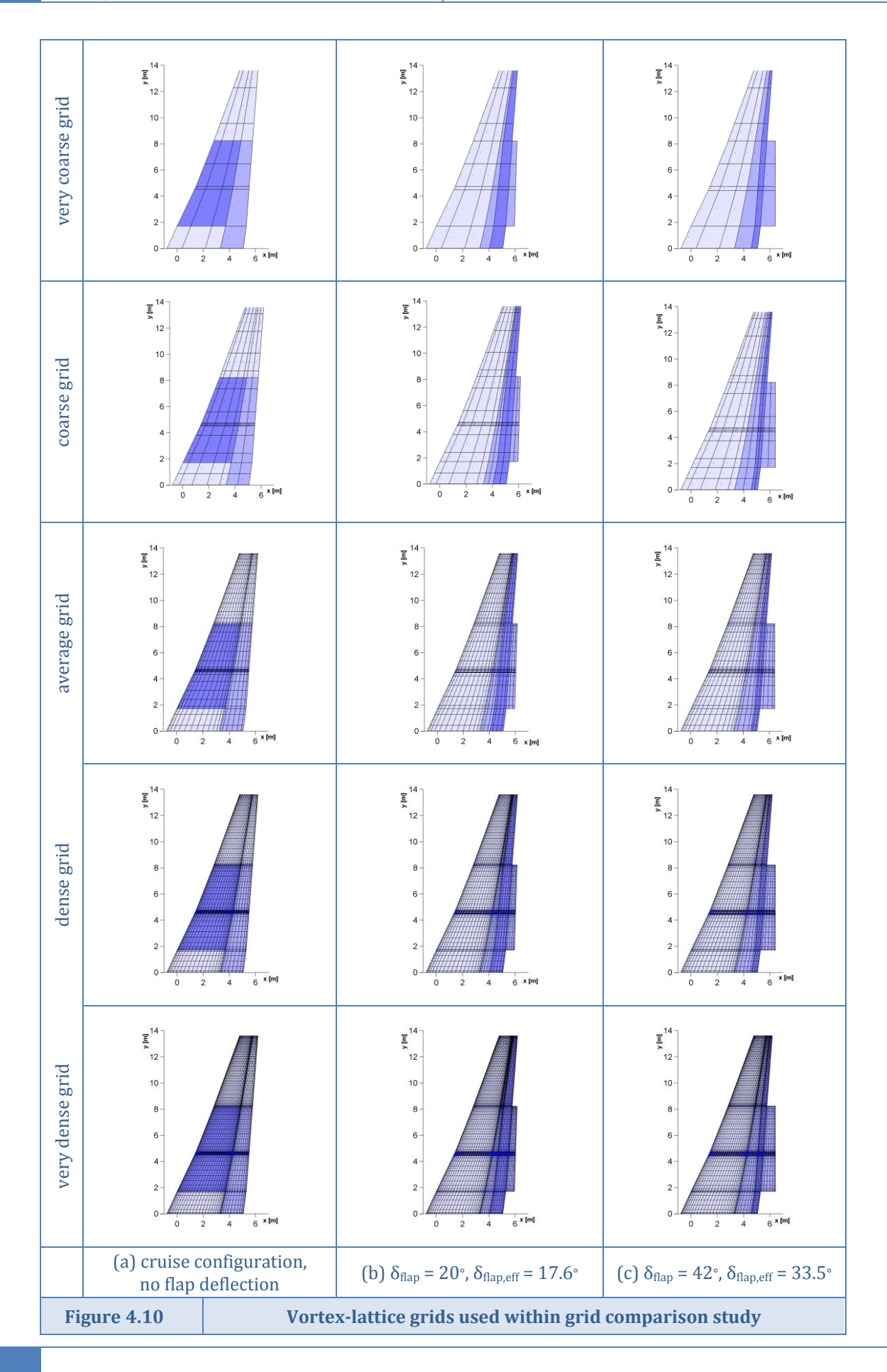
The lift curves for all grid settings are provided in figure 4.12. The top row shows the lift curves obtained from the result datadecks of AVL. The bottom row shows the lift curves obtained after interpolation of the aerodynamic results on the structural grid. Just as concluded from the spanwise c_I-distributions, the very coarse grid provides unsatisfactory results. Considering the total lift values directly obtained from AVL, no significant difference is seen between results using grids other than the very coarse grid setting. This observation however changes when considering the lift curves obtained using the interpolated aerodynamic results on the structural grid. In this case, the coarse grid setting underestimates lift as well. Due to the coarse vortex spacing, the difference between the re-cambered vortex-lattice grid and flattened structural grid are too large to ensure correct force values are obtained at the structural keypoint locations. Therefore this second grid setting should be avoided in the high-lift device analysis routine as well.

Required calculation effort per investigated grid type, flap deflection and angle-of-attack is compared in figure 4.9. It is observed that the calculation time increases exponentially with grid density. The high computational effort required for calculations using dense and very dense grids is the result of the required inversion of the large vortex influence matrix in obtaining the vortex-lattice solution. Since aerodynamic loading has to be determined for each aeroelastic iteration within the sizing tool, calculation time requirements cause the dense and very dense grids to be considered inapplicable.

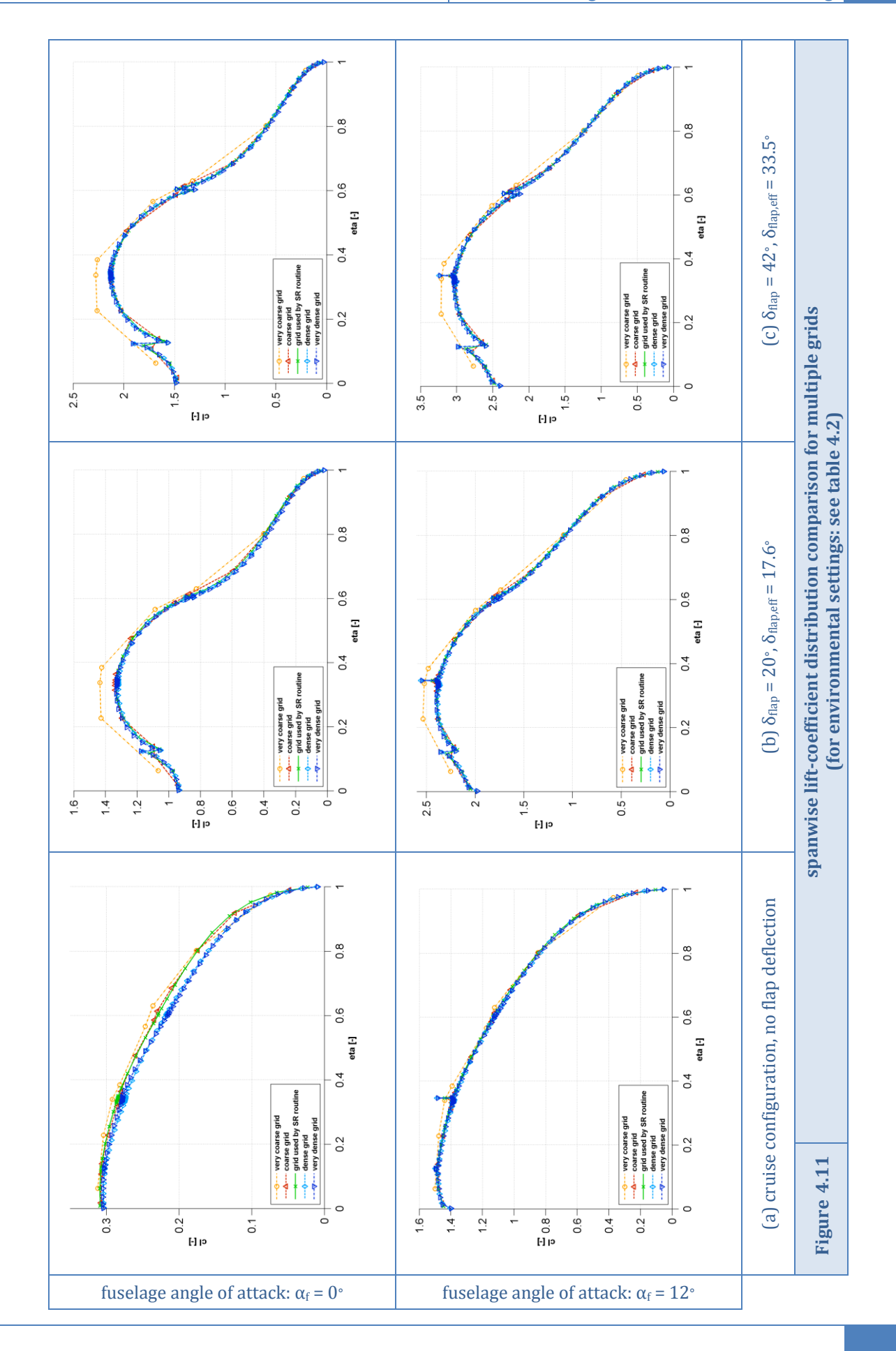
It is concluded that the average grid setting provides accurate results for usage in the conceptual and preliminary wing design phases, for an acceptable requirement on calculation time.



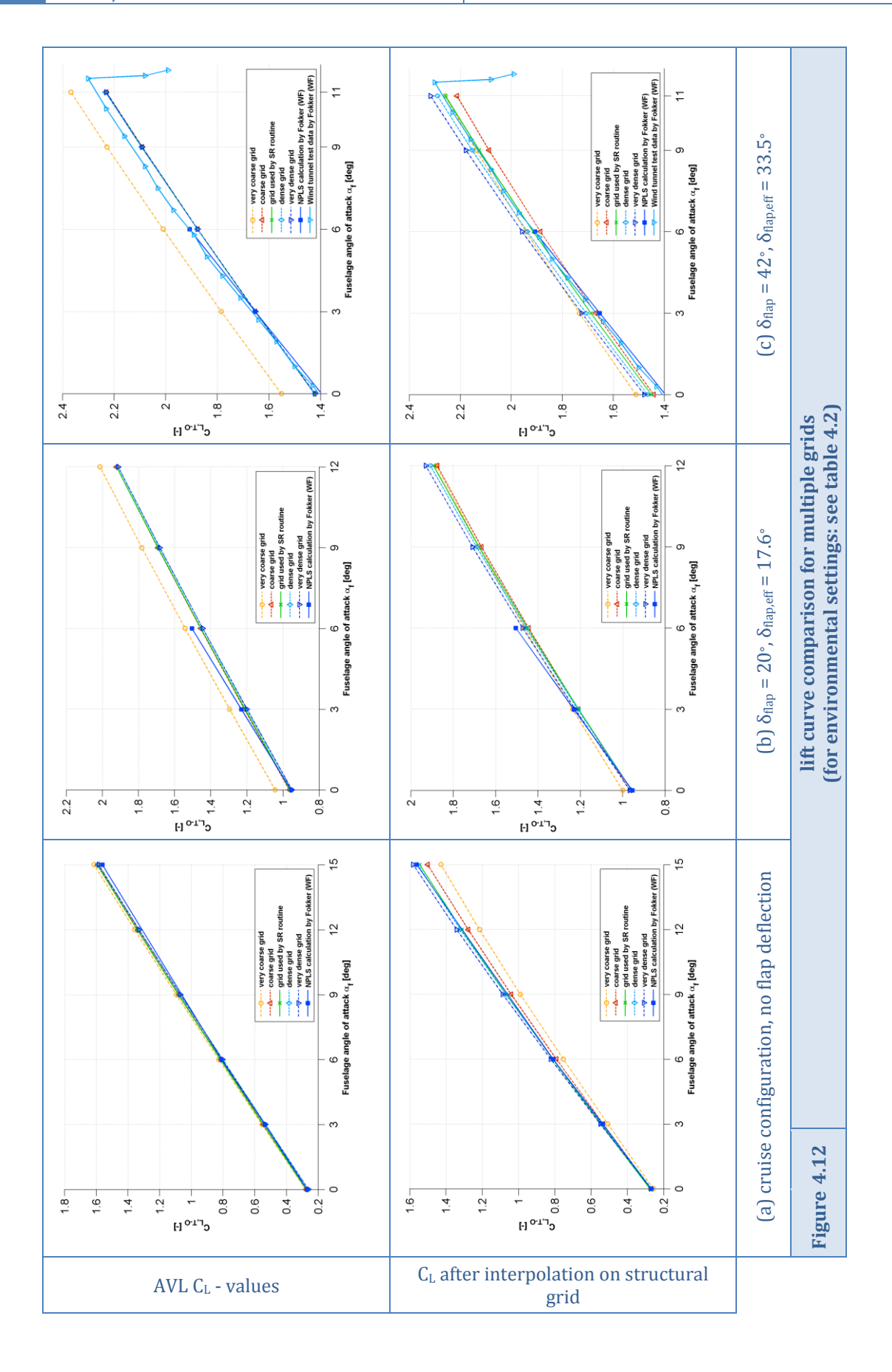
¹⁶ section 3.4.2 describes the way in which the uncambered vortex-lattice grid is adjusted to include camber in order to provide a sound basis for force interpolation.





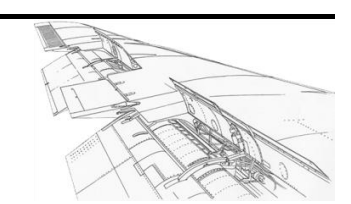






Chapter 5

Method application in preliminary wing sizing



The generated high-lift device analysis routine is used to perform initial sizing on the iGreen forward-swept wing model. The results provided in this chapter show the kind of the sizing studies that can be performed using the structural sizing routine for wings including high-lift devices.

The finalized aeroelastic analysis routine for wings including high-lift devices described in chapter 3 is utilized to perform an initial sizing of the iGreen wing model. A description of the geometry of this forward-swept wing was provided in section 3.2.1. Since the intent of the current chapter is to show initial sizing results, the aeroelastically converged calculation results presented at the end of chapter 3 are used as basis for structural sizing. This implicates sizing is performed 'out-the-loop'. Performing intermediate sizing during the aeroelastic iterations and studies on differences in convergence behaviour between both methods is left for future research.

As was described in section 3.7, the sizing robot 'S_BOT' is capable of considering multiple critical loadcases in order to size the wing according to the highest occurring loads. The current sizing however considers a single loadcase: the application of resulting aerodynamic loads obtained after aeroelastic convergence in combination with gravitational acceleration settings at sea level conditions. The results discussed hereafter show the ideal material distribution for the wing applicable to this particular loadcase only. Since the structure of the wing will encounter larger stresses when considering the entire flight envelope of the aircraft, material distributions will be different for the actual wing to be designed.

The preliminary sizing is limited to the torsion boxes of both the main wing and trailing edge flap of the iGreen wing and the flap support systems. Table 5.1 lists the boundary settings used during the application of S_BOT. A convergence checker is added to the S_BOT routine, based on the change in shell thickness per element layer. If for 99% of all shell elements, the thickness does not change more than a predefined convergence limit, the sizing is considered converged. For the iGreen wing sizing, this convergence limit is set to 0.1 [mm]. Stopping the sizing routine when 99% of the elements are within the convergence limit greatly reduces the amount of S_BOT iterations required per analysis. The very gradual convergence of shell thickness of the remaining elements would introduce slow program behaviour, while the overall thickness distribution does not change significantly. Aside a convergence checker, extraction macros for creating result datadecks for importing in MatLab are also added to the S_BOT programme.

Figure 5.1 shows overall mass convergence for the iGreen optimization region. When comparing the total wing mass after convergence, an increase in total mass for increasing flap deployment setting is observed. The larger loads imposed on the wing result in higher structural stresses which cause the structural sizing routine S_BOT to add skin thickness and thereby wing weight. The number of iterations required for convergence also increases with increasing flap deployment setting, which has an increased total running time of the sizing



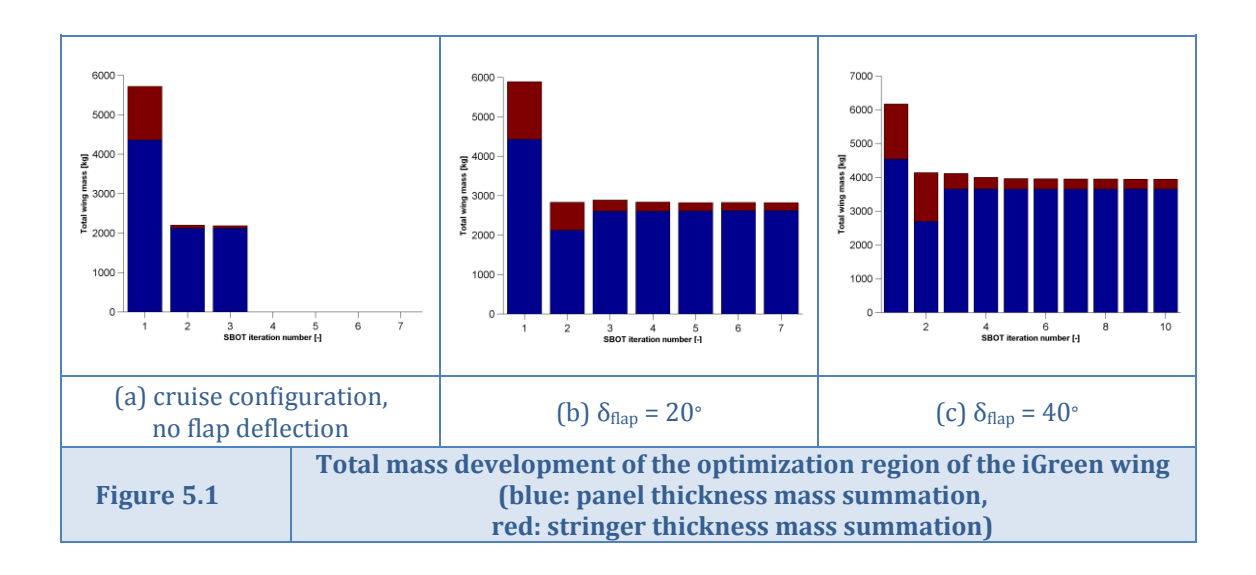
routine as a consequence. Since for each sizing iteration, a structural finite element solution has to be obtained, running time of the sizing routine is relatively large.

Element specific mass results are presented in figure 5.2 for clean wing in cruise conditions, in figure 5.3 for 20° flap setting and in figure 5.4 for the maximum flap deflection of 40°. Since the first iterations involve the largest change in wing thickness, results are provided for iteration numbers one to three and for the iteration which resulted in convergence. To allow for fair comparison of the mass distribution, element specific mass results are provided, expressed in mass per unit shell area. The uppermost row of each figure represents the structure in its undeformed shape. The entire upper and lower skin, as well all spar and all rib elements are set to their respective initial skin thickness value and therefore have a constant specific mass. Sizing on the loadcase with undeflected flap shows quick convergence to an updated, almost constant specific mass distribution, as seen in figure 5.2. This is the result of the very low aerodynamic loads imposed on the structure. The development of specific mass distributions for the loadcases involving flap deflection clearly show the results of wing bending on the one hand and stress introduction of the flap support system on the other hand. When considering the wing skin panels in the left column of figures 5.3 and 5.4, a gradual increase in element specific mass from the tip to the root of the wing is seen. This is the consequence of increasing wing bending moment when moving inboard. The development of the mass distribution of the rear spar can be seen in the right column of the aforementioned figures. The largest load transfer from flap support system to the rear spar occurs at the middle support. This leads to the material addition at the part of the rear spar in between this flap support system and the wing root, to ensure proper load transfer to the clamped wing box. As can be seen from comparison of mass distribution in the third and fourth row of the figures, this addition of material at the spar is partly translated to the skin during the sizing iterations in between the third and final iteration.

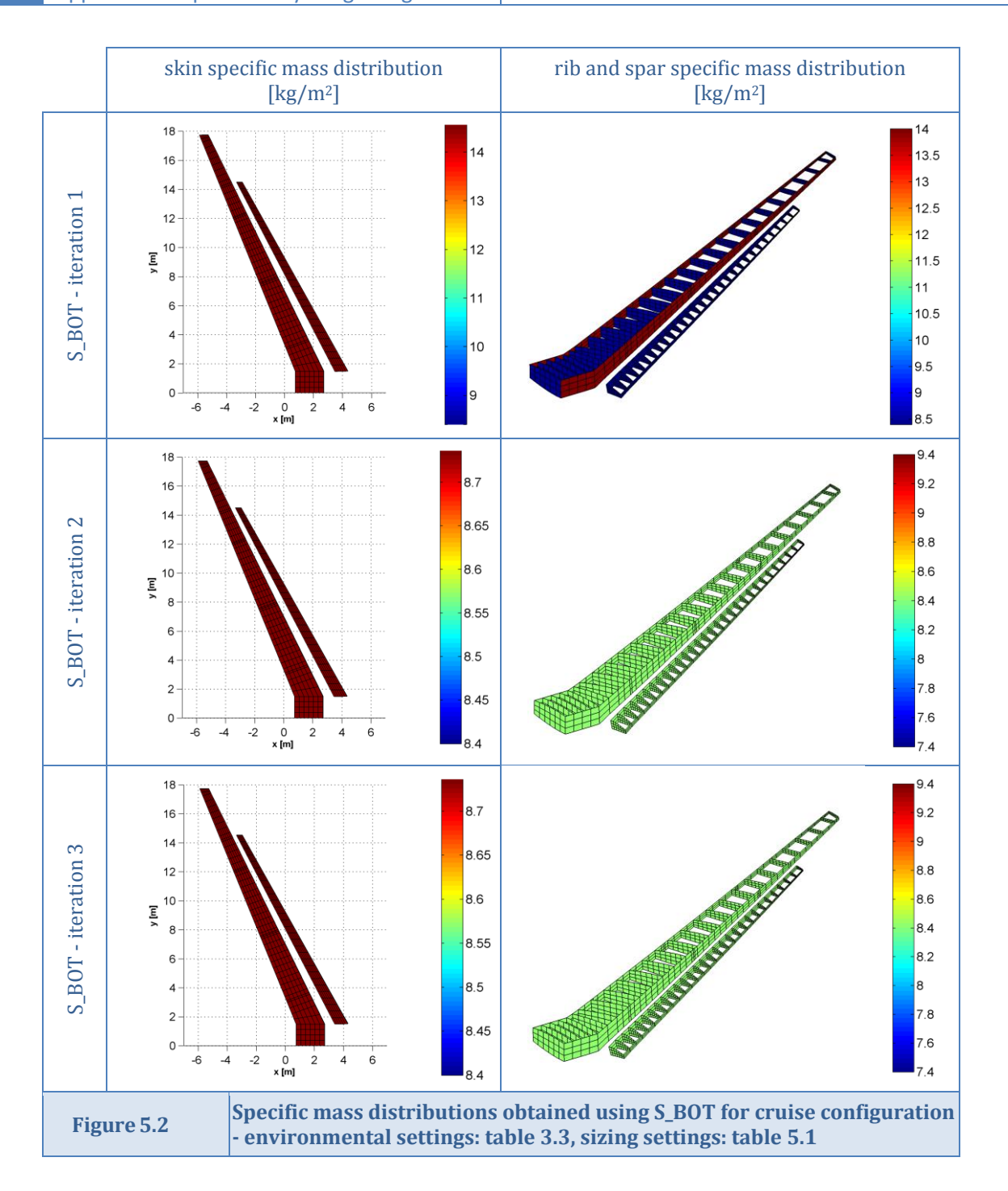
The total mass and mass distribution results show explicable behaviour. However, further research is needed on the mechanisms defining the redistribution of material across the wing structure, before performing actual mass estimations of wing setups during preliminary design. Also worth investigating is intermediate sizing during aeroelastic iterations instead of afterwards, in order to incorporate the change in loading distribution for changing structural wing properties.



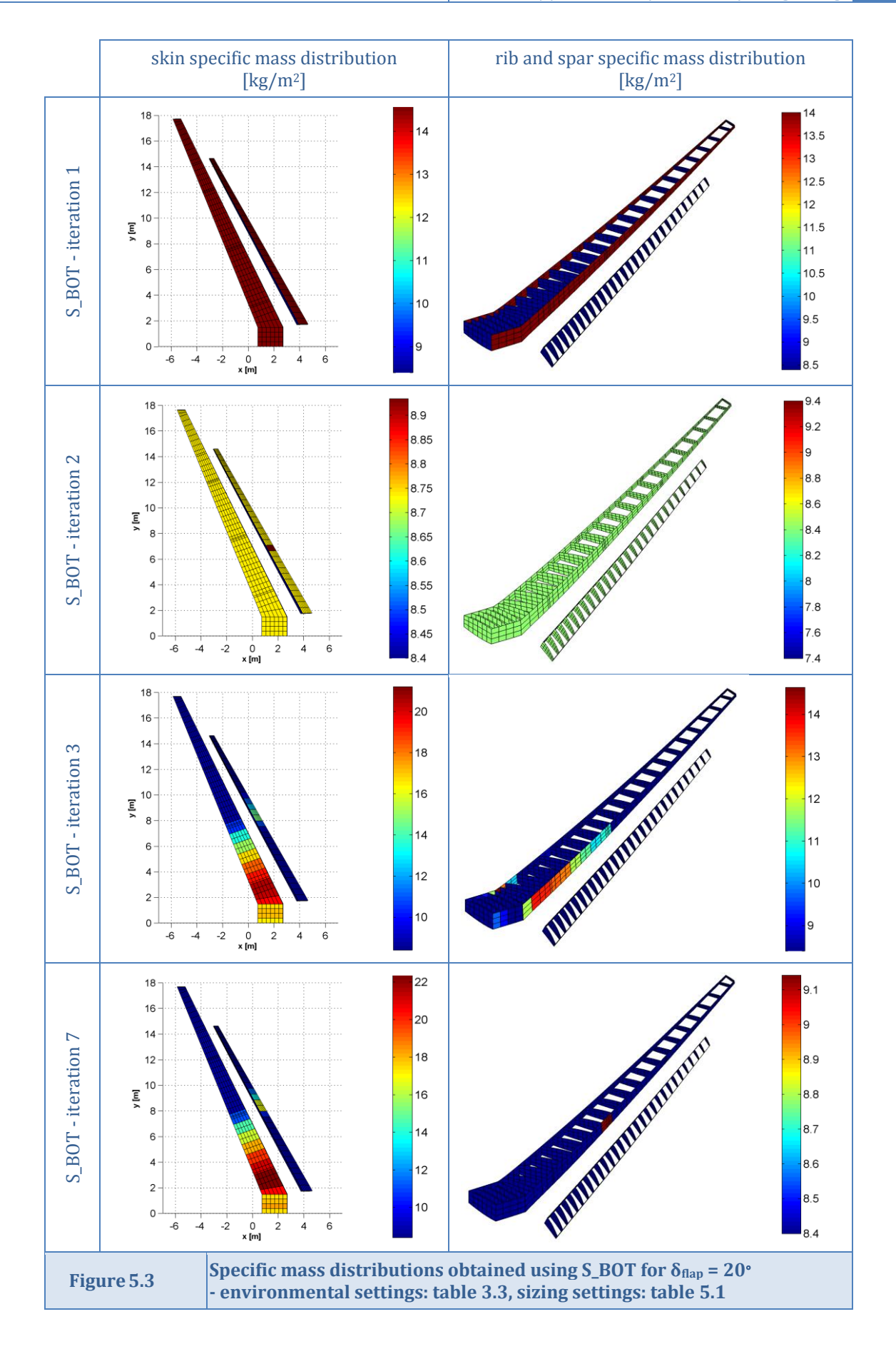
Table 5	.1	Gener	al sizing se	ettings for the	iGreen wing n	nodel used wit	hin S_BOT
area	sizing r	egion	parts	general safety factor	additional safety factor	minimum shell thickness [m]	yield criterion
main wing	torsion	box	shells	1.5	1.03	0.003	von Mises
	torsion	box	shells	1.5	1.03	0.003	max. stress
flap	supp	ort	shells	1.5	1.00	0.003	max. stress
	syste	em	beams	1.5	1.00	0.002	max. stress

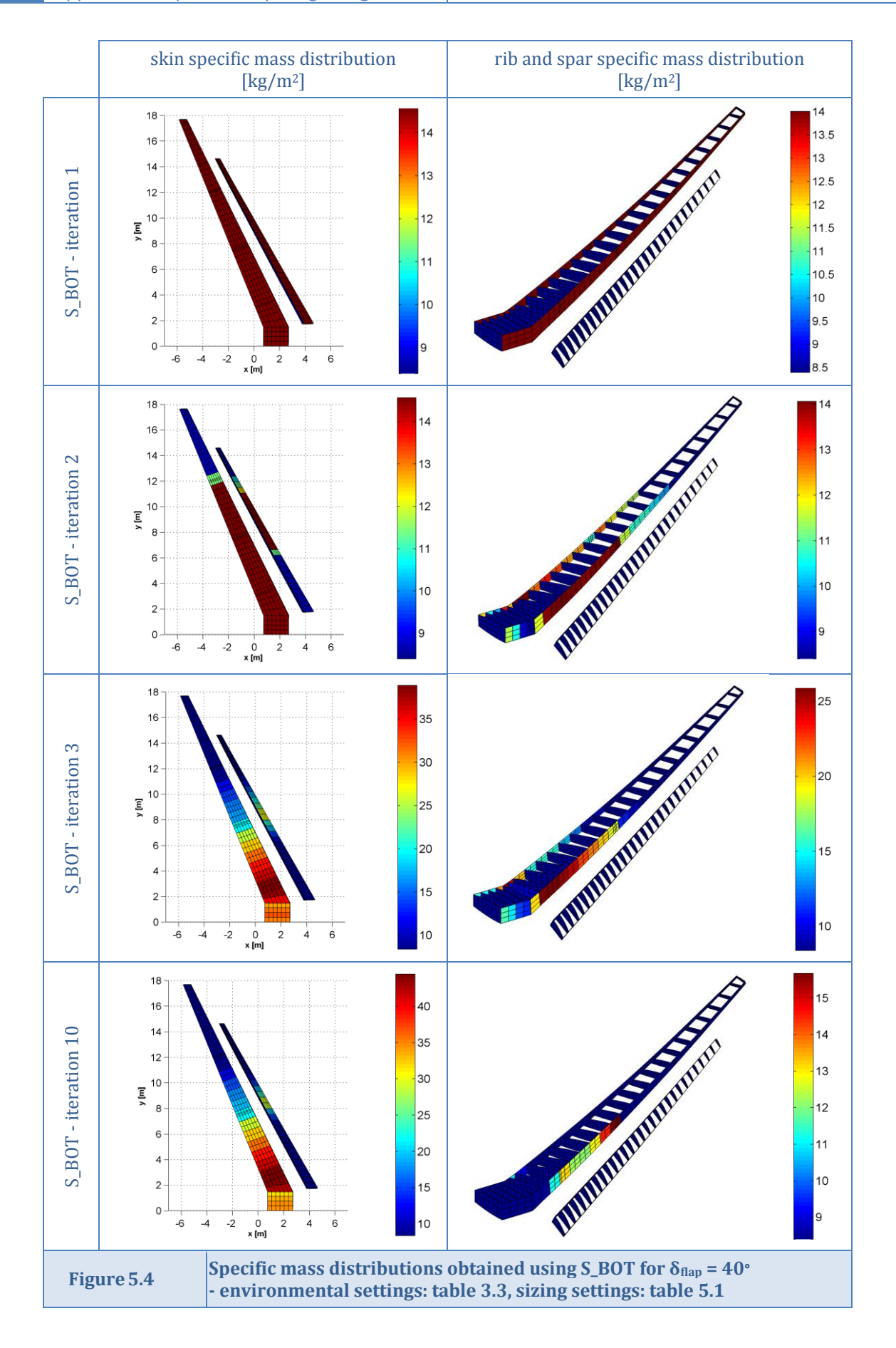






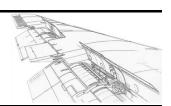






Chapter 6

Conclusions and Recommendations



This chapter provides the main conclusions concerning the development of the aeroelastic analysis tool for structural sizing of high-lift devices. Using these conclusions and experience gained during the tool development, recommendations for future work are provided thereafter.

6.1 Conclusions concerning the developed aeroelastic analysis tool for structural sizing of high-lift devices

The aeroelastic analysis tool developed during this thesis provides a solid basis for enhancement of the understanding of interconnections and sensitivities between the aerodynamic and structural disciplines involved in preliminary high-lift device design.

The main goal of this thesis was to develop an initial solution to the requirement for improved high-lift system representations on preliminary design level. The highly complex design of high-lift devices involves different areas of expertise, such as structural and aerodynamic design. These fields of expertise underlie the research performed in the framework of this master thesis. In order to fulfil the overall thesis goal, two main objectives were defined. First objective was to construct an aeroelastic representation of wings including high-lift systems. Hereby the main focus was set on rapid estimation of aerodynamic loads. Possible incorporation in the wing design chain of the German Aerospace Centre was to be kept in mind. Based on the construction of the aeroelastic representation, the understanding of the interconnections between structural and aerodynamic discipline involved in the design of high-lift systems was to be enhanced. Structural sizing and weight estimation formed the main focus of this second objective.

In order to achieve better understanding of the disciplines involved, a literature research was conducted on the current high-lift design process, parametric modelling techniques and aerodynamic calculation methods. From this research, it became clear that during the preliminary design stage, the current design of high-lift systems is based mainly on aerodynamic considerations, while other disciplines are barely taken into account. Furthermore, focus has been set on the generation of high-fidelity aerodynamic analysis tools involving computational requirements which are not applicable to preliminary design. However, several parametric modelling techniques exist that allow interconnecting multiple disciplines within high-lift system design. This allows for structural considerations to as well be taken into account in the early design phases. Concerning aerodynamic calculation methods, research shows that low to medium fidelity methods are available, providing satisfactory results for preliminary design phases using considerably lower computational resources.

An aeroelastic analysis tool was developed for preliminary structural sizing of wings incorporating high-lift devices, in order to create a solid basis for initial design of high-lift systems. The model generator developed during the preceding internship was used to construct structural base wing models used in the aeroelastic tool chain. This wing model is thereafter used to generate a connection to aerodynamic vortex-lattice software in order to perform rapid load estimations. Knowing the structural wing model and corresponding aerodynamic loads, deformation of the wing is obtained using finite element software. An iterative process is set up, updating the jig-shape of the wing model to its actual in-flight shape after which the corresponding load distribution is attained. Thereafter, a structural sizing routine was incorporated in order to perform initial structural sizing and weight estimation of the wing model. Herewith, the tool chain is completed and can be used to enhance understanding of the aeroelastic interconnections in high-lift device design.

To ensure that performance of the aerodynamic load estimation method is within acceptable preliminary design accuracy, results were compared to available load distributions on the Fokker-100 wing. Large similarities were found between the calculated loads and data provided by the Fokker report, thereby validating the applied aerodynamic method. Also, grid convergence studies were performed to show grid independence of the results on the one hand and to determine proper grid density for required calculation accuracy and computational demands on the other hand. The results of this study show that grid setups exist, for which obtained aerodynamic result data does not significantly change for additional density increase. Since computational requirements increase drastically for denser grids, the attained minimum grid density providing independent results is advised to be used in performing calculations using the aeroelastic analysis routine.

To show an indicative application of the aeroelastic analysis routine, the forward-swept wing box of a medium-sized transport aircraft was structurally sized for three different trailing edge flap settings. Results of the performed sizing are promising and form the starting point for implementation of the routine in preliminary aircraft design. Improved knowledge on the high-lift system using the developed preliminary analysis tool will enable designers to consider relevant sensitivities in both the structural and aerodynamic disciplines in early design phases.

Taken together, the above findings show that improving the high-lift system representation is feasible and beneficial for preliminary design level purposes. Due to extended knowledge of the aeroelastic behaviour of wings incorporating high-lift devices, designers are able to make more substantiated design decisions incorporating both structural and aerodynamic constraints. Once fully developed, this representation model has the potential to significantly influence the overall design process, by shifting knowledge of the parametric design space definitions to earlier stages.



6.2 Recommendations for future work on high-lift system investigations during preliminary design

The findings of the research performed in this master thesis show that the developed aeroelastic analysis routine has the potential to serve as basis for making design decisions in preliminary wing design phases. For the methodology to become generally applicable, future research should concentrate on the recommendations listed hereafter.

- Extending the analysis routine with a viscous flow coupling method
 Since the flow physics of high-lift systems involves multiple viscous flow effects, extending
 the analysis routine with a viscous flow coupling method is required to improve the
 accuracy of the aerodynamic load calculation. When analyzing existing wing models, this
 coupling can be based on the usage of existing experimental wind tunnel data or results of
 higher-fidelity calculations involving viscosity. To perform analysis on new wing designs, it is
 necessary to incorporate a viscous calculation method to obtain a proper basis for viscousinviscid flow coupling. For this matter, the two-dimensional viscous/inviscid flow solver
 MSES shows promising results for the multi-segmented airfoil sections under consideration.
 Otherwise, the viscous flow correction method applied in the validation of the
 aerodynamic results can serve as an initial solution for this problem.
- Incorporation of high-lift devices other than single-slotted flaps
 To be able to perform a analysis on the high-lift system of the complete wing, leading edge high-lift device definitions should be incorporated in the wing model representation. Research showed that modern transport aircraft mainly use slats as leading edge device, so one should focus on this particular type. Room has already been reserved in the source code of the aeroelastic analysis routine, and most of the calculation principles used for trailing edge devices are directly usable for leading edge devices as well. Trailing edge high-lift device definitions should be improved by incorporating a larger variety in deployment mechanisms and by generating improved representations of fairings containing the mechanisms.
- Extending the parametric wing model with elements having purposes other than adding high-lift capabilities
 - A very useful extension is the inclusion of spoiler panels, which can serve a double function. First, the possibility to analyse the effects of spoiler extension on the wing aeroelastic behaviour becomes available. A second, more profound effect of including spoiler panels is the possibility to control the gap between the main wing and extended trailing edge device. The effects of this extension are expected to have a significant influence on the aeroelastic analysis method when viscous flow effects are included in the aerodynamic calculation. Other wing-related elements considered a useful extension include: incorporation of tank volumes to simulate effects of fuel weight and distribution, inclusion of engines and gears and finally the addition of control surfaces. The latter should not require too much effort, since these are programmable as simplified versions of high-lift devices.

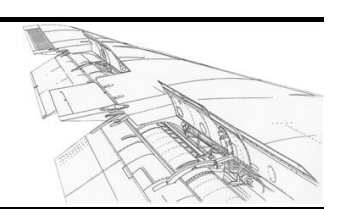


Investigating the effectiveness of the parametric modelling technique used within the aeroelastic analysis routine
 Using the model generator, a structural model representation of the wing is obtained. The use of this structural definition as a basis for deducing the aerodynamic model can pose severe consistency problems. Since in the current aerodynamic load determination an inviscid vortex-lattice calculation is applied, local discontinuities in the nose roundness have no direct influence to the obtained aerodynamic results. However, when extending the analysis routine by incorporating flow solvers which do depend on the actual geometrical definition of the skin, consistency problems might become of influence. This lack of

consistency across disciplines was identified as the largest threat of the applied discrete geometrical parameterization method during the literature research. Another interesting investigation might consider comparing the easiness of modelling and requirements on computational resources of the current and other identified parameterization methods.

- Incorporation of the aeroelastic high-lift device analysis routine in the wing design chain of the German Aerospace Centre
 Increasing the amount of disciplines involved in the high-lift system analysis is possible, providing a more solid basis for multidisciplinary design decisions during preliminary design.
 One could for example explicitly model hydraulic actuating systems to incorporate aeroelastic wing deformation effects in the design of the hydraulic system.
- Extension of material definitions within the structural model
 The current wing design incorporates a two material layers consisting of a homogeneous type of material: the first layer represents the actual wing ribs, spars or skin and the second layer represents the influence of stringers. This definition can be extended for the usage of composite materials by increasing the number of material layers. The sizing routine incorporated in the developed tool is capable of performing sizing of composite materials, by both adjusting layer thickness and fibre directions.
- Incorporation of methodologies checking for unwanted aeroelastic behaviour
 Divergence, flutter or the onset of wing buffet are examples of unwanted aeroelastic wing behaviour. Airplane controllability investigations are also among the possibilities. Since aeroelastically converged pressure distributions along the wing are obtained using the analysis routine, aileron effectiveness as well as the possible occurrence of aileron reversal can be assessed.
- Validation of the structural stress and displacement results as well as mass distribution results obtained using the external structural finite element software.
 Unfortunately, no extensive high-lift system mass data was available to the author. Verification of the structural sizing results could therefore not be performed during the thesis, which is however strongly advised before putting the analysis routine into practice.
- Performing mass sensitivity studies on high-lift system design parameters using the structural sizing method incorporated in the aeroelastic high-lift device analysis routine Exploring the complete primary geometrical design space will help in enhancing the understanding of sensitivities of design parameters on both the high-lift system specific mass and mass of the complete wing setup. Among others, primary geometrical design parameters include: span, chord and spanwise positioning of flaps, as well as the geometry and location of support systems. Knowing the influence of high-lift system parameter changes on wing mass can serve as a great aid in making design decisions during the preliminary design of wings.

References



- Moerland, E. "Internship report: Parametric high-lift device modelling using multibody dynamics." German Aerospace Centre, institute for air transportation systems and technology assessment, Hamburg, Germany, 2009.
- 2. Rudolph, P. K. C. "High-Lift Systems on Commercial Subsonic Airliners ". NASA, 1996.
- 3. Van Dam, C. P. "The aerodynamic design of multi-element high-lift systems for transport airplanes," *Progress in Aerospace Sciences* Vol. 38, No. 2, 2002, pp. 101-144.
- 4. EASA. "Certification Specifications for Large Aeroplanes." European Aviation Safety Agency, 2009.
- 5. Ruijgrok, G. J. J. *Elements of Airplane Performance*. Delft: Delft University Press, 1996.
- 6. Reckzeh, D. "Aerodynamic design of the high-lift-wing for a Megaliner aircraft," *Aerospace Science and Technology* Vol. 7, No. 2, 2003, pp. 107-119.
- 7. Niu, M. C.-Y. *Airframe structural design practical design information and data on aircraft structures*. Hong Kong: Conmilit Press, 1988.
- Anderson, R. D., Flora, C. C., Nelson, R. M., Raymond, E. T., and Vincent, J. H.
 "Development of Weight and Cost Estimates for Lifting Surfaces with Active controls."
 NASA, 1976.
- 9. Roskam, J. *Airplane design Pt 5. Component weight estimation*. Lawrence, Kansas, USA: DARcorporation, 1999.
- 10. Raymer, D. P. Aircraft design: a conceptual approach. Reston: AIAA, 1982.
- 11. Torenbeek, E. *Synthesis of subsonic airplane design*. Dordrecht, The Netherlands: Kluwer Academic, 1982.
- 12. Nagel, B., Anhalt, C., Monner, H. P., and Breitbach, E. "Adaptive Spaltkontrolle an Hochauftriebsklappen," *DGLR 2004 Deutscher Luft- und Raumfahrtkongress*. Bremen, Germany, 2004.
- 13. Balaji, R., Bramkamp, F., Hesse, M., and Ballmann, J. "Effect of flap and slat riggings on 2-D high-lift aerodynamics," *Journal of Aircraft* Vol. 43, No. 5, 2006, pp. 1259-1271.
- 14. Obert, P. I. E., and Slingerland, D. I. R. "Aerodynamic Design of Transport Aircraft," *AE4-211*. Delft University of Technology, Faculty of Aerospace Engineering, 2007.
- 15. Smith, A. M. O. "High-lift Aerodynamics," *Journal of Aircraft* Vol. 12, No. 6, 1975, pp. 501-530.
- 16. Anderson, J. D. *Fundamentals of aerodynamics*. Boston, MA [etc.]: McGraw-Hill Higher Education, 2007.
- 17. Rogers, S. E. "Progress in high-lift aerodynamic calculations," *31st Aerospace Sciences Meeting & Exhibit*. Vol. AIAA 1993-0197, Reno, NV, 1993.
- 18. Mack, M. D., and McMasters, J. H. "High reynolds number testing in support of transport airplane development," *17th Aerospace ground testing conference*. Vol. AIAA 1992-3982, AIAA, Nashville, Tenessee, USA, 1992.
- 19. Flaig, A., and Hilbig, R. "High-lift design for large civil aircraft," *AGARD conference proceedings* 515. AGARD, Neuilly-sur-Seine, 1992.
- 20. Wentz, W. H., Jr.; Seetharam, H. C. . "Development of a Fowler flap system for a high performance general aviation airfoil ". NASA, 1974, p. 115.



- 21. Airbus. "Airbus Photo Gallery," http://www.airbus.com/en/myairbus/multimedialibrary, accessed: 23-11-2010. 2010.
- 22. Van Dam, C. P., Paris, J. K., and Vander Kam, J. C. "High-lift design methodology for subsonic civil transport aircraft." Vol. 2, 2000, pp. 111-120.
- 23. Reckzeh, D. "Aerodynamic Design of Airbus High-Lift Wings," *Airbus*. Braunschweig, Germany, 2005.
- 24. Romijn, E. "Picture of A380-861 single slotted Fowler flap system fully deployed." 2010.
- 25. Mavris, D. N., DeLaurentis, D. A., Bandte, O., and Hale, M. A. "A Stochastic Approach to Multi-disciplinary Aircraft Analysis and Design," *36th Aerospace Sciences Meeting & Exhibit*. Vol. AIAA 1998-0912, AIAA, Reno, NV, 1998.
- 26. Wild, J. "Multi-objective constrained optimisation in aerodynamic design of high-lift systems," *International Journal of Computational Fluid Dynamics* Vol. 22, No. 3, 2008, pp. 153 168.
- 27. Vandenbrande, J. H., Grandine, T. A., and Hogan, T. "The search for the perfect body: Shape control for multidisciplinary design optimization." Vol. 15, 2006, pp. 11088-11103.
- 28. Ledermann, C., Hanske, C., Wenzel, J., Ermanni, P., and Kelm, R. "Associative parametric CAE methods in the aircraft pre-design," *Aerospace Science and Technology* Vol. 9, No. 7, 2005, pp. 641-651.
- 29. Kulfan, B. M., and Bussoletti, J. E. ""Fundamental" parametric geometry representations for aircraft component shapes." Vol. 1, 2006, pp. 547-591.
- 30. Samareh, J. A. "Survey of shape parameterization techniques for high-fidelity multidisciplinary shape optimization," *AIAA Journal* Vol. 39, No. 5, 2001, pp. 877-884.
- 31. Athanasopoulos, M., Ugail, H., and Castro, G. G. "Parametric design of aircraft geometry using partial differential equations," *Advances in Engineering Software* Vol. 40, No. 7, 2009, pp. 479-486.
- 32. Straathof, M. H., Van Tooren, M. J. L., Voskuijl, M., and Vos, R. "Development and Implementation of a Novel Parametrization Technique for Multidisciplinary Design Initialization," *51st AIAA/ASME/ASCE/AHS/ASC Structures, Structural Dynamics, and Materials Conference*. Orlando, Florida, USA, 2010.
- 33. Wu, H.-Y., Yang, S., Liu, F., and Tsai, H.-M. "Comparison of three geometric representations of airfoils for aerodynamic optimization," *16th AIAA Computational Fluid Dynamics Conference*. AIAA, Orlando, Florida, USA, 2003.
- 34. Samareh, J. A. "Multidisciplinary Aerodynamic-Structural Shape Optimization Using Deformation (MASSOUD)," *8th AIAA/USAF/NASA/ISSMO Symposium on Multidisciplinary Analysis and Optimization*. Vol. AIAA 2000-4911, Long Beach, California, U.S.A., 2000.
- 35. Nagel, B., Rose, M., and Heinrich, R. "An Alternative Procedure for FE Wing Modelling," *DGLR-2006-048*, 2006, p. 9.
- 36. Samareh, J. A. "Novel multidisciplinary shape parameterization approach," *Journal of Aircraft* Vol. 38, No. 6, 2001, pp. 1015-1024.
- 37. La Rocca, G., Krakers, L., and Van Tooren, M. J. L. "Development of an ICAD generative model for blended wing body aircraft design," *9th AIAA/ISSMO Symposium on Multidisciplinary Analysis and Optimization*. Atlanta, Georgia, USA, 2002.
- 38. Strohmeyer, D., and Seubert, R. "Improvement of a Preliminary Design and Optimization Program for the Evaluation of Future Aircraft Projects," *7th AIAA/USAF/NASA/ISSMO Symposium on Multidisciplinary Analysis and Optimization*. St. Louis, USA, 1998.



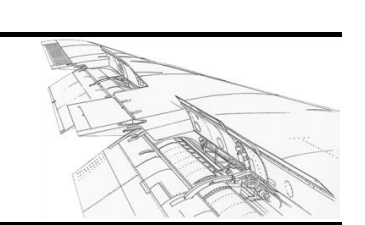
- 39. Werner-Westphal, C., Heinze, W., and Horst, P. "Improved representation of high-lift devices for a multidisciplinary conceptual aircraft design process," *Journal of Aircraft* Vol. 46, No. 6, 2009, pp. 1984-1994.
- 40. Rose, M., and Nagel, B. "Advanced Branch and Bound Method to Interplate Acoustic Data on Structural Finite Element Meshes," *ICSV13 Vienna 2006 The Thirteenth International Congress on Sound an Vibration*. Vienna, Austria, 2006.
- 41. Dvorak, F. A. W., F. A. . "A viscous/potential flow interaction analysis method for multielement infinite swept wings, volume 1 ". NASA, 1974, p. 91.
- 42. Dillner, B., and May, F. W. "Aerodynamic isues in the design of high-lift systems for transport aircraft," *Improvement of Aerodynamic Performance through Boundary Layer Control and High-lift Systems*. AGARD Cp-365, Brussels, Belgium, 1984.
- 43. Rumsey, C. L., and Ying, S. X. "Prediction of high-lift: Review of present CFD capability," *Progress in Aerospace Sciences* Vol. 38, No. 2, 2002, pp. 145-180.
- 44. Finck, R. D., Ellison, D. E., Malthan, L. V., and al, e. *USAF Stability and Control DATCOM*, 1978.
- 45. IHS. "ESDU: Engineering Sciences Data Unit main webpage," http://www.esdu.com/, accessed: 25-11-2010. 2010.
- 46. ESDU: Gilbey, R. W. e. a. "Information on the use of Data Items on high-lift devices," *ESDU 97002 with amendments A to D*. IHS ESDU, 2007.
- 47. ESDU: Dovey, J. R. J. e. a. "Maximum lift of wings with trailing-edge flaps at low speeds," *ESDU 91014 with amendment A*. IHS ESDU, 1995.
- 48. ESDU: Dovey, J. R. J. e. a. "Wing lift coefficient increment at zero angle of attack due to deployment of leading-edge devices at low speeds," *ESDU 96032*. IHS ESDU, 1996.
- 49. Roskam, J. *Airplane design Pt 6. Preliminary calculation of aerodynamic, thrust and power characteristics*. Lawrence, Kansas, USA: DARcorporation, 2000.
- 50. Howe, D. *Aircraft conceptual design synthesis*. London: Professional Engineering Publishing, 2000.
- Drela, M. "Newton Solution of Coupled Viscous/Inviscid Multielement Airfoil Flows,"
 21st Fluid Dynamics, Plasma Dynamics and Lasers Conference. Vol. AIAA 1990-1470,
 AIAA, Seatlle, WA, USA, 1990.
- 52. Valarezo, W., and Chin, V. "Maximum lift prediction for multielement wings," *AIAA* 30th Aerospace Sciences Meeting and Exhibit. AIAA, Reno, NV, USA, 1992.
- 53. Vos, d. i. R. "Aircraft Design and Operation," *AE4-240*. Delft University of Technology, 2010.
- 54. Obert, P. I. E. "A procedure for the determinations of trimmed drag polars for transport aircraft with flaps deflected." Vol. 1, Fokker B.V., Amsterdam, The Netherlands, 1986, p. 142.
- 55. Wild, J. "Multi-objective constrained optimisation in aerodynamic design of high-lift systems," *International Journal of Computational Fluid Dynamics* Vol. 22, No. 3, 2008, pp. 153-168.
- 56. Thiede, P. "EUROLIFT advanced high-lift aerodynamics for transport aircraft," *Air & Space Europe* Vol. 3, No. 3-4, pp. 105-108.
- 57. Brezillon, J., Dwight, R., and Wild, J. "Numerical Aerodynamic Optimisation of 3D High-Lift Configurations," *26th Congress Of The International Council Of The Aeronautical Sciences*. Anchorage, AK (USA), 2008.
- 58. Antunes, A. P., Da Silva, R. G., and Azevedo, J. L. F. "A study of transport aircraft highlift design approaches." Vol. 1, Reno, NV, 2007, pp. 329-346.
- 59. Liersch, C. M., and Wunderlich, T. F. "A Fast Aerodynamic Tool for Preliminary Aircraft Design," *12th AIAA/ISSMO Multidisciplinary Analysis and Optimization Conference*. Victoria, British Columbia Canada, 2008.



- 60. Van Dam, C. P., Vander Kam, J. C., and Paris, J. K. "Design-oriented high-lift methodology for general aviation and civil transport aircraft," *Journal of Aircraft* Vol. 38, No. 6, 2001, pp. 1076-1084.
- 61. Drela, P. d. i. M. "Athena Vortex Lattice (AVL) source page," http://web.mit.edu/drela/Public/web/avl/, accessed: 06-04-2010. Massachusets, USA, 2008.
- 62. Ramamurthy, R. S., and Dutt, H. N. V. "Analysis of wing flap configurations by a nonplanar vortex lattice method," *Journal of Aircraft* Vol. 25, No. 2, 1988, pp. 97-98.
- 63. Mook, D. T., and Nayfeh, A. H. "Numerical simulations of dynamic/aerodynamic interactions," *Computing Systems in Engineering* Vol. 1, No. 2-4, 1990, pp. 461-482.
- 64. Rossow, V. J. "Validation of vortex-lattice method for loads on wings in lift-generated wakes," *Journal of Aircraft* Vol. 32, No. 6, 1995, pp. 1254-1262.
- 65. iGreen_HAP_6. "AEROFLUB Aeroelastik in der Flugzeugbewertung," *German Aerospace Centre (DLR)*. 2009.
- 66. Kruse, M. "LamAir kick-off: Aerodynamischer Entwurf," *German Aerospace Centre* (*DLR*). 2009.
- 67. Eclipse-Foundation. "Eclipse modeling tools." Vol. 2011, The Eclipse Foundation, 2010.
- 68. Mason, W. H. *Applied Computational Aerodynamics Lecture Notes*: Virginia Polytechnic Institute and State University, 2003.
- 69. Burley, C., and Kourakis, K. "GNU Fortran G77 compiler for Win 32." 2002.
- 70. Sigur, S. "Barycentric Coordinates." Paideia school, Atlanta, USA, 1998.
- 71. Obert, P. I. E. *Aerodynamic Design of Transport Aircraft*. Delft: IOS press under the imprint Delft University press, 2009.
- 72. Heinrich, R., Kroll, N., Neumann, J., and Nagel, B. "Fluid-Structure Coupling for Aerodynamic Analysis and Design: A DLR Perspective (Invited)," *46th AIAA Aerospace Sciences Meeting and Exhibit*. Vol. AIAA 2008-561, Reno, Nevada, U.S.A., 2008.
- 73. Gardiner, A. "Fokker-100 (F-28-0100) high-lift flaps fully deployed while approaching HAM/EDDH." 2005.
- 74. Saunders, C. R., Hertog, R. J. d., and Sluis, J. C. v. d. "Fokker 100 Type Specification." Fokker Aircraft B.V., Amsterdam, 1995.

APPENDIX A



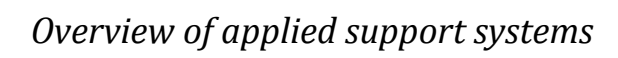


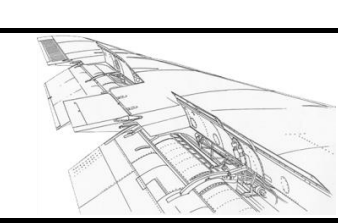
		25	÷		0	0	0	0	0	+	
Based on: [2]		m Ci	1	1	+	+	+	+	+	+	D
Based		simp licity	‡	+	‡		ŀ	I	+	0	IB: inboard, MS: midspan, OB: outboard, TP:tapered
	othe	r appl.	some fig superso	hter a/c, onic a/c	VTOL a/c		hybrid lar	ninar flow a/c	some fighter a/c		ırd, TF
		380									000
		350								ID(4) OD(0) TD	풀
	<u> </u>	340 330								IB(1x) OB(6x), TP	
	Airbus	321								IB(1x) OB(6x), TP IB(1x) OB(4x)	Ö
	₹	320								IB(1x) OB(4x)	Ë,
		310								(2v) TD	spa
		300								(3x), TP (3x), TP	ig
	1 4	L1101								IB(3x) OB(4x)	Ε
	MD	-80/87								(6x), TP	AS.
	IVID-	787								(6X), TP	÷,
										ID(4x) OD(6x)	arc
		777								IB(1x) OB(6x)	90
	ರಾ	767								IB(1x) OB(5x)	2.
	i.	757								IB(1x) OB(4x)	m
_	Boeing	747					IB(3x)	MS(5x) OB(5/6x)			_
io i		737					IB(1x)			OB(4x)	
at		727					IB(1x)			OB(4x)	
1 12		707				IB(1x)	ì			MS(5x) OB(5x)	
Types of leading edge devices and their application		Disadvantages	radius of curvature on upper wing surface is too tight, causes flow separation	bad low-speed, high-lift characteristics	large drag penalty at cruise speeds	not able to accommodate varying angles of attack (therefore only adequate for inboard wing sections), used as two-position device	slave linkage required for deployment, used as two-position device (deployment biased towards optimum landing configuration	limited spanwise bending stiffness requires more panels, rigging problems at cruise conditions, complicated and expensive	only two-positions possible, deployment biased towards optimum landing configuration	in general, slave tracks are required for third position (eliminated on newer airliners), increased complexity of the system	
eading edge		Advantages			simplicity	simplicity	more tolerant to AOA changes	improved airfoil shape at deployment		intermediate sealed takeoff position for best L/D performance	
Types of I		Schematic	7	1	Į	L	L	L		Ţ	
Table A.1		Subtype	Hinged LE	Variable camber LE		Simple Krüger	Folding, bull-nose Krüger	VC Krüger	Two- position slat	Three- position slat	
[Tab		Туре	Nose	Flap	Fixed Slot		Krüger flap			Slat	



		유島	:	÷		0	+	‡	‡	‡	
Based on: [2]		CI Max	:	+	,	+	‡	‡	‡	‡	te
ased		sim -pli- citv	ŧ	‡	‡	+	+		ı	I	rustga
Bi		max defl.		20°	30° - 35°	40°	55°	55°	60° -	up to 80°	IB: inboard, MS: midspan, OB: outboard, NTG: no thrustgate
	othe	er appl.	early a/c	as flaperon	a/c with slow cruise speeds	comeback at modern a/c					ard, NTC
		380 350									utbo
	σ	340				(2x, NTG)					
	Airbus	330 321				(2x, NTG)			(2x)		ō,
	⋖	320				(2x, NTG) OB(1x)			(=//)		par
		310 300				OB(1x)		IB(1x)	(2x)		nids
	LH	L1101						(2x)	(21)		<u>S</u> :
	MD.	-80/87					(2x)				9,≥
		787 777				OB(1x)			(1x)		oar
	_	767				OB(1x)			(1x)		inb
	Boeing	757							(2x)		ä
	8	747 737				(747SP: 2x)				(747: 2x) (2x)	
		727								(2x)	
		707					(2x)				
ınd their application		Disadvantages	low lift increase	low deployment angle due to early flow separation	little Fowler motion, small slotrequires rounded cavity on lower surface which imposes drag penalty at cruise conditions		very few mechanisms qualify (vane is trapped between spoiler and lower cove panel, must be sealed to improve TO L/D)	adds quite some complexity, challenge in mechanism (extract without slave linkages, keep contact with spoilers for sealed TO L/D)	step farther in complexity	very complex and heavy structure, high maintenance costs, significant edge losses create large drag, very high nose-down pitching moments	
Types of trailing edge devices and their application		Advantages	simplicity, good attitude and glideslope control device	simplicity, can be used as flaperon	simplicity	simplest of all Fowler flaps (low complexity), lowest weight and cost	only slightly heavier than single slotted flap	retractable vane creates second overlap: increases Fowler motion and total developed wing chord	more Fowler motion than articulating vane/ main flap with same stowed chord length	very high Fowler motion, highest sectional lift capabilities	
Types of tr		Schematic		1	/						
Table A.2		Subtype	Split flap	Plain flap	Simple slotted flap	Single slotted Fowler flap	Fixed vane/main double-slotted flap	Articulating vane/main double- slotted flap	Main/aft double- slotted flap	Triple- slotted flap	
Tab		Туре	Non-	slotted Flap			Slotted	<i>Flap</i>			

APPENDIX B





ST: Slave tracks, IB: inboard, OB: outboard

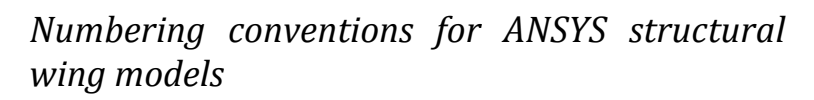
[2]		actuation Ioads (Iow: ++, high:)	;	i	·	+
Based on: [2]		Fowler motion develop ment	ŀ	i		+
П		simpli- city	‡	+	1	+
		other appl.				
		other appl. 380				
اہا		350				
Or		340				
ati	Airbus	330				IB(3x) OB(12x)
lic l	Air A	321				(10x)
dd		320				(10x) IB(2x) OB(6x)
[a]		310				IB(2x) OB(6x)
eir		300 LH L1101				IB(2x) OB(6x)
th		LH L1101				(14x)
ק		MD-80/87				(12x)
ar		787				(4.4.)
ns		777				(14x)
iSI	g	767				(12x)
au	Boeing	757		(0.)	(00 (00)	(10x)
Ch C	<u>&</u>	747		(6x)	(20x/22x)	(2. 07)
ne		737		(2x) (2x)		(6x+ST)
e n		727	(0)	(2x)		(8x)
gp		707	(6x)			(20x)
Types of leading edge mechanisms and their application		Comments				Relatively low actuation loads, since actuation loads are normal to the air loads
Types		Used for LE type	Simple Krüger	Folding, bull- nose (rigid) Krüger	Variable Camber (VC) Krüger	Slats
Table B.3		Subtype	without slave link	with slave link	with slave links to flex the Krüger panel	
Tabl		Туре	Simple hinge with	goose-neck fitting	Four bar linkage	Circular arc track

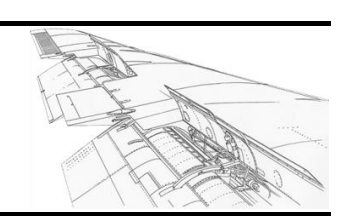


FMD: fowler motion development, FAS: fairing aerodynamic shaping possibilities, SCM: streamwise conical motion adaptability

						3ti can	TWISC COIIICA	i illutiuli aua	ptability		
			SCM		+	+	+	+	+	+	+
n: [2]			FAS	ŀ		‡	++/+	ı	+++ (not req'd)	0	0
Based on: [2]			FMD	·		‡	‡	‡	I	‡	‡
			simplic ity	‡		ŀ	i	ı	+	+	+
	О	the	r appl.								
			r appl. 380								
			350								
		'n	340								IB(2x) OB(3x)
	4	Allbus	330 321				(, [,])				IB(2x) OB(3x)
		₹	321				(+5x!)				IB(1x) OB(2x) IB(1x) OB(2x)
			310							IB(2x) OB(3x)	ID(1X) OD(2X)
딜			300							IB(2x) OB(4x)	
ij	L	Н.	L1101							(10x)	
ica	N	۱D-	-80/87	(4x)						(1011)	
ld			787								
ab			777				(4x)				
Ė			767	(2x)				OB(2x)			
he		Doeing	757							(x)	
d t		S S	747			(747SP: 4x)				(x)	
l ä l	'	_	737							(x)	
IS			727							(x)	
Sm			707						(x)		
es of trailing edge mechanisms and their application			Disadvantages	requires pivot far below wing, extra side load reaction required		counter rotation is faced at initial deployment, actuation power requirements can become high	actuation power requirements can become high	most of the links must be doubled for fail-safety, very expensive and complex, large maintenance (large amount of joints placed in series)	cuts vanes into segments, penetrates main flap panels	reaction to flap air loads results in large couple at carriage rollers leading to high maintenance requirements	
Types			Advantages	simplicity	fairing depth reduction of 30-35% compared to simple hinge	can be completely buried in airfoil when used as end supports (so no fairing required)	not clear if better or worse than upside-down linkage, deep but short fairing required				reduced roller loads when compared to hooked- track, very low actuation power required
Table B.4			Subtype		Upright four- bar linkage	Upside-down four-bar linkage	Upside- down/upright four-bar linkage	Complex four- bar linkage	Internal circular arc track	Hooked-track support	Link/track mechanism
Tabl			Туре	Simple hinge			four-bar linkages			mechanisms including tracks	

APPENDIX C





			Remark				[P]	[P, S]			Remark				[A]	[P, S]			Remark				B	[P, S]			Remark				ТВО				Remark	
ADDITIONAL WING PARTS (engine, gear)	eypoints	Convention:WPNSXX (6-digit)	# Meaning		7 Gear 8 Tank 9				lines	×	# Meaning		7 Gear 8 Tank 9				areas	Convention:WPNSXX (6-digit)	# Meaning		6 Engine 7 Gear 8 Tank				ment types	Convention: WTSE (4-digit)	# Meaning		6 Engine element 7 Gear element 8 Tank element 9	0 Point element 1 Line element 2 Area element 3 Volume element			material numbers	Convention: TEE (3-digit)	# Meaning	
DITIONAL WI		Conventior	Range	6 -	6 - 9	1 - 9		01 - 99		Conventior	Range	6 - 1	6 - 9	1 - 9	ŀ	01 - 99		Convention	Range	1 - 9	6 - 9	1 - 0	ŀ	01 - 99	ele	Convention	Range	1 - 9	6 - 9		6 - 0	1 - 9	mate	Convent	Range	01 - 99
AD			Indicates	Keference	Part	Part number	Sub Index	Index			Indicates	Keference	Part	Part number	Sub Index	Index			Indicates	Reference	Part	Part number	Sub Index	Index			Indicates	Reference	Element Type	4	(= Mesh type)	Index			Indicates Material type	Index
			Digit	>	d.	z	တ	×			Digit	>	۵	z	ဟ	×			Digit	>	۵	z	S	×			Digit	*	-		Ø	ш			Digit	. Ш

		Remark		(or: base - HLD2)	T. link type [S]			Remark				- Annual Control	Nelliain	ТВР				Remark	(incl MPC rigid link Only point type MP		[7,8]		Remark	
LINKS	keypoints	# Meaning		1 Base wing 2 LNK: base - HLD1 3 HLD1 4 LNK: HLD1 - HLD2 5 HLD2			lines tion: WTNXX (5-diait)		1 Link 2 Actuator attachment 3 Actuator		areas	Convention: WTNXX (5-digit)				element types	: WTSE (4	# Meaning	2 Link element 3 Revolute element 4 Rigid body element	0 Point element 1 Line element 2 Area element 3 Volume element		material numbers	nge # Meaning	
		Range #	1 - 9	- 0	1 - 9	П	Convention:	Range 1 - 9	- e	1 - 9		Conven	1 - 9	- 9	1 - 9		Conver	Range		6 - 0	1 - 9	mg	Range 2 - 2	11
		Indicates	Reference	Туре	Link number Index			Indicates	Туре	Link number Index		ootooibal	Reference	Туре	Link number Index			Indicates	Element Type	Subtype (= Mesh type)	Index		Indicates Material type	Index
		Digit	>	-	z×			Digit	-	z×		į	ž Š	-	z×			Digit	-	ø	ш		Digit	. Ш

			Remark			T				Remark							Remark								Remark					i	Kemark	
GENERAL WING PARTS (wing, moveables)	keypoints	S	# Meaning		Surface, lower			lines	WTRRSS (# Meaning	1 Ribs, upper 2 Ribs, lower	Spars, lower			areas	WTRRSS (# Meaning		1 Skin, upper 2 Skin, lower 3 Ribs	-			element types	Convention: WTSE (4-digit)	# Meaning	1 Wing/moveable el.	0 Point element 1 Line element 2 Area element 3 Volume element		material numbers	Convention: TEE (3-digit)	# Ming/moveable mat.	
VERAL WING		Conventio	Rang	1 - 9	- 5	- [-	01 - 99		Convention:	Range	-		01 - 99			Convention:	Sang	5			1.	01 - 99	ele	Convent	Range		6 - 0	1 - 9	mat	Conven	1 - 1 01 - 99	1
GEI			Indicates	Reference	Туре	Rib	Spar			Indicates		adk:	Rib	Spar			Indicates	Kererence	Type		Rib	Spar			Indicates	Element type	Subtype (= Mesh type)	Index		- In the second	Material type Index	
			Digit	>	-	RR	SS			Digit		-	RR	SS			Digit	>	-		R	SS			Digit	-	σ	ш				!



ADDITIONAL WING PARTS (engine, gear)	
LINKS	T == 2 Link Element T == 2 Link Element S == 1: Simple Revolute Joint, Type A ECAM188 S == 2 Simple Revolute Joint, Type A ECAM188 S == 2 Simple Alleron Mechanism LINK11 S == 2 Simple Alleron Mechanism E 2 S == 2 Simple Alleron Mechanism E 2 Target S == 2 Simple Alleron Mechanism E 2 Target TARGE 170 S == 2 Simple Alleron Mechanism Target TARGE 170 S == 2 Simple Alleron Mechanism Target Tar
GENERAL WING PARTS (wing, moveables)	

APPENDIX D

Fokker 100 wing geometry

